FTIR Studies of TiO_2 – Pigmented Polymer Photodegradation

Changqing Jin

University of Newcastle upon Tyne

A thesis submitted to the University of Newcastle upon Tyne
for the degree of Doctor of Philosophy

June 2004

Abstract

A novel method (*in-situ* quantitative infrared spectroscopy of evolved CO_2) for studying photo-degradation has been developed and applied to the study of several different polymers including a series of polyethylene and poly (vinyl chloride) samples containing TiO_2 pigments with different photo-activities. Infrared (IR) analysis was used to monitor carbon dioxide emitted from samples exposed to ultraviolet irradiation (UV) in atmospheres of differing composition. The experiments were conducted in a specially constructed cell that permits simultaneous UV exposure of the sample and IR interrogation of the vapour in the cell. It has been demonstrated that the *in-situ* gas-phase method permits a fast and convenient way of assessing the durability of pigmented and unpigmented polymer. A single test on one material occupied about 7 hours – very much less than conventional artificial weathering exposures. Excellent correlation between the CO_2 method and the conventional method for measuring carbonyl groups in the polyethylene films has been demonstrated.

The TiO_2 pigments used included anatase and rutiles with different surface treatments. Anatase-pigmented material gave significantly higher CO_2 emission than unpigmented polyethylene. The rutile-pigmented polyethylenes either gave reduced CO_2 emission or enhanced emission, according to the surface treatment. The ranking of the pigments as protectants or pro-degradants coincided with that obtained from much more time-consuming laboratory testing and field experience. Similar results were obtained for the poly (vinyl chloride).

The CO_2 method is a convenient way to study the factors (humidity, oxygen concentration and UV intensity or wavelength), which influence the rate of carbon dioxide evolution *i.e.* the rate of photo-oxidation of the polymers.

Blown polyethylene (PE) film was exposed to UV irradiation while held under tensile stress in a specially designed metal frame. The chemical degradation was followed using the FTIR carbonyl index. Tests were conducted on unpigmented PE and on a series of five PEs containing TiO_2 pigments with different photo-activities. The yield strengths measured in tensile tests on unexposed films were typically 10 % greater in the longitudinal (machine) direction than in the transverse direction. UV exposures were conducted with stress applied both parallel and transverse to the machine direction. For

all six materials, tensile stress accelerated carbonyl group development. Some samples cracked during UV exposure in tension and did so in a shorter time if the stress was applied in the machine direction than if it was transverse to it. The carbonyl index at the onset of cracking was lower for longitudinal samples than for transverse samples. Unpigmented PE was slightly more sensitive to transverse strain and the anatase-pigmented PE slightly more sensitive to longitudinal strain.

Declaration

This thesis records the work carried out in the School of Chemical Engineering and Advanced Material, University of Newcastle upon Tyne between October 2000 and September 2003. Except where otherwise stated this work is believed to be original. Extracts from this work have been accepted for publication in the following journal and conference papers:

(1) J White*, T.A. Egerton, P.A. Christensen, and Changqing Jin, Phtomechnical Oxidation of Anisotropic Polyethylene, at the SPE ANTEC 2004 conference.

(2) C Jin, T.A. Egerton, P.A. Christensen and J White*, Effect of Anisotropy on Photo-mechanical Oxidation of Polyethylene, Polymer, 2003. 44(19): p. 5969-5981.

(3) Changqing Jin, T.A. Egerton, P.A. Christensen, N. MacDonald and J White*, Rapid Method to Assess Effect of Pigments on Photodegradability of Polymer, at the SPE ANTEC 2003 conference.

The paper 'Rapid Method to Assess Effect of Pigments on Photodegradability of Polymer' was selected for 2003 SPE Polymer Analysis Division Netzsch Instruments the Frank Giblin Memorial Award in Polymer Analysis.

ACKNOWLEDGEMENT

I would like to acknowledge my sincere thanks to my supervisors, without whom this thesis would never have been completed. Firstly, Dr. Terry Egerton, for his valuable scientific guidance, advice, suggestions and stimulating discussion throughout this work and during the preparation of this thesis. Secondly, Professor Jim R. White particularly for his enthusiasm for the project and encouragement at times of despair, but also for all the time he has put in together with Dr. Terry Egerton to help me turn files of spectra into chapters of this thesis. Finally, Dr. Paul Christensen for his continual support, advice, his logical thinking and push me when I was little lazy throughout the course of the project.

I am most grateful to Huntsman Tioxide for the award of a University Postgraduate Studentship for my study and the continual support for the project. My sincere thanks also go to Dr. Les A Simpson, Mme. Christine Spriet and Mr. Neil Macdonald for their valuable advice and helpful discussions.

In particular, I would like to thank Mr John Lawson, for his kindly teaching and guiding me side by side to understand using the equipment involved in this project.

I would also like to express my thanks to Mr Mike Foster for his help with the mechanical testing of the polymer material. All past and present members of the TAE/PAC research group for their warmly help and making the lab an enjoyable place to work. I would like thank Ian Tooley for his warm help at the beginning of this project and the students James, Samia, Raghu, Rob, Paola, and the others for their encouragement and moral support.

I would also like to thank the help and advice of the mechanical and glass blowing workshops in the department of chemistry for constructing the FTIR cells and accessories used in this work.

I would like to thank my wife Fang Tian and my daughter Luyang Jin and other members of my family for their patience, encouragement and support for my study, and my friends for their concern and their help to make this work a success.

Contents

Chapter 1: Introduction

Chapter 2: Experimental

Chapter 3: Photooxidation of Unpigmented Polyethylene

Chapter 4: Pigmented Polyethylene

List of Figures

Chapter 1

Chapter 2

Chapter 3

Chapter 4

Chapter 5

Chapter 6

Chapter 7

Lists of Tables

Chapter 1

Chapter 2

Chapter 3

Chapter 4

Chapter 5

Chapter 6

List of Abbreviations

Abs	absorbance
AM	air-mass
a.u.	absorbance units
ATR	attenuated total reflectance
CI	carbonyl index
EPL	effective path length
EPR	electron paramagnetic resonance
ESR	electron spin resonance
FTIR	fourier transform infrared
GC-MS	gas chromatography-mass spectrometry
GPC	gel permeation chromatography
LDPE	low density polyethylene
ID	internal diameter
IRE	internal reflection element
MCT	mercury cadmium telluride
PAS	photo-acoustic spectroscopy
PCD	photocatalytic degradation
PD	photochemical degradation
PE	polyethylene
PET	poly(ethylene terephthalate)
Phr	parts per hundred resin
PVC	poly(vinyl chloride)
R-A	reflection-absorbance
RH	relative humidity
S/N	signal to noise ratio
SEM	scanning electron microscopy
SIMS	secondary ion mass spectrometry
UV	ultraviolet
WOM	weather-ometer

XPS	X-ray photoelectron spectroscopy
Xe	xenon

List of main Symbols

A	absorbance	N	Avogadeo's number
A	the absorption coefficient	*h*	planck's constant
C	velocity of light	λ	wavelength (nm)
D	film thickness	n	molar number
d_p	penetration depth (m)	P	pressure (Nm^{-2})
E	energy (J)	R	ideal gas constant ($JK^{-1}mol^{-1}$)
E_{bg}	band gap energy (eV)	T	transmittance (%)
Ec	energy of conduction band (eV)	V	volume (m^3)
E_v	energy of valence band (eV)	ν	frequency (s^{-1})
e^-	photogenerated electron	η	refractive index
ε	molar absorption coefficient		
h^+	photogenerated hole		
I	UV intensity ($mWm^{-2}\ nm^{-1}$)		
I_o	incident light intensity (quanta s^{-1})		
ID	internal diameter (mm)		
l_{eff}	effective pathlength (m)		
L	pathlength (m)		
Log (I_o/I)	optical density (a.u.)		

CHAPTER 1

INTRODUCTION

1.1 GENERAL CONCEPT

The purpose of this project is to develop infrared spectroscopy to measure carbon dioxide produced from UV irradiated polymers and hence to measure the effectiveness of different TiO_2 pigments on photostability of polymer materials. It is essential firstly to understand some fundamental concepts relevant to this project.

A pigment is a particulate material used to colour and opacify a coating or film which may be a paint, an ink, a sheet of plastic or paper, a ceramic glaze, a tablet coating, a fabric and many other forms of coating [1-7].

A polymer is a high-molecular-weight organic compound, natural or synthetic, whose structure can be represented by a repeated small unit, the monomer (*e.g.*, polyethylene, rubber, cellulose). Synthetic polymers are formed by addition or condensation polymerization of monomer. If two or more different monomers are involved, a copolymer is obtained. Some polymers are elastomers, some plastics [8-10].

1.1.1 Pigments

A pigment should be:

i) Insoluble in the coating, plastic, paper or any other binder system it is used in.

ii) Chemically inert and non toxic.

iii) Heat and light stable.

iv) As pure and consistent as possible to produce even coloration and prevent cross contamination.

The most significant difference between a pigment and a dye is that the latter may be soluble in some applications.

Typical examples of pigments include:

a) Natural earth colors such as iron oxides and their synthetic analogues.

b) Complex organic compounds such as phthalocyanine blues and greens, and

c) Titanium dioxide.

It is generally accepted that a pigment will provide significant opacity whereas cheaper particulate fillers and extenders may be virtually transparent in the end applications due to their lower refractive index. Although they often provide functional properties such as viscosity and flow control, the latter are usually natural products such as calcium carbonate (ground chalk), clay, talc etc. Some compounds such as synthetic silica (SiO_2) meet the first four criteria for pigments but are virtually transparent in a binder system and are used for specific application properties.

Pigments are widely used for the coloration of thermoplastic in many commercial applications [7, 11]. Although they are used primarily to impart colour or opacity to the polymer, they can nevertheless have a marked influence on the thermal and photochemical stability of the polymer material. This effect on the durability of polymer material has a substantial significance.

1.1.2 TiO_2 as pigment

Titania is very white and has a very high refractive index – surpassing that diamond. Titanium dioxide is by far the most widely used white pigment. The interest of TiO_2 as a pigment for the paint industry stems from its high refractive index (2.73 for rutile and 2.55 for anatase TiO_2, whereas the refractive index for diamond is 2.42). The refractive index determines the opacity that the material confers to the matrix in which the pigment is housed. Hence, with its high refractive index, relatively low levels of titania pigment are required to achieve a white opaque coating. It provides whiteness and opacity to such products such as paints and coatings (including glazes and enamels), plastics, paper, inks, fibres and food and cosmetics [3, 7, 12, 13]. One of the major advantages of the material for exposed applications is its resistance to discoloration under UV light.

From the 1920s TiO_2 pigment production had increased by 1988 to an estimated 2.9 million tonnes per year [3]. The main reasons for this are that TiO_2 possesses a very high light scattering efficiency and it is an inert, non-toxic material that is safe to use.

1.1.3 Durability of Polymer

Durability, which is the resistance to destructive effects caused by the environment, is of great importance for products such as paint, textiles, plastics and rubber, since breakdown of the surface may result in severely reduced mechanical strength and will certainly detract from appearance.

There is always concern regarding the durability of polymeric materials because they can sometimes degrade very rapidly. If the useful lifetime of these materials can be predicted their maintenance and replacement can be planned. The deterioration of a material depends on how and to what extent it interacts with its surroundings. Degradation of plastic during outdoor exposure is influenced to varying degrees by all natural meteorological phenomena. Heat, radiation (ultraviolet and infrared), rain, humidity, atmospheric contaminants, thermal cycling, and oxygen content of air all contribute to the degradation of plastic subjected to outdoor exposure [14]. All of these factors influence the durability of polymeric materials.

Since the mechanism of breakdown of pigmented polymer is extremely complex, it is convenient to evaluate the photoactivity of titanium dioxide pigments through studying the oxidation of simple materials in order to assess the effects of pigments. Hence, polyethylene (PE), poly (vinyl chloride) (PVC) and other polymer types, *e.g.* poly (ethylene terephthalate) (PET), paints etc were selected and pigmented to different degrees with titanium dioxide. Fundamentals of TiO_2 chemistry relevant to the research and the methods of durability testing will be described in more detail.

1.2 TITANIUM DIOXIDE

Titanium dioxide has been found extensive use as a white pigment in a variety of formulations, being best known for its incorporation into paints and polymers. As early as 1929 it was known that the pigment "titanium white", *i.e.* TiO_2, was

responsible for fading in paints and several major studies into the photosensitizing action of TiO_2 followed [15]. Because of its photosensitizing action, TiO_2 appeared initially to be unsuitable as a pigment for paint, since it caused chalking, *i.e.* the photodegradation of the organic polymer 'binder' of the paint [16]. However, this undesirable feature was largely eliminated by coating the pigment with a hydrous layer of an inert oxide, such as silica, alumina or zirconia [15, 16]. In poly(vinyl chloride) (PVC) TiO_2 is used in window profile, facia boards, *etc.* and in polyethylene (PE) to give the familiar white plastic bag. In Europe 50% of the TiO_2 is used in paint, 25% in paper and 20% in plastic. The remaining 5% is used in both pigmentary applications such as inks, floor coverings, sealants, foods and other similar products and in nonpigmentary applications such as ceramics, welding rods and catalyst support *etc* [17].

1.2.1 Structure of Titanium Dioxide

Titanium is abundant in many minerals, occurring in four common ores: ilmenite ($FeTiO_3$), rutile (TiO_2), anatase (TiO_2) and leucoxene ($TiO_{2\cdot x}$ $FeO_{\cdot y}$ H_2O) [7]. Titanium dioxide occurs in nature in three crystalline forms, Anatase, Brookite and Rutile [18]. The anatase and brookite forms can be transformed to rutile by heating at 700°C and 900°C, respectively. The anatase crystal modification is most frequently used in photocatalysis, *i.e.* particularly in the form of the commercially available Degussa P25 powder (70% anatase / 30% rutile). Most TiO_2 pigments are rutile. Brookite is not commonly available.

Anatase and rutile each have titanium atoms surrounded by six adjacent oxygen atoms in regular but slightly different octahedral arrangements, and each oxygen atom is surrounded by 3 adjacent titanium atoms, therefore the titanium dioxide formula is TiO_2. Anatase has a tetragonal structure, which consists of TiO_6 octahedra sharing four-edges, and the structure may be derived from NaCl by removal of half the sodium cations (Figure 1-1 a). The bridging oxygens are displaced towards one another to produce a shorter O-O distance.

The rutile structure is also tetragonal with the TiO_6 octahedra sharing two edges and two corners (Figure 1-1 b). Reduction of the bridging O-O occurs as with anatase. However, displacement of the oxygens towards each other is greater for rutile, thus explaining the slightly greater density and smaller molar volume of the latter. The crystallographic parameters of anatase and rutile are shown in Table 1-1 [19-21].

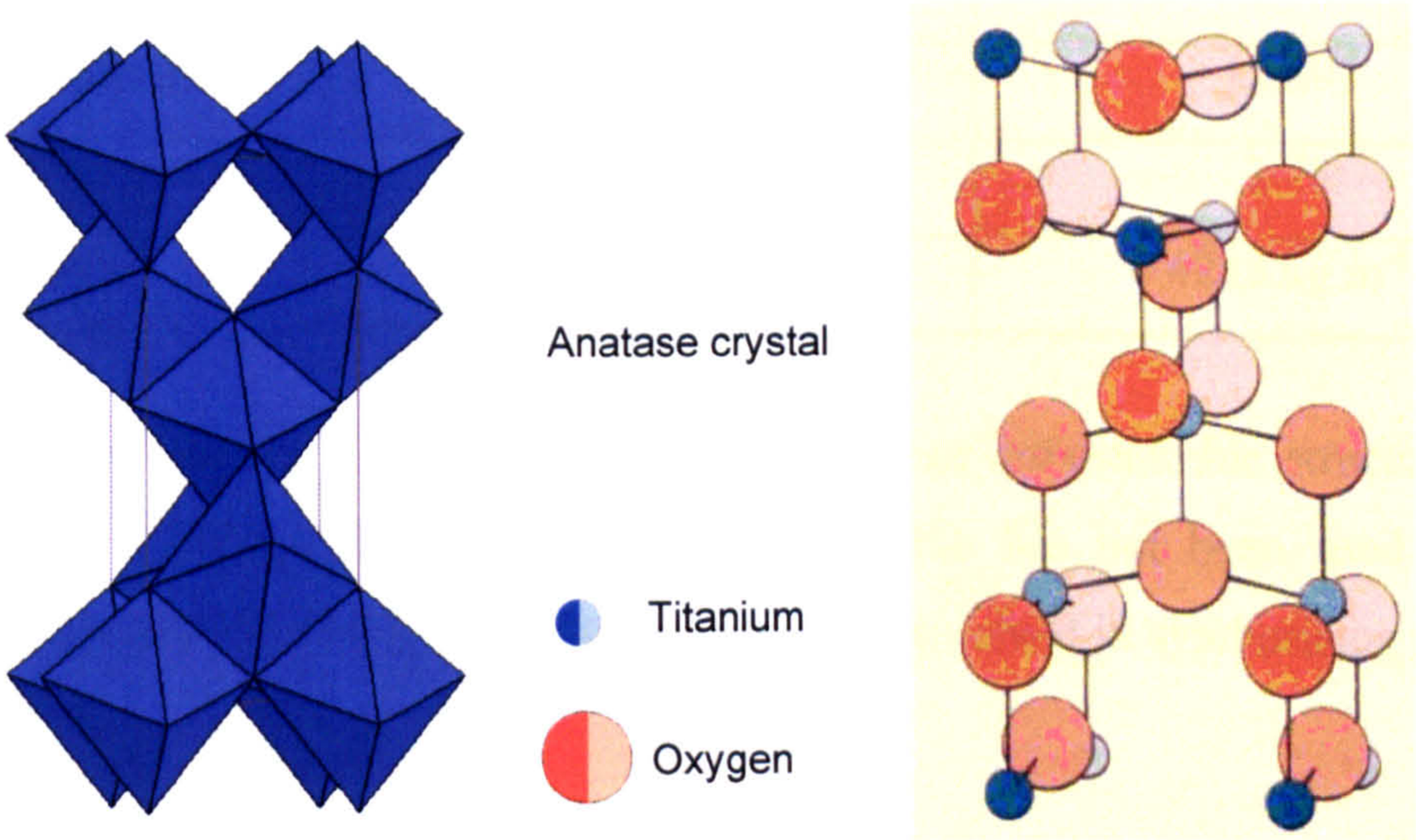

(a)

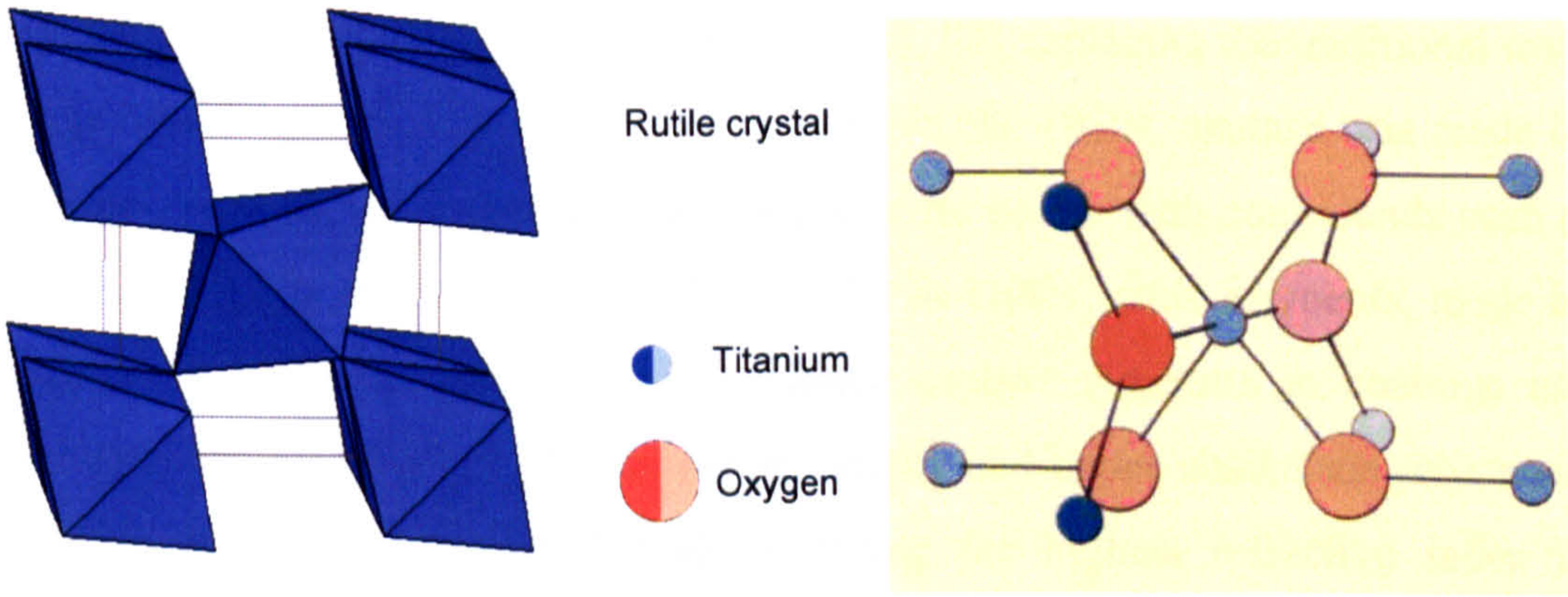

(b)

Figure 1-1 The crystal structure of the anatase and rutile forms of TiO_2, (a) anatase (b) rutile (in Polyhedral and ball-stick display).

Table 1-1 Crystallographic and physical parameter of Anatase and Rutile.

Parameter	Anatase	Rutile
Unit cell	4 TiO_2	2 TiO_2
Unit cell dimensions	a=b=3.7842 A c=9.5146 A	a=b = 4.5936 A c=2.9587 A
Ti-O bond lengths	1.934A (4 per octahedra) 1.980A (2 per octahedra)	1.949A (4 per octahedra) 1.980A (2 per octahedra)
O-Ti-O bond angles	90°, 78.1°, 101.9°	90°, 81.21°, 98.79°
Molar volume	20.156	18.693
Refractive index	2.55	2.73
Density	3895 kg m^{-3}	4243 kg m^{-3}

Brookite is the third crystal phase of TiO_2 and has an orthorhombic structure with TiO_6 octahedra sharing three edges and a corner but has not been used in any photocatalysis studies, probably due to the difficulty involved in synthesising it in the laboratory.

1.2.2 Manufacture of TiO_2

Titanium dioxide has been manufactured commercially since 1918 and has increased to be the most commonly used white pigment, with an average world-wide production of over 3 million tonnes every year [22, 23], replacing the traditional toxic pigments based on lead, zinc and antimony [24]. In the 1930s, anatase was made by the sulphate process and it competed as a pigment for paints with compounds such as lithopone and white lead $(PbCO_3)_2 Pb(OH)_2$ [17]. In 1940s, rutile pigments, made by seeding the sulphate process, began to replace anatase pigments in coatings and plastics applications because of their higher opacity and better chalk/fade resistance. The higher opacity is associated with it having the highest refractive index of colourless, stable compounds. Pigments based on rutile replaced anatase because of its light-scattering advantage of about 20% [17, 25, 26].

TiO_2 pigment is manufactured in four stages [25, 27]:

1) Titanium ore is converted to a purified intermediate, either aqueous titanyl sulphate solution (the sulphate process) or anhydrous titanium tetrachloride (the chloride process).
2) The intermediate is converted into crystalline, size-optimised pigment particles.
3) The surface of the pigment particles is coated by aqueous precipitation techniques.
4) The pigment is finished by grinding with or without dry after-treatments.

TiO_2 pigments are produced from a variety of ores by either of two processes, the sulphate and the chloride process. Sulphate is batch manufacture; chloride is a continuous process. Size-optimised pigment particles from either process are surface-treated from an aqueous environment with inorganic oxides and hydroxides, generally in a batch mode. The product is filtered, washed and dried. The dried pigment can receive a finishing treatment with organics and must then be ground and packed or slurried with appropriate dispersants.

1.2.3 The Sulphate Process

The Sulphate process [23, 25, 27] was the first commercial process for the manufacture of TiO_2. Originally this used ilmenite as a raw material, but beneficiated ores with a much higher TiO_2 content have been used more recently.

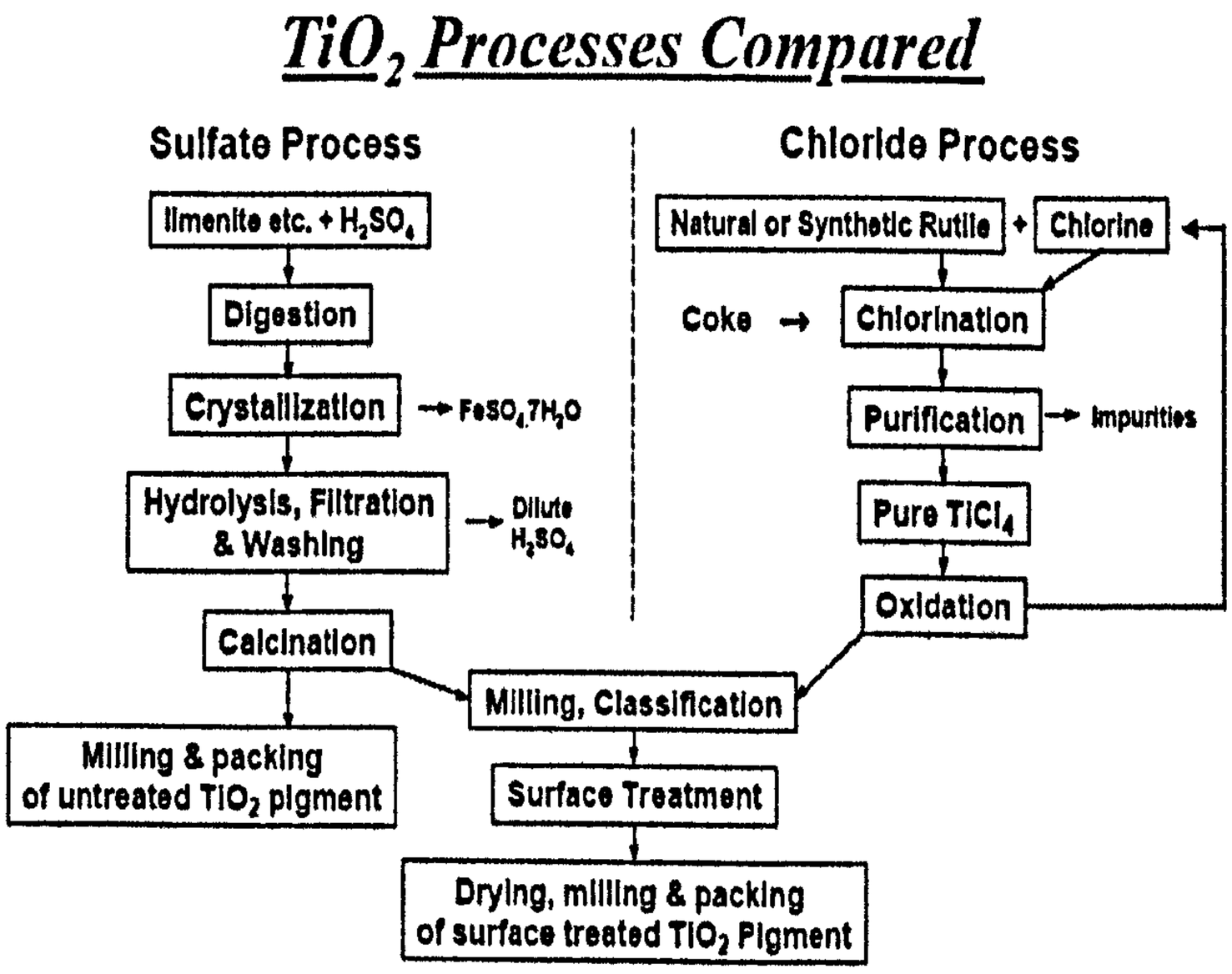

Figure 1-2 Compares the essential process steps in each process.

The ore is first dried, ground, and classified to ensure efficient sulphation by agitation with concentrated sulfuric acid in a batch or continuous exothermic digestion reaction. Figure 1-2 shows the process steps. The following chemical reactions are involved:

$$FeTiO_3 + 2H_2SO_4 \rightarrow TiOSO_4 + FeSO_4 + 2H_2O \qquad (1.1)$$

$$Fe_2TiO_5 + 4H_2SO_4 \rightarrow TiOSO_4 + Fe_2(SO_4)_3 + 4H_2O \qquad (1.2)$$

Controlled conditions maximize conversion of TiO_2 to water-soluble titanyl sulphate ($TiOSO_4$) using the minimum acid. The resultant dry, green-brown cake of metal sulphates are dissolved in water or weak acid, and the solution treated to ensure that only ferrous-state iron is present. The solution temperature is reduced to avoid premature hydrolysis and clarified by settling and chemical flocculation.

The purified titanyl sulphate liquor is filtered to remove final insoluble impurities. The solution is evaporated to a precise composition and hydrolyzed to produce a suspension ("pulp") consisting predominantly of clusters of colloidal hydrous titanium oxide. Precipitation is carefully controlled to achieve the necessary particle size, usually employing a seeding or nucleating technique. The washed pulp is treated with chemicals which adjust the physical texture in the calcination step. This process can produce either anatase or rutile crystal forms depending on additives used prior to calcination.

1.2.4 The Chloride Process

The chloride process[23, 25, 27] was commercialised by Du Pont in the early 1950s. The process route is illustrated in Figure 1-2. Its process depends on the following chemical reaction:

$$TiO_2 \text{ (ore)} + 2Cl_2 + C \rightarrow TiCl_4 \text{ (impure gas)} + CO_2 \qquad (1.3)$$

$$TiCl_4 \text{ (impure gas)} \rightarrow TiCl_4 \text{ (pure liquid)} \qquad (1.4)$$

$TiCl_4$ (pure gas) + O_2 (gas) → TiO_2 (pure solid) + $2Cl_2$ (1.5)

The feedstock for the chloride process is a mineral rutile or synthetic enriched ore containing over 90% TiO_2. Ore is mixed with a source of carbon and the two are reacted, in a fluidized bed, with chlorine at approximately 900°C. The reaction yields titanium tetrachloride, $TiCl_4$, and the chlorides of all the impurities present. The mixed chlorides are cooled and the low-volatile chloride impurities (*e.g.* iron, manganese and chromium) are removed from the gas stream with any un-reacted solid starting materials. The $TiCl_4$ vapor is condensed to a liquid, followed by fractional distillation to produce an extremely pure, colorless, mobile liquid $TiCl_4$ intermediate product.

The second critical stage in the chloride process is oxidation of the $TiCl_4$ to TiO_2 pigment particles. Pure titanium tetrachloride is reacted with oxygen in an exothermic reaction to form titanium dioxide and liberate chlorine, which is recycled to the chlorination stage. After cooling, the gas stream passes through a separator to collect the pigment particles.

In both processes, the raw pigment may either be dried, milled, packed and sold or more likely, especially for rutile pigments, surface-treated to produce a range of special products for various applications. The end-product is either sold as a dry pigment or, especially in North America, converted to a slurry for the manufacture of water-based paints.

1.2.5 Surface Treatments

'Pure' TiO_2 base pigments, whether anatase or rutile, provide high opacity and excellent colour but have a relatively reactive surface [28]. The majority of commercial pigments are therefore coated with an inorganic treatment or coating, and often an organic treatment [29].

Reasons for surface treating titanium dioxide pigment

Nearly all commercial TiO_2 pigments have a surface treatment or coating to:

i) Improve wetting and dispersion in different media (water, solvent or polymer).

ii) Reduce photoactivity.

iii) Increase air in the film in flat latex paints.

Depending on the end application, the surface treatment is usually a combination of alumina, silica and/or zirconia, deposited onto the core TiO_2 particles from either the chloride or sulfate base pigment process, by a wet precipitation process. The coatings on TiO_2 pigments are deposited under very closely controlled conditions of time, temperature and pH to develop the required characteristics. The final analysis of a surface coating shows only part of the expertise in making high performance TiO_2 pigments. Order of addition and precipitation as well as the processes parameters are critical to making the optimum product.

Finally, a polyol or other organic chosen to enhance the wetting of the pigment in a resin system and/or dry bulk handling characteristics is added.

Following surface treatment, the pigment is dried, milled and packed.

1.2.6 Comparison of Titanium Dioxide Crystal Types

Both anatase and rutile TiO_2 produce high opacity due to their high refractive index in comparison with extenders, fillers and early pigments (See Table 1-2).

In fact, examination of the basic properties of the two crystal forms shows several differences – in specific gravity, hardness, refractive index. Although anatase TiO_2 was the first to be produced commercially, and represented a step-change in optical performance over the pigments that preceded it, the rutile form of TiO_2 offers still higher opacity and durability [30]. This is a consequence of the higher refractive index.

Table 1-2 Refractive Index of TiO_2 and Fillers [7].

Materials	*Refractive Index*
Rutile TiO_2	2.73
Anatase TiO_2	2.55
Lithopone	2.13
Zinc oxide	2.02
White lead	2.00
Calcium carbonate (chalk, whiting)	1.57
'China' clay	1.56
Talc	1.50
Silica	1.48

1.3 MECHANISMS OF POLYMER PHOTODEGRADATION

Photochemistry is the study of the chemical reactions of atoms or molecules that have been electronically excited by absorption of light, typically with wavelength in the range of 200 nm to *ca.* 700 nm. In thermal reactions heat is transferred to the respective ground state species, generating a Maxwell – Boltzmann energy distribution. In contrast, photochemical excitation proceeds via the absorption of discrete quanta of energy [31]. More detailed in-depth reviews of photochemistry can be found in some excellent books [31, 32]. Here is just a simple introduction to the basic processes underlying the photochemical degradation of polymer.

1.3.1 Primary Photophysical Processes

The energy E (in joules) of a single photon is given by the Planck equation

$$E = h\nu = \frac{hc}{\lambda} \qquad (1.6)$$

where h is Planck's constant (6.6265×10^{-34} J s), ν is the frequency of radiation (s^{-1}), c is the velocity of light (2.9979×10^{8} ms^{-1}), and λ is the wavelength (m) of monochromatic light. In practice an Einstein (*i.e.*, the amount of energy in 1 mole of photons) can be obtained for a given wavelength by multiplying the energy of the

photon by Avogadro's number ($N=6.023 \times 10^{23}$). The energy of the photon can be calculated using equation 1.6. Therefore the energy of the photon is inversely proportional to the wavelength. For example one Einstein associated with a wavelength of 300 nm gives 398.3 kJ mol^{-1} of energy.

When a system is irradiated, the light may be transmitted, scattered, refracted, or absorbed. The first law of photochemistry, formulated by Grotthus (1817) and Draper (1843) [33], states that only light which is absorbed by a molecule is effective in producing a reaction which changes the molecule. This implies that there must be some overlap between the range of wavelengths of the light entering the system and those absorbed by the starting material. The other law is the photochemical equivalent law proposed by Einstein in 1912: that each photon or quantum absorbed activates only one molecule [14].

Furthermore, the intensity of radiation transmitted through a layer of solution obeys the Lambert-Beer law:

$$\text{Log}\,(I_0/\,I) = A = \varepsilon Lc \quad (1.7)$$

Where I_0 is the intensity of incident light, I the intensity of transmitted light, A the absorbance, ε the molar absorption coefficient, L the pathlength through the sample, and c the concentration of solute.

Photochemically induced changes are caused by absorption of a photon resulting in electronically excited states. Each absorbed photon activates only one macromolecule or chromophore in their ground state S_0; thus, excited singlet states (Sn) are generated. The energies of the higher singlet states deactivates thermally very fast by vibrational relaxation to the lowest excited singlet (S_1) state or, after intersystem crossing, the first triplet state (T_1). Both S_1 and T_1 are the starting species for all the following photophysical or photochemical processes encountering photodegradation [34]. This differentiates photodegradation from thermal oxidation arising from the ground state S_0.

Therefore, all chemical reactions can only take place *via* electronically excited states. The excited singlet molecule may undergo the following processes dissipating the excited energy (see Figure 1-3)[14]:

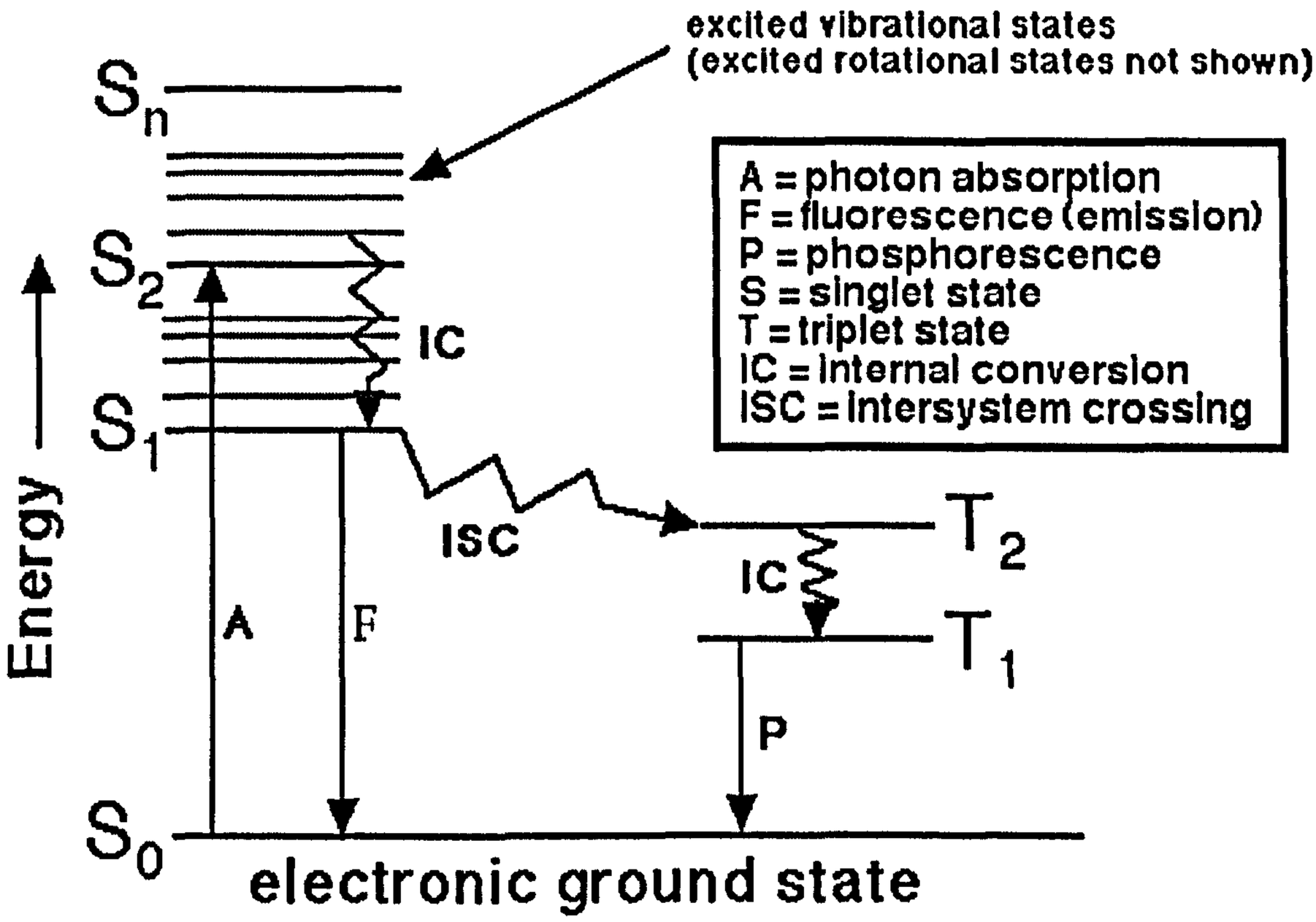

Figure 1-3 Modified Jablonsky energy diagram[35].

Dissociation process: either at the excited singlet (S_1) or the excited triplet state (T_1), which is formed by intersystem crossing.

Radiative process: emission of fluorescence ($S_1 \rightarrow S_0 + h\nu'$) or phosphorescence ($T_1 \rightarrow S_0 + h\nu''$).

Transfer process: transfer of the excited energy to another molecule.

$S_1 + Q_s \rightarrow S_0 + Q_s^*$ or $T_1 + Q_T \rightarrow S_0 + Q_T$

where Q_s and Q_T are quenchers of the excited singlet and excited triplet state, respectively.

The excited energy may also be dissipated as heat. In addition, the formation of an excimer with the same kind of molecule ($A^* + A \rightarrow E_m^*$) or an exciplex with a different kind of molecule ($A^* + B \rightarrow E_p^*$) may occur.

1.3.2 General Mechanism of Photodegradation of Polymer

A polymer system absorbs ultraviolet light and is susceptible to photochemical degradation. The general mechanism of photooxidation of hydrocarbon polymers is based on the following steps [36]:

Initiation: $RH \xrightarrow{hv} R^{\bullet} + H^{\bullet}$ (1.8)

Propagation: $R^{\bullet} + O_2 \rightarrow RO_2^{\bullet}$ (1.9)

$RO_2^{\bullet} + RH \rightarrow ROOH + R^{\bullet}$ (1.10)

Branching: $ROOH \rightarrow RO^{\bullet} + {}^{\bullet}OH$ (1.11)

$RH + {}^{\bullet}OH \rightarrow R^{\bullet} + H_2O$ (1.12)

$RO^{\bullet} \rightarrow$ chain scission processes (1.13)

Termination: $R^{\bullet} + R^{\bullet} \rightarrow R - R$ (1.14)

$R^{\bullet} + RO^{\bullet} \rightarrow ROR$ (1.15)

$RO_2^{\bullet} + R^{\bullet} \rightarrow ROOR$ (1.16)

$RO_2^{\bullet} + RO_2^{\bullet} \rightarrow$ Products (1.17)

Where RH is the polymer, $R^{\bullet}$ is the polymer alkyl radical, $RO^{\bullet}$ is the polymer alkoxyl radical, $ROO^{\bullet}$ is the polymer peroxy radical (polymer alkylperoxy radical), ROOH is the polymer hydroperoxide, and $HO^{\bullet}$ is the hydroxyl radical.

This mechanism occurs in both thermal- and photo-oxidation of almost all polymers [36]; however, the initiation steps differ in each case:

i) In thermal degradation, initiation results from the thermal dissociation of chemical bonds in macromolecules;

ii) In photodegradation, initiation results from photodissociation of chemical bonds (from the singlet or triplet excited states) in a macromolecule.

The carbonyl groups in the chain are formed mainly by the chain branching reaction in which polymer oxy radicals can be a source of formation of in-chain ketone groups [37]:

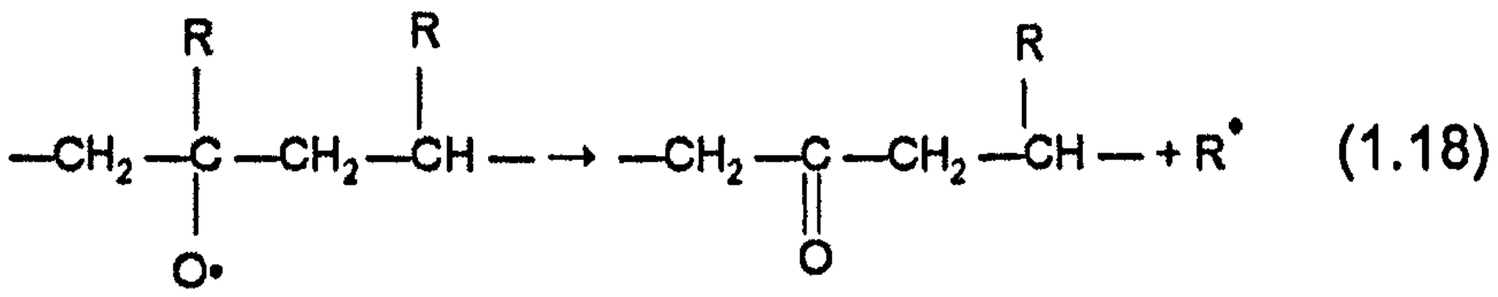

(1.18)

Chain scission in polymeric alkoxy radicals ($PO^{\bullet}$) has generally been attributed to the β-scission reaction, which results in fragmentation of the polymer chain with formation of end carbonyl (or aldehyde) groups and end-polymer alkyl radicals.

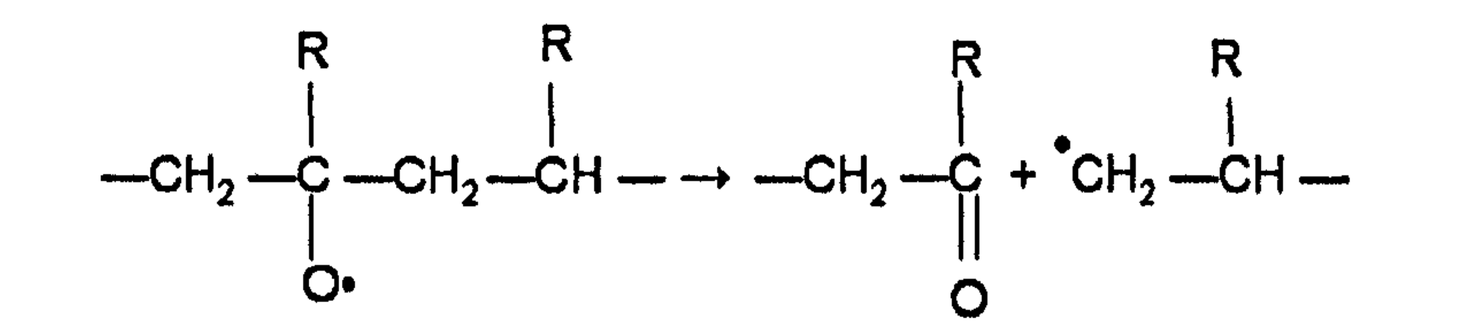

(1.19)

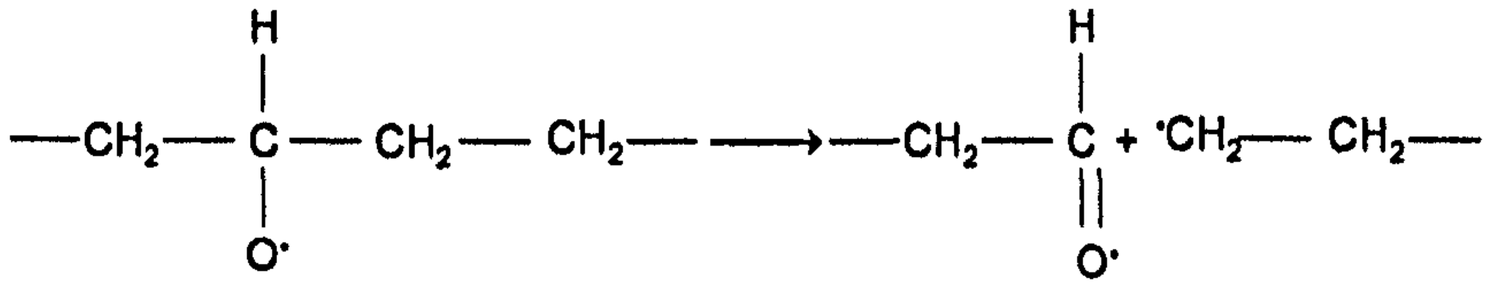

(1.20)

The CO_2 molecules are formed mainly from carboxylic esters which photodegrade by undergoing reactions similar to the Norrish I and Norrish II type reactions of ketones, as shown in Figure 1-4.

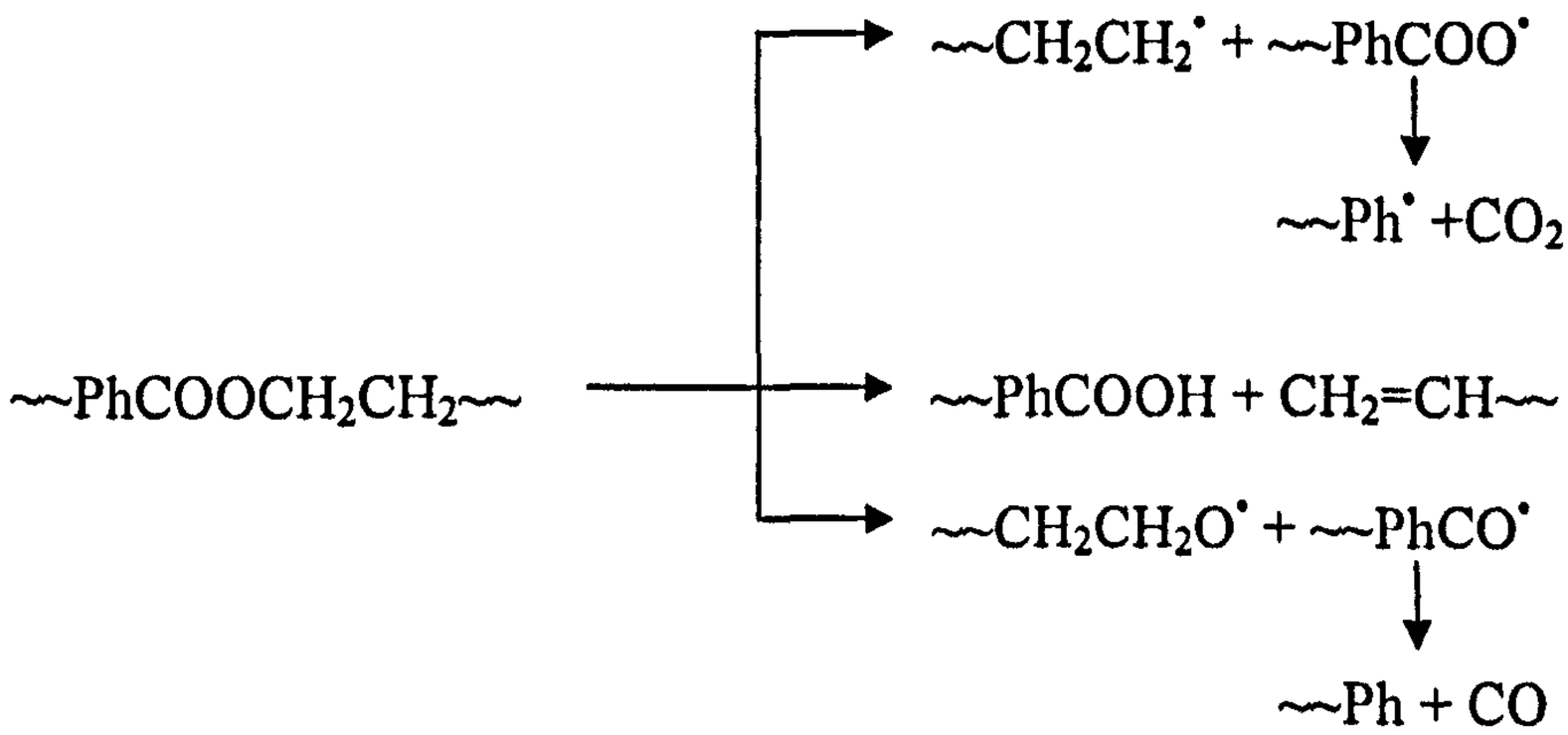

Figure 1-4 Ester photolysis reactions [37].

The incorporation of titanium dioxide pigments can have beneficial effect on the durability of the system because of their ability to absorb the radiation and, consequently, protect the polymer – *i.e.* to reduce the extent of the initiation reaction (1.8).

1.3.3 Photodegradation of Unpigmented Polyethylene (PE)

Polyethylene is one of the most widely studied polymers, particularly concerning its degradation under environmental conditions [38-54]. It has a very simple structure, the simplest one of commercial polymers. A molecule of polyethylene is nothing more than a long chain of carbon atoms, with two hydrogen atoms attached to each carbon atom.

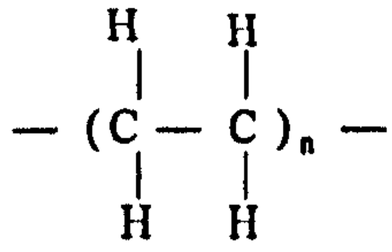

Figure 1-5 Chemical structure of PE.

Sunlight photolytic degradation and/or photooxidation can only occur when the polymer contains chromophores that absorb wavelengths of the solar spectrum which are present at the earth's surface (> 290 nm) [55]. Table 1-3 lists the longest-wavelength absorption bands of some typical organic chromophores [56]. These wavelengths have sufficient energy to cause a dissociative (cleavage) process resulting in degradation.

Table 1-3 Some Chromophores correspond to actual long-wavelength Absorption

Chromophore	Wavelength λmax (nm)	ε_{max}	Transition type
C~C	<180	1000	σ, σ^*
C-H	<180	1000	σ, σ^*
C=C	180	10,000	π, π^*
C=C-C=C	220	20,000	π, π^*
C=O	280	20	n, π^*
C=C-C=O	350	200	n, π^*
C=C=C=O	220	30	π, π^*
N=N	350	100	n, π^*

Therefore, on the basis of their chemical structure, conventional saturated polymers in a pure form are not expected to photodegrade [57]. However, although pure polyethylene does not contain functional groups capable of absorbing UV radiation, polyethylene is known to absorb UV radiation and photodegrade. There must be some chromophores existing in polyethylene. Chromophores [36, 58] that can absorb sunlight are:

1) Internal in-chain impurities such as hydroperoxides or carbonyls formed during storage, processing or weathering.

2) Extrinsic impurities as polymerisation catalyst residues, additives (*e.g.* pigments, dyes or antioxidants), pollutants from the atmosphere or metal traces from processing equipment.

3) Parts of the molecular structure of the polymer.

4) Charge transfer complexes between oxygen and the polymer chain[59].

The photodegradation of low density polyethylene (LDPE) has been studied from a mechanistic point of view. It was shown that, similar to other hydrocarbon polymers, it follows the generally accepted oxidation reaction scheme: formation of free radicals, reaction of these with oxygen producing peroxy radicals, cleavage of the O-O bond of the hydroperoxides and formation of carbonyl containing groups [57].

Depending on the history and form of the polymer, different kinetics for these general reactions are observed, but the mechanism has been shown to be always the same. In the case of the photo-degradation of LDPE films one aspect that has received particular attention is the relationship between initiation and the depth of penetration of light [38, 60-62]. In general, most authors assume that the photochemical process is a surface phenomenon [63, 64]. This assumption is based on the distribution of the light intensity in the polymer film if not pigmented, oxygen starvation is more important; it falls very strongly from the surface to the bulk.

Giesse and De Paoli [38] have studied the kinetics of the photodegradation of films of LDPE of different thickness by means of transmission and Attenuated Total Reflectance (ATR) infrared spectrophotometry. From these experiments they have related the kinetics of formation of carbonyl containing photoproducts in the bulk of the films with the kinetics in the upper surface layers of the same films. Their results indicate that at the very beginning of the reaction the concentration of oxidation product is higher in bulk of the films than on the upper surface layer penetrated by the infrared beam. With increase of irradiation time the situation is reversed, with an increase of oxidation product concentration on the surface. These results are in contrast to the generally accepted idea that photo-oxidation phenomena are restricted to a thin surface layer of polymers.

1.3.4 Photodegradation of Unpigmented Poly (vinyl chloride) (PVC)

PVC is another representative commercial polymer that has provided a variety of products. According to the structure of the repeating units of PVC, $[-CH_2-CHCl-]_n$, pure PVC is not expected to absorb light of wavelength above 220 nm. However in practice, it is very sensitive to near-ultraviolet light, and photodegradation of PVC takes place on exposure to most light sources, including solar radiation. This is explained by assuming that the photodegradation of PVC is a sensitised process, initiated by trace quantities of extraneous impurities and anomalous structures in PVC introduced as a result of the processing. Extrusion or injection-moulding procedures involve subjecting polymers to both heat and mechanical stresses with consequent scission of the polymer chain to give macroalkyl radicals, which are effective

initiators for thermal oxidation. A mechanism regarding the mechano-oxidation of PVC during processing to give centres capable of absorbing UV to induce further degradation is illustrated in Figure 1-6.

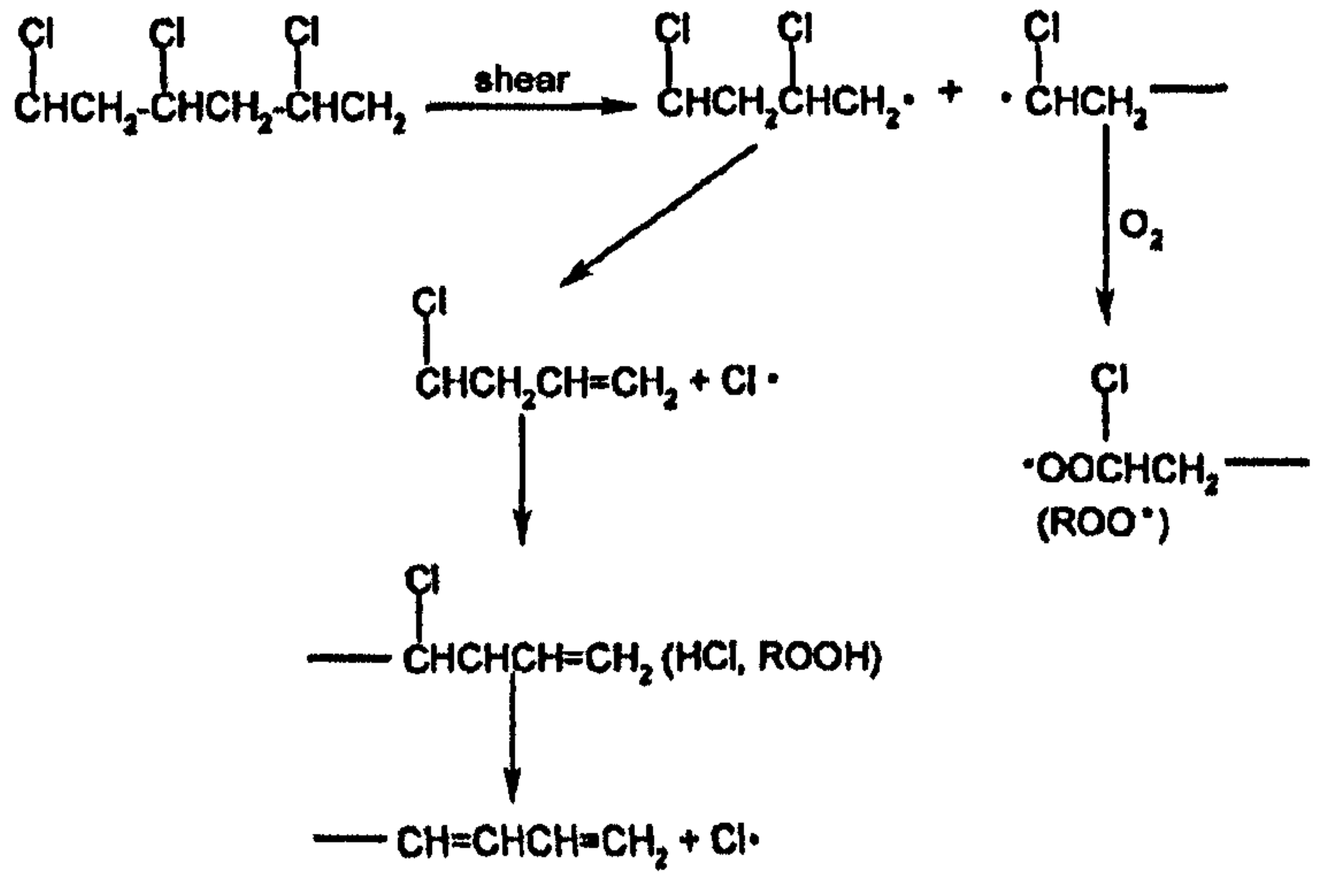

Figure 1-6 Mechano-oxidation of poly(vinyl chloride) during processing [65, 7].

The photo-oxidation of PVC is initiated by $Cl^{\bullet}$ atoms, which formed during generation of polyenes of increasing length by successive photochemical excitation. The first step involves absorption of light by a chromophoric defect identified as a α-chlorinated diene. The polymer is subsequently photo-oxidised and discoloration is then caused by residual polyenes. The mechanism of the photodegradation of PVC is shown in Figure 1-7.

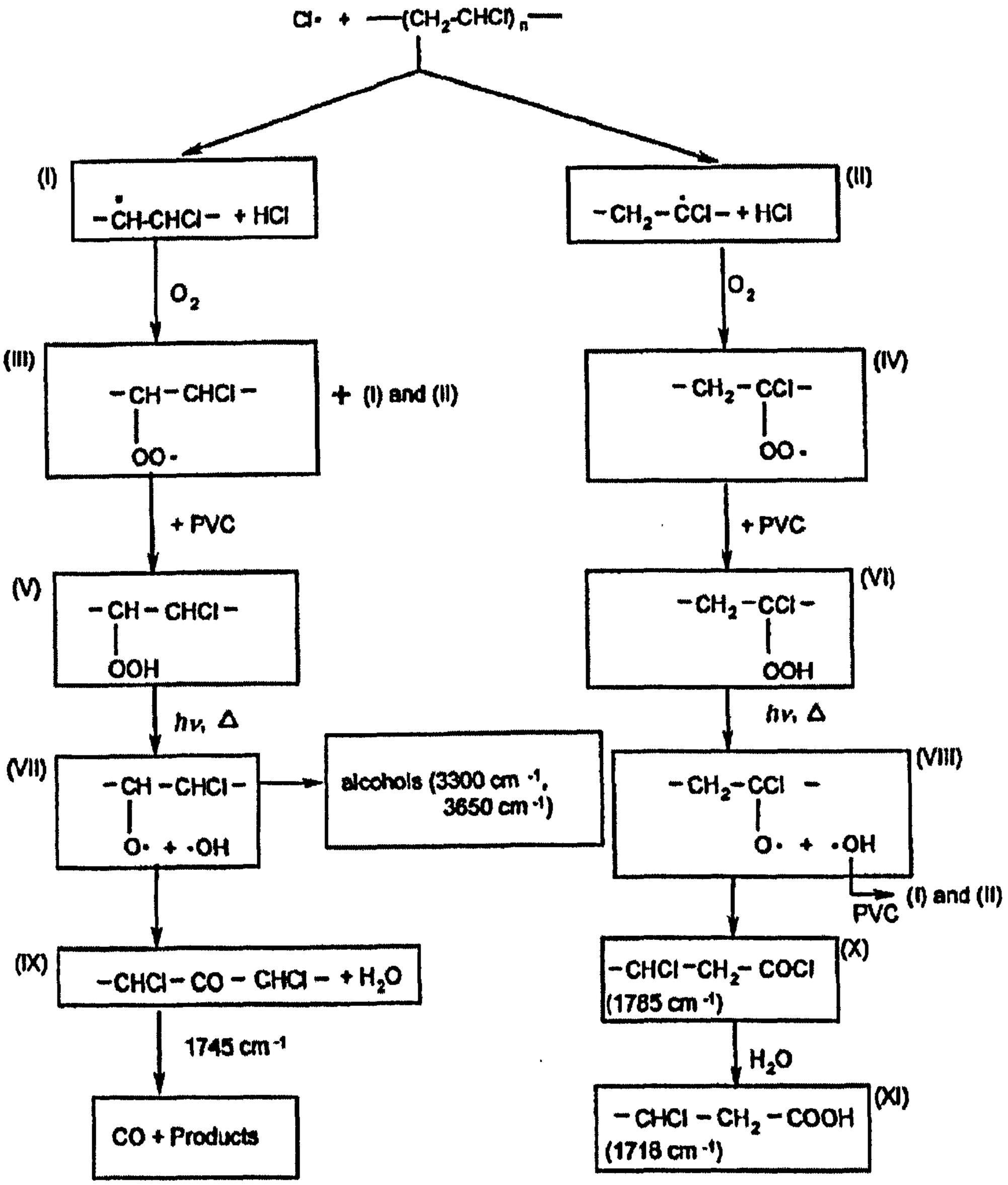

Figure 1-7 Mechanism of photodegradation of PVC [66].

1.4 PHOTOCATALYSIS AND TITANIUM DIOXIDE

In recent decades, TiO_2 has replaced all other materials as a source of light scattering in paints, plastics and inks because appropriately sized TiO_2 particles provide more light scattering and at lower cost than other materials. But TiO_2 is also a photocatalyst [67-69], although the work represented in this thesis deals with its use as a polymer pigment. Increasing applications have been found for TiO_2 over recent years as for example: a heterogeneous catalyst for the oxidation of gas and liquid phase organic

pollutants [70-74] and as a photosensitizer for organic photosynthetic processes [75, 76]. Before dealing with the mechanism of TiO_2 photocatalysis, some basic principles of semiconductor theory are discussed below. Initial interest in semiconductor photoelectrocatalysis was prompted by the discovery by Fujishima and Honda [77] in which, is a cell comprising an illuminated n-TiO_2 photoanode and a Pt (under a positive bias) cathode, oxygen could be evolved from water at the anode and simultaneously hydrogen was produced at the cathode.

1.4.1 Band Theory

The energy levels of a semiconductor are generally considered in terms of band theory [78]; in a solid the electronic valence orbitals overlap to form a band. As a result of the large numbers of such orbitals, the band shows a correspondingly large number of closely-spaced orbitals covering a finite width of energy. If the topmost populated band is half full, the solid is a metal; it requires very little thermal energy to excite electrons from the filled part of the band into the empty orbitals, where they are free to move and give rise to metallic electronic conductivity, see Figure 1-8 (a). If the topmost occupied band is full, and there is a large energy gap between it and the lowest unoccupied band, then the material is an insulator, see Figure 1-8 (b). If, however, the band gap between the topmost filled band and lowest unoccupied band is not too large, see Figure 1-8 (c), such that electrons can be excited from the filled ('Valence') band to the unoccupied ('Conduction') band, the material is a semiconductor.

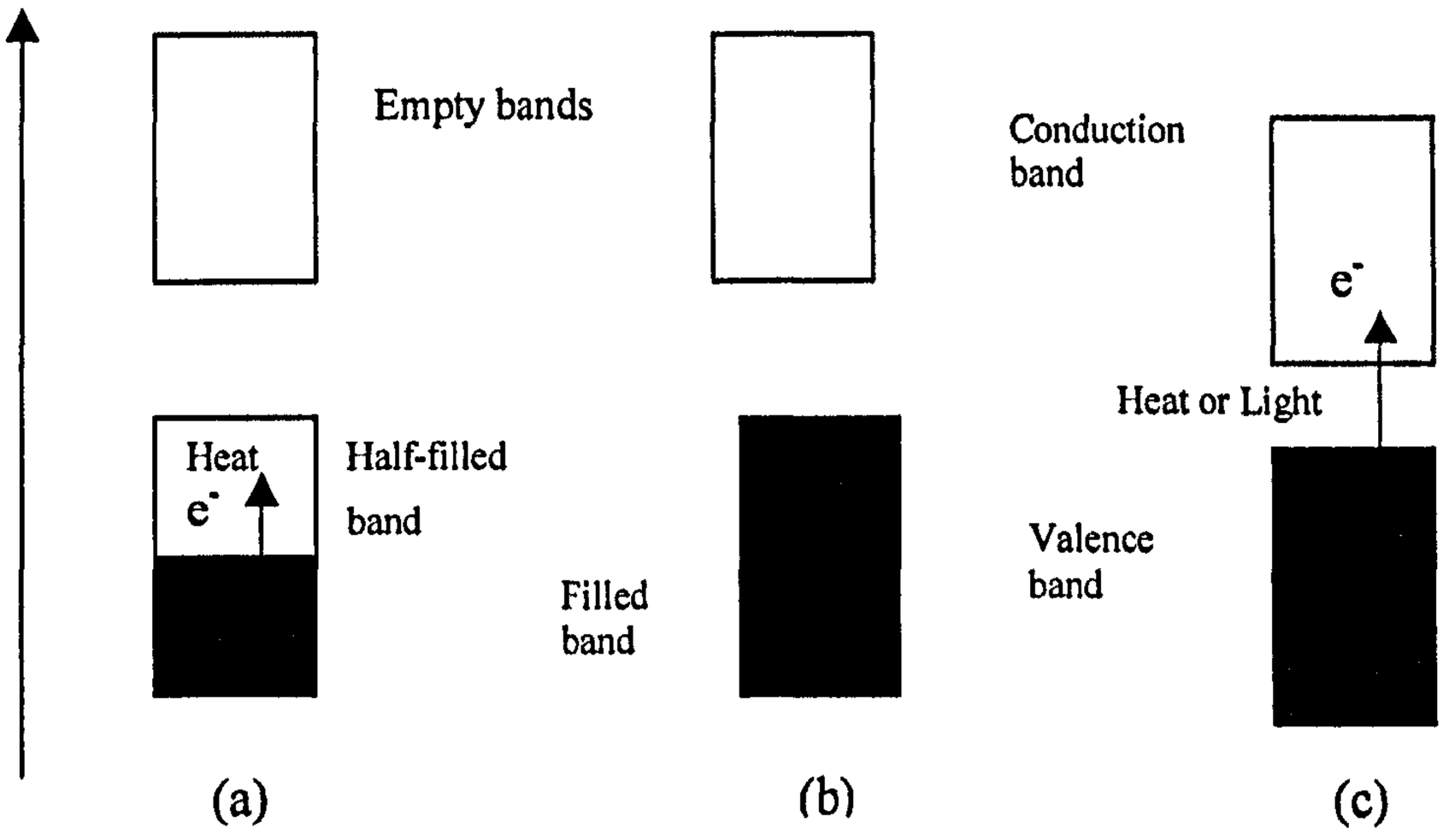

Figure 1-8 Schematic representation of the occupied an unoccupied bands of (a) metal, (b) an insulator and (c) a semiconductor [21].

In general, solids with bandgap energies less than ~ 3 eV are considered to be semiconductors. In a semiconductor the highest occupied and the lowest empty energy bands are particularly important. Semiconductors can be made conductive either by putting extra electrons into the conduction band or by removing electrons from the valence band. Removal of an electron from the valence band creates a positively charged vacancy called a hole. The hole can be regarded as a mobile entity because annihilation of a hole by a nearby electron effectively moves the hole in space. The electrical current can be carried by either electrons in the conduction band or holes in the valence band, or by both types of charge carriers. Mobile charge carriers can be generated by three different mechanisms, thermal excitation, photoexcitation, and doping. If the bandgap energy is sufficiently small (less than half an electron volt) thermal excitation can promote an electron from the valence band to the conduction band. In a similar manner, an electron can be promoted from the valence band to the conduction band upon the absorption of a photon of light, photoexcitation, provided that hv > Ebg mention by as band gap. The third mechanism of generating mobile charge carriers is doping. At room temperature, and

particularly in the case of TiO_2, a wide band gap semiconductor ($E_{bg} > 3.0$ eV), only the last two methods of electron excitation are appropriate, and these will be discussed in greater detail below.

Doping is used to impart conductivity and this is achieved by introducing new energy levels in the band gap by altering the crystal lattice. Two types of doping can be distinguished. For n-type doping, occupied donor levels are created very near the conduction band edge. In this case current is carried mainly by negative charge carriers. Likewise, p-type doping corresponds to the formation of empty acceptor levels near the valence band, creating positive charge carriers. In this particular case current is carried mainly by positive charge carriers.

Alteration in the TiO_2 lattice results in a loss of stoichiometry giving TiO_{2-x} and can be achieved by heating a semiconductor in a reducing atmosphere, *e.g.* hydrogen atmosphere [79]. This reductive treatment has been identified as giving rise to two types of donor sites; oxygen vacancies and titanium interstitials. Oxygen vacancies (V_0) can donate up to two electrons to the conduction band as follows:

Singly ionised vacancy: $V_o \rightarrow V_o^{\bullet} + e^{-}$ (1.21)

Doubly ionised vacancy: $V_o \rightarrow V_o^{\bullet\bullet} + 2e^{-}$ (1.22)

However, titanium interstitials can donate up to four electrons to the conduction band, but only the first two ionisation energies are expected to represent shallow donor levels as the resulting configuration should be stable [80]:

(quadruply ionised Ti interstitial) $(Ti)_i \rightarrow (Ti)^{\bullet\bullet\bullet\bullet} + 4e^{-}$ (1.23)

These energy levels are located just beneath the conduction band and electron promotion into this band is facilitated by thermal excitation, see Figure 1-9.

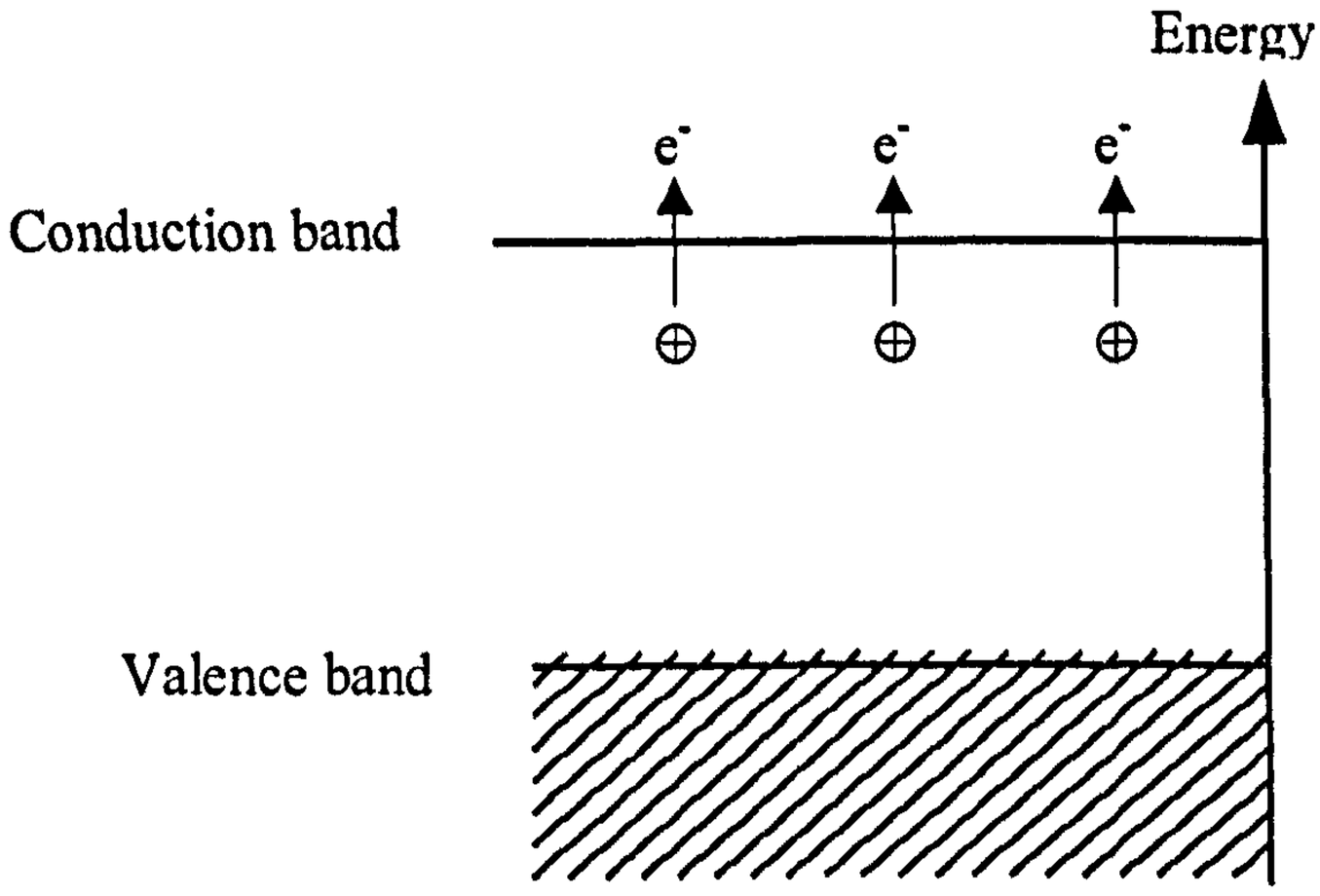

Figure 1-9 Charge carrier generation by n-type doping.

Thus, it can be said that doped TiO_2 is an n-type semiconductor because its conductivity derives from the fact that current is carried primarily by electrons (negatively charged, the majority carrier) in the conduction band.

The band gap energy dictates the light absorption characteristics of the semiconductor. Photoexcitation is achieved by irradiating a semiconductor with light of energy greater than the band gap energy. If a photon of light of energy greater than the band gap energy is absorbed it can excite an electron (e^-) from the valence band to the conduction band leaving behind a hole (h^+), see Figure 1-10. Although rapid recombination of electron and hole generally occurs (on the nanosecond time scale) separation of the electron-hole pair (e^- - h^+) can be effected by means of diffusion or the application of an electric field.

In the case of the anatase form of TiO_2, the wavelength of light must be less than ~ 385 nm and for rutile it must be less than ~ 405 nm, *i.e.* UV light. The absorption of a photon with the appropriate energy results in the excitation of an electron from the valence band to the conduction band leaving behind a positive charge, hole, which is mobile (Figure 1-10).

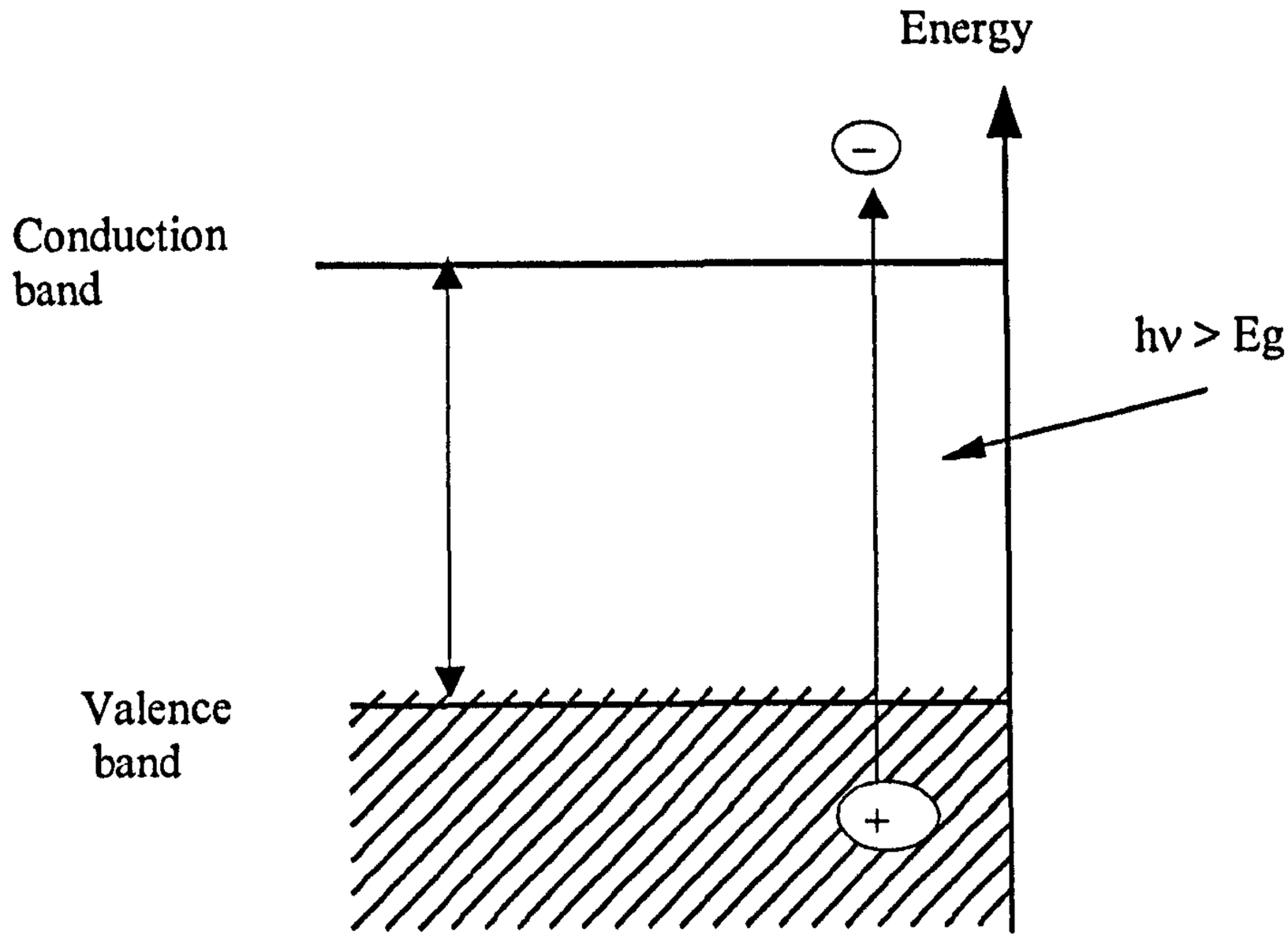

Figure 1-10 Charge carrier generation by photoexcitation of an n-type semiconductor.

1.4.2 Titanium Dioxide as a photocatalyst

The photocatalyst, which has received most attention and has been most well studied [81-93], is titanium dioxide owing to its high photocatalytic activity, biological and chemical inertness and insolubility in aqueous solution, including strong acids and alkalis [94-97]. The activity of the anatase form of TiO_2 has been frequently reported as being much greater than that of rutile [98]. There are a number of explanations for the greater photoactivity of the anatase phase, and these may be summarised as follows:

The band gaps are 3.23 eV and 3.03 eV for anatase and rutile, respectively [15]. The valence band edges of the anatase and rutile are found to be similar. The conduction band edges of the anatase are 0.2 eV more positive than that of the rutile form. The higher energy of the band edge position of anatase results in the electrons being more able to reduce reactants *e.g.* O_2 than in rutile [99].

Perhaps, because fewer electrons are trapped by O_2 the surface recombination rate associated with rutile is higher than that of anatase, resulting in fewer holes being available for hydroxyl radical generation [100]. This has important implications in pigment systems as a reduction in the number of photogenerated holes available for

hydroxyl radical generation leads to a decrease in the photocatalytic degradation of the organic substance. The higher rate is thought to be due to the fact that rutile has a lower capacity for oxygen adsorption, resulting in the reduction of electron transfer, leading to the build up of photogenerated electrons on the TiO_2 particle to increase the rate of recombination.

The final important difference between the anatase and rutile forms is the extent and nature of the surface hydroxylation. There is an abundance of experimental evidence, provided by infrared spectroscopy [101, 102], X-ray photoelectron spectroscopy (XPS) [103] and adsorption studies [104], which show that the exposure of the TiO_2 to water vapour or aqueous solution results in the surface undergoing hydroxylation. The surface hydroxylation process is believed to result from the chemisorption of water molecules on co-ordinately unsaturated Ti^{4+} surface. The chemisorption of water molecules on surface Ti^{4+} ions is expected, as it would fill vacant co-ordination sites, with proton transfer occurring with neighbouring oxide ions in order to obtain better charge neutralisation [105]. The proton transfer to the O^{2-} site results in the formation of two kinds of surface OH groups; those bound to one Ti^{4+} and those bound to two Ti^{4+} ions. The doubly-bonded OH groups are strongly polarised by the cations, resulting in acidic character due to the loosening of the hydrogen bond. In contrast to this, the singly-bound OH groups are generally basic in character, and this amphoteric behaviour is observed for both anatase and rutile [104, 106]. Surface hydroxylation of TiO_2 has been shown, by adsorption isotherms, to occur on not more than half of the surface of anatase and rutile and in addition chemisorbed water is bound directly to the surface Ti^{4+} ions. It has also been reported that further water has been found to physisorb on top of the hydroxyl groups by hydrogen bonding [103].

The extent and type of surface hydroxylation has been observed to depend on the geometry of the exposed crystal, with the (101) and (100) faces of rutile not permitting the dissociative chemisorption of water. The above differences in hydroxylation for the two crystal forms of TiO_2 are therefore important in explaining the differences in photocatalytic activity due to the reaction of the photogenerated holes with the adsorbed water or surface hydroxyl groups in order to form the primary oxidant $OH^{\bullet}$.

1.5 PHOTOCATALYSIS, DURABILITY AND WEATHERING

UV light, particularly in the wavelength range of 300–350 nm, in conjunction with other influencing factors of weather (oxygen, ozone, water, and industrial pollution), can create havoc on plastics. Since pigmentary TiO_2 absorbs much of the UV light it comes into contact with, one of the more useful properties it can impart in plastics is durability. Therefore many outdoor plastics contain high levels of TiO_2 to aid in their protection.

When TiO_2 is exposed to UV light, electrons from the valence band are excited to the conduction band and positive holes in its crystal lattice are created. Free electrons and holes can reach the crystal surface and react.

$$\text{holes} + OH^- \Rightarrow OH^\bullet \qquad (1.24)$$

$$\text{electrons} + O_2 \Rightarrow O_2^\bullet \qquad (1.25)$$

$$O_2^\bullet + H_2O \Rightarrow HO_2^\bullet + OH^- \qquad (1.26)$$

Thus by absorbing UV radiation, TiO_2 prevents direct photochemical attack. However, by absorbing UV radiation, TiO_2 also generates free radicals, which can oxidize the plastic.

By surface treatment one can greatly lessen the generation of free radicals, possible reasons for this are:

a) The formation of a barrier which reduces oxygen diffusion to the TiO_2 surface or lessens radical release from this surface or

b) Providing hole and electron recombination sites or hydroxy radical recombination sites.

The presence of alumina, zirconia, and silica all can work by forming a physical barrier to oxygen.

1.6 ROLE OF WATER AND OXYGEN IN PHOTOCATALYSIS

Earlier work by this group highlighted the influence of a moist oxygen atmosphere in the photo-oxidation of pigmented and unpigmented paint films causing a difference in durability [107, 108]. This work emphasised the importance of maintaining a consistent atmosphere in the gas cell in order to obtain reproducible results, and experimental methods were developed to achieve this.

The significant role of water in weather-induced degradation of plastics lies in the combination of its unique physical properties with its chemical reactivity. Chemical processes involving water include hydrolysis of the polymer, reaction with the polymer in the excited state, or the hydrolysis of intermediates. Some polymeric materials exposed to high humidity degrade at an accelerated rate due to the "plasticizing" action of sorbed water, which enhances the accessibility of atmospheric oxygen into the materials. Water can also cause leaching of additives, which may include pigments and stabilizers within the matrix [57].

Chalking of plastics surfaces containing TiO_2 pigment is a result of degradation of binder or polymer under the influence of the weather, where water takes part in the photochemical reaction. More specifically, as outlined below (1.6.1), water plays a key role in the generation of the catalytically active $OH^{\bullet}$ radicals at the surface of TiO_2. Another important component of the chemical environment that influences polymers is oxygen. Oxygen is involved in a number of photochemical degradation (PD) and photocatalytic degradation (PCD) reactions that result in degradation of the materials. The mechanisms of photodegradation are different for PD and PCD processes. For TiO_2-pigmented polyethylene, the formation of an electron-hole pair on the pigment surface in the presence of oxygen and water can produce reactive species, which can eventually cause oxidation of the polymer [43, 109].

1.6.1 $OH^{\bullet}$ as the Primary Oxidant

It is assumed that the hydroxyl radical ($OH^{\bullet}$) is the primary oxidant in TiO_2 photocatalysis [110-112]. The assumption is based on the fact that the TiO_2 surface readily hydroxylates. There is also widespread agreement that, after excitation with

supraband gap light (1.27), the primary oxidant ($OH^{\bullet}$) is produced by reaction of the photogenerated hole (h^+) with adsorbed water (1.28) or hydroxyl group (1.29) on the TiO_2 surface.

$$TiO_2 + h\nu \rightarrow TiO_2 (h^+ + e^-) \qquad (1.27)$$

$h\nu > E_{bg}$ (3.23 eV Anatase, 3.02 eV Rutile)

$$TiO_2 (h^+) + H_2O_{ads} \rightarrow OH^{\bullet} + H^+ \qquad (1.28)$$

$$TiO_2 (h^+) + OH_{ads}^- \rightarrow OH^{\bullet} \qquad (1.29)$$

Evidence to support the production of the hydroxyl radical is found from numerous electron paramagnetic resonance (EPR/ESR) [113-116] spectroscopic studies. The importance of hydroxyl radical formation has been demonstrated by a kinetic isotope study on the photocatalysed oxidation of isopropanol in TiO_2 slurries by Cunningham and Srijaranai [117]. They reported that substitution of deuterium for hydrogen on the organic reactant had no effect on the observed initial rate of reaction; however, replacement of H_2O with D_2O led to a decrease in the rate of reaction. The results imply that the formation of $OH^{\bullet}$ ($OD^{\bullet}$) through reaction involving the solvent is the rate limiting step.

The primary role of the hydroxyl radical is believed to be the oxidation of the organic substance; however, formation of hydrogen peroxide *via* a termination reaction has also been reported (1.30).

$$2OH^{\bullet} \rightarrow H_2O_2 \qquad (1.30)$$

The hydrogen peroxide can undergo decomposition to form further species that are useful in the oxidative process, *i.e.* HO_2^- and H^+ (1.31):

$$H_2O_2 \rightarrow HO_2^{\bullet -} + H^+ \qquad (1.31)$$

1.6.2 Effects of Oxygen

The absence of oxygen has been found to have a dramatic effect on the rates and efficiencies of photocatalytic degradation. Barbeni *et al* have pointed out that both O_2 and H_2O are essential species in the photomineralization of 4-chlorophenol in the presence of irradiated TiO_2[118]; no photodegradation occurs in the absence of either O_2 or H_2O, or both[118]. Adsorbed oxygen traps e^- and thereby delays electron-hole recombination[112]. The principle is that molecular oxygen suppresses electron-hole recombination through the removal of photogenerated electrons in the conduction band by adsorbed oxygen, generating the superoxide species ($O_2^{\bullet -}$) hence increases the rate of photodegradation[119, 111, 15].

$$TiO_2(e^-) + O_2 \rightarrow O_2^{\bullet -} \qquad (1.32)$$

The superoxide species ($O_2^{\bullet -}$) is a highly active oxidising species and can attack either the organic molecules or adsorbed intermediates, or after protonation, can generate hydrogen peroxide(1.33) [120].

$$2HO_2^{\bullet -} \rightarrow H_2O_2 + O_2 \qquad (1.33)$$

Hydrogen peroxide has been found to play an important role in increasing the rate of photo-oxidation [121]. Studies carried out in the presence of hydrogen peroxide have shown a dramatic increase in the rate of photodegradation. This is believed to be because hydrogen peroxide is a better electron acceptor than oxygen and is more effective at preventing the accumulation of the electrons at the surface on the titanium dioxide particles, thus suppressing the electron-hole recombination reaction further [121, 97]. The addition of hydrogen peroxide has been shown to enhance considerably the rate of photodegradation by the generation of additional hydroxyl radicals, most probably *via* the following reaction [119]:

$$TiO_2(e^-) + H_2O_2 \rightarrow TiO_2 + OH^- + OH^{\bullet} \qquad (1.34)$$

A number of other electron scavengers which have been shown to enhance the photocatalytic degradation rate at illuminated TiO_2. These include: methyl viologen, metal salts, halogenated electron acceptors [122], persulphate and iodate [123].

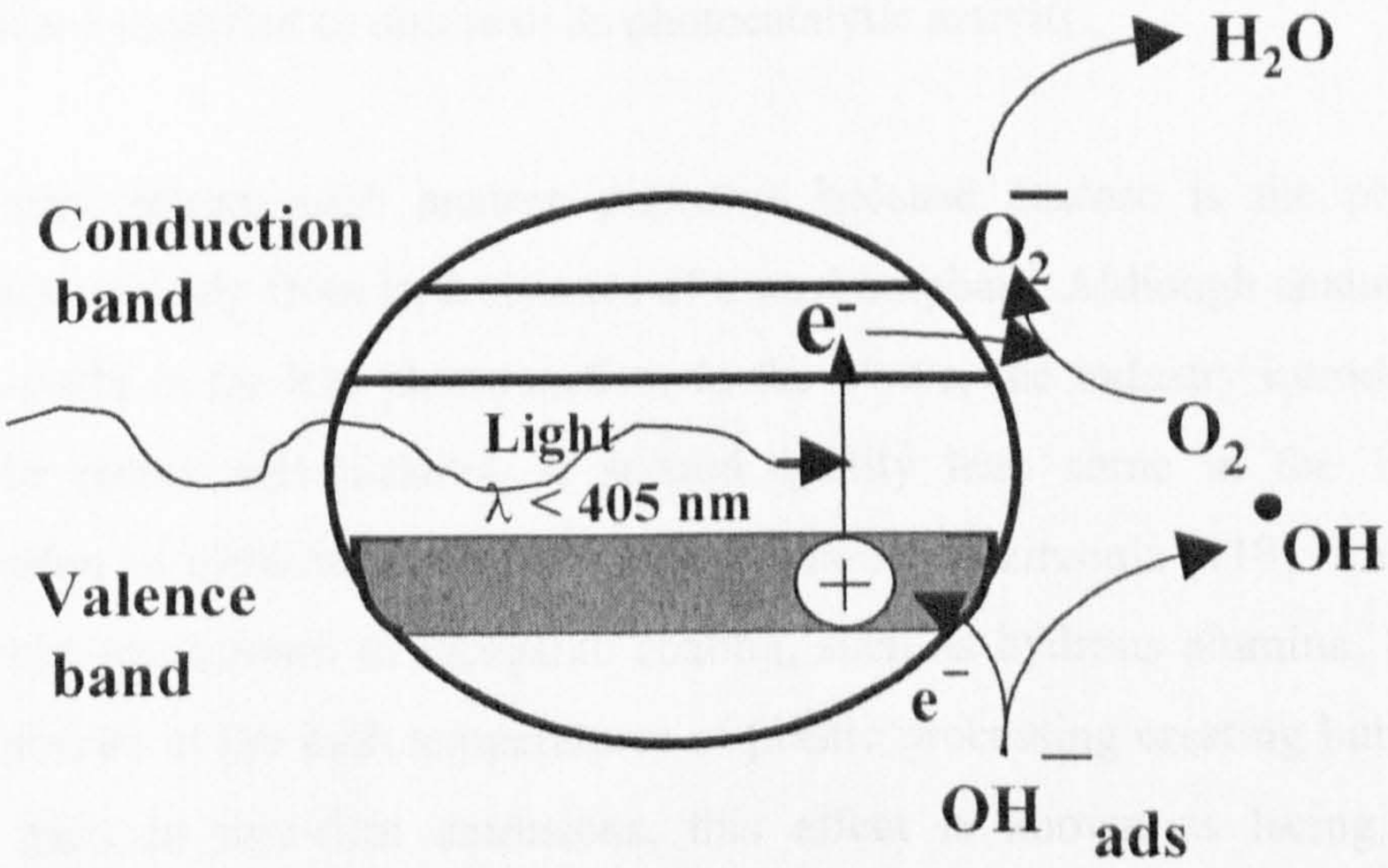

Figure 1-11 Schematic illustration of the common radical formation [15].

1.7 TIO_2 AS A PIGMENT IN POLYMER

Fillers are widely used in polymer materials to provide characteristics to suit a particular commercial application. Titanium dioxide has found especially polyethylene (PE), to give the familiar white plastic bags, and in poly (vinyl chloride) (PVC), as used in window profile, facia boards, *etc* [7]. Its presence affects the photodegradation of paints and polymers in two ways. Firstly, by absorbing incident UV, the titanium dioxide protects the polymer from direct photochemical reaction of the organic polymer. Secondly, a small portion of the absorbed UV leads to the generation of highly reactive hydroxyl radicals at the TiO_2 pigment surface, which catalyse polymer breakdown [124]. Titanium dioxide pigment is used to opacify plastic materials. Unpigmented plastic is translucent or transparent and therefore not aesthetically appealing. In some applications, TiO_2 is used to improve photostability.

The requirements for TiO_2 in plastic are good dispersability in a polymer system, and good heat stability. Plastic objects are usually much thicker than films. Hence, opacity can be achieved with less TiO_2. The vast amount of plastic produced, however, makes

the plastic industry a major user. In order to make use of the excellent optical properties of TiO_2 and use its high UV absorption characteristics to protect the organic resin (plastic), from direct photochemical oxidation without initiating the photocatalytic degradation of the plastic or binder, the TiO_2 used in plastic is usually rutile, surface modified to diminish its photocatalytic activity.

The industry started with anatase pigments because anatase is the product that crystallises naturally from hydrolysates of titanyl sulphate. Although anatase is easier to make, rutile is far less photoreactive. In the 1940s, the industry introduced rutile grades for paints and plastics. A second quality leap came in the 1960s with encapsulation of rutile in amorphous silica, alumina or zirconia [119]. It is desirable to minimize the amount of inorganic coating, such as hydrous alumina, because its water vaporises at the high temperatures of plastic processing creating bubbles in the finished part. In thin-film extrusions, this effect is known as lacing. Uncoated pigments for plastic are often treated with an organic polyol, silane or siloxane to enhance dispersibility and reduce water content [125-127].

Alternative approaches to reduce photocatalytic activity involve attempts to (a) recombine holes and electrons at the TiO_2 surface *via* semiconductor mechanisms and (b) prevent hydroxylation of the TiO_2 surface, *i.e.* interfere with reaction of the chalking sequence.

Day and Egerton have [13, 22, 128] used surface analytical methods to study the effects of TiO_2 surface coatings on photocatalytic activity.

1.8 PHOTODEGRADATION MECHANISMS IN POLYMERS PIGMENTED WITH TIO_2

As outlined above, the practical photodegradation of a pigmented system is a result of at least two separate processes (a) the direct homogeneous photochemical oxidation of

the organic medium and (b) the heterogeneous photo-catalytic oxidation caused by the titanium dioxide pigment. These two different processes have different mechanisms of reaction [107].

1.8.1 Photocatalytic Degradation Mechanism

Allen and Katami [129] suggest there are three mechanisms of the photosensitised oxidation of polymers by titanium dioxide and for that matter other white semiconducting pigments such as ZnO.

The formation of an oxygen radical anion by electron transfer from photoexcited TiO_2 to molecular oxygen is the first step. A recent modification of this scheme involves a process of ion-annihilation to form singlet oxygen, which then attacks any unsaturation in the polymer.

$$TiO_2 + O_2 \xrightarrow{h\nu} TiO_2^{+\bullet} + O_2^{-\bullet} \qquad (1.35)$$

$$TiO_2^{+\bullet} + O_2^{-\bullet} \longrightarrow TiO_2 + {}^1O_2 \text{ (ion-annihilation)} \qquad (1.36)$$

$$TiO_2^{+\bullet} + O_2^{-\bullet} + H_2O \longrightarrow TiO_2 + HO^{\bullet} + HO_2^{\bullet} \qquad (1.37)$$

$$2\,HO_2^{\bullet} \longrightarrow H_2O_2 + O_2 \qquad (1.38)$$

$$RCH = CHR + {}^1O_2 \longrightarrow RCH = C(OOH)\,R \qquad (1.39)$$

Formation of reactive hydroxyl radicals by electron transfer from water catalysed by photoexcited TiO_2. The Ti^{3+} ions are reoxidised back to Ti^{4+} ions to start the cycle over again.

$$H_2O \xrightarrow{(Ti02)h\nu} H^+ + e^- \text{ (aq)} + {}^{\bullet}OH \qquad (1.40)$$

$$[Ti^{4+}] + e^- \longrightarrow [Ti^{3+}] \qquad (1.41)$$

$$[Ti^{3+}] + O_2 \longrightarrow [Ti^{4+}] + O_2 \qquad (1.42)$$

Irradiation of TiO_2 creates an exciton (h^+) that reacts with the surface hydroxyl groups to form a hydroxyl radical. Oxygen anions are also produced and are adsorbed on the surface of the pigment particle. They produce active perhydroxyl radicals.

$$TiO_2 \xrightarrow{h\nu} e^- + h^+ \qquad (1.43)$$

$$OH^- + h^+ \longrightarrow HO^\bullet \qquad (1.44)$$

$$Ti^{4+} + e^- \longrightarrow Ti^{3+} \qquad (1.45)$$

$$Ti^{3+} + O_2 \longrightarrow [Ti^{4+}\text{--}O^{2-}] \text{ adsorbed} \qquad (1.46)$$

$$[Ti^{4+}\text{--}O^{2-}] \text{ adsorbed} + H_2O \longrightarrow Ti^{4+} + HO^- + HO_2^\bullet \qquad (1.47)$$

1.8.2 Practical Effects of the two Mechanisms

The practical weathering of a pigmented system is a result of at least two separate processes (a) the direct homogeneous photochemical oxidation of the organic medium and (b) the heterogeneous photo-catalytic oxidation caused by the titanium dioxide pigment. With the photochemical reaction, after weathering, the surface is degraded and pigment particles are left standing proud on the surface. This protrusion leads to an irregular surface on the film which has the visual effect of lowering the gloss. Because the pigment particles are acting in a protective capacity, they prevent the passage of ultra violet light and the area immediately below the pigment particles is screened. So during the early stages of weathering, the particles remain adhered to the film surface so that the onset of chalking is delayed [107, 130]. See Figure 1-12 (a).

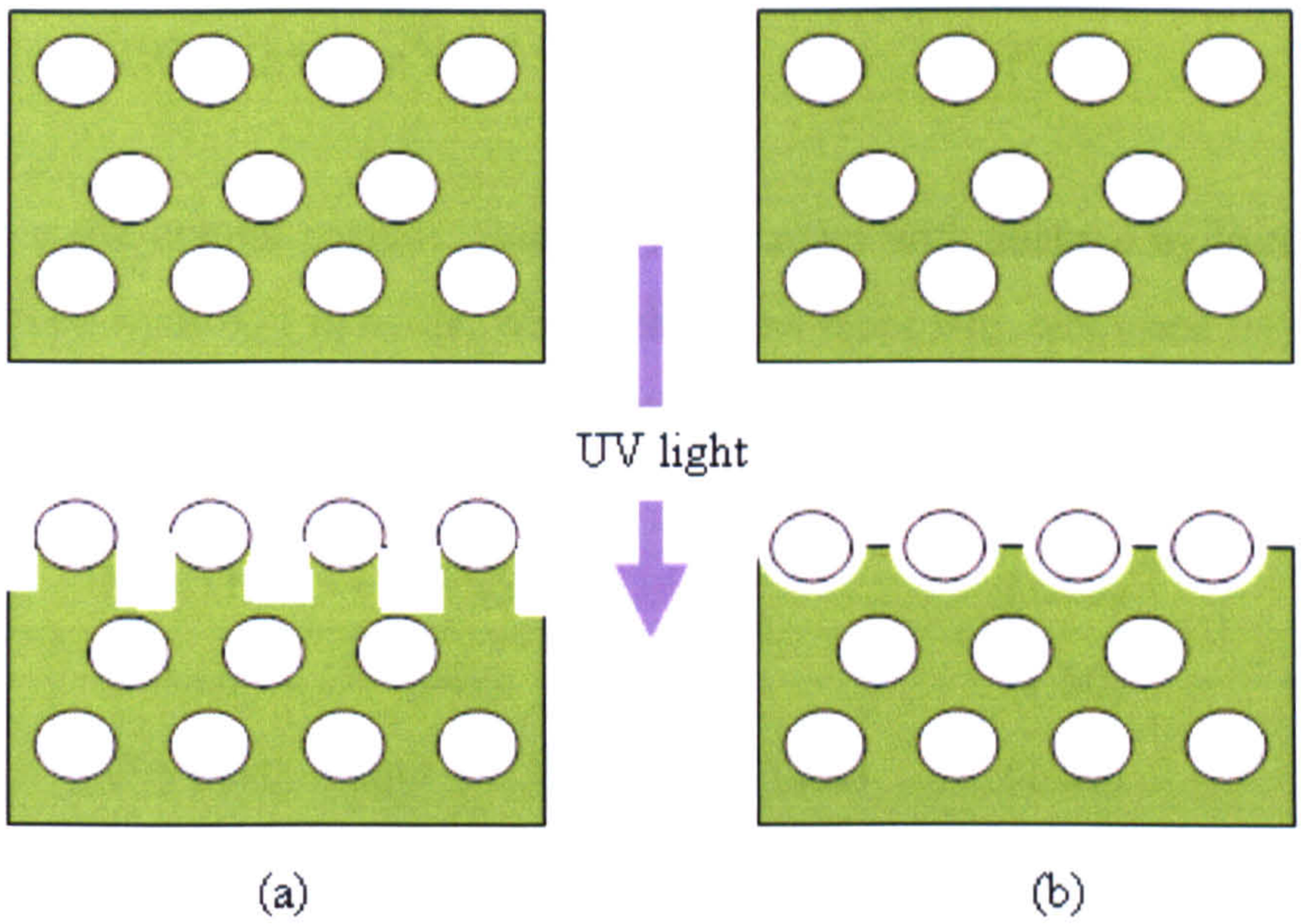

Figure 1-12 Schematic show the comparison of degradation mechanisms. (a) Photochemical; (b) Photocatalytic [130].

With photocatalytic degradation, which occurs at the surface of the pigment, the area around the particles is affected most, and because the surface remains fairly flat the gloss is not so pronounced and remains higher than with the other mechanism. However, because the photocatalytic mechanisms occur all the way round the particles, they are no longer adhered to the surface and consequently will show a degree of chalking earlier in the degradation process than with the photochemical mechanisms [130]. See Figure 1-12 (b).

Obviously, in most real systems, both mechanisms will operate. Which of them predominates, will depend on the choice of pigment and polymer and various other factors [130].

1.8.3 Square root relationship for TiO_2 photocatalytic degradation

According to Egerton and King [131], for the photocatalysed reaction, an $I^{0.5}$ (intensity of UV) dependence of reaction is exactly what would be predicted for a process in which recombination of the electrons and holes generated by UV radiation of titanium dioxide is the controlling step in the mechanism. This is explained as follows:

$$TiO_2 + hv \rightarrow e^- + h^+ \qquad (1.48)$$

On reaching the crystal surface, positive holes react with surface hydroxyl groups to form adsorbed hydroxyl radicals, whilst electrons react with adsorbed oxygen to form the O_2^- radical ion which then attacks a water molecule to form the $HO_2^\bullet$ radical.

$$h^+ + OH^-_s \rightarrow OH^\bullet (ads) \qquad (1.49)$$

$$e^- + O_2 \rightarrow O_2^- (ads) \qquad (1.50)$$

$$O^-_2 (ads) + H_2O \rightarrow OH^-_s + HO_2^\bullet (ads) \qquad (1.51)$$

Either the hydroxyl, $OH^\bullet$, or perhydroxy, $HO^\bullet_2$, radical may initiate breakdown of the organic medium, but it is likely that only one of the processes (1.49) and (1.50) is rate determining. The process involving the other radical completes the reaction and preserves overall charge neutrality. In the treatment that follows, sequence (1.49) is assumed to be rate determining but this choice does not affect the conclusions since a completely analogous set of equations leads from sequence (1.50). In the case of oxidation of anatase TiO_2 pigmented polyethylene film to final production of CO_2, then

$$\text{Rate of } CO_2 \text{ formation} = k_3 h = r \qquad (1.52)$$

where h is the hole concentration, and in the interior of the crystal

$$\text{Rate of hole formation} = k_1 I \qquad (1.52)$$

and

$$\text{Rate of } e^- - h^+ \text{ recombination} = k_2 h^2 \qquad (1.53)$$

where the simplifying assumption that h = e is made.

The steady state concentration of holes may be deduced by balancing their rate of formation against their rate of removal.

Thus

$$dh/dt = 0 = k_1 I - k_2 h^2 - k_3 h \qquad (1.54)$$

When I is large a large number of holes and electrons will be generated hence

$$k_2 h^2 >> k_3 h$$

$$\therefore \quad k_1 I \approx k_2 h^2$$

$$i.e. \quad h \approx (k_1 I / k_2)^{0.5} \qquad (1.55)$$

and $r = k_3h = (k_3^2k_1/k_2)^{0.5}I^{0.5} = KI^{0.5}$ (1.56)

It is that under conditions of high recombination the rate of oxidation depends on the square root of light intensity.

1.9 TEST METHOD FOR DURABILITY OF POLYMERS

1.9.1 A short review of relevant methods

In order to improve upon any given system there needs to be some way of evaluation current performance, a way of benchmarking a product against others and being able to give a definitive answer as to which performs the best. The ideal test would be quick to perform, and have a correlated performance with real world situations. Many factors (heat, radiation, humidity, atmospheric contaminants, oxygen content *etc*) affect degradation of polymer during outdoor exposure. None of these factors are constant in any one location, and weather conditions vary widely with location. To attain maximum accuracy in predicting the useful life of an outdoor plastic, all components of the anticipated exposure environment must be considered [57].

An ideal method of testing polymer products durability would be to expose them to that climate to which the material will be exposed during subsequent use [132]. One result of the world's increasing economic integration is that it is often impossible for producers to know where their materials will be used. In this case, it is important to know how the material will react to extreme climates. In the course of time, Florida has come to be considered as a reference climate owing to its moist, warm weather, followed by Arizona, with its hot, dry climate [14, 133].

There are problems associated with the use of outdoor exposure to the weather for the evaluation of the outdoor durability of polymer materials [14]. It is difficult to extrapolate outdoor exposure results from one location or time to another due to the variability of climatic condition. It is not convenient and economic to wait years for the results of outdoor weathering because of competition and market demand. In order to improve upon any given system there needs to be some methods to evaluate current performance, to occupy the market with own product against others and being able to give a definitive answer as to which performs the best. The ideal test would be quick

and easy to perform, and have a correlated performance with real world situations. There is a need for accelerated weathering in the laboratory. This is intended to identify and measure the same changes in the properties of polymeric material that would occur during the normal service life of these materials. This is a demanding goal to aim at, since apart from the desired acceleration of the aging processes that do occur naturally, accelerated time testing generally poses the danger of initiating degradation processes other than those occurring in general practice, or, by the same token, changes occurring outdoors may not take place during accelerated weathering [133].

It is clear that there is a need for a reliable fast test which could determine polymer durability in significantly shorter time than current methods and which would obviate the necessity to send panels to Florida or Arizona for natural weathering thus saving both time and money. There are two general ways to accelerate durability testing [133]:

i.) Use higher intensity or shorter wavelength radiation to simulate more extreme conditions than those expected during the service life of the product. The advantage of these techniques is that gloss loss and colour retention characteristics can be acquired in times of 1-2 months. However, for such accelerated exposure to provide data which can be extrapolated to long times and which will correlate with natural exposure results, there must be no change in either the relative rates of degradation processes occurring or the type of degradation chemistry. Unfortunately these methods run the risk of producing a poor correlation between accelerated and natural exposure data. The use of artificially high UV intensities to increase the reaction rate can provide misleading results because it also alters the relative rates of both parallel and sequential reactions [131].

ii.) The second method is using more sensitive techniques to evaluate the degradation process. Whilst it is recognized that it is possible for a polymer to fail due solely to physical effects, in general before the physical

properties change the chemical properties will change. Certain techniques can be used to measure in short times (several minutes or hours) changes within the polymer that can provide durability information correlated to the natural weathering.

In a typical study of polymer UV degradation, samples are exposed (outdoors or in the laboratory) and the consequent changes are measured after various periods of time using a range of chemical and mechanical characterization methods. Molecular mass distributions can be measured using gel permeation chromatography (GPC)[134]; spectroscopic methods (including infrared analysis) and luminescence methods can be used to follow the growth and decay of key intermediates, such as carbonyl groups or hydroperoxide groups [31]; X-ray diffraction and thermal analysis methods may be valuable in the case of crystallizing polymers [135]; standard tensile and impact tests are used to determine the effect of degradation on engineering properties, often complemented by microscopic examination (light optical microscopy and scanning electron microscopy) to determine the mechanisms of failure [136, 60]. These methods are necessarily slow because of the long exposure time required to develop measurable changes and the subsequent time occupied by the analysis procedure.

Another approach is to monitor carbon dioxide emission by chromatographic analysis [137]. Such investigations are limited by the slow rate of accumulation of CO_2 and the low measurement sensitivity, especially when the polymers contain protective pigments. More recently, Searle and Worsley [138] reported using a closed system incorporating FTIR continuous monitoring and gas chromatography-mass spectrometry (GC-MS) sampling has been developed to study the generation under UVA illumination of volatile photodegradation products from model plasticised and TiO_2 pigmented films. The rate of CO_2 evolution from the irradiated films can be used as a photoactivity index to rank pigment photoactivity successfully within 6 h [138, 139].

Chemiluminescence has also been promoted as a sensitive probe for polymer oxidation [140, 141]. Although there is some dispute over the source of the luminescence, it is probably associated with recombination of radicals produced by

peroxide decomposition. The disadvantage of this method is that it operates at temperatures higher than those at which UV photo-oxidation data are required.

1.9.2 Artificial Exposure methods

As solar energy is the main factor in polymer degradation, simulation of the solar spectral energy distribution, or its specific components, is a prime consideration in artificial weathering of polymeric materials. The commonly used light sources include carbon-arc, xenon-arc, and fluorescent sunlamp. Each of these light sources has its own specific spectral energy distribution. Filters can also be employed to modify the distribution to suit particular purposes or to obtain a better match to the solar energy spectrum. Next is the simple introduction of details of commercial artificial acceleration devices based on these three light sources.

1.9.2.1 Carbon Arc [133]

The enclosed carbon arc lamp was the original artificial weathering UV source. The spectral output has little comparison with natural sunlight. The main radiation consists of three high intensity peaks between 350-450 nm. It is being progressively phased out of international test specifications but is still widely used in industry for company specifications.

1.9.2.2 Xenon Arc sources[133]

Xenon-arc produces the best match to natural sunlight. This light source provides a much better simulation of sunlight than carbon arc sources. Xenon-arc contains UV radiation of wavelengths shorter than the cut off level of solar radiation; filters are used to remove the shorter wavelengths. A high intensity of infrared radiation is emitted so some kind of IR filter (*e.g.* water filter) must be used to remove infrared in order to prevent overheating of the samples. The close simulation of natural sunlight and the ability to control the source automatically combine to make Xenon arc sources a useful alternative as an artificial sunlight simulator.

1.9.2.3 Fluorescent Tube Lamps[133]

These sources are much cheaper to run than xenon-arc and have the advantage that they produce little infrared heating. They are available with different spectral outputs, the most common being UVA and UVB tubes. The UVB spectrum has a peak intensity at around 313 nm, with a high intensity at wavelengths below the solar cut off (*i.e.* 270-290 nm). They provide a strong acceleration, but are also likely to induce unwanted or unnatural chemical reaction. UVA tubes provide a much closer reproduction of the solar spectrum up to around 350 nm and can therefore produce a much closer correlation with natural exposure.

1.9.3 Physical test methods

During the lifetime of polymers they undergo deterioration in physical and mechanical properties, especially when exposed to a combined prolonged effect of UV radiation, temperature, humidity, air pollutants, mechanical stresses, oxygen and thermal cycling. Two basic changes that occur are destruction and structural modification of the materials. These processes of irreversible change in materials are very significant under the enhancing detrimental influence of UV and temperature [142].

The physical test methods commonly used for evaluating the oxidative stability of polymers are tensile strength and elongation, and impact strength. Tensile strength and ultimate elongation are sensitive mechanical properties and their measurements are widely used in the evaluation of degradative effects of the polyolefins. Elongation is a more useful measure of oxidative degradation than tensile strength. Tensile strength may not be markedly affected by sample embrittlement, whereas elongation is much more sensitive and can provide evidence of degradation more readily [143]. Polyethylene and certain other plastics show a comparatively small initial elongation up to quite high stresses and then elongates steadily without further increase in stress "drawing". The results of these measurements, monitored as a function of time under given atmospheric conditions, are dependent on size, shape, and preparation of specimens [57].

1.9.4 Physico-Chemical test methods used to follow degradation

Chemical measurements focus on monitoring the changes of components of material to assess their durability. These methods include: Fourier transform infrared (FTIR) spectroscopy [144], XPS [128, 145, 146], , chemiluminescence [147, 148], iodometric titration [149, 145, 150], oxygen adsorption [151], impedance spectroscopy [152, 153], oxygen uptake [154] and secondary ion mass spectroscopy (SIMS) [155]. Their validity depends on the nature of the material and the mode of deterioration. If a technique is relevant to the characterisation of a polymer then it is often an appropriate means of assessing the degraded material. Since most of the degradation results from irreversible chemical reactions of polymer molecules, changes in molecular composition provide a logical method for measuring the course of polymer degradation. As hydrocarbon polymers degrade, many different changes in polymer composition occur. Fourier transform infrared spectroscopy is used to study the changes in the functional groups (carbonyl, vinyl, vinylidene, alkene, and hydroxyl) of plastic. Since FTIR method is a non-invasive, chemically specific and sensitive technique, it has received the most attention over recent years [156].

1.9.5 FTIR technique in the Study of Polymer oxidation

Infrared spectroscopy has been an indispensable method for the study of polymer degradation and stabilisation. The FTIR technique has three important characteristic that contribute to its usefulness.

(i) No two dissimilar molecules can have the same IR spectrum.

(ii) Infrared spectra of mixtures are additive and absorption is proportional to concentration.

(iii) Infrared spectra can be obtained non-destructively on any type of polymer or additive sample-solid, liquid, or even gas.

Traditional (dispersive) infrared techniques experience difficulties due to the '1 wavenumber at a time' nature of data acquisition. This leads to either a poor signal to noise ratio in a spectrum or a very long time needed to obtain a high quality spectrum. Both these situations cause problems with kinetic work. The first gives inherently large errors, the second prohibits *in-situ* work. These problems can be overcome using

Fourier transform infrared spectroscopy (FTIR) which is based on the interferometer originally designed by Michelson and a mathematical procedure developed by Fourier that converts response from the 'time' to the 'frequency' domain [157]. Traditional FTIR spectroscopy uses simple transmission sampling techniques. However, 'difficult' samples and experiments need specialised sampling accessories. Some common FTIR techniques are described below.

a) Transmission

This is the most simple and basic of the infrared spectroscopic sampling techniques. Essentially infrared radiation is passed through a sample and the transmitted radiation is measured (see Figure 1-13). The spectra obtained will be representative of the whole of the sampled area and 'localised' (*e.g.* surface) properties can quite easily be lost in the 'bulk' properties depending on the size and nature of the sample. The polymeric films should be sufficiently thin to allow observation of spectral absorbance values in the linear domain, which is generally an absorbance value of less than I for the major portions of the spectra. This need for thin films usually means that polymer film samples should be prepared in the 10-100 μm range of thickness. The disadvantage of transmission is that the samples must be thin enough to transmit light.

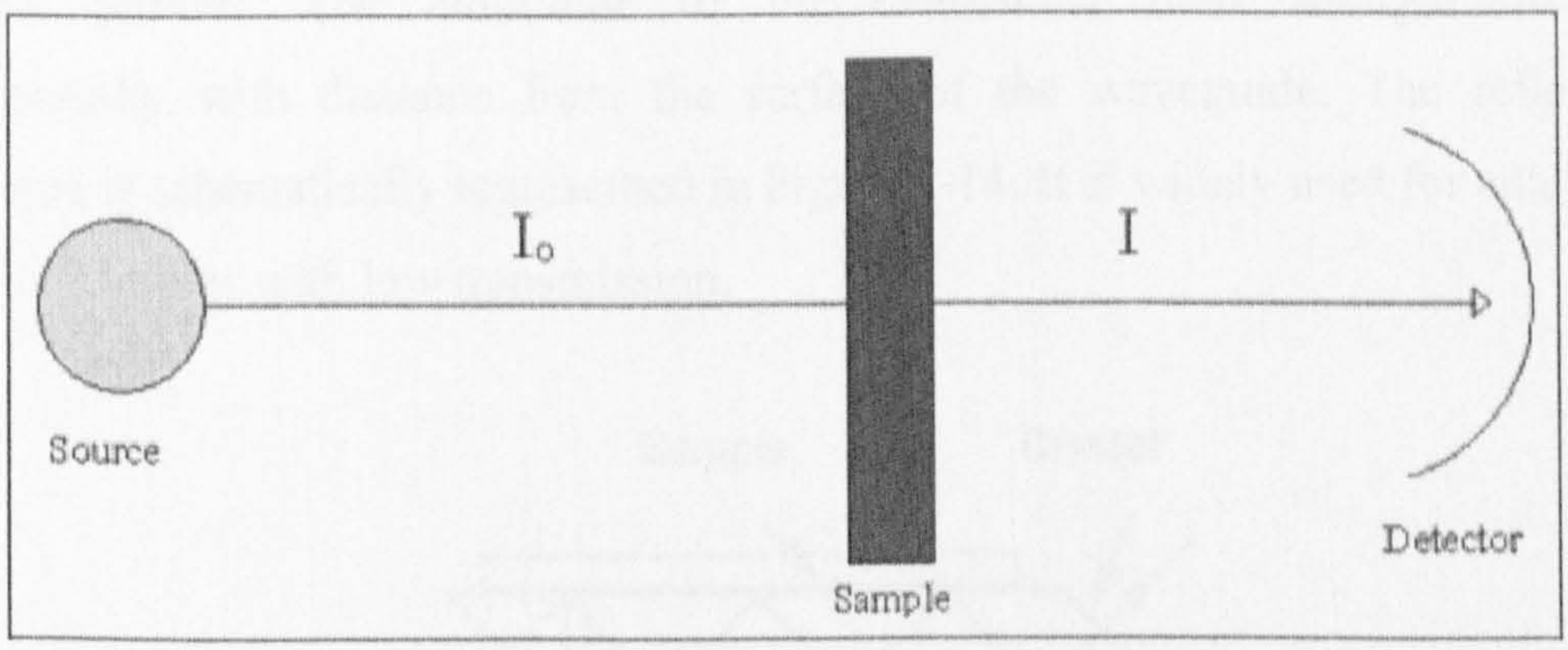

Figure 1-13 Schematic representation of the radiation path and contact type for transmission technique.

In the transmission experiment the transmitted radiation or transmittance (T) is given by

$$T = \frac{I}{I_0} = \exp(-\alpha \ell) \qquad (1.57)$$

where I is the transmitted intensity

I_o is the incident intensity

α is the absorption coefficient

ℓ is the sample thickness

b) Attenuated Total Reflectance (ATR)

The well-established sampling technique of attenuated total reflectance (ATR) [158, 159, 43, 160] is based upon contact between an infrared transparent crystal, also called an internal reflection element (IRE) or an optical waveguide, and a surrounding medium of lower refractive index. When infrared radiation, directed inside the waveguide, is totally reflected at the interface between the two, a standing evanescent wave is established and the radiation acts as if it penetrates a small distance into the surrounding medium. When a material, which selectively absorbs infrared radiation, is in close contact with the reflecting surface the radiation loses energy during each reflection in contact with the sample at the wavelength where the material absorbs. The resultant attenuated radiation is measured and an infrared spectrum of the material plotted. The amplitude of the evanescent field strength decreases exponentially with distance from the surface of the waveguide. The reflectance technique is schematically represented in Figure 1-14. It is widely used for analysis of polymer samples with low transmission.

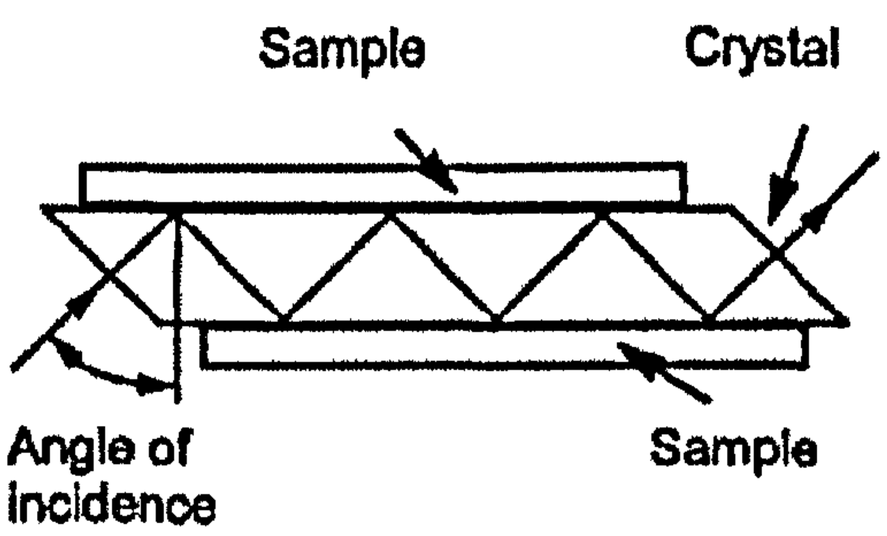

Figure 1-14 Schematic representation of the radiation path and contact type for ATR/FTIR technique.

The depth of penetration (d_p) depends on a number of factors, including the angle of incidence and refractive index, but is approximately equal to the wavelength of the IR light. It can be calculated by using the following equation [43, 159]:

$$d_p = \frac{\lambda}{2\pi n_1 (\sin^2\theta_{eff} - n_{21}^2)^{1/2}} \qquad (1.58)$$

Where d_p penetration depth, in mm

λ wavelength, in mm

n_1 refractive index of the ATR crystal

$n_{21}=n_2/n_1$ ratio of the refractive indexes of the sample (n_2) and of the crystal (n_1)

θ_{eff} effective angle of reflection incidence, in degrees

The effective angle of incidence is calculated by using Eq. (1.59):

$$\theta_{eff} = \theta_{IRA} - \sin^{-1}\left[\frac{\sin(\theta_{IRA} - \theta_{IRE})}{n_1}\right] \qquad (1.59)$$

Where θ_{IRA} angle measured in the accessory's scale, in degrees

θ_{IRE} angle of the crystal's face, in degrees

The effective path length of the beam (*EPL*) is influenced by the refractive indexes of the sample and of the ATR crystal, the wavelength and the number of reflections (*N*) inside the crystal. The relationships among these variables are [43]:

$$N = (l/t)\cot\theta_{eff} \qquad (1.60)$$

and

$$EPL = N \bullet d_p \qquad (1.61)$$

where l and t are the length and thickness of the ATR crystal, respectively. The crystal length in particular is defined as the distance between the centers of the entrance and exit apertures.

c) Photoacoustic Spectroscopy (PAS)

The origin of Photoacoustic Spectroscopy (PAS) [161] date back to the discovery of the photoacoustic effect by Alexander Graham Bell in 1880 [162]. Photoacoustic spectroscopy (PAS) is based on the principle that modulated IR radiation striking the surface of a sample will cause the surface to alternately heat and cool with IR absorption [163, 164]. This cyclic heating is conducted to a coupling gas. A standing sound wave that can be detected by a microphone develops.

Photoacoustic spectroscopy is now commonly used in the analysis of a variety of materials. It is a non-destructive technique that is applicable to almost all types of samples. It offers minimal or no sample preparation, the ability to look at opaque and scattering samples, and the capability to perform depth profiling experiments. PAS can be used for both qualitative and quantitative analysis. In particular, depth profiling experiments are also useful for the characterization of surface-coated and laminar materials and for studies of weathering, aging, curing, and the diffusion of species into or out of a polymer matrix.

1.9.6 The FTIR Method Related to Carbonyl Groups

FTIR is a way of looking at samples using infrared radiation. The entire spectrum can be scanned in a few seconds or less. So the FTIR method is widely used for investigating the chemical changes that occur during oxidation of polyolefins. Most of the early studies using FTIR are based on the use of transmission IR spectroscopy *i.e.* the transmission of IR beam through a thin film of sample during weathering [55, 165-168]. This technique was used to monitor carbonyl group development to evaluate the extent of photodegradation of polyethylene[43, 159, 169]. The carbonyl (CO) and hydroxyl (OH)/hydroxyperoxide (OOH) frequencies are the best known of the characteristic infrared absorption bands formed upon photo-oxidative degradation of polymers [170]. These strong bands fall in regions of the spectra where few other absorptions are found.

1.9.6.1 Carbonyl Groups

A carbonyl group is a carbon-oxygen double bond. Oxygen can have only two bonds, so nothing else can be bonded to oxygen, but carbon forms four bonds, so there are two "bonds" left over by which other atoms can be bonded to the carbon. If the carbonyl group is joined only to alkyl groups or aryl groups, the compound is a ketone; if it is joined to at least one hydrogen atom, the compound is an aldehyde. A carbonyl group looks like.

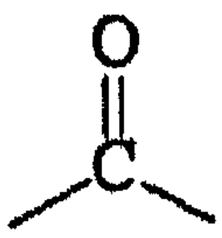

In FTIR absorption spectra, the carbonyl group bands occur within 60 cm^{-1} around 1700 cm^{-1}[157]. Variation from the normal position (1710-1720 cm^{-1}) is caused by effects which include geometric effects, force constant effects, resonance and /or mesomeric effects, hydrogen bonding to the carbonyl group lowers the carbonyl frequency and intermolecular effects.

Gulmine [43] summarized that the absorption band around 1714 cm^{-1}, which can be assigned to the C=O stretching vibration of a ketone group, grows in intensity with extended aging, and at the same time new bands begin to appear. These absorption bands indicate that more than one oxidation product is formed, as detailed in Figure 1-15. These new bands show up after 100 h of exposure in the Weather – Ometer (WOM)-equipment and after 24 h using the Weathering Tester (QUV) equipment. The irradiance differences of the two chambers are reflected in faster aging in QUV conditions, with carbonyl splitting beginning with only 24 h exposure. The carbonyl bands were assigned to C=O stretching vibrations in aldehydes and/or esters (1733 cm^{-1}) carboxylic acid groups (1700 cm^{-1}) and γ-lactones (1780 cm^{-1}) [171-174].

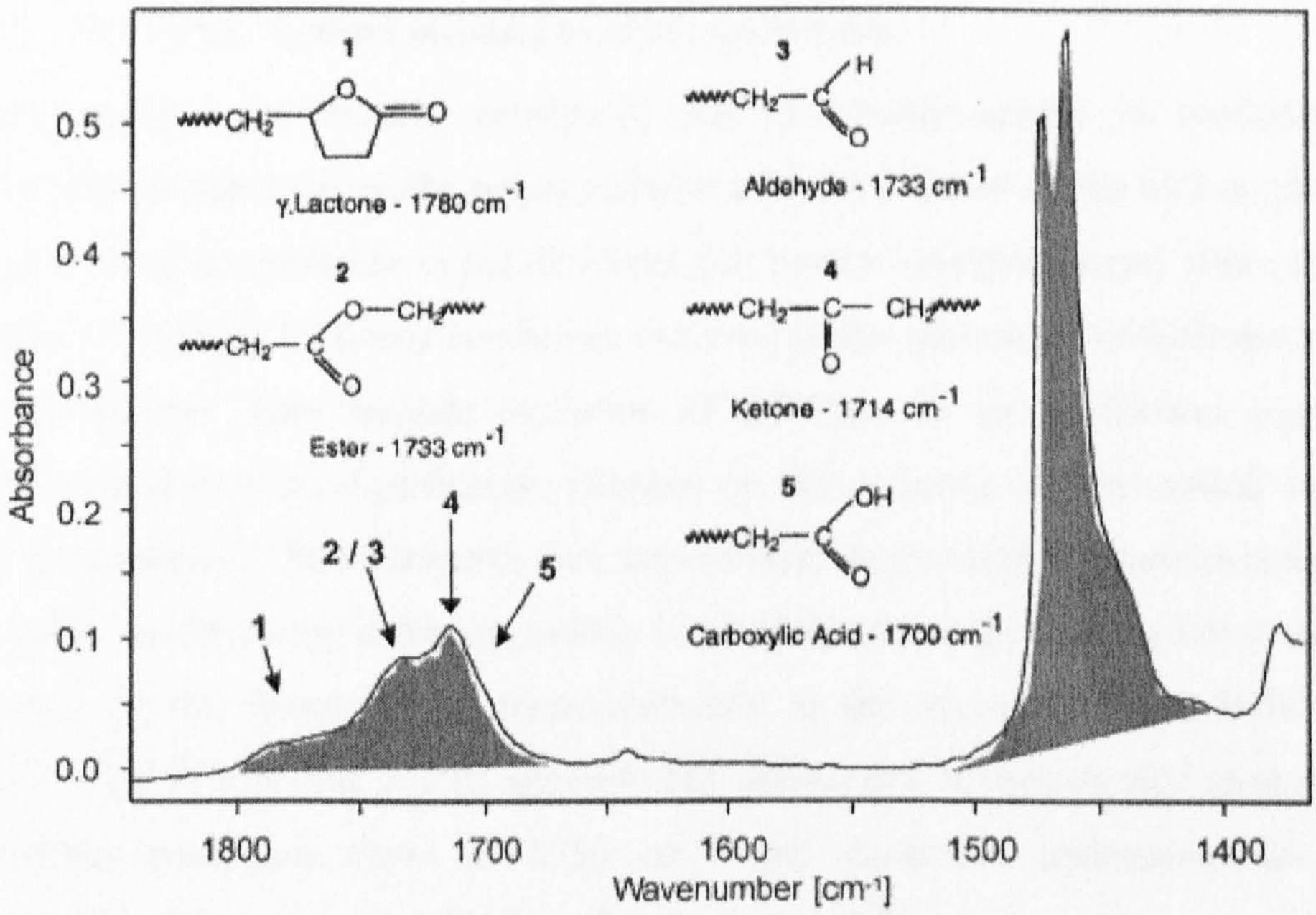

Figure 1-15 FTIR–ATR spectrum of LDPE aged during 400 h under WOM conditions showing the formation of various bands that can be assigned to stretching vibrations of various carbonyl groups formed by the polymer oxidation processes [43].

1.9.6.2 *Carbonyl index*

The carbonyl index (measured at 1710-1720 cm^{-1} is commonly used for the determination of the extent of photodegradation of polymer. Allen *et al* [175, 176] defined that the oxidation rates were determined *via* the well-established carbonyl index method:

$$\text{Carbonyl Index(C.I.)} = [(\log I_0/I)/D]100 \quad (1.62)$$

where D is film thickness in μm

I_0 is the initial light intensity at 1710 cm^{-1}

I_t is the transmitted light intensity at 1710 cm^{-1}

Gulmine *et al*[159] defined the carbonyl index as the ratio between the integrated band absorbance of the carbonyl around 1714 cm^{-1} and that of the PE-polymer bands (1470 cm^{-1}), characterizing the degree of oxidation for each polyethylene sample. In this thesis, Allen's C.I. was used to represent the extent of PE degradation.

1.9.7 The FTIR Method Related to Hydroperoxides

Hydroperoxides are usually considered the key intermediates in oxidation of polyolefins initiated thermally or photochemically. The nature of the hydroperoxides in polyolefins, in particular in polyethylene, has been investigated many times in past decades [177-180]. Different conditions can lead to the generation of hydroperoxides in polyethylene. They include oxidation of PE films in air by thermal aging or radiation, and may be significantly changes by the presence of free radical sources such as peroxides. The hydroperoxides formed were determined by chemical methods and /or by spectroscopy methods, mainly infrared spectroscopy. All the films showed evidence of the formation of hydroperoxides in the region of 3410-3600 cm^{-1}. Gugumus [178] reported that IR spectroscopy allows free hydroperoxide groups with absorption maximum close to 3550 cm^{-1} and associated hydroperoxides with absorption maximum around 3410 cm^{-1} to be distinguished.

1.9.8 Review of FTIR Used in PE Degradation

An enormous literatures has been reported around the world using IR spectroscopy to monitor degradation of polyethylene [11, 41, 43, 61, 159, 173, 174, 181-190].

The effect of natural weathering on the chemical structure of low density polyethylene (LDPE) was studied in Ankara, by Akay *et al* [190]. Formation of carbonyl and vinyl groups was investigated by IR spectroscopic measurement. The most important spectral changes occurred in the carbonyl region, and the changes in the unsaturation region corresponding to vinyl groups were considered to be of secondary importance.

Allen and Katami [129] reported the effect of TiO_2 pigments on thermal and photochemical oxidation and stabilisation of polyolefin films. They concluded for thermal oxidative degradation over the temperature range 50-90 °C, the titanium dioxide pigments behave as thermal (catalytic) sensitizers. Satoto and Subowo [167] reported that transmission FTIR was able to distinguish between the degree of photodegradation of two high-density polyethylene films exposed to natural sunlight at different latitudes (Indonesia and Japan) on the basis of measuring the growth of the carbonyl features.

Gijsman *et al* [165] used the FTIR method to study aging of polyethylene in accelerated (Xenon) tests and outdoors. By measuring the different rates of change in the carbonyl features and the degree of unsaturation of the polymer chain, the data show clearly the difference in chemical changes in polyethylene films. Jakubowicz *et al* [191] reported that the FTIR spectra of the carbonyl groups show that photooxidition gives rise to a broad absorption band in the 1800-1680 cm^{-1} region. A detailed examination of this region gave many absorption peaks corresponding to different types of carbonyl compounds.

1.10 THE NOVEL FTIR METHOD TO MONITOR CO_2 EVALUTION

The final degradation products of polyethylene (PE) are the same regardless of whether the initiating system is UV light or heat (with or without chemical accelerators), provided air (oxygen) is present. These final products are carbon dioxide and water, no matter whether the starting material is LDPE, HDPE or LLDPE.

The same final products are formed from PE, even though there are a number of ways to initiate the oxidation. For other polymers also, ignoring any intermediate product, *i.e.* both of the photochemical oxidation of the organic medium and the photo-catalytic oxidation, lead to the same final products CO_2, water and other simple molecules.

Gas-phase CO_2 has strong doublet absorption near 2360 and 2340 cm^{-1} in infrared region. The absorption at 2360 cm^{-1} is measured. It is possible to evaluate the progress of photodegradation by monitoring the CO_2 evolution.

Christensen *et al* [107, 124, 192-194] have used of *in-situ* quantitative infrared spectrometry to measure the carbon dioxide generated during the UV-induced oxidation of an acrylic paint pigmented with titanium dioxide. They showed that, for pigments of widely differing activity, the ranking judged from the amount of carbon dioxide evolution mirrors the results of conventional paint weathering tests.

Worsley and Searle [138, 139] reported a new testing procedure that enables a rapid assessment of TiO_2 photoactivity to be made. The kinetics of CO_2 production from solution cast unplasticised PVC (UPVC) films pigmented with 50% by weight TiO_2 under UV-A illumination (365 nm) monitored by Fourier transform infrared spectroscopy in a closed loop flow system have been measured. A range of TiO_2 samples with differing photoactivities ranging from unclassified materials (unsuitable for structural or coatings applications) through grade C (interior use), grade B (non-demanding external) and grade A (demanding external coatings and structural UPVC) have been tested. The rate of CO_2 evolution from the irradiated films can be used as a photoactivity index to rank pigment photoactivity successfully within 6 h. In addition, the technique appears sensitive to differences in grade A pigment performance allowing rapid assessment of even the most photostable materials.

To develop a rapid, reliable and sensitive method to predict the change in optical and mechanical properties of TiO_2 pigmented polymers, the above described technique for CO_2 evolution has been adapted to use with polymer films or disks (PE, PVC). The results show that FTIR spectroscopy can be used in conjunction with a suitable artificial light source to provide a reproducible measure of the carbon dioxide evolution to evaluate the durability of polymer films.

1.11 STRAIN ENHANCED PHOTODEGRADATION OF POLYMER

The application of a large external stress or loading on a polymer will result in a decrease in its useful lifetime, primarily *via* physical creep, although it is possible that chemically degrading mechanisms may also be affected adversely. It has been shown that stress accelerates the photo-oxidative degradation of polymers [195, 196]. The book by Davis and Sims [197] suggests that polymers are likely to fail more rapidly if weathered under load, but it does not refer to any quantitative studies of this effect. Significant research has been conducted into the acceleration of the thermo-oxidative degradation of thermoplastics. Much of this work was conducted in the former Soviet Union and reviewed in a monograph [198]; further discussion is included in a

review[199]. Much of the data obtained on stress-assisted thermo-oxidation of polymers can be fitted to the rate law that is usually attributed to Zhurkov [200, 201];

$$r = A \exp[-(\Delta G - B\sigma) / RT] \qquad (1.63)$$

Where r is the rate of a process that has an activation energy, ΔG, σ is the stress, R is the gas constant and T is the absolute temperature, and A and B are constants.

Photo-oxidation involving the ultraviolet (UV) component of solar radiation is generally accepted as the principal cause of the outdoor degradation of polymers, and O'Donnell and White [195] described a study designed to investigate whether stress-assisted photo-oxidation could be described in a similar manner as thermo-oxidation. They concluded the measurements of molecular weight on samples conditioned under various combinations of stress and UV illumination show that tensile stress accelerates molecular degradation in polystyrene. Accordingly, when polystyrene samples were tensile tested after such treatment, those samples which were conditioned under stress generally failed more readily than those which were conditioned in the unstressed state.

Benachour and Rogers [196] noted the photodegradation of low density polyethylene films is greatly enhanced by uniaxial elongation, and the enhancement process is closely related to the morphological changes induced upon drawing of the polymer films. The necking development region shows more degradation due to its highly disrupted structure. The enhancement can be reduced by annealing or relaxation, and stress (applied load, or stored energy) appears to be the dominant factor of enhancement. The mechanical tests confirmed that the oxidation is concentrated in the surface layers.

1.12 DICHROIC RATIO

Dichroic ratio measurements can be used to quantify molecular orientation in some polymers. The absorption of infrared radiation occurs to a maximum degree when the direction of the electric vector of the radiation is parallel to the direction of the dipole

moment changes involved in the various vibrational modes of the absorbing molecule. If the direction of the electric vector lies at an angle to the direction of the dipole movement change, the component of the former resolved along the latter direction is involved in the absorption process, which thus occurs less strongly. This is the directional property that makes infrared spectroscopy useful for orientation studies. More details can be referenced with books, on polymer spectroscopy [202].

1.13 RESEARCH OBJECTIVES

The aims of this research consist of three main parts, which are: (1) to use FTIR spectroscopy to study photodegradation of polyethylene; (2) to measure effects of strain on photodegradation of polyethylene; (3) to use the *in-situ* FTIR method to study PVC material.

In the study of photodegradation of polyethylene, the first objective was to investigate whether the *in-situ* FTIR method can be used in conjunction with a suitable artificial light source to provide a reproducible measure of the photoactivity of the unpigmented PE film or of films pigmented with commercial grade TiO_2 polyethylene. The second objective was to develop a rapid, reliable and sensitive *in-situ* FTIR method to provide real time information on the degradation of the PE films. This should not only distinguish showed between effects of pigment grades on photodegradation of polymer but also show good correlation with conventional methods of monitoring, *e.g.* carbonyl group development in the sample. The third objective is using *in-situ* FTIR spectroscopy to probe the mechanism of the photodegradation of pigmented and unpigmented polyethylene films in order to understand the parameters which relates to the durability of practical PE films.

In the study of the effects of applying strain, FTIR spectroscopy was used to study strain effects on the photodegradation of the polyethylene and also measure dichroism of polyethylene films. I*n-situ* FTIR method was extended to determine the effect of a constant strain on the rate of carbon dioxide evolution and hence evaluate the effects of different TiO_2 pigments on photodegradation of strained polyethylene.

In the study of the PVC material the objectives were, firstly to evaluate whether the FTIR gas-phase technique could be extended to distinguish between the differences in the photoactivity of the rigid PVC panels (2 mm thickness) of different compositions, and secondly, to elucidate whether the FTIR CO_2 method was able to test the gas phase HCl signal from the volatile production of photodegradation of PVC samples. .

1.14 REFERENCES

1. Schroder, J., *Progress in Organic Coatings,* 1988. **16**(1): p. 3-17.
2. Allen, N.S., C. Vasiliou, G.P. Marshall, and W. Chen, *Polymer Degradation and Stability,* 1989. **24**(1): p. 17-31.
3. Day, R.E., *Polymer Degradation and Stability,* 1990. **29**(1): p. 73-92.
4. Allen, N.S., H. Khatami, and F. Thompson, *European Polymer Journal,* 1992. **28**(7): p. 817-822.
5. Singh, R.P., J. Lacoste, R. Arnaud, and J. Lemaire, *Polymer Degradation and Stability,* 1988. **20**(1): p. 49-58.
6. Allen, N.S., A. Chirinos-Padron, and J.H. Appleyard, *Polymer Degradation and Stability,* 1984. **9**(1): p. 15-22.
7. Kemp, T.J. and R.A. McIntyre, *Progress in Reaction Kinetics and Mechanism,* 2002. **26**(4): p. 337-374.
8. Young, R.J. and P.A. Lovell, *Introduction to Polymers*. 1991, London: Chapman & Hall.
9. Sperling, L.H., *Introduction to physical polymer science*. 2001, *Wiley-Interscience*: New York.
10. Stevens, M.P., *Polymer chemistry: an intruduction*. 1999, New York: Oxford University Press.
11. Allen, N.S., M. Edge, T. Corrales, A. Childs, C.M. Liauw, F. Catalina, C. Peinado, A. Minihan, and D. Aldcroft, *Polymer Degradation and Stability,* 1998. **61**(2): p. 183-199.
12. Egerton, T.A. and A. Tetlow, *in Industrial Inorganic Chemicals: Production and Uses (Royal Society of Chemistry, 1995) Chapter 13.*
13. Day, R.E. and T.A. Egerton, *Colloids and Surfaces,* 1987. **23**(1-2): p. 137-155.
14. Hamid, S.H., M.B. Amin, and A.G. Maadhah, *Handbook of Polymer Degaradation*. ed. IV. 1992, New York.
15. Mills, A. and S. LeHunte, *Journal of Photochemistry and Photobiology a-Chemistry,* 1997. **108**(1): p. 1-35.
16. Pappas, S.P. and R.M. Fischer, *Journal of Paint technology,* 1974. **46**: p. 65.
17. Braun, J.H., *Journal of Coatings Technology,* 1997. **69**(868): p. 59-72.
18. Cotton, F.A. and G. Wilkinson, *Advanced Inorganic Chemistry. 1988, Chichester: Wiley Interscience. Ch. 18-A.*
19. http://ruby.colorado.edu/~smyth/min/tio2.html.
20. Gopal, M., W.J.M. Chan, and L.C. DeJonghe, *Journal of Materials Science,* 1997. **32**(22): p. 6001-6008.
21. Finklea, H.O., *Semiconductor Electrodes*. Finklea, H. O. ed. Vol. Ch.2. 1988, Amsterdam: Elsevier.
22. Day, R.E., *Polymer Degradation and Stability,* 1990. **29**(1): p. 73-92.

23. Egerton, T.A., *Titanium Compounds, Kirk-Othmer Encyclopedia of Chemical Technology, 4th Edition,24,*. John Wiley and Sons (1997).
24. Gaskell, D., *Chemistry in Britain,* 1995. **31(6)**: p. 430-432.
25. Braun, J.H., A. Baidins, and R.E. Marganski, *Progress in Organic Coatings,* 1992. **20**(2): p. 105-138.
26. McNeil, L.E. and R.H. French, *Acta Materialia,* 2000. **48**(18-19): p. 4571-4576.
27. Tioxide-Group, *Manufacture and general properties of titanium dioxide pigments*. 1999.
28. Schiller, M., F.W. Muller, and C. Damm, *Journal of Photochemistry and Photobiology A: Chemistry,* 2002. **149**(1-3): p. 227-236.
29. Gesenhues, U., *Journal of Photochemistry and Photobiology a-Chemistry,* 2001. **139**(2-3): p. 243-251.
30. Johnson, R.W., E.S. Thiele, and R.H. French, *Tappi Journal,* 1997. **80**(11): p. 233-239.
31. Rabek, J.F., *Chapman & Hall,* 1995.
32. Calvert, J. and J. Pitts, *Photochemistry*. 1970, New York: Wiley and Sons.
33. Wayne, R.P., *Principles and Applications of Photochemistry*. 1988, Oxford: Oxford University Press.
34. Pospisil, J. and S. Nespurek, *Progress in Polymer Science,* 2000. **25**(9): p. 1261-1335.
35. Wayne, R.P. and C.E. Wayne, *Photochemistry*. 1996, New York: Oxford University Press Onc.
36. Rabek, J.F., *Photodegradation of Polymers*. 1995, London: Chapman and Hall.
37. Rabek, J.F., *Photodegradation of Polymers*. 1996, New York: Springer.
38. Giesse, R. and M.A. Depaoli, *Polymer Degradation and Stability,* 1988. **21**(2): p. 181-187.
39. Wu, Q., B. Qu, Y. Xu, and Q. Wu, *Polymer Degradation and Stability,* 2000. **68**(1): p. 97-102.
40. Gobin, K. and G. Manos, *Polymer Degradation and Stability,* 2004. **83**(2): p. 267-279.
41. Valadez-Gonzalez, A. and L. Veleva, *Polymer Degradation and Stability,* 2004. **83**(1): p. 139-148.
42. Mendes, L.C., E.S. Rufino, F.O.C. de Paula, and A.C. Torres Jr., *Polymer Degradation and Stability,* 2003. **79**(3): p. 371-383.
43. Gulmine, J.V., P.R. Janissek, H.M. Heise, and L. Akcelrud, *Polymer Degradation and Stability,* 2003. **79**(3): p. 385-397.
44. Cruz, S.A. and M. Zanin, *Polymer Degradation and Stability,* 2003. **80**(1): p. 31-37.
45. Jakubowicz, I., *Polymer Degradation and Stability,* 2003. **80**(1): p. 39-43.
46. Jipa, S., T. Zaharescu, B. Gigante, C. Santos, R. Setnescu, T. Setnescu, M. Dumitru, L.M. Gorghiu, W. Kappel, and I. Mihalcea, *Polymer Degradation and Stability,* 2003. **80**(2): p. 209-216.
47. Basfar, A.A., K.M. Idriss Ali, and S.M. Mofti, *Polymer Degradation and Stability,* 2003. **82**(2): p. 229-234.
48. Fallani, F., G. Ruggeri, S. Bronco, and M. Bertoldo, *Polymer Degradation and Stability,* 2003. **82**(2): p. 257-261.
49. Glastrup, J., *Polymer Degradation and Stability,* 2003. **81**(2): p. 273-278.

50. Abdel-Hady, E.E., *Polymer Degradation and Stability,* 2003. **80**(2): p. 363-368.
51. Tavares, A.C., J.V. Gulmine, C.M. Lepienski, and L. Akcelrud, *Polymer Degradation and Stability,* 2003. **81**(2): p. 367-373.
52. Avila, A.F. and M.V. Duarte, *Polymer Degradation and Stability,* 2003. **80**(2): p. 373-382.
53. Suarez, J.C.M. and E.B. Mano, *Polymer Degradation and Stability,* 2001. **72**(2): p. 217-221.
54. Qayyum, M.M. and J.R. White, *Polymer Degradation and Stability,* 1993. **39**(2): p. 199-205.
55. Gijsman, P., G. Meijers, and G. Vitarelli, *Polymer Degradation and Stability,* 1999. **65**(3): p. 433-441.
56. Turro, N.J., *Modern Molecular Photochemistry*. 1978, Menlo Park, California: The Benjamin/Cummings Publishing Co., Inc.
57. Hamid, S.H., M.B. Amin, and A.G. Maadhah, *Handbook of Polymer Degradation*. 1992.
58. Allen, N.S., M. Edge, T. Corrales, M. Shah, D. Holdsworth, F. Catalina, C. Peinado, and E.P. Collar, *Polymer,* 1996. **37**: p. 2323-2333.
59. Gijsman, P., G. Meijers, and G. Vitarelli, *Polymer Degradation and Stability,* 1999. **65**: p. 433-441.
60. White, J.R. and A. Turnbull, *Journal of Materials Science,* 1994. **29**(3): p. 584-613.
61. Badr, Y., Z.I. Ali, and R.M. Khafagy, *Radiation Physics and Chemistry,* 2000. **58**(1): p. 87-100.
62. Lacoste, J., D.J. Carlsson, S. Falicki, and D.M. Wiles, *Polymer Degradation and Stability,* 1991. **34**(1-3): p. 309-323.
63. Balakrishnan, S. and D. Ramaswamy, *Jocca-Surface Coatings International,* 1991. **74**(4): p. 117 et seq.
64. Schnabel, W., *Polymer degradation*. 1981, Munich: Hanser International.
65. Scott, G., *Polymer Degradation and Stability,* 1985. **10**(2): p. 97-125.
66. Gardette, J.L., S. Gaumet, and J. Lemaire, *Macromolecules,* 1989. **22**(6): p. 2576-2581.
67. Finklea, H.O., *Semiconducter Electrodes*. 1988, *Elsevier*: Amsterdam. p. Ch. 2.
68. Chun, H., W. Yizhong, and T. Hongxiao, *Chemosphere,* 2000. **41**(8): p. 1205-1209.
69. Bahnemann, D.W., M. Hilgendorff, and R. Memming, *Journal of Physical Chemistry B,* 1997. **101**(21): p. 4265-4275.
70. Minero, C., C. Aliberti, E. Pelizzetti, R. Terzian, and N. Serpone, *Langmuir,* 1991. **7**(5): p. 928-936.
71. Sabate, J., M.A. Anderson, H. Kikkawa, M. Edwards, and C.G. Hill, *Journal of Catalysis,* 1991. **127**(1): p. 167-177.
72. Sabin, F., T. Turk, and A. Vogler, *Journal of Photochemistry and Photobiology a-Chemistry,* 1992. **63**(1): p. 99-106.
73. Herrmann, J.M., J. Disdier, P. Pichat, S. Malato, and J. Blanco, *Applied Catalysis B-Environmental,* 1998. **17**(1-2): p. 15-23.
74. Minabe, T., D.A. Tryk, P. Sawunyama, Y. Kikuchi, K. Hashimoto, and A. Fujishima, *Journal of Photochemistry and Photobiology a-Chemistry,* 2000. **137**(1): p. 53-62.
75. Bard, A.J., *Science,* 1980. **207**: p. 139.

76. Hidaka, H., T. Nakamura, A. Ishizaka, M. Tsuchiya, and J.C. Zhao, *Journal of Photochemistry and Photobiology a-Chemistry,* 1992. **66**(3): p. 367-374.
77. Fujishima, A. and K. Honda, *Nature,* 1972. **238**(5358): p. 37-38.
78. West, A.R., *Solid State Chemistry and its application*, in *Solid State Chemistry and its application*, A.R. West, Editor. 1985, *J. Wiley and Sons*: Xhichester. p. P497.
79. Khader, M.M., F.M.N. Kheiri, B.E. Elanadouli, and B.G. Ateya, *Journal of Physical Chemistry,* 1993. **97**(22): p. 6074-6077.
80. Goodenough, J.B., *Prog. Solid State Chem.,* 1971. **5**: p. 145.
81. Aliskandarani, M., C. DupuyMaillard, M. PetitRamel, J.P. Percherancier, H. Brun, and B. Pouyet, *Fresenius Environmental Bulletin,* 1996. **5**(9-10): p. 569-573.
82. Ohtani, B., M. Kakimoto, S. Nishimoto, and T. Kagiya, *Journal of Photochemistry and Photobiology a-Chemistry,* 1993. **70**(3): p. 265-272.
83. Pelizzetti, E., C. Minero, V. Carlin, and E. Borgarello, *Chemosphere,* 1992. **25**(3): p. 343-351.
84. Tseng, J.M. and C.P. Huang, *Water Science and Technology,* 1991. **23**(1-3): p. 377-387.
85. Liu, H., S.A. Cheng, J.Q. Zhang, C.N. Cao, and S.K. Zhang, *Chemosphere,* 1999. **38**(2): p. 283-292.
86. Noorjahan, M., V.D. Kumari, M. Subrahmanyam, and P. Boule, *Applied Catalysis B-Environmental,* 2004. **47**(3): p. 209-213.
87. Huang, X.J., G. Ye, L.C. Wang, W. Liu, N.C. Cai, and J.H. Liu, *Chemical Journal of Chinese Universities-Chinese,* 2003. **24**(8): p. 1459-1463.
88. Gao, Y., W. Yu, B.H. Chen, Y.X. Ma, and H.L. Li, *Rare Metals,* 2003. **22**(2): p. 137-143.
89. Ao, C.H., S.C. Lee, and J.C. Yu, *Journal of Photochemistry and Photobiology a-Chemistry,* 2003. **156**(1-3): p. 171-177.
90. Ku, Y. and C.B. Hsieh, *Water Research,* 1992. **26**(11): p. 1451-1456.
91. Chemseddine, A. and H.P. Boehm, *Journal of Molecular Catalysis,* 1990. **60**(3): p. 295-311.
92. Kato, K., *Nippon Seramikkusu Kyokai Gakujutsu Ronbunshi-Journal of the Ceramic Society of Japan,* 1993. **101**(3): p. 245-249.
93. Sauer, M.L. and D.F. Ollis, *Journal of Catalysis,* 1996. **163**(1): p. 215-217.
94. Mills, A. and S. Morris, *Journal of Photochemistry and Photobiology a-Chemistry,* 1993. **71**(3): p. 285-289.
95. Hsiao, C.Y., C.L. Lee, and D.F. Ollis, *Journal of Catalysis,* 1983. **82**(2): p. 418-423.
96. Gerischer, H., *Electrochimica Acta,* 1993. **38**(1): p. 3-9.
97. Ollis, D.F., E. Pelizzetti, and N. Serpone, *Environmental Science and Technology,* 1991. **25**(9): p. 1522-1529.
98. Pelizzetti, E. and M.E. Schiavello, *Photochemical Conversion and Storage of Solar Energy*. 1991, *Kluwer*: Dordrecht.
99. Schindler, K.M. and M. Kunst, *Journal of Physical Chemistry,* 1990. **94**(21): p. 8222-8226.
100. Sclafani, A., L. Palmisano, and M. Schiavello, *Journal of Physical Chemistry,* 1990. **94**(2): p. 829-832.
101. Yates, D.J.C., *Journal of Physical Chemistry,* 1961. **65**: p. 746.
102. Boehm, H.P., *Advances in Catalysis,* 1966. **16**: p. 249.

103. Sham, T.K. and M.S. Lazarus, *Chem. Phys. Letts.*, 1979. **68**: p. 426.
104. Jackson, P. and G.D. Parfitt, *J.Chem.Soc.Faraday Trans 1*, 1971. **67**: p. 2469.
105. Boehm, H.P., *Adv. Catalysis*, 1966. **16**: p. 249.
106. Boehm, H.P., *Faraday Disc. Chem. Soc.*, 1971. **52**: p. 264.
107. Christensen, P.A., A. Dilks, T.A. Egerton, and J. Temperley, *Journal of Materials Science*, 1999. **34**(23): p. 5689-5700.
108. Christensen, P.A., A. Dilks, T.A. Egerton, E.J. Lawson, and J. Temperley, *Journal of Materials Science*, 2002. **37**(22): p. 4879-4887.
109. Allen, N.S., M. Edge, D. Holdsworth, A. Rahman, F. Catalina, E. Fontan, A.M. Escalona, and F.F. Sibon, *Polymer Degradation and Stability*, 2000. **67**(1): p. 57-67.
110. Anpo, M., T. Shima, S. Kodama, and Y. Kubokawa, *Journal of Physical Chemistry*, 1987. **91**(16): p. 4305-4310.
111. Schiavello, M., *Electrochimica Acta*, 1993. **38**(1): p. 11-14.
112. Pelizzetti, E. and C. Minero, *Electrochimica Acta*, 1993. **38**(1): p. 47-55.
113. Liu, G., J. Zhao, and H. Hidaka, *Journal of Photochemistry and Photobiology A: Chemistry*, 2000. **133**(1-2): p. 83-88.
114. Jenkins, C.A., D.M. Murphy, C.C. Rowlands, and T.A. Egerton, *Journal of the Chemical Society-Perkin Transactions 2*, 1997(12): p. 2479-2485.
115. Howe, R.F., *Colloids and Surfaces a-Physicochemical and Engineering Aspects*, 1993. **72**: p. 353-363.
116. Gratzel, M. and R.F. Howe, *Journal of Physical Chemistry*, 1990. **94**(6): p. 2566-2572.
117. Cunningham, J. and S. Srijaranai, *Journal of Photochemistry and Photobiology a-Chemistry*, 1988. **43**(3): p. 329-335.
118. Barbeni, M., E. Pramauro, E. Pelizzetti, E. Borgarello, M. Gratzel, and N. Serpone, *Nouveau Journal De Chimie-New Journal of Chemistry*, 1984. **8**(8-9): p. 547-550.
119. Gerischer, H. and A. Heller, *Journal of Physical Chemistry*, 1991. **95**(13): p. 5261-5267.
120. Nelson, S.F., M.F. Teasely, and P.L. Kapp, *J. Am. Chem. Soc.*, 1986. **108**: p. 5503.
121. Sun, L.Z. and J.R. Bolton, *Journal of Physical Chemistry*, 1996. **100**(10): p. 4127-4134.
122. Muzyka, J.L. and M.A. Fox, *Journal of Organic Chemistry*, 1991. **56**(14): p. 4549-4552.
123. Walker, G.M. 1998, *University of Newcastle*.
124. Christensen, P.A., A. Dilks, T.A. Egerton, and J. Temperley, *Journal of Materials Science*, 2000. **35**(21): p. 5353-5358.
125. Allen, N.S., *Polymer Degradation and Stability*, 1994. **44**(3): p. 357-374.
126. Andrady, A.L. and N.D. Searle, *Journal of Applied Polymer Science*, 1989. **37**(10): p. 2789-2802.
127. Andrady, A.L., A. Torikai, and K. Fueki, *Journal of Applied Polymer Science*, 1989. **37**(4): p. 935-946.
128. Egerton, T.A., G.D. Parfitt, Y. Kang, and J.P. Wightman, *Colloids and Surfaces*, 1983. **7**(4): p. 311-323.
129. Allen, N.S. and H. Katami, *Polymer Degradation and Stability*, 1996. **52**(3): p. 311-320.

130. Kaempf, G., W. Papenroth, and R. Holm, *Journal of Paint technology,* 1974. **46**: p. 56.
131. Egerton, T.A. and C.J. King, *Journal of the Oil & Colour Chemists Association,* 1979. **62**: p. 386-390.
132. Brown, R., *Handbook of polymer testing: physical nethods.* 1999, New York: Marcel Dekker, INC.
133. Johnson, B.W. and R. McIntyre, *Progress in Organic Coatings,* 1996. **27**(1-4): p. 95-106.
134. O'donnell, B., J.R. White, and S.R. Holding, *Journal of Applied Polymer Science,* 1994. **52**(11): p. 1607-1618.
135. Rabello, M.S. and J.R. White, *Journal of Applied Polymer Science,* 1997. **64**(13): p. 2505-2517.
136. O'donnell, B., M.M. Qayyum, L. Tong, and J.R. White, *Plastics Rubber and Composites Processing and Applications,* 1994. **21**(5): p. 297-307.
137. Vink, P., T.P.M. Koster, H.F.N. Fontijn, and A. Mackor, *Polymer Degradation and Stability,* 1995. **48**(1): p. 155-160.
138. Searle, J. and D. Worsley, *Plastics Rubber and Composites,* 2002. **31**(8): p. 329-335.
139. Worsley, D.A. and J.R. Searle, *Materials Science and Technology,* 2002. **18**(6): p. 681-684.
140. Jacobson, K., B. Stenberg, B. Terselius, and T. Reitberger, *Polymer Degradation and Stability,* 1999. **65**(3): p. 449-455.
141. Jacobson, K., B. Stenberg, B. Terselius, and T. Reitberger, *Polymer Degradation and Stability,* 2000. **68**(1): p. 53-60.
142. Kovacevic, V., D. Hage, M. Braver, I. Mudri, and Z. Cerouecki, *Polimeri,* 1986. 7((12)): p. 351-355.
143. Hamid, S.H. and W.H. Prichard, *Journal of Applied Polymer Science,* 1991. **43**: p. 651-678.
144. Busca, G., H. Saussey, O. Saur, J.C. Lavalley, and V. Lorenzelli, *Applied Catalysis,* 1985. **14**(1-3): p. 245-260.
145. Allen, N.S., M.J. Parker, C.J. Regan, R.B. McIntyre, and W.A.E. Dunk, *Polymer Degradation and Stability,* 1995. **47**: p. 117.
146. Lacoste, J., Y. Deslandes, P. Black, and D.J. Carlsson, *Polymer Degradation and Stability,* 1995. **49**(1): p. 21-28.
147. Johnson, B.W. and R. Mcintyre, *Progress in Organis Coatings,* 1996. **27**(1-4): p. 95-106.
148. Broska, R. and J. Rychly, *Polymer Degradation and Stability,* 2001. **72**(2): p. 271-278.
149. Allen, N.S., C.J. Regan, R.B. McIntyre, and W.A.E. Dunk, *Prog. Org. Coatings,* 1997. **32**: p. 9.
150. Mielewski, D.F., D.R. Bauer, and J.L. Gerlock, *Polymer Degradation and Stability,* 1991. **33**: p. 93.
151. Macker, A., T.P.M. Koster, and L. Kui-Wen. in *Proceeding of the XVth International Conf. Organic Coatings, Science and Technol.* 1989. Athens.
152. Geenhen, F.M., H.J.W. Lenderink, E.P.M. Van Westing, and J.H.W. De Wit. in *Proceedings FATIPEC Conference*. 1990. Nice.
153. Dings, M., R. De Longe, S.M. Peters, E.J.H. Koot, F.M. Greenhen, E.P.M. Van Westing, and J.H.W. De Wit. in *Proceedings FATIPEC Conference*. 1990. Nice.

154. Scheirs, J., S.W. Bigger, and N.C. Billingham, *Polymer Testing,* 1995. **14**(3): p. 211-241.
155. Gerlock, J.L., T.J. Prater, S.L. Kaberline, and J.E. De Vries, *Polymer Degradation and Stability,* 1995. **47**: p. 405.
156. Urban, M.W., *Vibrational Spectroscopy of Molecules and Macromolecules of Surfaces*. 1993, New York: John Wiley and Sons Ltd.
157. Smith, B.C., *Fundamentals of Fourier transform infrared spectroscopy*. 1996: Boca Raton : CRC Press.
158. Murphy, B., P. Kirwan, and P. McLoughlin, *Vibrational Spectroscopy,* 2003. **33**(1-2): p. 75-82.
159. Gulmine, J.V., P.R. Janissek, H.M. Heise, and L. Akcelrud, *Polymer Testing,* 2002. **21**(5): p. 557-563.
160. Gugumus, F., *Polymer Degradation and Stability,* 1996. **52**(2): p. 131-144.
161. Urban, M.W., *Journal of Coatings Technology,* 1987. **59**(745): p. 29-34.
162. Almeida, E., M. Balmayore, and T. Santos, *Progress in Organic Coatings,* 2002. **44**(3): p. 233-242.
163. Rosencwaig, A., *Photoacoustics and Photoacoustic Spectroscopy*. 1980, New York: Wiley.
164. Bertrand, L., *Applied Spectroscopy,* 1988. **42**(1): p. 134-138.
165. Gijsman, p., j. Hennekens, and K. Janssen, *Advances in Chemistry Series: Polymer Durablity,* 1996. **37**: p. 621.
166. Singh, R.P., J. lacoste, R. Arnaud, and J. Lemaire, *Polymer Degradation and Stability,* 1988. **20**.
167. Satoto, R., W.S. Subowo, R. Yusiasih, Y. Takane, Y. Watanabe, and T. Hatakeyama, *Polymer Degradation and Stability,* 1997. **56**(3): p. 275-279.
168. Gerlock, J.L., C.A. Smith, E.M. Nunez, V.A. Cooper, R. Liscombe, and D.R. Cummings, *Adv. Chem.series, Polymer Durability,* 1996. **249**: p. 335.
169. Gesenhues, U., *Polymer Degradation and Stability,* 2000. **68**(2): p. 185-196.
170. Fechine, G.J.M., M.S. Rabello, and R.M. Souto-Maior, *Polymer Degradation and Stability,* 2002. **75**(1): p. 153-159.
171. Khabbaz, F., A.-C. Albertsson, and S. Karlsson, *Polymer Degradation and Stability,* 1998. **61**(2): p. 329-342.
172. Setnescu, R., S. Jipa, and Z. Osawa, *Polymer Degradation and Stability,* 1998. **60**(2-3): p. 377-383.
173. Khabbaz, F., A.-C. Albertsson, and S. Karlsson, *Polymer Degradation and Stability,* 1999. **63**(1): p. 127-138.
174. Valadez-Gonzalez, A., J.M. Cervantes-Uc, and L. Veleva, *Polymer Degradation and Stability,* 1999. **63**(2): p. 253-260.
175. Allen, N.S. and M. Edge, *Fundamentals of Polymer Degradation and Stabilisation.* 1992: Chapman and hall, Chichester.
176. Allen, N.S., M. Edge, T. Corrales, A. Childs, C. Liauw, F. Catalina, C. Peinado, and A. Minihan, *Polymer Degradation and Stability,* 1997. **56**(2): p. 125-139.
177. Fanton, E., A. Tidjani, and R. Arnaud, *Polymer,* 1994. **35**: p. 433.
178. Gugumus, F., *Polymer Degradation and Stability,* 1995. **49**(1): p. 29-50.
179. Gugumus, F., *Polymer Degradation and Stability,* 2002. **75**(1): p. 55-71.
180. Fanton, E., B. Pellereau, R. Arnaud, and J. Lemaire, *Polymer Photochemistry,* 1985. **6**(6): p. 437-451.

181. Costa, L., M.P. Luda, and L. Trossarelli, *Polymer Degradation and Stability,* 1997. **58**(1-2): p. 41-54.
182. Gijsman, P. and J. Sampers, *Polymer Degradation and Stability,* 1997. **58**(1-2): p. 55-59.
183. Lee, A.W., J.P. Santerre, and E. Boynton, *Biomaterials,* 2000. **21**(8): p. 851-861.
184. Ciuprina, F., G. Teissedre, and J.C. Filippini, *Polymer,* 2001. **42**(18): p. 7841-7846.
185. Kurtz, S.M., O.K. Muratoglu, F. Buchanan, B. Currier, R. Gsell, K. Greer, G. Gualtieri, R. Johnson, S. Schaffner, and K. Sevo, *Biomaterials,* 2001. **22**(13): p. 1731-1737.
186. McLaughlin, W.L., J. Silverman, M. Al-Sheikhly, W.J. Chappas, L. Zhan-Jun, A. Miller, and W. Batsberg-Pedersen, *Radiation Physics and Chemistry,* 1999. **56**(4): p. 503-508.
187. Haider, N. and S. Karlsson, *Polymer Degradation and Stability,* 1999. **64**(2): p. 321-328.
188. Uhniat, M., M. Sudol, and S. Kudla, *Polymer Degradation and Stability,* 2000. **71**(1): p. 75-82.
189. Akay, G. and T. Tincer, *Polymer Engineering and Science,* 1981. **21**(1): p. 8-17.
190. Akay, G., T. Tincer, and H.E. Ergoz, *European Polymer Journal,* 1980. **16**: p. 601-605.
191. Jakubowicz, I., D. Gardiner, S. Jamtvedt, D. Kockoott, M. Schlosser, and P. Trubiroha, *Polymet Testing,* 2000. **19**: p. 729-753.
192. Christensen, P.A., A. Dilks, T.A. Egerton, and E.J. Lawson, *Journal of Materials Science,* 2002. **37**: p. 1-9.
193. Christensen, P.A., T.A. Egerton, E.J. Lawson, and J. Temperley, *Journal of Materials Science,* 2002. **37**(17): p. 3667-3673.
194. Dilks, A., *Pure and Applied Studies of the Photodegradation of Titanium Dioxide Pigmented Paint Film*. 1999, *University of Newcastle upon Tyne PhD thesis*: PhD thesis.
195. O'Donnell, B. and J.R. White, *Journal of Materials Science,* 1994. **29**(15): p. 3955-3963.
196. Benachour, D. and C. Rogers, E., *Photodegradation and Photostabilization of Coating,* 1981. **17**: p. 263-274.
197. Davis, A. and D. Sims, *Weathering of Polymers*. 1983: Applied Science, Barking,.
198. Popov, A., N. Rapoport, and G. Zaikov, *Oxidation of Stressed Polymers*. 1991, New York: Gordon and Breach.
199. White, J.R. and A. Turnbull, *Journal of Materials Science,* 1994. **29**: p. 584-613.
200. Zhurkov, S.N., V.S. Kuksenko, and V.A. Petrov, *Doklady Akademii Nauk Sssr,* 1981. **259**(6): p. 1350-1353.
201. Zhurkov, S.N., V.A. Zakrevskyi, V.E. Korsukov, and A.F. Kuksenko, *Journal of Polymer Science A2,* 1972. **10**: p. 1509.
202. Fawcett, A.H., *Polymer Spectroscopy*. 1996, New York: John Wiley & Sons, Inc.

CHAPTER 2

EXPERIMENTAL

This chapter describes the experimental procedures employed in this work. The first part describes the materials and details of tensile test sample preparation, followed by exposure conditions and characterisations. The characterisation techniques used include (i) a novel *in-situ* FTIR method to measure the carbon dioxide generated during the UV-induced oxidation of various polymers and (ii) the conventional FTIR transmittance method to monitor the carbonyl group development during UV irradiation. A UV/Visible spectrophotometer was used to obtain the transmittance and absorbance of polymer films and neutral density filters. The second part describes tensile testing and analysis.

2.1 MATERIALS AND CHEMICALS

2.1.1 Polyethylene Film (PE)

The materials used in the study of pigment activity were based on a low density polyethylene, LDPE Riblène MR10 (Polimeri Europa). PE film samples containing titanium dioxide pigment of various kinds were tested. The TiO_2 pigments used included the rutile and anatase forms. Anatase is a photocatalyst for many reactions and can be expected to be a pro-degradant for the polymer matrix whereas rutile has less photoactivity. Surface coatings of various kinds are applied to reduce the photoactivity of TiO_2 and different commercially available and experimental rutiles were included in this study. The samples were provided by Huntsman Tioxide, (Calais, France) in the form of lay-flat, blow moulded tube with wall thickness ~ 100 μm. The pigmented samples all had a pigment loading of 5 phr (parts per hundred resin). The details of the PE films are listed in Table 2-1 for the first batch of samples, received in September 2000 and in Table 2-2 for a second batch of samples, received in February 2003.

Table 2-1 The polyethylene film based TiO_2 pigmented samples (batch 1) used in this study with information regarding crystal form and coating of the pigment.

Pigment	Crystal	Production process	Uncoated or coated
U-1	Unpigmented	Not applicable	
A-1	Anatase	Sulphate process	Coated: Al_2O_3
R1-1	Rutile	Sulphate process	Coated: Al_2O_3
R2-1	Rutile	Sulphate process	Coated: Al_2O_3
R3-1	Rutile	Chloride process	Coated: Al_2O_3/SiO_2
R4-1	Rutile	Chloride process	Coated: $Al_2O_3/SiO_2/ZrO_2$

N.B. U-1 represents a sample of unpigmented PE film supplied as part of batch 1 (-1); A represents anatase TiO_2 pigment and R1, R2-R4 are codes to replace the commercial names of different grades of rutile TiO_2 pigments. PE A-1 represents anatase pigmented PE film and the PE R1-1 expresses rutile R1 pigmented PE film.

Table 2-2 The polyethylene film based TiO_2 pigmented samples (batch 2) used in this study with information regarding crystal form and coating of the pigment.

Pigment	Crystal	Production process	Comments
U-2	Unpigmented		Blown film 100 μm
A-2	Anatase	Sulphate process	Coated: Al_2O_3
R1-2	Rutile	Sulphate process	Coated: Al_2O_3
R2-2	Rutile	Sulphate process	Coated: Al_2O_3
R3-2	Rutile	Chloride process	Coated: Al_2O_3/SiO_2
R4-2	Rutile	Chloride process	Coated: $Al_2O_3/SiO_2/ZrO_2$
R5-2	Rutile	Chloride process	Coated:Al_2O_3/SiO_2
R6-2	Rutile	Chloride process	Coated: Al_2O_3/SiO_2
R7-2	Rutile	Chloride process	Coated: Al_2O_3/SiO_2
R8-2	Rutile	Chloride process	Coated: Al_2O_3/SiO_2
R9-2	Rutile	Chloride process	Coated: Al_2O_3/SiO_2
R2D	Rutile	Sulphate process	Coated: Al_2O_3 Drawn 250 μm
UD100	Unpigmented		Drawn film 100 μm
UD250	Unpigmented		Drawn film 250 μm

N.B. '-2' means batch 2. D represents the film made by drawn technique. R5-R9 are codes representing the commercial names of other different grades of rutile TiO_2 pigments in batch 2 samples. UD means unpigmented drawn film.

2.1.2 Polyvinyl chloride (PVC)

PVC can be made tough and rigid, in which case it is known as unplasticized PVC (PVC-U). Alternatively, by the inclusion of plasticizers, it can be made soft and flexible; in this form it is known as plasticized PVC (PVC-P). PVC samples were also supplied by Huntsman Tioxide as rectangles 10×15 mm^2 with thickness of 2 mm. These samples were made by dry-blending a batch containing all the PVC-U components except the TiO_2. The TiO_2 is added after melting the other ingredients on a two-roll mill. Dispersion of the TiO_2 is effected by cutting and remixing the softened PVC-U as it is being rolled. The details of PVC samples used in this study are listed in Table 2-3.

Table 2-3 Composition of the PVC sheet samples used in this study

Material \ Sample	PVC 1	PVC 2	PVC 3	PVC 4	PVC5
PVC resin S 6636	100.0	100.0	100.0	100.0	100.0
Harochem PDF (dibasic lead phosphite)	4.0	4.0	4.0	4.0	4.0
Harochem P28G (neutral lead stearate)	0.5	0.5	0.5	0.5	0.5
KM 323B	6.0	6.0	6.0	6.0	6.0
K 175	1.5	1.5	1.5	1.5	1.5
Omyalite 95T ($CaCO_3$ filler)	6.0	0.0	0.0	0.0	6.0
Loxiol G60	0.6	0.6	0.6	0.6	0.6
Wax PE 520	0.0	0.0	0.0	0.0	0.0
Stavinor CA PSE (calcium stearate)	0.3	0.3	0.3	0.3	0.3
Uniwax 1750 (stearic acid)	0.2	0.2	0.2	0.2	0.2
Loxiol G30	0.9	0.9	0.9	0.9	0.9
TiO_2 R1 (SAF R20)	3.0	3.0	**0.0**	**9.0**	**0.0**
TiO_2 R3 (H101335/50)	0.0	0.0	0.0	0.0	**3.0**

(Composition concentration in phr, differences from PVC 1 highlighted in **bold**)

2.1.3 Saturated Salt Solution

The saturated salt solutions[1] employed to give known humidities in the gas-phase atmosphere were copper (II) sulphate pentahydrate (Aldrich), sodium nitrite (Aldrich) and acetic acid potassium salt (Aldrich). Water used in all experiments was supplied by a Milli-Q water purification system (Millipore Corp.) with resistivity > 18 MΩ cm.

2.2 SAMPLE PREPARATION

2.2.1 *In-situ* Samples

The polymer samples employed in the gas-phase experiments to measure CO_2 evolution under UV irradiation were received from the industrial sponsor. The samples, which were used for the research measurements, were cut from blown film into discs (*ca.* 0.55 cm^2, 0.1 mm thickness and weight of 11 ± 1 mg) with the aid of a steel punch. The details of composition have been described in section 2.1.

2.3 UV IRRADIATION - ULTRAVIOLET SOURCES

2.3.1 In *In-situ* FITR Spectroscopy Studies

Although UV accounts for only about 5% of the spectral composition of sunlight, it is responsible for most of the photochemical damage to polymeric material outdoors. To simulate the damage caused by sunlight it is not necessary to reproduce the entire spectrum of sunlight. It is only necessary to simulate this UV component.

A 150 W high-pressure Xenon arc lamp (Oriel) with broad band output from 300-800 nm was used as the source of UV radiation. The source was fitted with a 100 mm water filter to reduce sample heating effects. The spectral distribution of the radiation system was measured by using a UV-Visible Radiometer (Optronic Laboratories Model 730A) (see Figure 2-1). The UV light was projected onto the sample in the FITR compartment *via* a 1 m flexible light guide (Oriel, Model 77556), which was connected to the light source *via* a beam turning assembly fitted with a dichroic mirror, see Figure 2-2. The spectral distribution of irradiation falling on the specimen

in the dynamic FTIR cell for different filter combinations is given for different filter combinations.

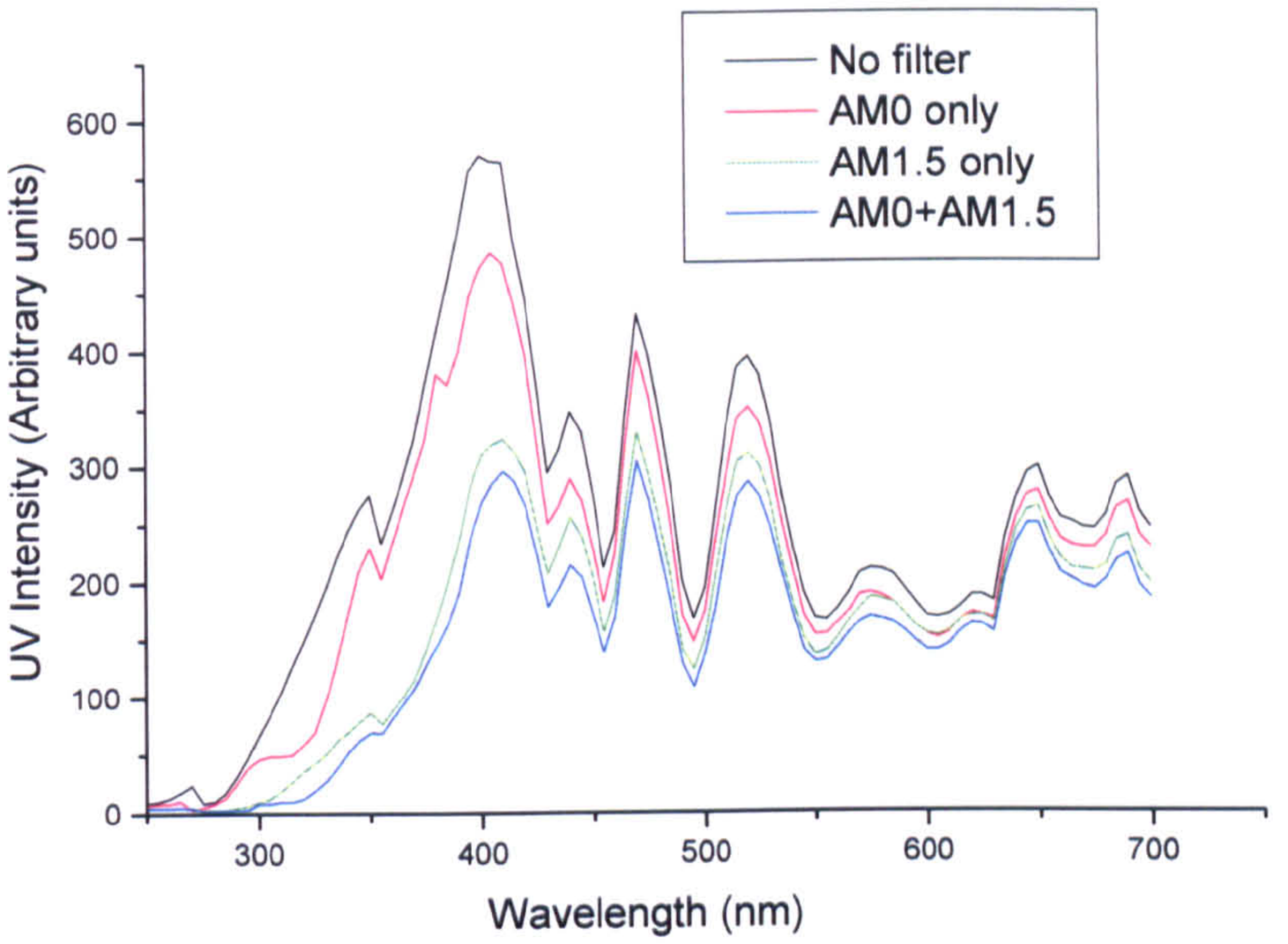

Figure 2-1 Spectral output from the 150 W Xenon lamp, fitted with a 100mm pathlength water filter, with and without the AM0 or AM1.5 or AM0+AM1.5 solar filter in place.

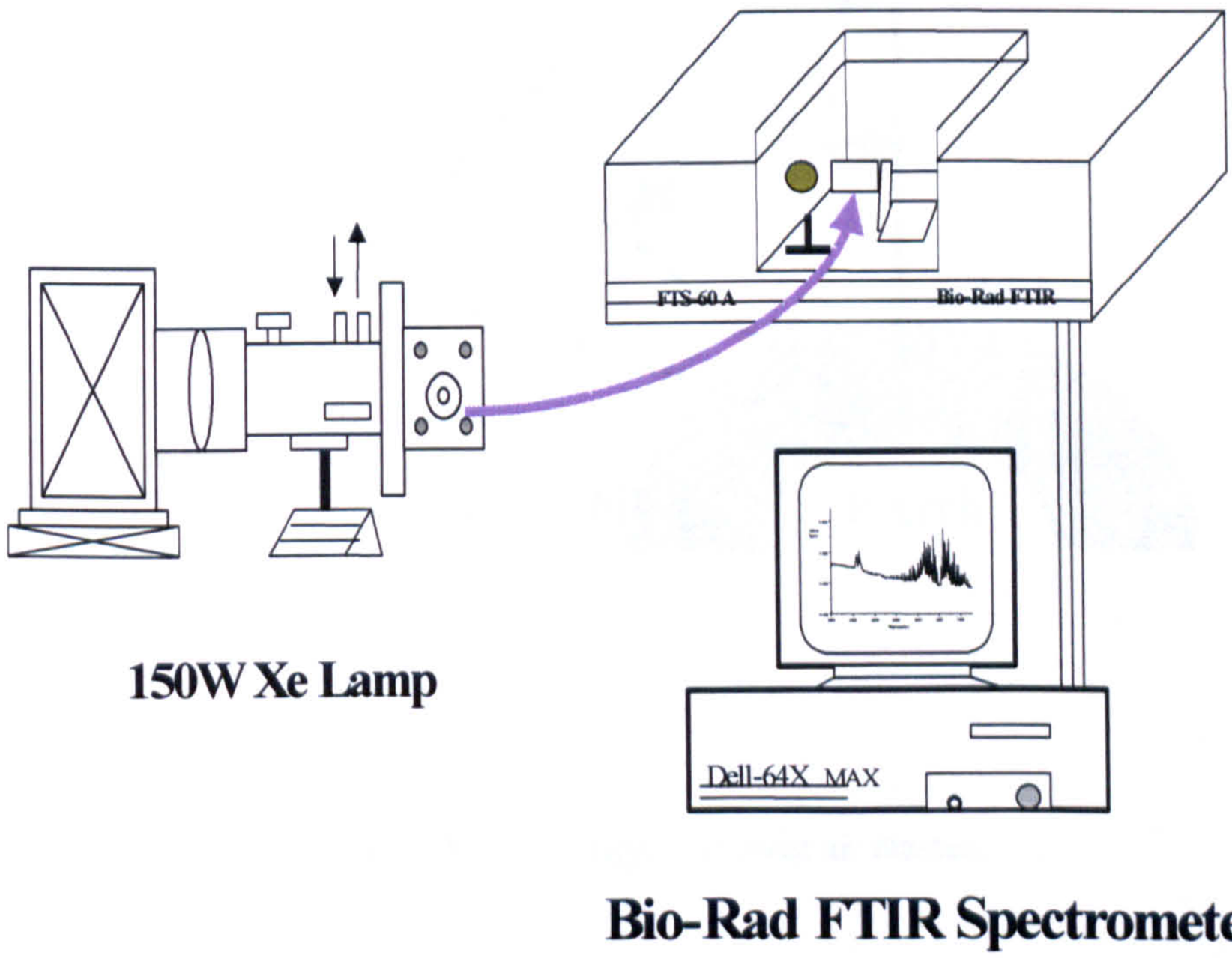

Figure 2-2 The light source and FTIR system used in the *in-situ* FTIR studies. The system consists of a Bio-Rad FTIR spectrometer and a 150 W high-pressure Xe lamp (Oriel) fitted with water and solar filters connected to a 1 m flexible optical guide *via* a beam turning assembly.

The solar filters were employed in order to modify the spectral output of the Xenon arc lamp to match specific natural solar conditions. A variety of filters known as air-mass (AM) filters fits into the filter holder. The spectral distribution required determined which air mass filters should be used. The direct radiation that reaches the ground from the sun passes through the atmosphere *i.e.* the air-mass, and the filters are designed to simulate this. Some of the common air-mass filters are shown in Figure 2-3 with their corresponding Zenith angles. AM0 corrects the output of a xenon lamp to better match the solar spectrum found outside the earth's atmosphere. AM1.5 Direct simulates the direct solar spectrum when the sun is at a zenith angle of 48.2° which is an American Standard Test Method (ASTM E891). It requires AM0 filter also. The (Oriel) AM filters which were employed for the *in-situ* studies were types AM1.5D or AM0, or the two combined together, as the experiments required.

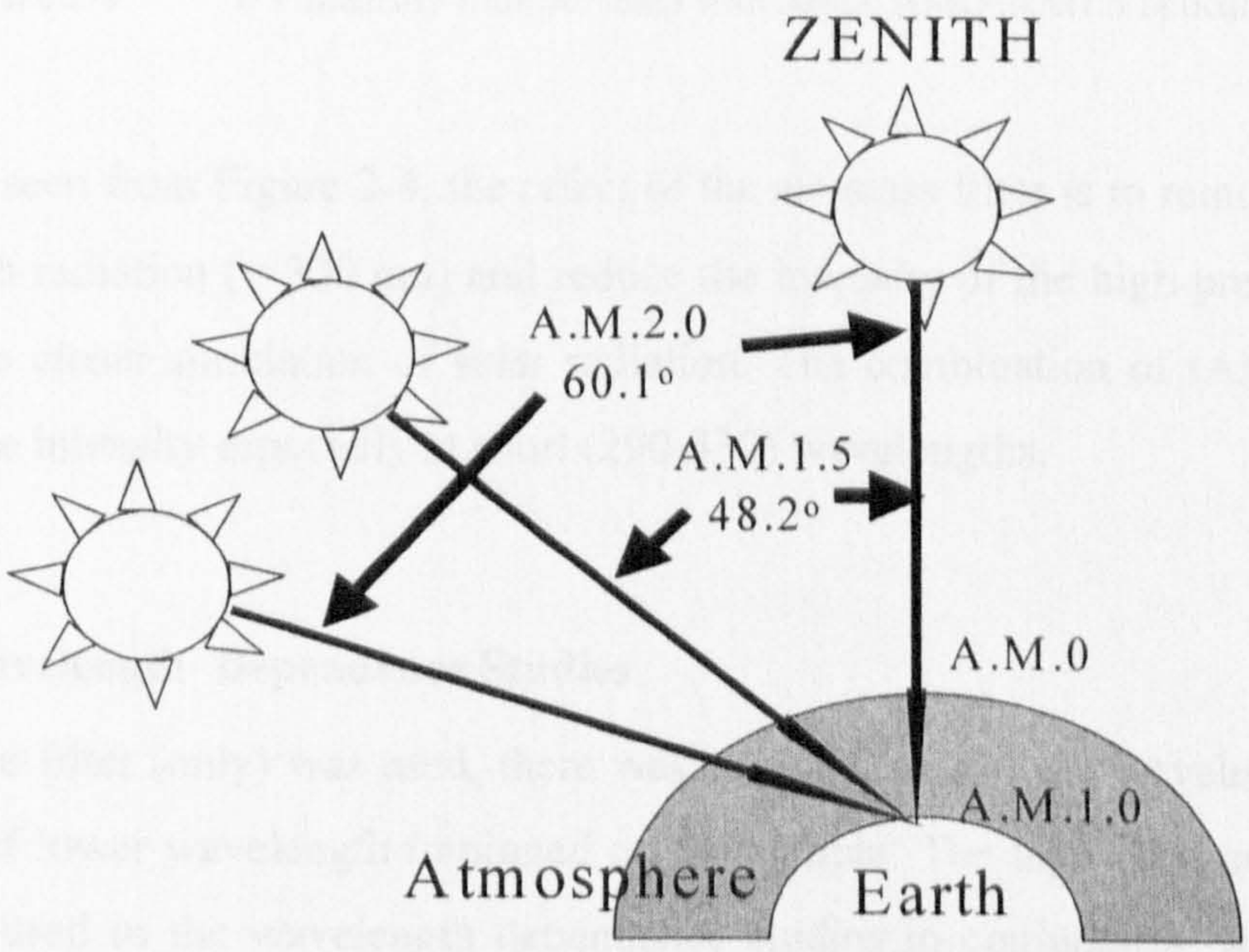

Figure 2-3 Diagram of solar air masses.

The effects of the AM0 and AM0+AM1.5D solar filter on the UV region of the lamp output can be clearly seen from Figure 2-4 below.

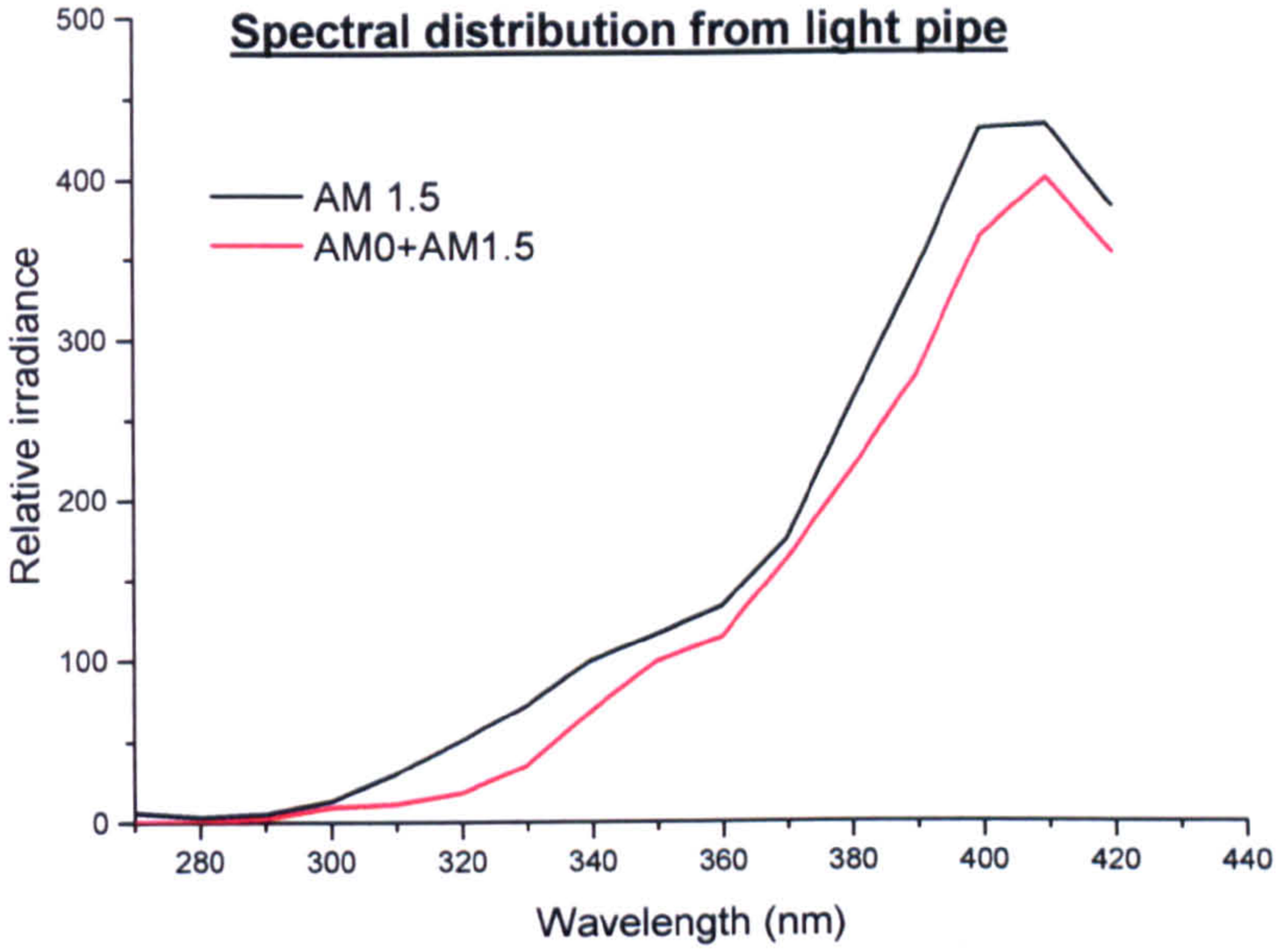

Figure 2-4 UV Intensity from Xe lamp with AMO, AMO+AM1.5 optical filter.

As can be seen from Figure 2-4, the effect of the air-mass filter is to remove the short wavelength radiation (< 300 nm) and reduce the intensity of the high-pressure xenon source into closer simulation of solar radiation. The combination of (AM0+AM1.5) changes the intensity especially at short (290-330) wavelengths.

2.3.2 Wavelength Dependence Studies

Even if one filter (only) was used, there was a cut off at 290 nm wavelength and no radiation of lower wavelength impinged on the sample. The high-pressure xenon arc lamp was used in the wavelength dependence studies in conjunction with different AM solar filter combinations. Unfiltered light gives shorter wavelength UV. Selected solar filters (AM0 or AM1.5) were used either singly or in combination to remove short wavelength UVC radiation. The more filters used, the more short wavelength UV light is removed. In these experiments different filters were used to select defined portions of the UV spectrum and the effects on carbon dioxide evolution rates were monitored. The output of the Xe lamp intensity was monitored during the course of experiments. It was stable in single run and relatively stable over short periods (see Table 2-4). The spectro-radiometer was used to give relative values of irradiance to monitor the effects of lamp age and filters. Results presented in any given graph

Table 2-4 UV Lamp Intensity Measurements:

Date	Time	Intensity× 10^{-8}(@350nm) AM0+AM1.5 W/cm^{2}nm		Intensity× 10^{-8}(@400nm) AM0+AM1.5 W/cm^{2}nm		Background (@350&400nm)
		Reading	True	Reading	True	
26/02/02	9:30	0.014	0.013	0.060	0.059	0.001
Tues	10:50	0.011	0.010	0.055	0.054	0.001
	10:55	0.011	0.010	0.060	0.059	0.001
	1:40(pm)	0.013	0.010	0.063	0.060	0.003
	2:30	0.012	0.011	0.062	0.061	0.001
	3:30	0.010	0.010	0.061	0.061	0.000
27/02/02	9:30	0.013	0.012	0.061	0.060	0.001
Weds	10:30	0.013	0.012	0.060	0.059	0.001
	12:00	0.013	0.012	0.063	0.062	0.001
	2:30(pm)	0.012	0.010	0.063	0.061	0.002
	3:10	0.015	0.010	0.073	0.068	0.005
28/02/02	10:30	0.013	0.012	0.060	0.059	0.001
Thurs	12:00	0.014	0.013	0.060	0.059	0.001
	1:30(pm)	0.013	0.012	0.060	0.059	0.001
	2:30	0.011	0.013	0.060	0.058	-0.002
1/03/02	9:30	0.011	0.011	0.056	0.056	0.000
Fri	10:30	0.015	0.012	0.060	0.057	0.003
	4:30(pm)	0.011	0.011	0.056	0.057	0.000-1

for a series of experiments are directly comparable, but those in different figures should not be compared directly, because of possible changes in light intensity associated with replacement of a failing lamp or because of changes in background levels of CO_2 associated with different vacuum greases used from one set of experiments to another. One source of fluctuation of UV intensity was the connection between the port of the Xe lamp and the head of the light pipe, which was not fixed. When the head of the light pipe was put into the port of the Xe lamp, there was a gap

causing the light entry direction change each time the connection was made. This problem was tackled by putting Sellotape on the head of the light pipe fitting to the port of the Xe lamp. During the course of this work it was discovered that the UV intensity fell significantly over a period of several months. Although suspicion was initially on the UV lamp, it was eventually discovered that the water filter cell windows had become contaminated. Although this allowed measurements to be made at different levels, the problem was eliminated by regular inspection, and cleaning whenever the intensity fell.

2.3.3 Light Intensity studies

The same Xe lamp described above was employed in the light intensity studies. The UV intensity was varied using neutral density filters (Oriel). Neutral density filters with 7%, 30% and 55% transmittance (see Figure 2-5), were positioned in series with the AM solar filters or without any AM filter as required.

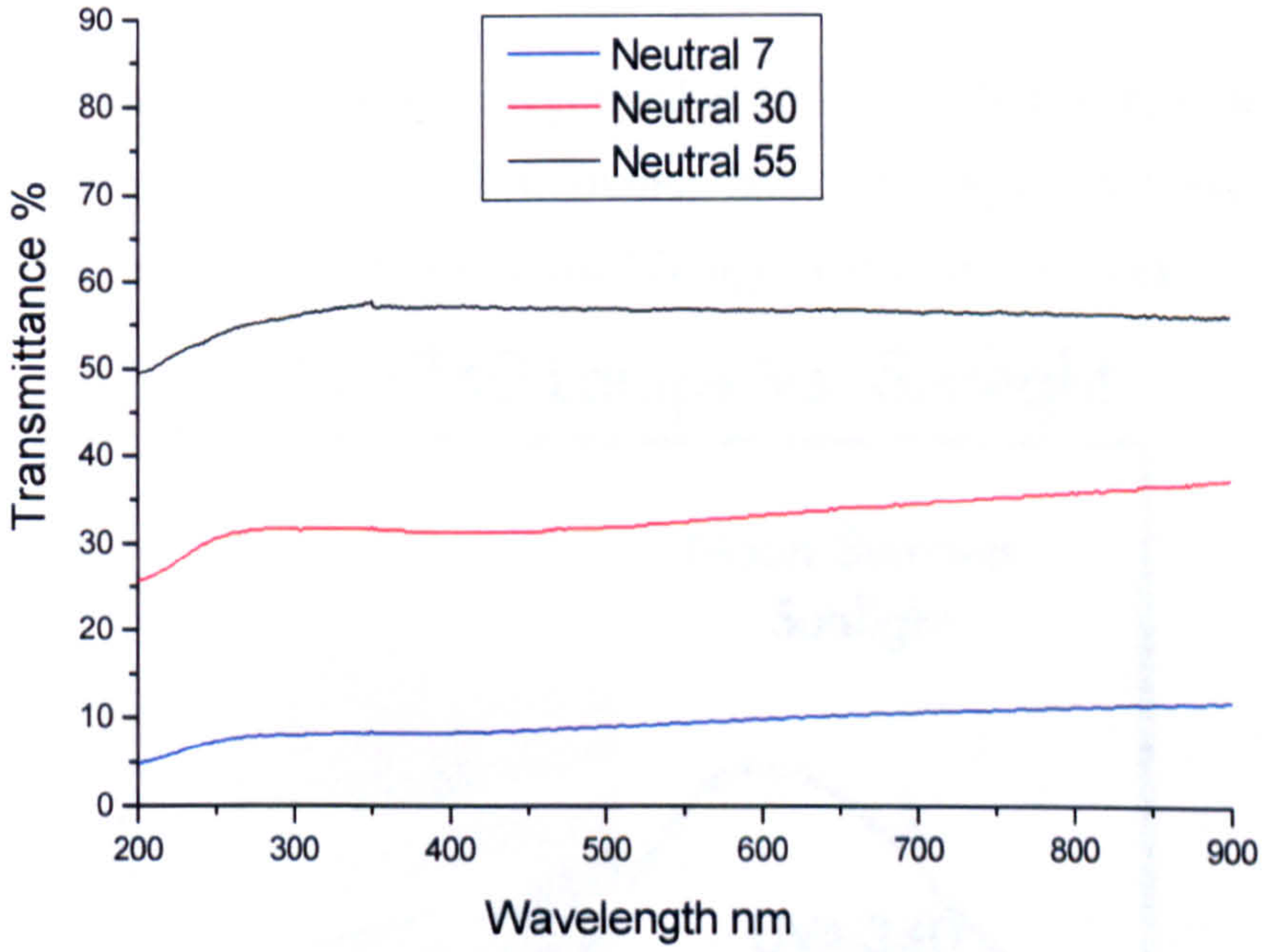

Figure 2-5 UV/Visible spectra of the neutral density filters used in the light intensity studies. Spectra were recorded on a Shimadzu UV 160A UV/Visible spectrophotometer operating at slow scan speed.

2.3.4 UV used in *Ex-situ* FTIR Transmittance Spectroscopy Studies

2.3.4.1. QUV machine- Accelerated Weathering Tester

For comparative *ex-situ* FTIR Transmittance Spectroscopy studies, most samples were irradiated in a QUV machine (Q-Panel Company, Cleveland, Ohio, USA). The QUV machine — the QUV Accelerated Weathering Tester is designed to provide laboratory simulation of the damaging forces of weather for the purpose of predicting the relative durability of materials exposed to the outdoor environment. Rain and dew are simulated by a condensation system. The damaging effects of sunlight are simulated by fluorescent UV lamps. Exposure temperature is automatically controlled, as is the daily sequence of UV periods and condensation periods [2].

The UV spectrum is divided into three regions:

— UV-A Region, 315 to 400 nm wavelength

—UV-B Region, 280 to 315 nm

—UV-C Region, below 280 nm

Fluorescent UV lamps are usually categorized as UV-A or UV-B lamps, depending on the region into which most of their output falls. The type UVA-340 lamp was employed in all *ex-situ* experiments as the UV light source in this work.

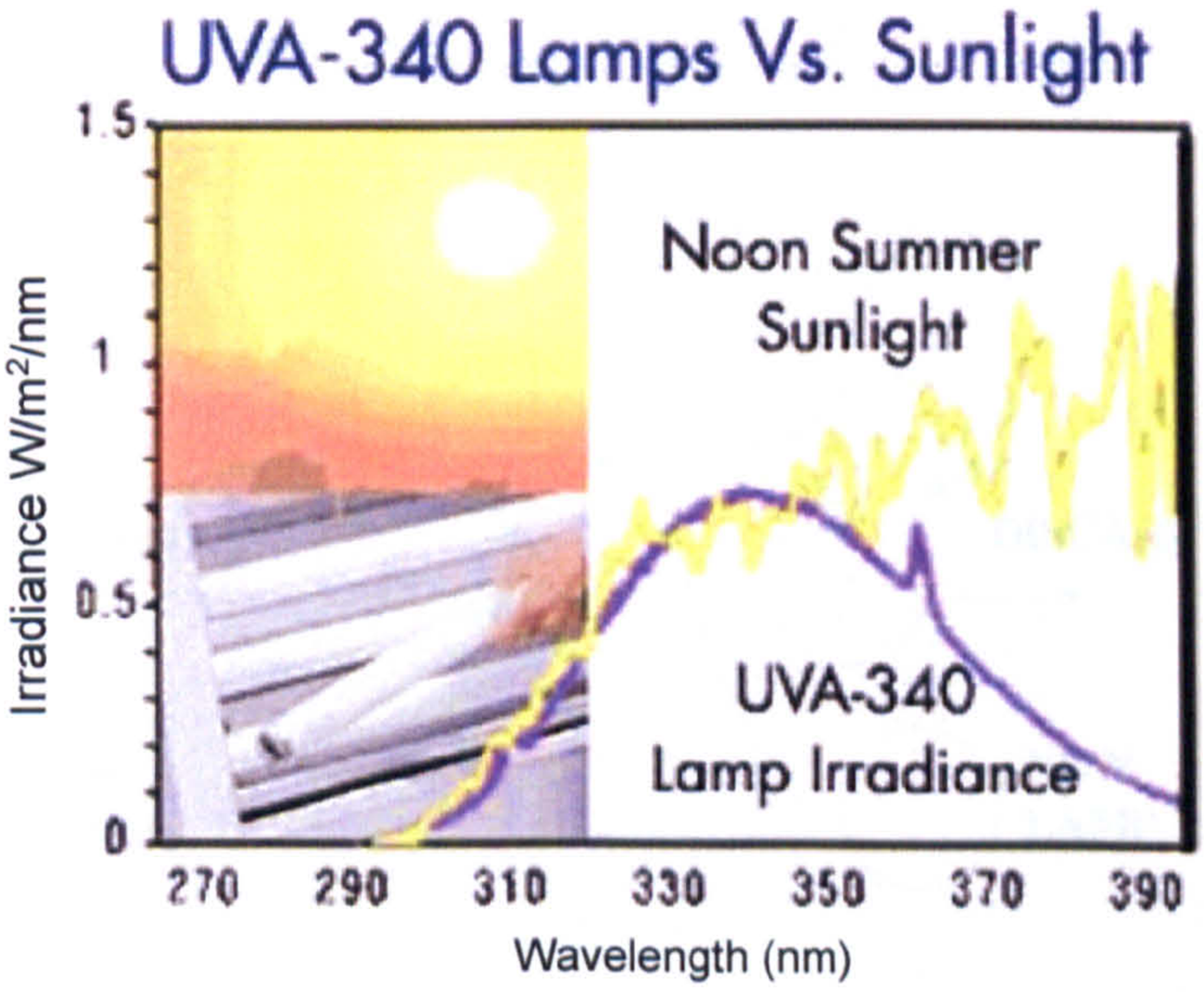

Figure 2-6 Output for UVA fluorescent tube compared with UV portion of sunlight (data from Q-Panel Company).

The UVA-340 lamp is claimed by Q-Panel company to give an excellent simulation of sunlight in the region from 365 nm down to the solar cut-off of 295nm. The UVA-340 produces only those UV wavelengths found in sunlight. The output of the tubes matches closely the UV portion of sunlight at the earth's surface as shown in Figure 2-6 above [3].

a). Lamp Aging and Replacement

The light energy of these UVA-340 fluorescent tubes decreases with time. During the first 100 hours of lamp's operation, there is a relatively rapid decline in output, followed by a more gradual decline over the remaining life. Tubes must be discarded after 1600 hours. However, the 8 tubes are not changed at one time, since this would cause a large fluctuation in radiation intensity. Instead, after every 400 hours of lamp operation, the oldest tube in each bank is discarded and a new tube installed. Thus, each bank will have lamps near the following ages: 0 hours, 400 hours, 800 hours, and 1200 hours. The total output from the bank is an average of several lamps, and does not change substantially with time. An interval of 400 hours of light operation works out to about 4 to 6 weeks, depending on the UV/Condensation cycle chosen. Every 400-450 hours of lamp operation, Q-Panel Company specifies that lamp location should be changed according to the scheme given below in Figure 2-7. After this is done, the lamp service time monitor should be reset to zero.

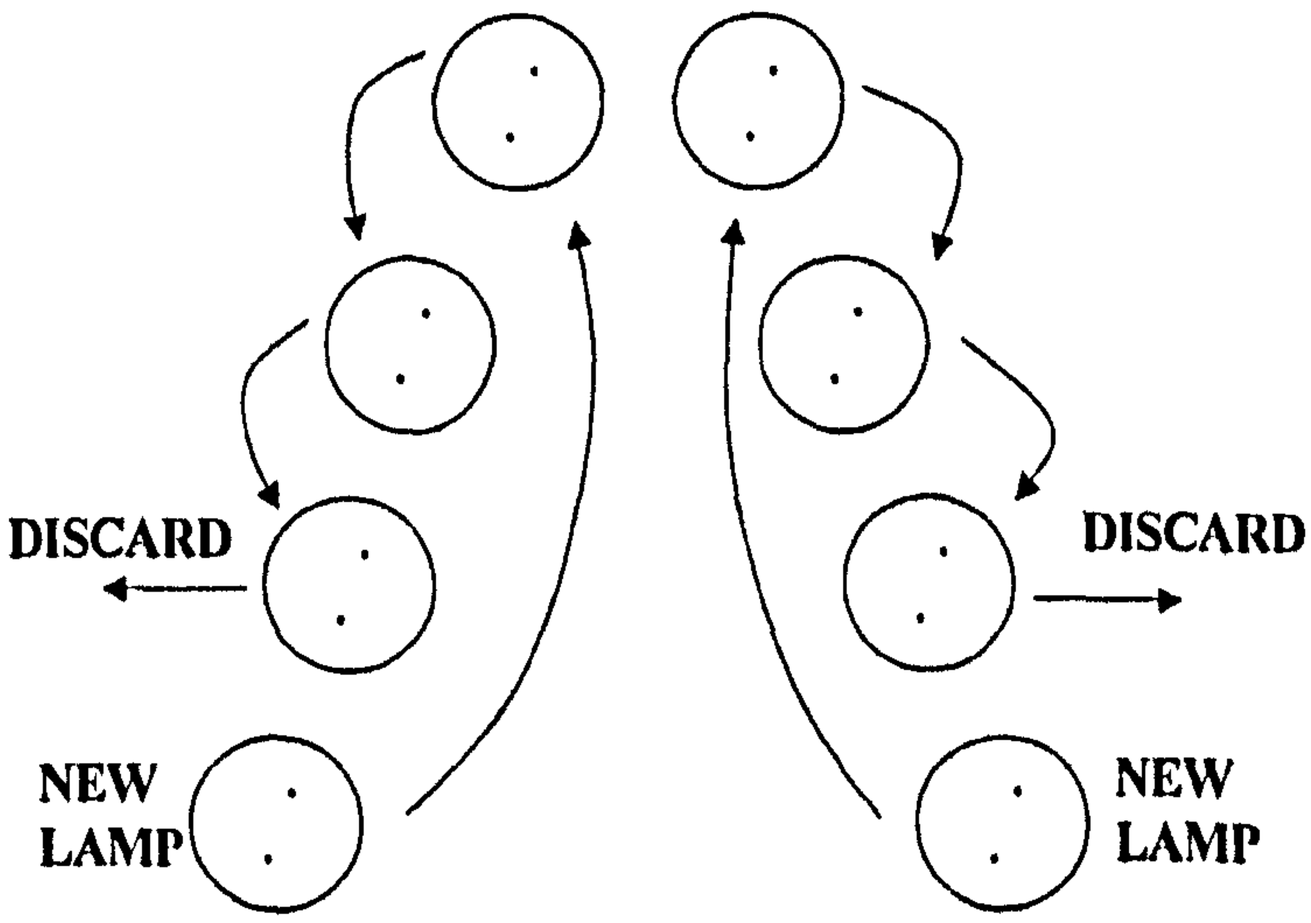

Figure 2-7 Scheme for replacing and rotating the UV lamps in the QUV machine.

b). Ultraviolet Exposure

The samples were exposed to UV radiation from fluorescent UVA-340 tubes in the QUV machine. The QUV machine was operated as a simple constant temperature enclosure set at 42° C (no temperature or humidity cycling). The lamps were cycled as described above. Normal samples (unstrained) were held on a standard panel holder containing 2 panels (75×150 mm) by a metal ring attached with a magnet plate (same size as the ring) put on the holder back (see Figure 2-8)

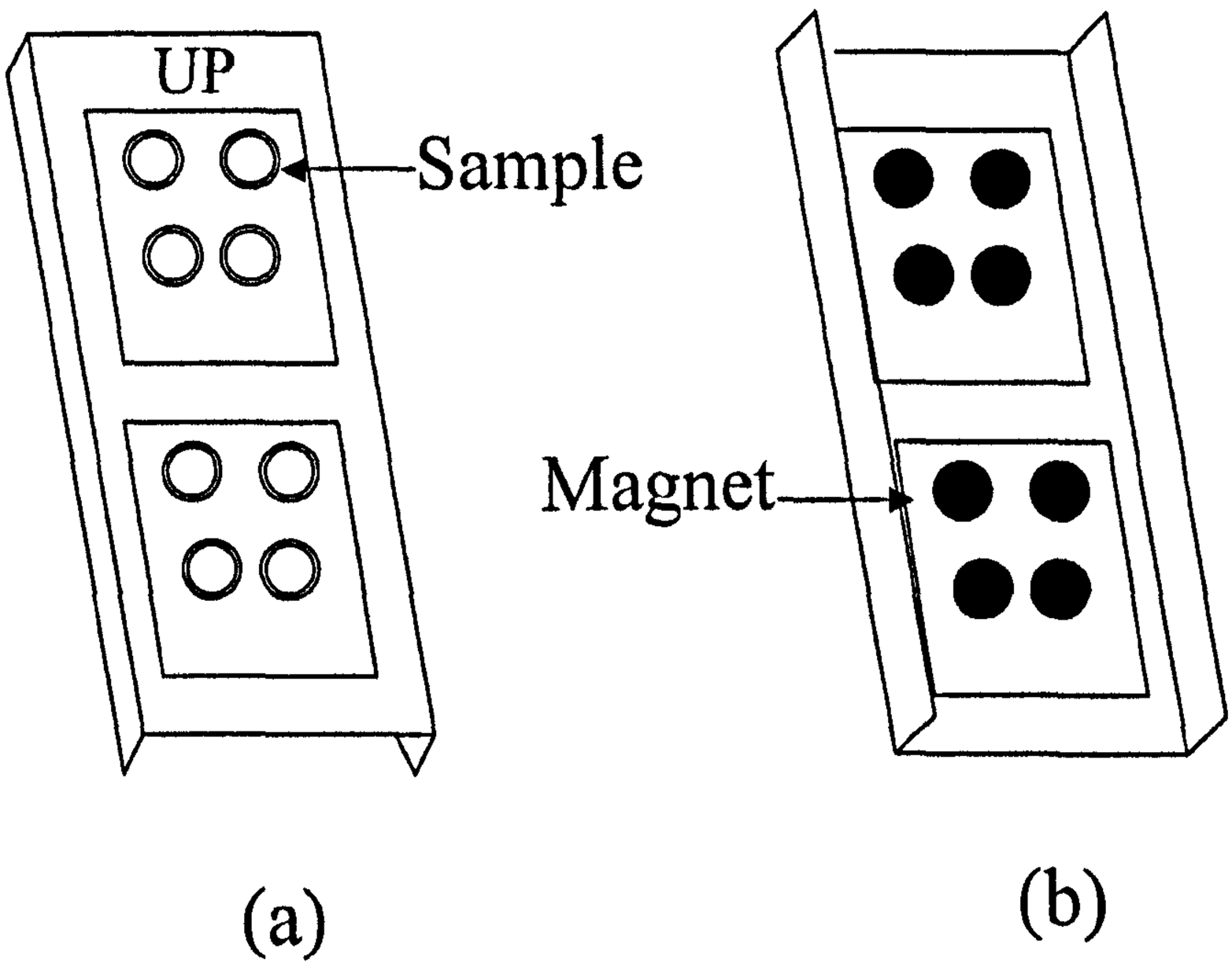

Figure 2-8 Showing samples were held on standard panel holder containing 2 panels (75×150 mm) by a metal ring attached with a magnet put on the holder back. (a) The face of panel with samples to the UV lamp. (b) The back of panel with glued magnet.

2.3.4.2. Room UV exposure procedure

A preliminary study was conducted using conventional methods to monitor carbonyl group development. The samples were exposed to UV radiation from fluorescent UVA-340 tubes supplied by Q-Panel Company (as shown in Figure 2-6).

The tubes were used in pairs and produced a uniform output over the central meter. The intensity of the radiation reaching the sample was controlled by adjusting the distance between the tubes and the sample surface. The tubes were replaced after about 8 months use when their output began to decay more rapidly, as checked using

a Bentham Spectroradiometer. All exposures were conducted in a constant temperature room at 30° C with fluctuation of ± 1.5°C. For continuously exposed samples open frames were used to hold the samples and tubes as shown below in Figure 2-9.

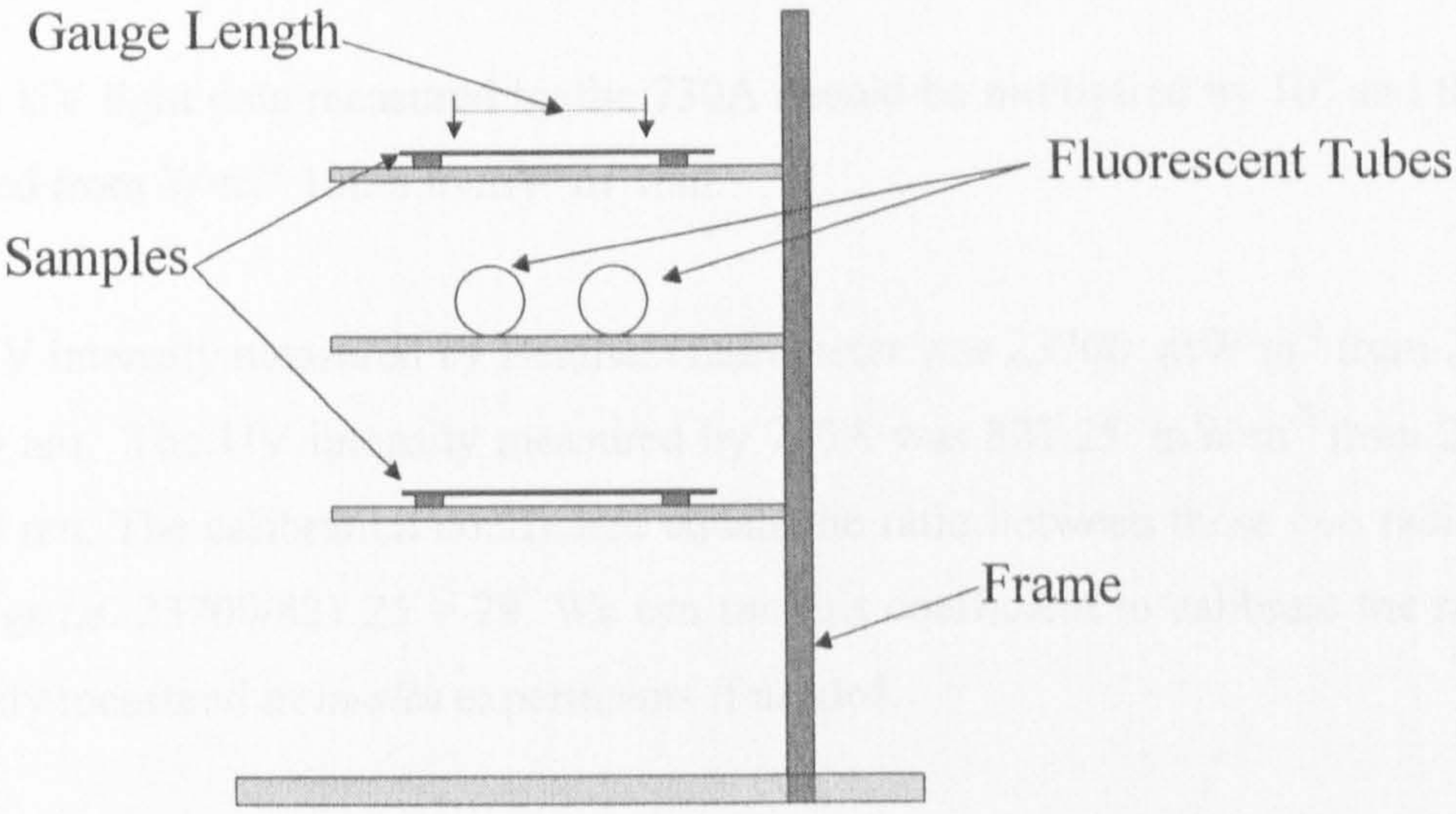

Figure 2-9 Apparatus used to hold samples and tubes during continuous exposure experiments in 'Room' UV exposure.

2.4 CALIBRATION OF 730A RADIOMETER:

A 730A radiometer was used for routine monitoring of lamp output (see section 2.3.1). The 730A radiometer was calibrated using a Bentham radiometer. Fluorescent tubes of type UVA-340 (Q-Panel Company) were used as the UV Radiation source. The distance between sensors of the both radiometer to the plane of two UV tube axes was 10 mm. The Bentham radiometer was calibrated using a standard lamp delivering wavelengths in the range 250-3000 nm (Bentham Instruments model CL2).

The measurement procedure is described as follows. The UV intensity at the position selected (10 mm from the axes of two tubes) was measured by the Bentham radiometer. The distribution of light spectra was recorded automatically with the Bentham radiometer using a step interval 5 nm. At the same time the UV intensity was integrated in units of $mW \cdot m^{-2}$ from 250 to 700 nm. The sensor of the 730A then

was replaced in the same position of the Bentham sensor. The readings were recorded with step interval 5 nm from 250nm to 700 nm in units of $W \cdot m^{-2} \cdot 10nm$.

Because: $W \cdot cm^{-2} \cdot (10nm)^{-1} = 10^6\ mW \cdot m^{-2} \cdot nm^{-1}$

So the UV light data measured by the 730A should be multiplied by 10^6 and the unit changed from $W \cdot m^{-2} \cdot 10nm$ to $mW \cdot m^{-2}.nm$.

The UV intensity measured by Bentham radiometer was 23700 $mW \cdot m^{-2}$ from 250 nm to 700 nm. The UV intensity measured by 730A was 821.25 $mW \cdot m^{-2}$ from 250 nm to 700 nm. The calibration coefficient equals the ratio between these two radiometer readings *i.e.* 23700/821.25 = 29. We can use this coefficient to calibrate the real UV intensity measured in *in-situ* experiments if needed.

2.5 FTIR SPECTROSCOPY STUDIES

2.5.1 The FTIR spectrometer

Infrared spectroscopy has long been recognised as a powerful tool for polymer characterisation. The uses of dispersive infrared spectroscopy for polymer studies have been clearly documented in the review by Krimm [4]. With the advent of FTIR spectroscopy numerous problems in the field of polymer physics and polymer analysis have become more readily accessible to spectroscopic investigation than with conventional dispersive instrumentation. The increased speed and higher signal-to-noise ratio of FTIR as compared to dispersive IR has lead to a substantially greater number of applications of IR in polymer research. This is a particular advantage for studies of pigmented films. The increasing use of *in-situ* infrared (IR) spectroscopy has been found not only in the study of degradation reaction of related polymers during both thermal and UV induced oxidation [5].

A Bio-Rad FTS-60A FTIR spectrometer was used for all experiments described in this thesis including *in-situ* monitoring of photogenerated gas phase carbon dioxide and *ex-situ* solid materials transmittance measurement. The Bio-Rad FTS-60A FTIR spectrometer uses a high-sensitivity, narrow band, liquid nitrogen cooled mercury

cadmium telluride (MCT) detector. Figure 2-2 shows the irradiation system incorporated in all studies of the *in-situ* volatile production (CO_2). As can be seen from Figure 2-2, the spectrometer control is a computer installed with Bio-Rad FITR software to communicate with the instrument. The absorbance spectra (100 scans at 4 cm^{-1} resolution) were recorded over the same period of time (5 hours) and, at the same time intervals of 20 minutes typically; the system also allowed versatile data handing and manipulation.

2.5.2 Advantages of Fourier transform techniques

The advantages of FTIR over dispersive IR spectroscopy have contributed to its widespread use. In conventional spectroscopy the light is dispersed and each wavelength is examined separately. Therefore the dispersive IR spectrometer takes a long time to obtain a spectrum of even the mid-IR range. The development of FTIR would have been impossible without the use of the Michelson interferometer, invented in 1880 by Albert Abraham Michelson[6]. The Michelson interferometer can scan all wavelengths simultaneously, unlike a dispersive instrument, which must examine them one at a time. But it was not until the late 1960s that the advent of fast computers allowed Fourier transform techniques to be routinely possible. This in turn led to a revolution in the use of infra-red spectroscopy as a chemical technique. The fundamental principle of the Michelson interferometer is introduced below.

The purpose of an interferometer is to take a beam of light, split it into two beams, and make one of the light beams travel a different path to the other. The operation of the interferometer is based on two plane mirrors which are mutually perpendicular, one is free to move and the other is fixed, and a beamsplitter which is placed between the two, at an angle of 45° (see Figure 2-10).

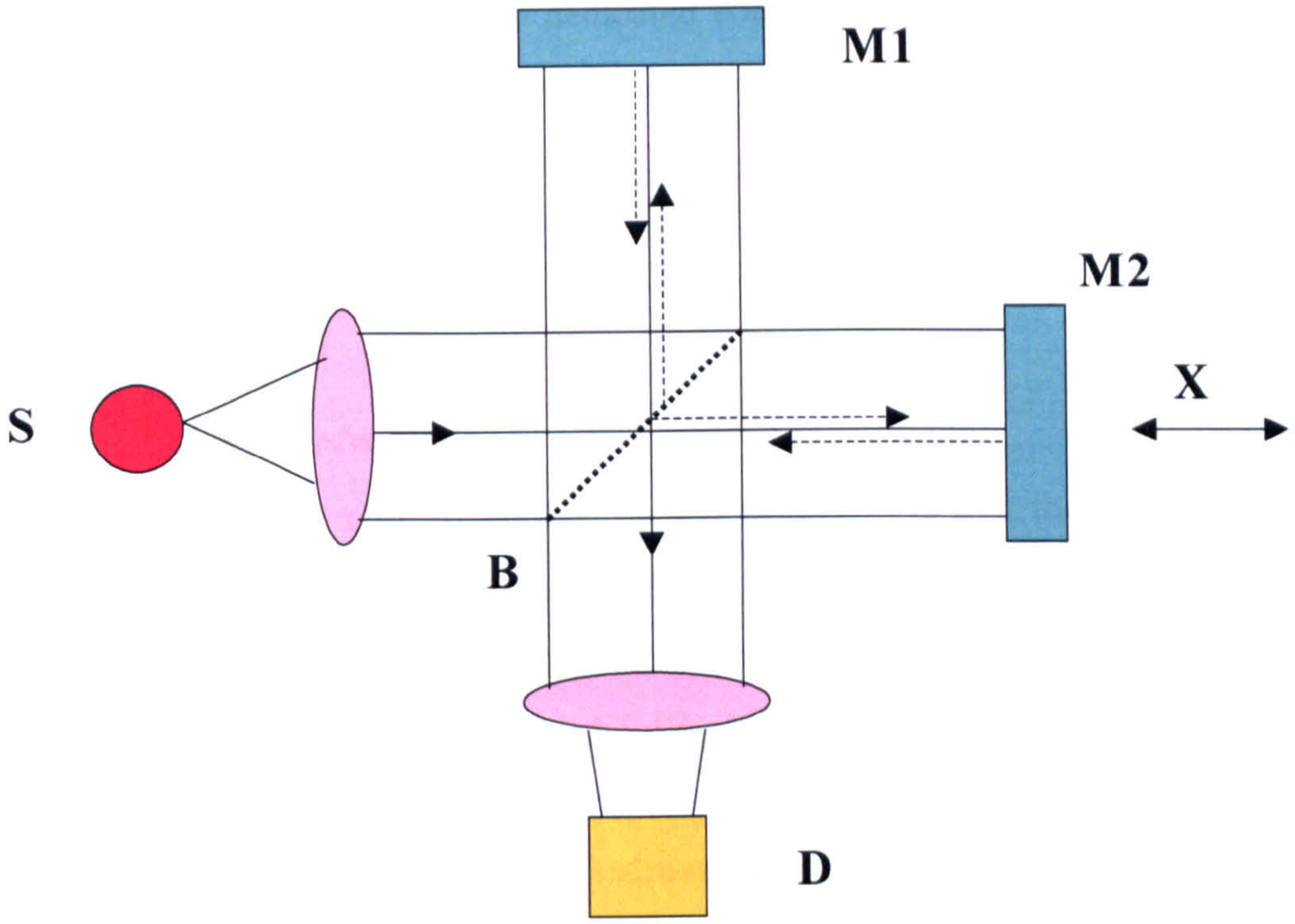

Figure 2-10 Schematic of a Michelson interferometer. S - source; D - detector; M1 - fixed mirror; M2 - movable mirror; X - mirror displacement, B-beamsplitter.

Collimated radiation from the source is directed into the interferometer and impinges on the beamsplitter. The beamsplitter is basically a thin film of germanium and allows 50% of the incident light to be transmitted to the fixed mirror and half to be reflected to the moving mirror. The two beams are reflected off the surfaces of the two mirrors, they recombine at the beamsplitter where constructive and destructive interference occurs depending on the position of the moving mirror with respect to the fixed mirror.

The interferogram is the resultant intensity at the detector after recombination and interference at the beam splitter. The resulting interference pattern for a monochromatic source is a modulated sine wave. For a broad band infrared source, the resulting pattern is the sum of the modulated sine waves at each frequency; in the presence of an absorbing sample the interferogram becomes modified. The superposition of waves of a range of amplitudes, frequencies and phases corresponds exactly to the mathematical operation known as a Fourier transform. The Fourier transform of a Fourier transform is the original function. Hence in a FTIR instrument, physical interference effects produce the first transform and then a Fourier transform

carried out on the interferogram by a dedicated computer gives the spectrum of the source modified by the detector response (both constant) and the sample.

There are 3 main advantages of the FTIR instrument over the dispersive instrument[6]:

1). Multiplex (Fellgett) advantage

One of the main defects with dispersive IR spectrometers is that these instruments have to scan each frequency individually with the use of a grating. Assuming it takes two seconds for each frequency to be completed, it could take several hours to obtain a spectrum of the mid-IR range. The FT-IR instrument can scan all frequencies simultaneously; it gains a significant speed advantage over dispersive instruments. In the two seconds it takes the dispersive instrument to collect just one frequency, the FTIR can collect the entire mid-IR range. The speed advantage is used both to look at rapidly changing samples and to improve sensitivity.

This speed advantage is useful to look at a sample that may be changing over time. It also offers a possibility to use '*in-situ*' monitors to follow reactions in real time. For rapid reactions and *in-situ* recorded spectra, FTIR is the only option - dispersive IR just is not fast enough.

The advantage of the increased speed coupled with the signal averaging ability of FTIR allows increased signal-to-noise ratio (SNR), that is, sensitivity, in a spectrum. If a time t_s is available for sampling in a dispersive IR spectrometer at a spectral resolution $\Delta\nu$ and for a spectral range ν_r, the time spent observing a resolution element $\Delta\nu$ is $t_{\Delta\nu}$, given by:

$$t_{\Delta\nu} = t_s \Delta\nu / \nu_r$$

For a constant resolution, the SNR is related to the number of scans added together [6]:

$$SNR \propto (N)^{1/2}$$

where N is the number of scans added together or time spent collecting data.

Therefore, the Fellgett or Mutiplex advantage M_A, is given by:

$$MA = (t_{\Delta\nu,FTIR}/t_{\Delta\nu,\ DISPERSIVE})^{0.5}$$
$$=(t_s/t_s\Delta\nu/\nu_r)^{0.5}$$
$$=(\nu_r/\Delta\nu)^{0.5}$$

2). Jacquinot's Advantage - Throughput

Dispersive instruments use slits in order to limit the frequency reaching the detector. This is the only means these instruments have of selecting which frequency is looked at, and the higher the resolution, the narrower the slit must be. Limiting the energy in this way means two things. First, the amount of energy reaching the detector is limited, so it may not be as sensitive as it could be. Secondly, if the sample is highly absorbing and transmits very little IR, the amount of energy actually reaching the detector is critical. FTIR systems have no slits and so can utilize their source output more efficiently to look at highly absorbing samples, low throughput samples and sampling accessories. For example, the Bio-Rad FTIR spectrometer used in these studies typically has a beam power of 112 mW in the sample compartment, whereas a dispersive instrument has a beam power < 2 mW [6]. In practice, the Jaquinot advantage is small at low resolution, when a dispersive instrument can use wide slits. The main advantage appears at high-resolution, when the slits must be narrowed or with strongly absorbing / scattering samples such as pigmented polymer.

3). Connes' advantage - Laser Sampling

A dispersive instrument has no way of knowing which frequency it is looking at. In order to be sure, it must be calibrated. Between the calibration tests the instrument may drift out of alignment. FTIR instruments avoid this calibration requirement by using a laser as an internal calibrator. The laser is used both to control the position of the moving mirror and to signal the capture of data. Because the frequency of the laser is known and dependable, the system always knows the exact location of every data point collected. The laser and source interferogram provide the spectrometer with the ability to calibrate the spectrum to a high degree of accuracy and precisely overlap spectra.

2.5.3 Data Manipulation[7]

In these studies the spectra were recorded as absorbance spectra, which represented a very convenient way in which to measure the amount of carbon dioxide produced from the photo-oxidation of the polymer samples or carbonyl group generated by UV irradiation in the polymer samples. When an interferogram is Fourier transformed, a single beam spectrum is obtained. A single beam spectrum is a plot of the raw detector response versus wavenumbers. A single beam spectrum obtained without a sample in the infrared beam is called a background spectrum. Different procedures were used for the measurement of gas-phase carbon dioxide and for measurement of carbonyl development in PE films. In the *in-situ* gas-phase experiments, a background spectrum contains the instrument and the environment contributions including a contribution from the cell internal atmosphere. In the carbonyl measurement, a background spectrum contains the instrument and the environment contributions only. To eliminate these contributions, the sample single beam spectrum is ratioed against the background spectrum to produce a transmittance spectrum. The absorbance spectrum can be calculated from the transmittance spectrum using the following equation.

$$A = -\log_{10} T$$

where: T = Transmittance; A = Absorbance.

So a background spectrum was recorded at the start of each section of the experiment in order to provide a reference to which the subsequent absorbance spectra could be normalised. This procedure allows changes with respect to a reference point to be obtained, thus giving rise to difference spectra with both positive and negative bands. Peaks pointing up (*i.e.* to + Abs.) are due to a gain in chromophore with respect to the background spectrum, and peaks pointing down (*i.e.* to –Abs.), are due to a loss of chromophore. The mathematical operation required to produce absorbance spectra was carried out automatically by the FTIR microcomputer.

2.5.4 Gas-phase Transmittance

FTIR analysis of gas phase carbon dioxide has been shown to be sufficiently sensitive to monitor quantitatively the evolution of carbon dioxide generated, either by the direct homogeneous oxidation, or indirectly by the UV induced heterogeneous photocatalytic degradation of acrylic emulsion paints pigmented with commercial grades of titanium dioxide pigments [5, 8-10]. The method was also postulated as offering a potentially simple and reliable technique to measure the durability of TiO_2 pigmented polymer (plastic) systems, given the high extinction coefficient of CO_2 in the infrared region. The work using the *in-situ* method was carried out with these polymers in the form of films or plates *etc*. At the heart of the equipment is a cell in which the sample is mounted and exposed to UV that arrives from a xenon lamp *via* a flexible light pipe and a calcium fluoride window. The preparation of the samples for the gas-phase experiment is as described previously in section 2.2. The cell employed in these studies is shown in Figure 2-11.

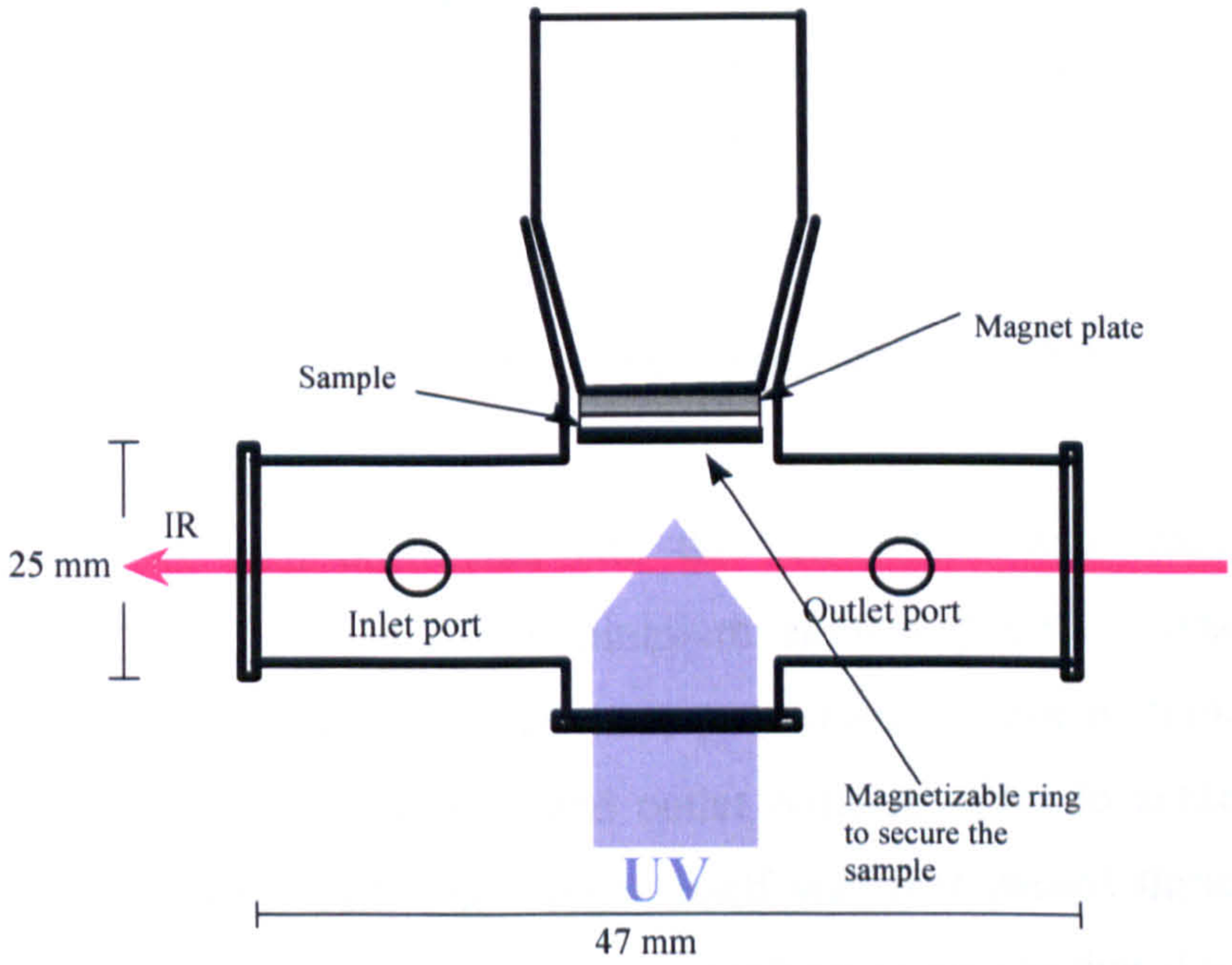

Figure 2-11 Schematic of the gas cell employed in the measurement of carbon dioxide gas from the UV-induced oxidation of polymer sample (side view).

During the research as detailed in section 2.6 various modifications to the cell were adopted, but the underlying approach remained the same. The cell that was fabricated from glass had an *ID* of 16 mm, path length of 47 mm and an internal volume, unless

otherwise stated, of 14 cm^3. The windows were all polished calcium fluoride windows (Crystran), 25 mm in diameter and 2 mm thick.

The sample, which was made into discs with the aid of a steel punch, was mounted in the gas-tight cell. A magnet substrate plate (13 mm Ø, 1.5 mm thickness) was glued on the head of a Quickfit cone (glass joint) then the sample disc was placed on the magnetic substrate plate and covered with a metal ring to clamp it on (see Figure 2-12).

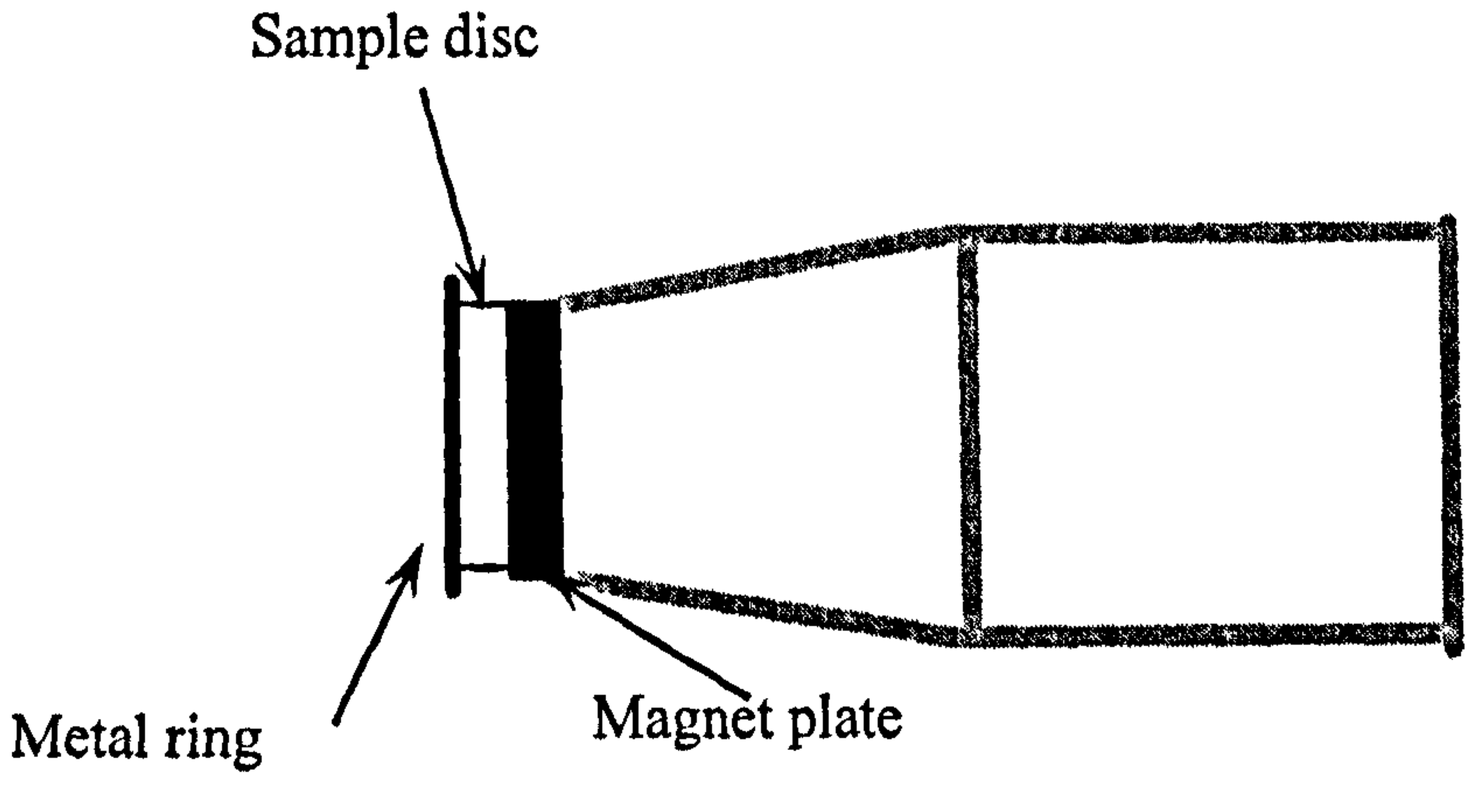

Figure 2-12 Showing sample clamped on the head of Quickfit cone.

The glass joint was then positioned into the cell sealed with vacuum grease (APIEZON or FOMBLIN) using the minimum amount possible consistent with adequate sealing. After assembly, the cell was purged for an hour with moist oxygen (BOC cylinder product) *via* the inlet and outlet ports in order to achieve a moist oxygen atmosphere in the cell. The oxygen itself was first passed through a water bubbler for half an hour and vented to the atmosphere to ensure that the residual air was purged out, see Figure 2-13. Humidity variations were achieved by using oxygen direct from the cylinder or passing it through a column of silica-gel.

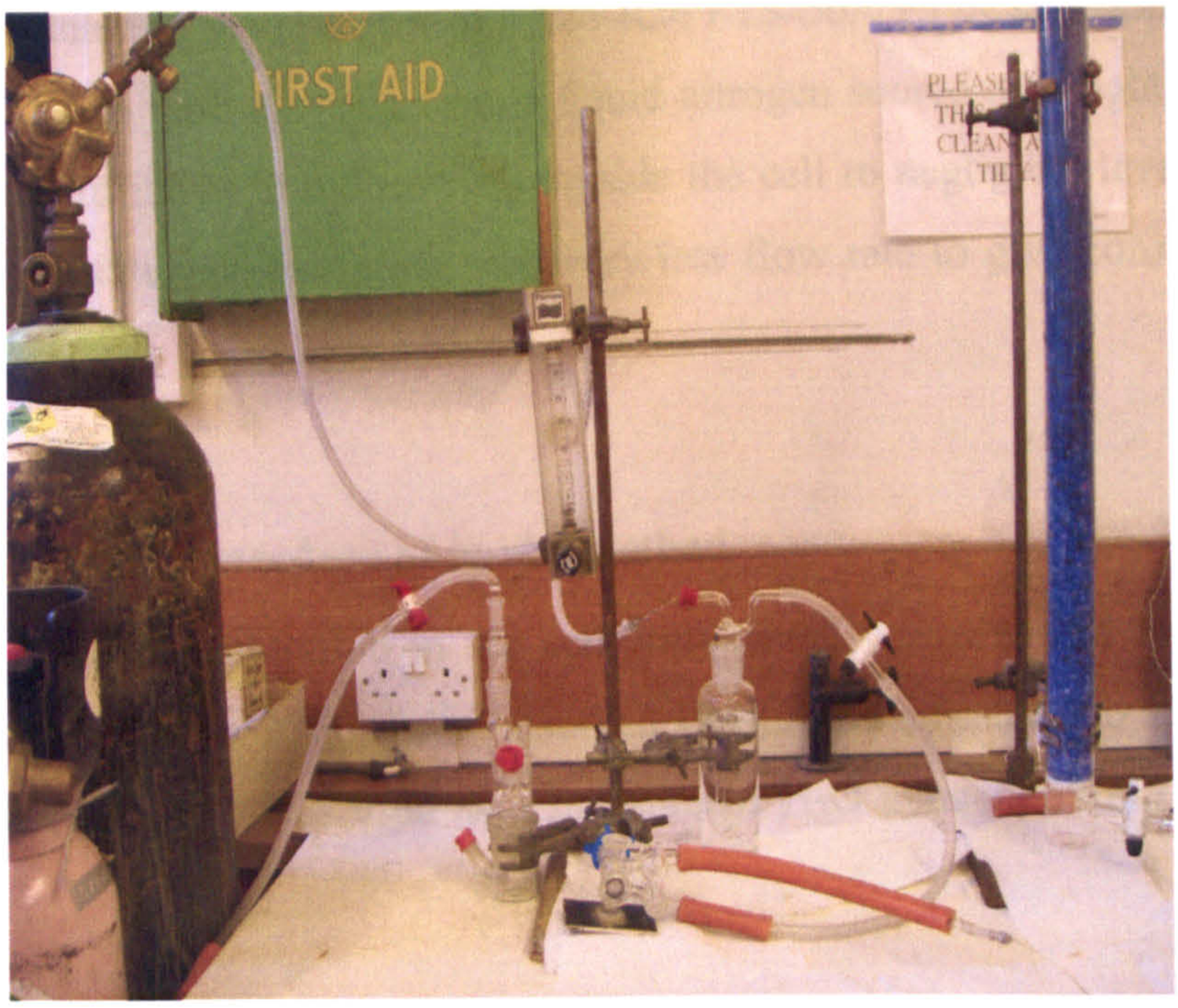

Figure 2-13 Picture showing the gas bubbler, silica-gel cylinder and gas-phase cell.

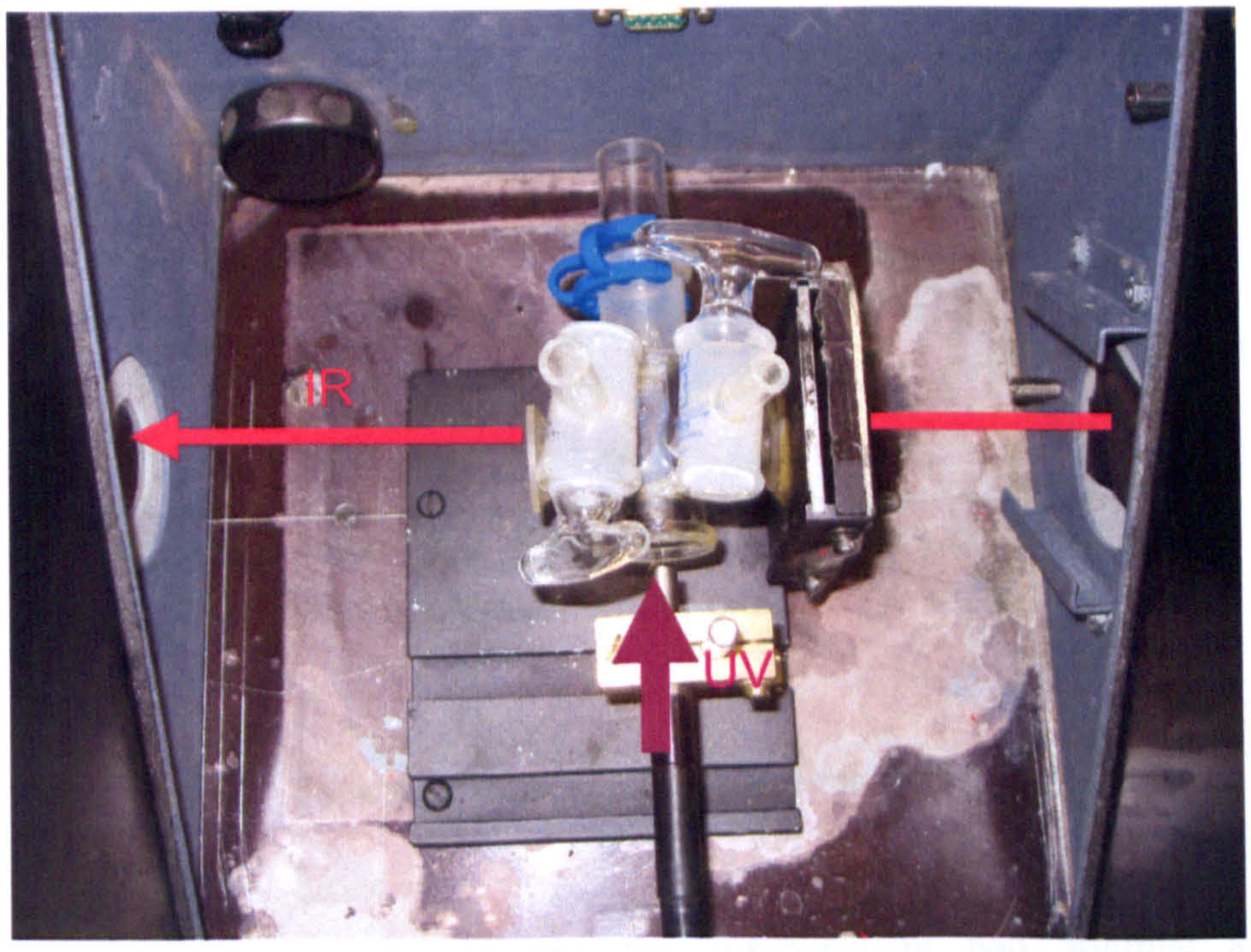

Figure 2-14 Picture showing the gas-phase cell and light pipe fixed in chamber.

Once the process of sparging was complete, the cell was positioned on the optical bench in the sample compartment of the FTIR. The flexible light guide was positioned such that the illuminated face was directly opposite the sample, see Figure 2-14. Then

the cell was mounted in the chamber of a Bio-Rad FTS-60A FTIR spectrometer. The chamber was flushed with nitrogen from a liquid nitrogen source overnight. Flushing for an hour was sufficient to reduce CO_2 outside the cell to negligible levels but the chamber had to be flushed overnight with very low flow rate to give constant water peaks in the IR.

2.5.5 Measurement Procedure of *in-situ* method

A measure of CO_2 concentration in the cell atmosphere was obtained from the IR absorbance peak height at 2360 cm^{-1}. Absorbance could be measured to 10^{-4}a.u. The peak height at 1560 cm^{-1} was used as a measure of H_2O concentration (see Figure 2-15).

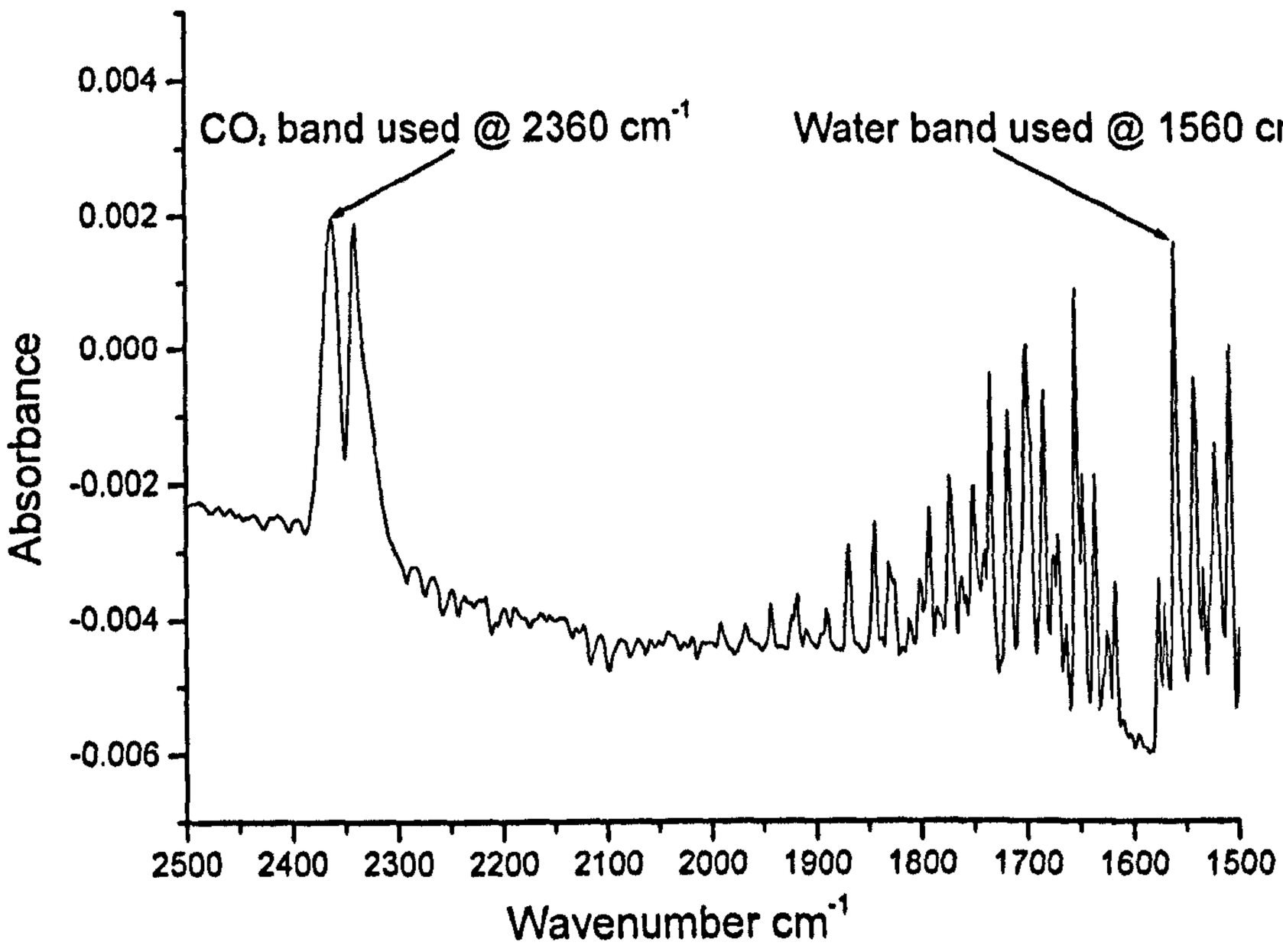

Figure 2-15 Typical gas-phase absorbance spectrum used in *in-situ* study.

After an hour flushing with nitrogen, the compartment had attained a stable atmosphere and the experiments were carried out. All spectra were averages of 100 scans, taken over ~40s, at 4 cm^{-1} resolution. A background (single beam) reference spectrum was recorded firstly in the dark and used to give a measure of the starting concentration of CO_2 and H_2O. Subsequent spectra were referenced to this. Sample

(absorbance) spectra were collected for one hour prior to UV exposure to measure any dark reaction or equipment leak. The light pipe was then connected to the UV source and the spectra of the evolution of CO_2 under UV were recorded. Generally the spectra were recorded at regular intervals over 3-4 hours. Finally, spectra were collected in the dark again to show whether changes continued and to check for leakage from the cell.

2.5.6 Moist Oxygen Atmosphere

Water and oxygen are two necessary constituents in the UV-induced photo-oxidation of polymeric materials. The importance of water has been highlighted in earlier work by this group on paint films [8, 9] and in particular they reported that degradation as a result of both accelerated and natural exposure was very slow in the absence of moisture. The purpose of the water bubbler system was to facilitate provision of high humidity to enhance the photo-oxidative process even though some moisture would be present in the gas cell without the use of the water sparge.

The water concentration in the gas cell was obtained by measuring the peak height at 1560 cm^{-1}, which is one of the rotational peaks in the water band, in the single beam reference spectrum prior to irradiation. It was not easy to measure and interpret the water absorbance specifically in terms of relative humidity in the cell because of the presence of residual low levels of water in the path of the infrared beam. Therefore to calibrate the water bands, the cell was purged with oxygen equilibrated to different, known, relative humidities by employing aqueous solutions saturated with different salts. The chemicals employed to produce the saturated salt solution are described in section 2.13. Table 2.5 shows values for the relative humidity of the saturated solutions [11] and the measured band intensity near 1560 cm^{-1} for the three solutions employed.

Table 2-5 The relationship between the relative humidity values for the saturated salt solutions employed and the corresponding water vapour band intensities near 1560 cm^{-1}, measured from the single beam reference spectrum of the gas cell atmosphere [11].

Salt solution	Relative humidity %	H_2O vapour band intensity near 1560 cm^{-1} / a.u.
$CuSO_4.5H_2O$	98	0.1411
$NaNO_2$	66	0.1148
CH_3COOK	20	0.0918

It shows that variations from 0.0918 to 0.1411 in the measured band intensity of the 1560 cm^{-1} feature corresponded to changes in relative humidity from 20 to 98 %. Using these data it is possible to plot a relative humidity vs. absorbance of water graph for the IR gas cell and this is shown in Figure 2-16.

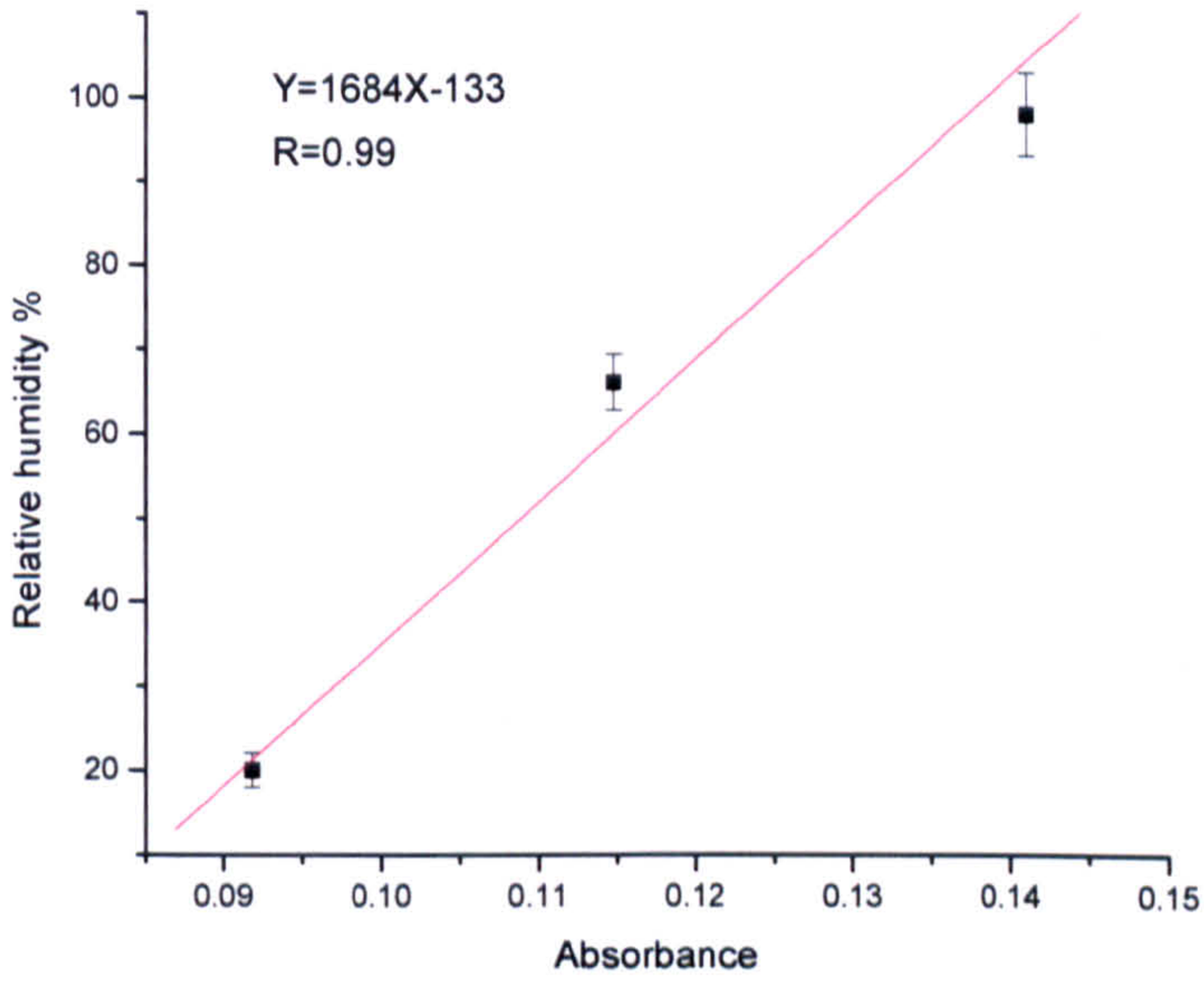

Figure 2-16 Response of relative humidity graph for the IR gas cell.

It is possible to calculate roughly the relative humidity in the gas cell using the above graph, but it was not possible to measure water peak development during photoreaction because the nitrogen used caused a small decrease with time.

2.5.7 Calibration of FTIR peak height for CO_2 pressure in the cell

It is known that for transmission FTIR the Beer's law relationship is valid [6]. The height of CO_2 absorbance at around 2360 cm^{-1} should be proportional to the pressure (concentration) of carbon dioxide of the cell. Experiments for Calibration of FTIR peak height for CO_2 pressure in the cell were conducted.

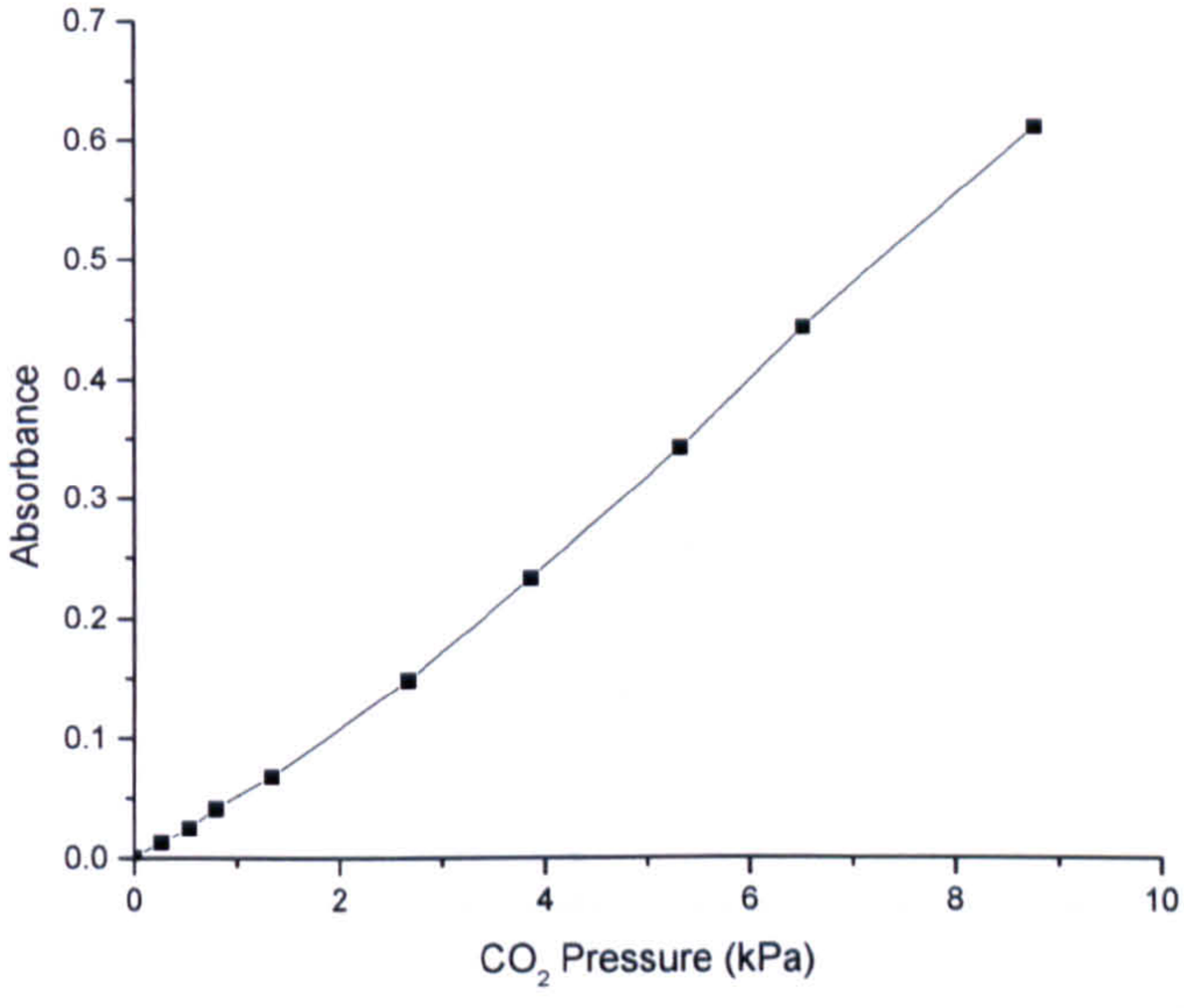

Figure 2-17 Graph showing absorbance CO_2 peak as a function of CO_2 pressure (Pa) (wide range) in the cell.

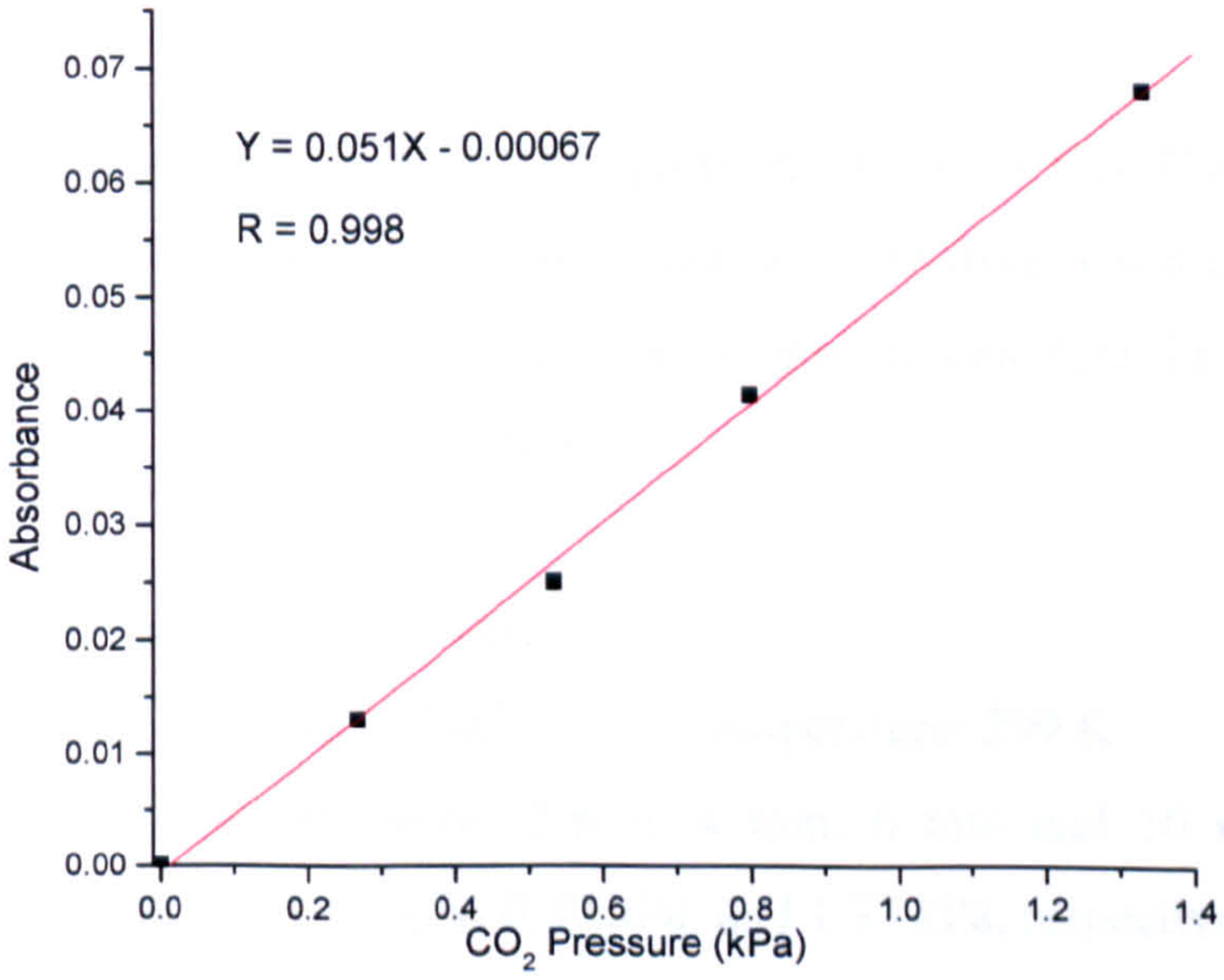

Figure 2-18 Graph showing linear fit absorbance of CO_2 peak as a function of CO_2 pressure (Pa) in experiment range.

Figure 2-17 shows the relationship between CO_2 absorbance with its pressure - *i.e.* its concentration in the cell. The CO_2 absorbance is fairly proportional to the pressure. Figure 2-18 show the expected linear relationship existing between CO_2 absorbance and its pressure in narrow range. The very narrow range from 0.001 to 0.1000 absorbance a.u. is relevant to *in-situ* experiments. The different pressures were achieved using a specially designed cell (see Figure 2-19). The cell firstly was evacuated to zero Pascal then filled with CO_2 gas to the experimental pressure.

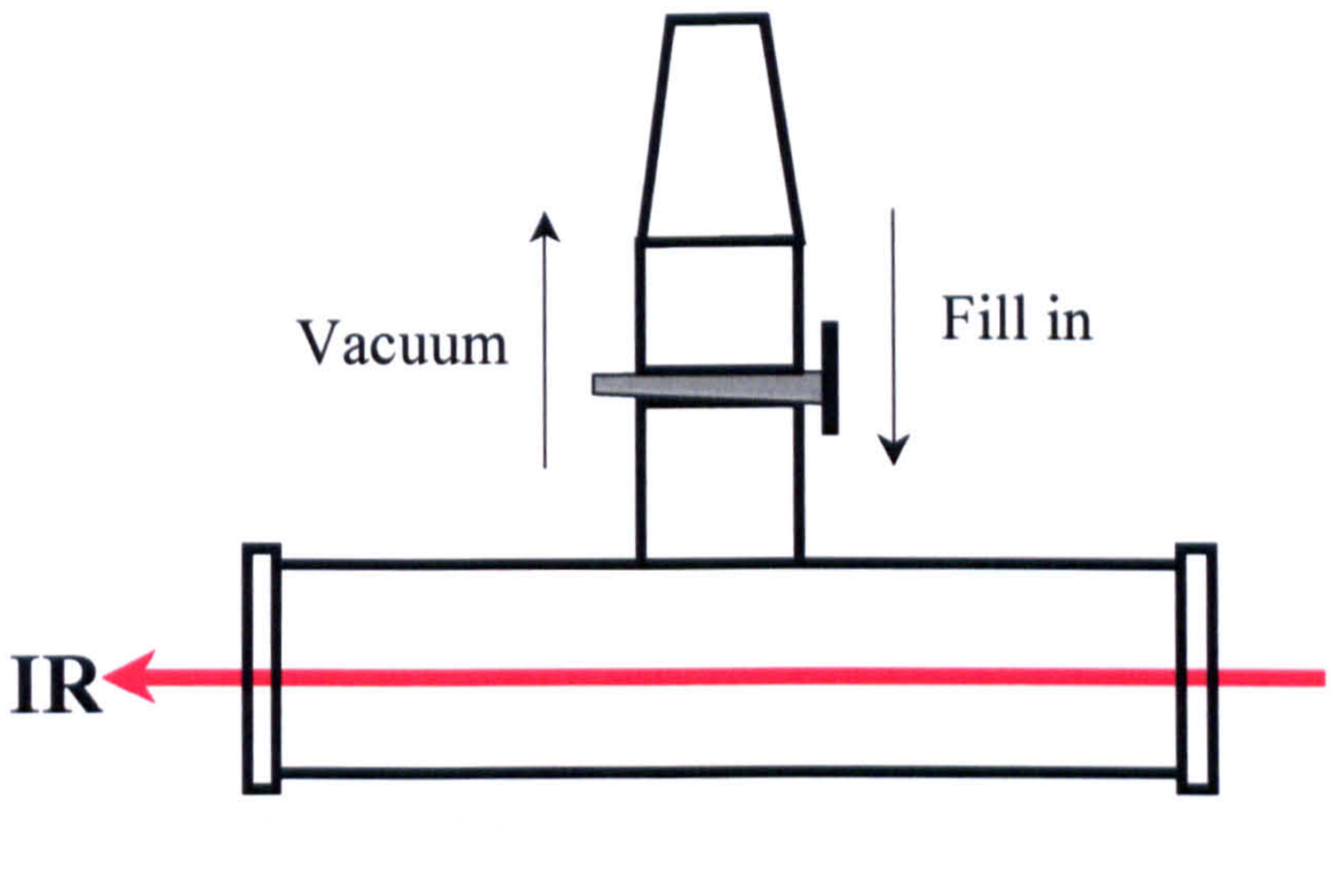

Figure 2-19 The cell used for measuring absorbance of CO_2 with different pressures.

The relationship of absorbance with CO_2 pressure in *in-situ* Gas-Phase experiment provides a method by which the carbon dioxide evolved from a real cell used in *in-situ* FTIR method can be calculated. A typical example to calculate the relationship of absorbance with CO_2 pressure is as follows.

The parameters for the experiment were:

Cell volume: $6.38\ cm^3 = 6.38\times10^{-6}\ m^3$ Temperature: 299 K

Pressures selected in the cell were: 2 mm, 4 mm, 6 mm and 10 mm ± 0.05 of mercury, roughly 0.26 kPa, 0.53 kPa, 0.80 kPa, and 1.33 kPa, respectively.

Assuming CO_2 behaves as an ideal gas.

$$PV = nRT \quad \text{where} \quad R=8.3145 J.mol^{-1}.K^{-1}$$

Hence, $n = PV/RT$

Thus if P = 0.53 kPa:

$$n_{CO_2\,(0.53\ kPa)} = 530\ Pa \times 6.38\times10^{-6} m^3 / 8.314 J\cdot mol^{-1}\cdot K^{-1} \times 299K$$
$$= 1.36\times10^{-6}\ mol$$

The experimental data presented in Figure 2.18, can be used in the equation

$$Y = 0.051X - 0.00067$$

where X Pa is CO_2 pressure; and Y is CO_2 absorbance,

Hence, when p = 0.53 kPa,

Abs (Y) $= 0.051\times0.53 - 0.00067 = 0.0263 = 263\times10^{-4}$ a.u.

Thus: one (Absorbance $\times10^{-4}$) corresponds to quantum of CO_2

$= 1.36\times10^{-6}/263$

$= 5.17\times10^{-9}$ mol CO_2

or 5.17×10^{-9} mol × 44g/mol

$= 2.27\times10^{-7}$ g

$= 0.227\mu g$

Using the same steps above for 0.26 kPa, 0.80 kPa, and 1.33 kPa obtained 0.234μg, 0.225μg and 0,224μg. The average is 0.228 μg.

Because the CO_2 results were obtained by 6.38×10^{-6} m^{-3} cell, this cell has the same path length as the cell used in the *in-situ* CO_2 experiments.

However the *in-situ* cell has a volume of 13.7 cm^3. Hence, for the cell used in real experiments, one Absorbance 10^{-4} corresponds to carbon dioxide in μg is:

$0.228\mu g.cm^{-3} \times 13.7\ cm^3 / 6.5 cm^3$

$= 0.48\mu g$

In a typical experiment with A-1 pigmented PE, the amount of CO_2 evolution was 32 units (absorbance × 10^{-4}) per hour with AM1.5 filter. This is equal to 0.48μg×32= 15.3 μg carbon dioxide emission per hour. For unpigmented PE CO_2 evolution was 20 Abs per hour with AM1.5 filter equivalent to 0.48μg × 20 = 9.6 μg carbon dioxide in the cell.

2.6 CELL DEVELOPMENT

2.6.1 Position of the sample holder

The cell initially used in these studies was designed in order to test whether the photostability of both unpigmented and pigmented polymer material could be assessed using a simple FTIR gas-phase technique by measuring the amount of CO_2 produced by the UV-induced photo-oxidation of polymer.

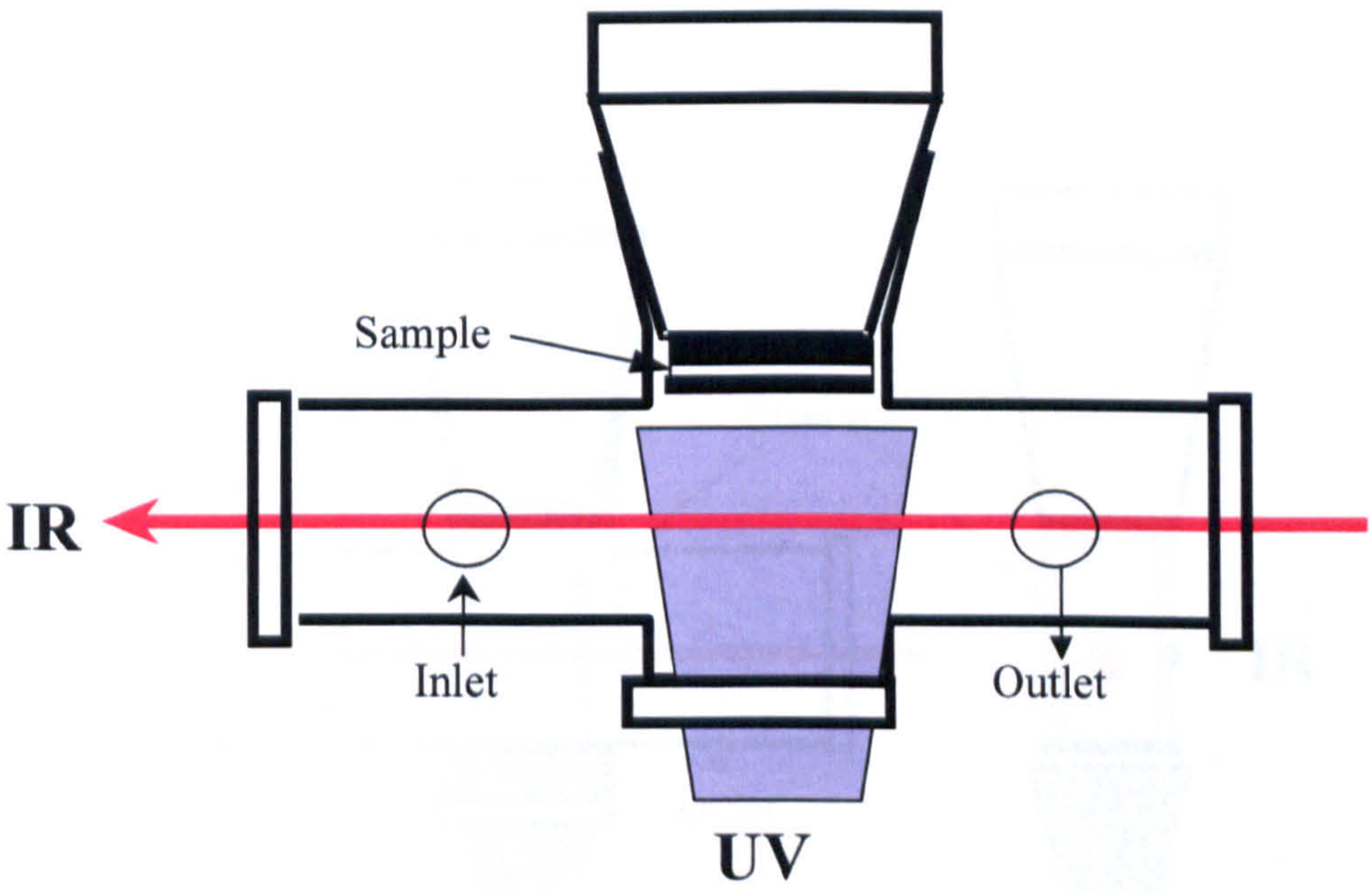

Figure 2-20 'old' cell.

In the initial experiments the background CO_2 was not negligible, and limited the usefulness of the method for measuring relatively photo stable films. Further, the background was not constant- it depended on which vacuum grease was used and also on the age of the Araldite adhesive used in the assembly of the cell. The cell was therefore modified as shown in Figure 2-20 and Figure 2-21. The most significant change was that the sample was placed nearer to the front of the window used to admit UV illumination.

Two thin glass strips were used to hold the magnetic disc near the front window. The IR beam can pass through the gap between the two glass arms of the holder. In the new cell, the sample holder blocks UV light from reaching any residual grease on the wall of the cell and hence minimized UV irradiation of such contaminate. Consequently, generation of background CO_2 was also minimized. With this improvement, the background CO_2 now appears to be mainly caused by the temperature rising in the cell. This is believed to be caused by desorption of CO_2 physisorbed on the internal surface of the cell wall. Figure 2-22 compares the background CO_2 evolution when a blank metal disk was placed in the back position and the front position respectively.

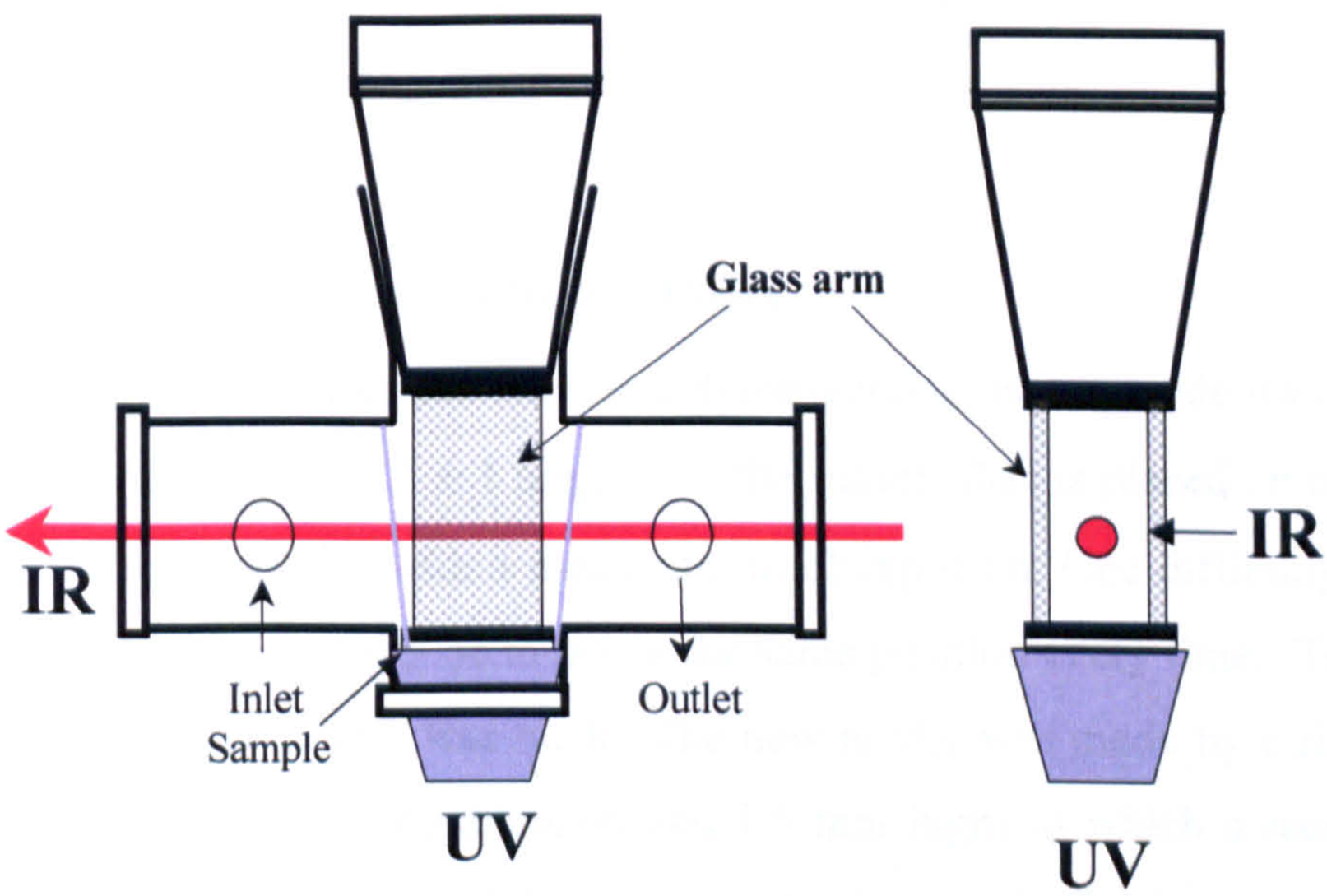

Figure 2-21 'New' cell.

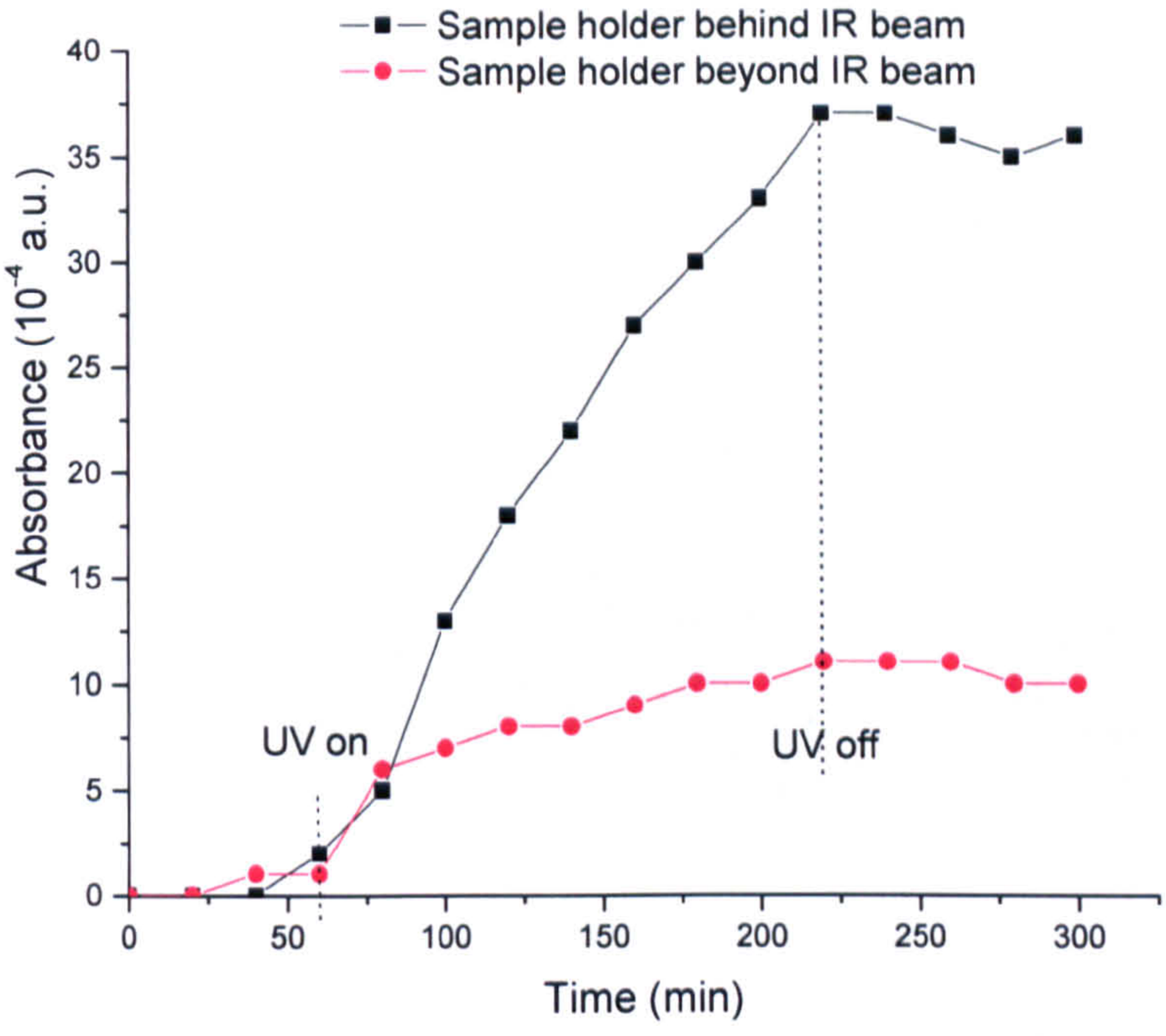

Figure 2-22 CO_2 build up measured when a blank metal disk was placed in the cell instead of a polymer sample. The CO_2 background signal was lower when the inactive sample was put in front of the IR beam.

It was found that UV intensity decreased significantly with the distance between the light pipe and the UV intensity detector, so the sample was placed at the front position in the cell to get increased CO_2 generation.

2.6.2 Positioning of the sample on the holder

The samples, which are used for the research measurements, are made into discs (ca. 55 mm^2, diameter 8.4 mm, 11 ± 1 mg). Then the sample disc is placed on a magnetic substrate plate and covered with a metal ring to clamp it on. One difficulty was that the metal ring could not easily be to put in the same position every time. To improve reproducibility, a new holder was made. The new holder was made by a ring (9 mm outside diameter, 8 mm inside diameter and 1.5 mm high) in which a recess with a diameter of 8.5 mm circle depth 1.3 mm was cut. The sample fits the recess. The thin (PE) samples were fixed in the ring by two very short metal wires about 1 mm long and 0.5 mm diameter. Thick samples, for example 2 mm rigid sheet PVC samples,

were clamped by another similar ring. The background CO_2 was significantly reduced by using this arrangement. Figure 2-23 shows the new holder.

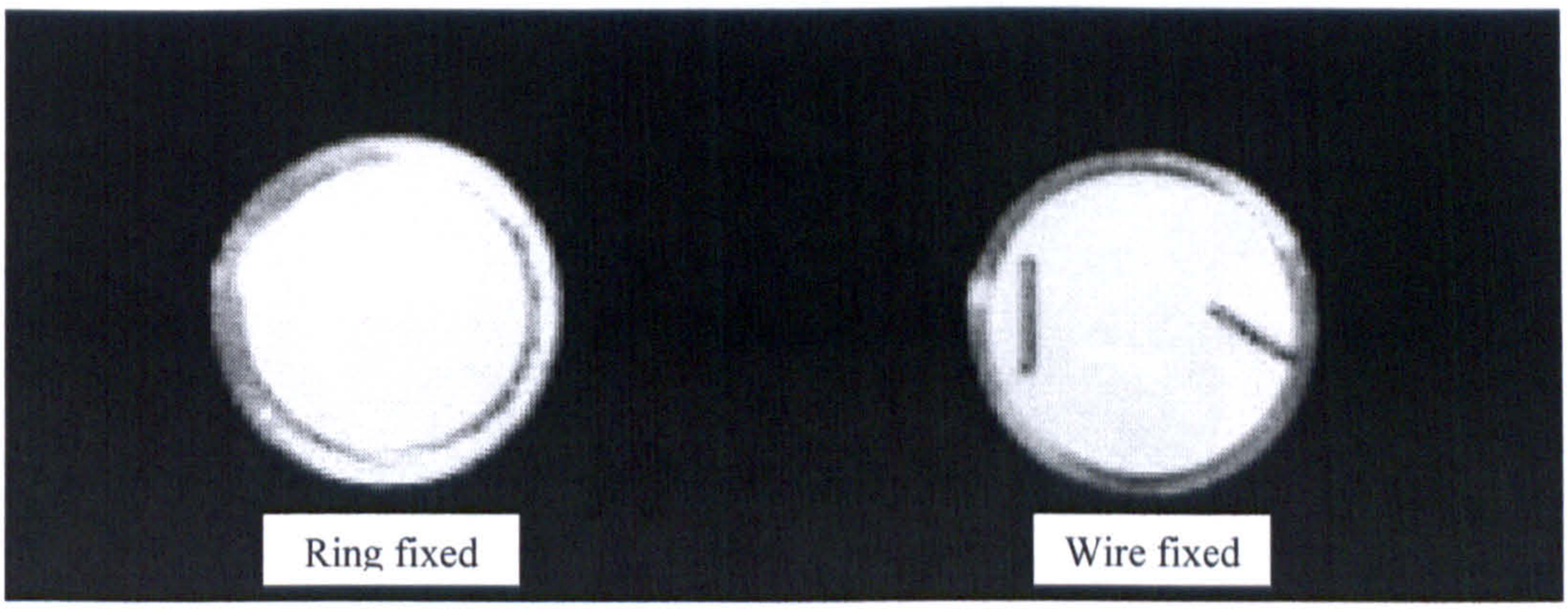

Figure 2-23 The new sample holder for PE and PVC samples.

There are two major advantages with new holder: one is increasing the irradiated area; the other is improved reproducibility.

2.7 UV-VISIBLE SPECTROSCOPY

Ultraviolet/visible spectroscopy involves the absorption of ultraviolet/visible light by a molecule causing the promotion of an electron from a ground electronic state to an excited electronic state. A Shimadzu UV 160A UV/Visible spectrophotometer was used to obtain the transmission absorption of polymer films to determine whether the polymer, in the form of particular unpigmented pure films, can absorb UV/Visible light or the extent of absorption.

2.8 EXPOSURE OF SAMPLES UNDER TENSILE STRESS

2.8.1 Samples preparation under tensile stress

A special testing frame was designed to conduct the photo-mechanical exposures. It consisted of a pair of flat rings that were placed on either side of the sample film (Figure 2-24). Bolts that passed through both rings (and the sample film) were used to clamp the film between the rings (Figure 2-25).

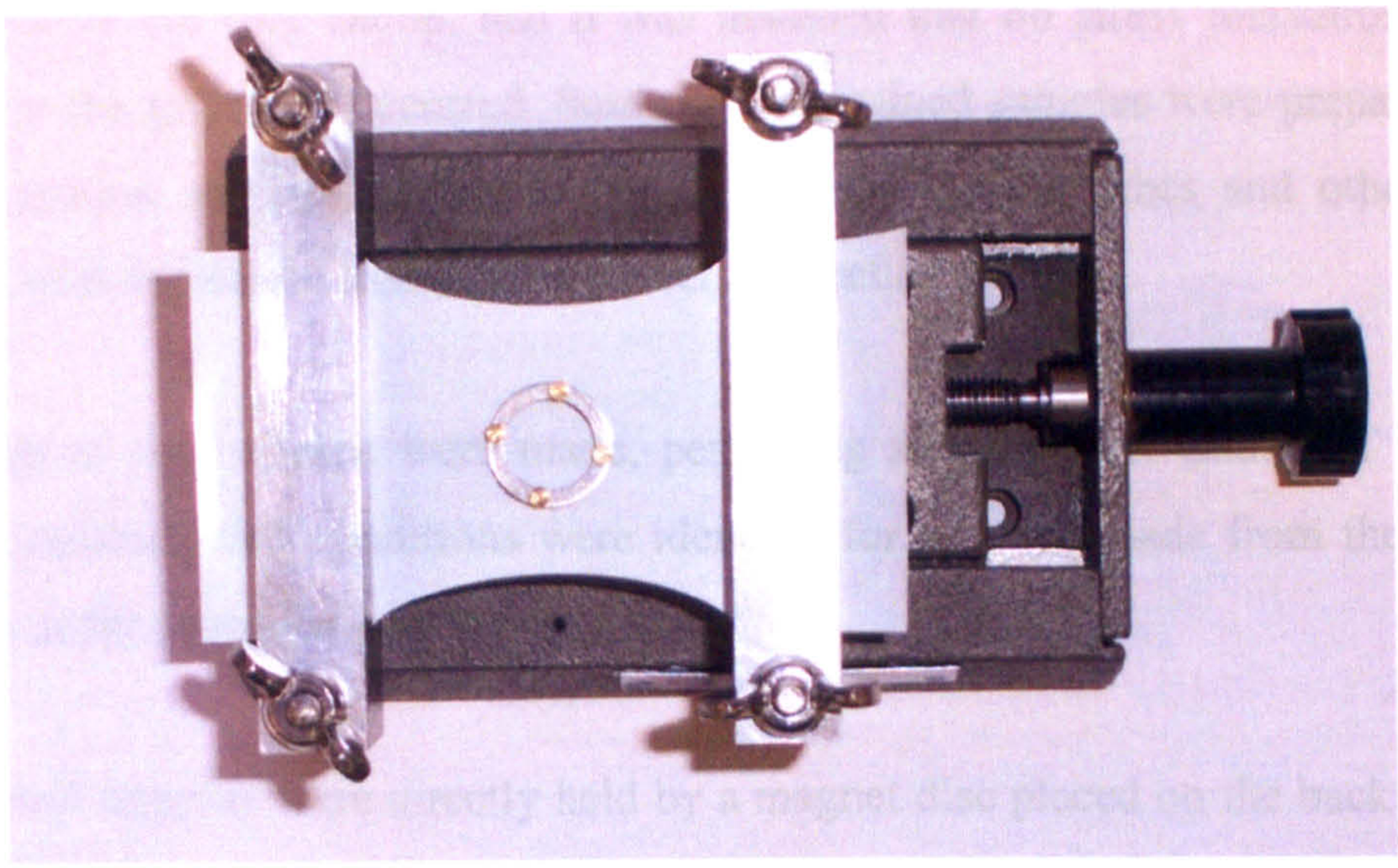

Figure 2-24 A special testing frame used to put strain on the tensile-test sample.

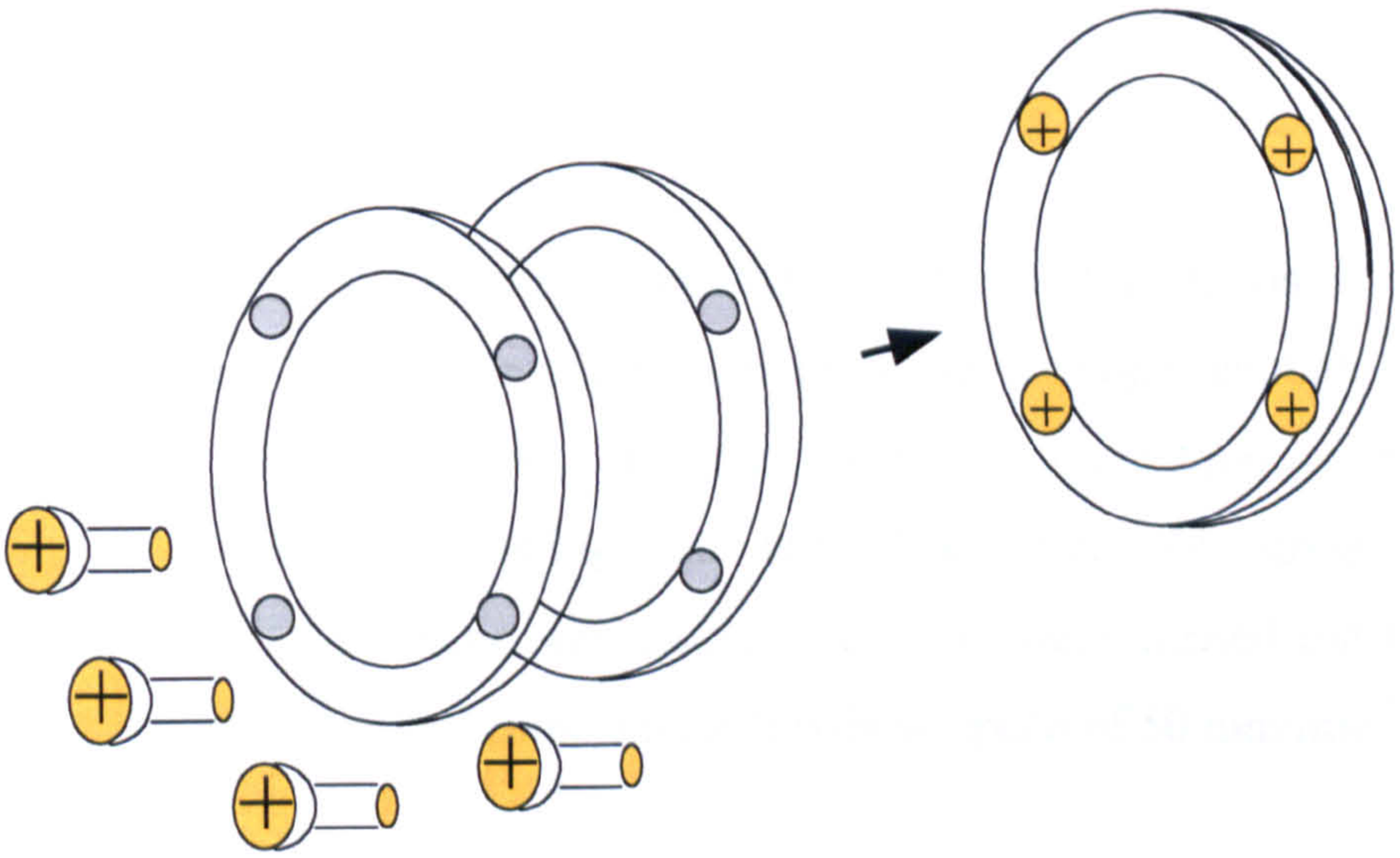

Figure 2-25 Rings used to maintain strain on the sample during UV exposure.

After clamping the rings onto the film, the surrounding film was cut away to leave a disc shaped sample mounted securely between the rings. Samples that were to be exposed in a stressed state were prepared by extending a piece of the lay-flat film 25 mm wide in a purpose-built stretching frame (Figure 2-24) with initial grip jaw separation 24.7 mm and final grip jaw separation 44.7 mm, giving an extension of 80 %. The film was held stretched in the frame while a portion of it was mounted in the ring-shaped holder, just as with the unstressed samples. When the ring with the

mounted film was cut away as before, it was noted that there was no movement of the sample within the ring clamp, and it was assumed that no stress relaxation due to slippage in the grips had occurred. Some of the strained samples were prepared with the deformation applied parallel to the axis of the lay-flat tubes and others were prepared with the tensile axis in the transverse direction.

Many sets of ring clamps were made, permitting simultaneous testing of multiple samples, ensuring that conditions were identical for samples made from the several materials under examination.

The strained samples were directly held by a magnet disc placed on the back panel in QUV machine. In some cases the sample broke within the mounting ring during UV exposure, before the planned termination of the test. In each case the fracture was perpendicular to the tensile strain axis, independent of the preferred orientation of the sample.

2.8.2 Stress Relaxation

Measurement of tensile stress-strain properties is the most common mechanical measurement on most polymer materials. The principle is simple enough. The test piece is stretched until it breaks, and the force and elongation is measured continuously or periodically during the test. The effect of stress on the photodegradation of polyethylene was studied. All tests were carried out using an RDP-Howden Ltd tensile test machine with a crosshead speed of 50 $mm \cdot min^{-1}$.

In order to assess the stress state of the samples prepared in the manner described in section 2.8.1, the stress relaxation behaviour of the materials was examined in a separate series of experiments. The sample dimensions matched those used in the hand-operated stretching frame as closely as possible and a 20 mm crosshead displacement was used. The strain was applied on the sample then kept fixed for least 4 hours during which the load was recorded periodically. The load fell approximately 30 % within the first few minutes; it had fallen to between 50 and 60 % of the initial value at the end of the first hour and thereafter fell very slowly. The pigmented

polyethylene gave slightly higher initial load than the unpigmented polyethylene (see Figure 2-26).

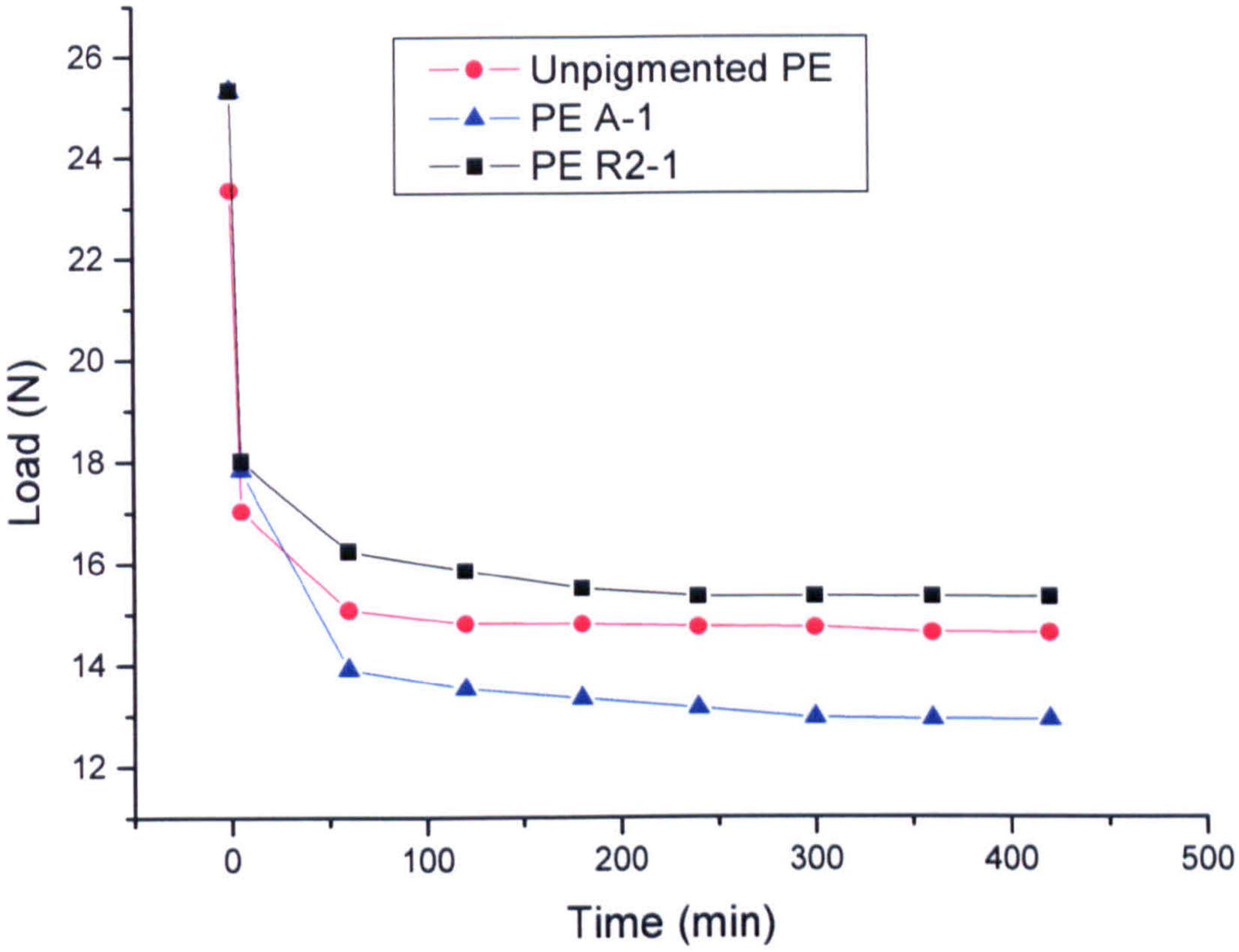

Figure 2-26 Showing the relationship of load decrease with relaxation time.

2.8.3 Ultraviolet exposure

The ring-mounted samples were transferred to a QUV machine (Q-Panel Company, Cleveland, Ohio, USA) in which the ultraviolet (UV) illumination was provided by UVA340 fluorescent tubes (Q-Panel Company). The details were described in section 2.3.41.

2.8.4 Calibration of thickness effect on FTIR results

When the film is extended it reduces thickness. This means that the path of the interrogating infrared beam through the sample is reduced and the absorption will be necessarily reduced. It is relatively straightforward to take this into account as long as the distribution of the absorbing groups is homogeneous, as is expected to be the case for the polyethylene resonances used here.

The heights of the peaks at 1374 cm^{-1} and 1301 cm^{-1}, should be proportional to the film thickness as predicted by Beer's law. In order to prove this, simple calibration experiments were carried out by measuring the absorbance of different thickness films using one disc, two discs up to seven disks together, respectively (see Figure 2-27).

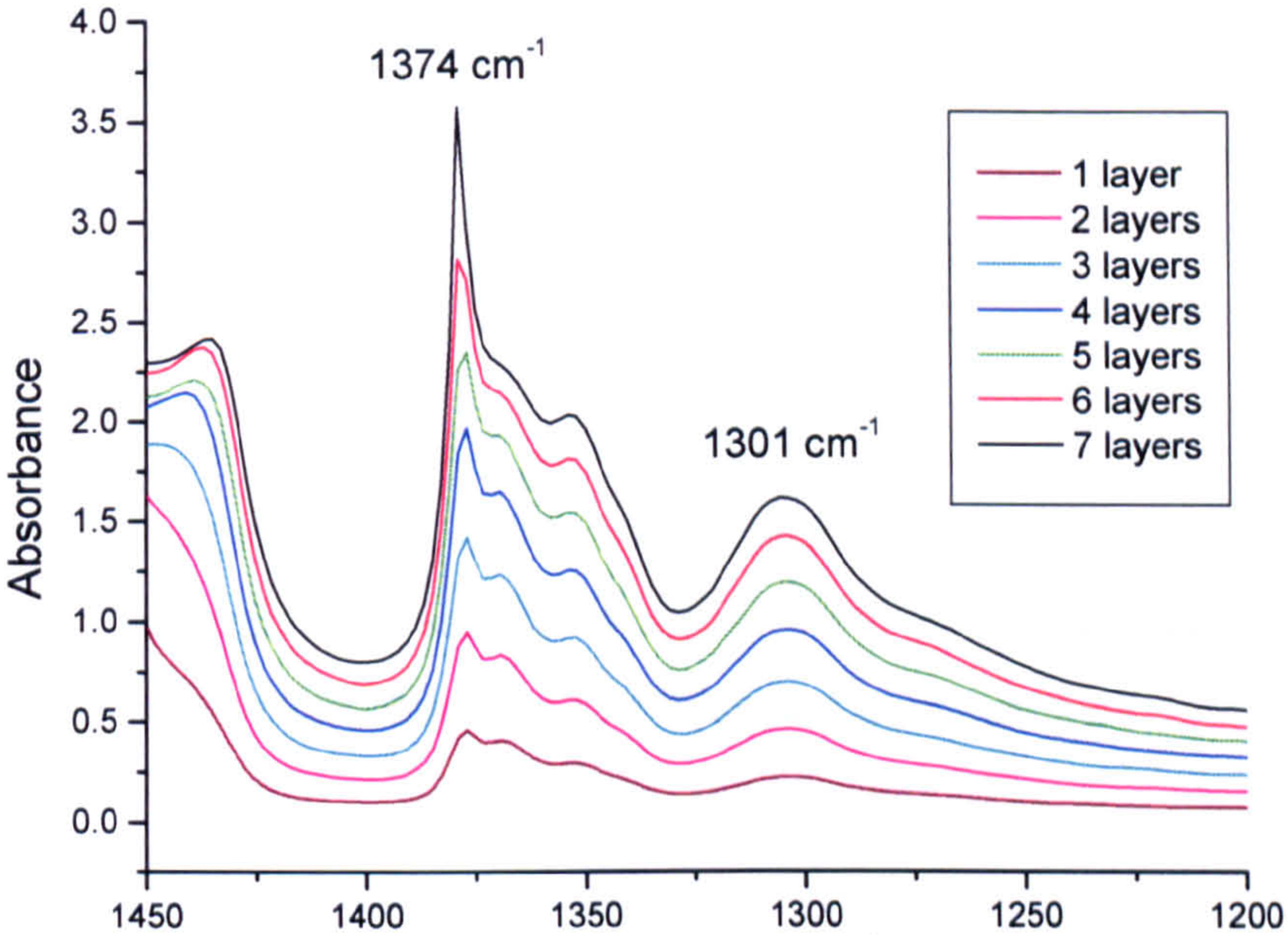

Figure 2-27 Showing relationship between Absorbance with different thickness (one layer sample disc thickness is 100 μm).

In the table below different thicknesses (obtained using stacks of disks) and their absorbance are shown.

Table 2-6 Absorbance of unpigmented PE film with different thickness at 1374 cm^{-1} and 1301 cm^{-1} .

Thickness (μm)	Absorbance at 1374 cm^{-1}	Absorbance at 1301 cm^{-1}
100	0.39	0.156
200	0.813	0.37
300	1.263	0.539
400	1.738	0.726
500	2.094	0.935
600	2.5	1.106
700	3.153	1.236

Using these data it is easy to plot an absorbance vs. thickness graph showing the linear relationship between them. The height of peaks at 1374 cm^{-1} and 1301 cm^{-1} can then be used to normalize the sample thickness. Both peaks have shown the linear relationship between the absorbance and its thickness in Figure 2-28.

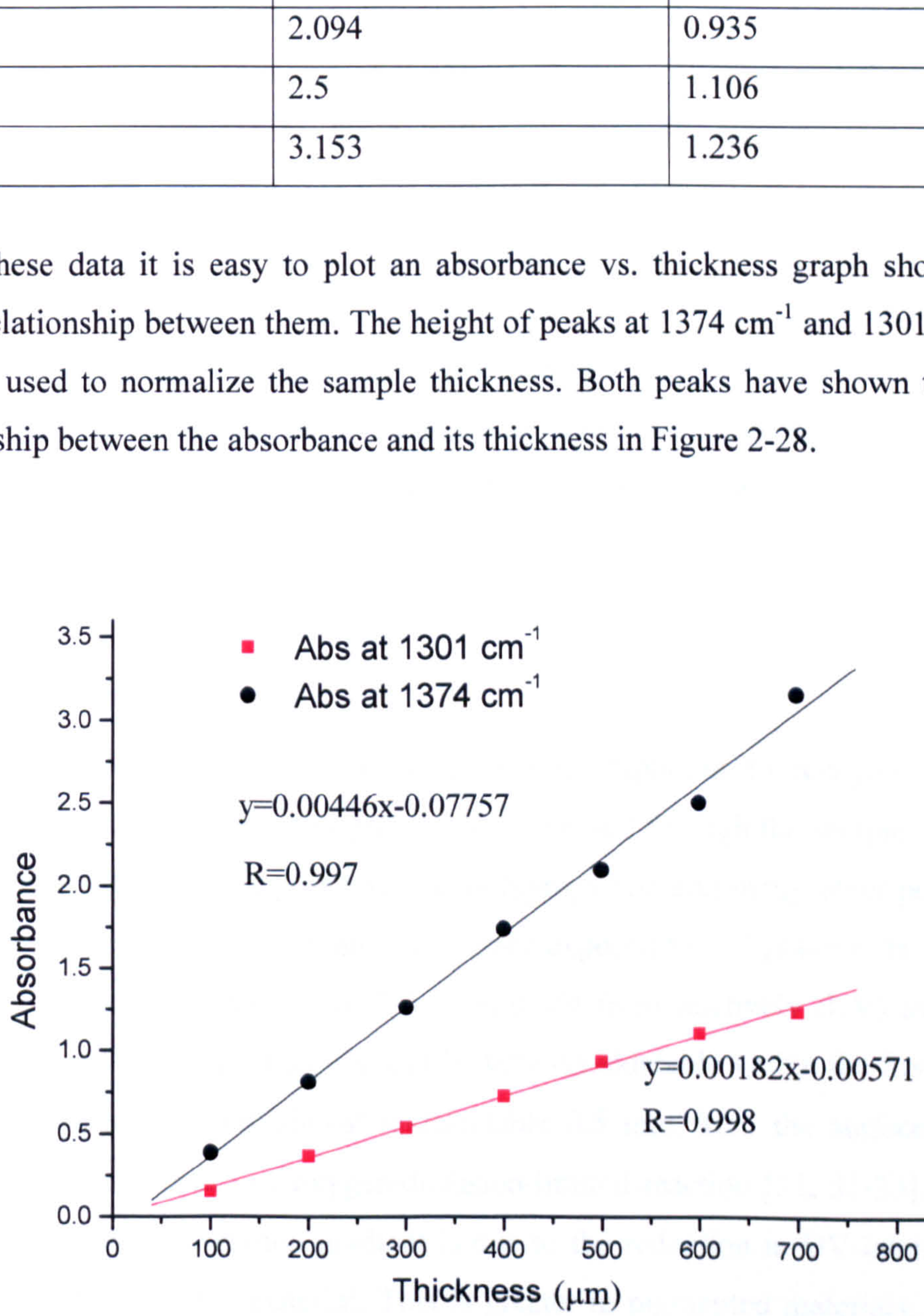

Figure 2-28 The relationship between absorbance at 1374 cm^{-1} and 1301 cm^{-1} and different numbers of disks (100μm thick).

2.8.5 Characterization

The exposed samples were removed from the QUV machine periodically and an infrared (IR) spectrum was obtained, using a Bio-Rad FTS60A spectrometer, with the sample still mounted in the ring clamp. The principal region of interest was 1700 – 1800 cm^{-1} in which carbonyl group stretching appears and absorbance measurements for this band were measured. In those cases, in which the sample broke within the mounting ring prematurely, the UV exposure and sequence of IR measurements was continued until the planned test duration had expired. A second use of the FTIR spectrum was for the monitoring of thickness when the films were deformed, using absorption bands produced by the polyethylene. Intensity measurements of bands centred at 1304 cm^{-1} (attributed to C–H wagging) and another in the range 1350–1380 cm^{-1} (attributed to C–H bending) [12] were made for this purpose (see section 5.2.7). The bands centred at 1304 cm^{-1} and in the range 1350–1380 cm^{-1} were also used to attempt to determine the dichroic ratio as a measure of molecular orientation in the samples [13, 14]. The presence of the pigments had no obvious effect on the bands attributed to polyethylene. TiO_2 does not absorb in this wavelength region though it may scatter if the particles are in a certain size range.

2.8.6 Multi-layered samples

When dealing with photodegraded samples it is important to recognise that the carbonyl groups may not be homogeneously distributed through the sample thickness. It is well established that in polyethylene, polypropylene and many other polymers a steep degradation gradient develops at a surface exposed to UV [14-30]. In relatively thick samples (of the order of say 2–3 mm) made from relatively (UV) transparent materials, the molecular degradation can be very considerable within the first 100 μm of the exposed surface yet almost undetectable 0.5 mm from the surface. This is primarily the consequence of oxygen-diffusion-limited reaction [22, 31-33]. Another contribution to the degradation gradient is due to the reduction in UV intensity as it penetrates deeper into the material. This is greater in pigmented materials, in which the UV intensity falls steeply with depth. It is less clear to what extent the gradient in oxidation plays a part in the observations made with unstrained and (thinner) strained samples. Triple-layered unstrained samples were mounted in the double-ring clamps and subjected to UV exposure. The layer facing the UV source is labelled layer 1 and

the one facing away from it is layer 3. Layer 3 receives UV radiation onto its outward facing surface by reflection within the equipment and onto the forward facing surface by transmission through layers 1 and 2 (where layer 2 is the middle layer). The samples were removed periodically and IR measurements were made on the individual layers before remounting them in the same sequence and returning them to the UV exposure unit.

2.9 REFERENCES

1. Robert, W., *CRC handbook of chemistry and physics*. 1988: Boca Raton, FL : CRC Press, c1988.
2. COMPANY, T.Q.-P., *Operating Manual Q.U.V. Accelerated Weathering Tester*.
3. O'Donnell, B. and J.R. White, *Polymer Degradation and Stability*, 1994. 44(2): p. 211-222.
4. Krimm, S., *Advantage Polymer Science*, 1960. **2**: p. 51-72.
5. Christensen, P.A., A. Dilks, T.A. Egerton, and J. Temperley, *Journal of Materials Science*, 1999. **34**(23): p. 5689-5700.
6. Smith, B.C., *Fundamentals of Fourier transform infrared spectroscopy*. 1996, Boca Raton, Florida 33431: CRC Oress LLC.
7. Christensen, P.A. and A. Hamnett, *Techniques and Mechanisms in Electrochemistry*. 1994, Glasgow: Blackie Academic and Professional.
8. Christensen, P.A., A. Dilks, T.A. Egerton, E.J. Lawson, and J. Temperley, *Journal of Materials Science*, 2002. **37**(22): p. 4879-4887.
9. Christensen, P.A., A. Dilks, T.A. Egerton, and J. Temperley, *Journal of Materials Science*, 2000. **35**(21): p. 5353-5358.
10. Christensen, P.A., A. Dilks, T.A. Egerton, and E.J. Lawson, *Journal of Materials Science*, 2002. **37**: p. 1-9.
11. Lidle, D.R., *CRC Handbook of Chemistry and Physics. 74th Edition ed. 1993, Florida: CRC Press, (1993)*.
12. Hendra, P.J. and W.F. Maddams, *In: A.H. Fawcett, Editor, Polymer spectroscopy, Wiley, Chichester/New York (1996), pp. 173?02 Chap. 7.*
13. Colthup, N.B., L.H. Daly, and S.E. Wiberley, I*ntroduction to infrared and Raman spectroscopy, Academic Press, New York (1964).*

14. Campbell, D., R.A. Pethrick, and J.R. White, P*olymer Characterization.* 2000: Stanley Thornes.

15. O'donnell, B., M.M. Qayyum, L. Tong, and J.R. White, P*lastics Rubber and Composites Processing and Applications,* 1994. 21(5): p. 297-307.

16. Furneaux, G.C., K.J. Ledbury, and A. Davis, P*olymer Degradation and Stability,* 1980. 1: p. 1;3:431.

17. Davis, A. and D. Sims, W*eathering of Polymers.* 1983: Applied Science, Barking,.

18. Jouan, X. and J.-L. Gardette, P*olymer Communications (Guildford, England),* 1987. 28(12): p. 329-331.

19. Jouan, X., C. Adam, D. Fromageot, J.-L. Gardette, and J. Lemaire, P*olymer Degradation and Stability,* 1989. 25(2-4): p. 247-265.

20. Gardette, J.-L., P*olymers & Polymer Composites,* 1997. 5(1): p. 7-13.

21. Gardette, J.L., S. Gaumet, and J.L. Philippart, J*ournal of Applied Polymer Science,* 1993. 48(11): p. 1885-1895.

22. Audouin, L., V. Langlois, J. Verdu, and J.C.M. de Bruijn, J*ournal of Materials Science,* 1994. 29(3): p. 569-583.

23. Girois, S., L. Audouin, J. Verdu, P. Delprat, and G. Marot, P*olymer Degradation and Stability,* 1996. 51(2): p. 125-132.

24. Girois, S., P. Delprat, L. Audouin, and J. Verdu, P*olymer Degradation and Stability,* 1997. 56(2): p. 169-177.

25. O'donnell, B., J.R. White, and S.R. Holding, J*ournal of Applied Polymer Science,* 1994. 52(11): p. 1607-1618.

26. Li, T. and J.R. White, P*olymer Degradation and Stability,* 1996. 53(3): p. 381-386.

27. Rabello, M.S. and J.R. White, P*olymer Degradation and Stability,* 1997. 56(1): p. 55-73.

28. White, J.R., P*lastics, Rubber and Composites Processing and Applications,* 1998. 27(3): p. 124-131.

29. Turton, T.J. and J.R. White, J*ournal of Materials Science,* 2001. 36(19): p. 4617-4624.

30. Turton, T.J. and J.R. White, P*olymer Degradation and Stability,* 2001. 74(3): p. 559-568.

31. Gillen, K.T., J. Wise, and R.L. Clough, P*olymer Degradation and Stability,* 1995. 47(1): p. 149-161.

32. Wise, J., K.T. Gillen, and R.L. Clough, P*olymer,* 1997. 38(8): p. 1929-1944.

33. Audouin, L., S. Girois, L. Achimsky, and J. Verdu, P*olymer Degradation and Stability,* 1998. 60(1): p. 137-143.

CHAPTER 3

PHOTOOXIDATION OF UNPIGMENTED POLYETHYLENE

3.1 INTRODUCTION

Polyethylene is one of the most widely studied polymers. There is a large amount of literature regarding the degradation of polyethylene under various environmental conditions (see section 1.3). This chapter reports the work aimed at assessing the resistance of unpigmented polyethylene to UV degradation by UV-visible spectroscopy and Fourier Transform Infrared (FTIR) techniques. FTIR techniques include an *in-situ* method to measure the evolution of carbon dioxide and the conventional *ex-situ* transmission IR measurement of development of carbonyl groups, such as ketones.

The unpigmented polyethylenes used in this study were based on a low density polyethylene; the details were described in section 2.1.1.

3.2 UV- VISIBLE TRANSMISSION RESULTS

As described in the introduction, section 1.3, UV degradation will occur only if UV is absorbed by the polymer. To determine the absorption of PE film used in these studies the unpigmented polyethylene film was scanned using a Shimadzu UV 160A UV/Visible spectrophotometer at the slow scan (5.9 nm per second) spectrometer setting. The UV-visible spectrum of unpigmented polyethylene film (U-1) demonstrates that as the wavelength decreases, low transmission starts in the visible region then gradually increases from ~ 400 nm to 225 nm in the UV region but the sample only starts to absorb strongly at wavelength less than 225 nm (Figure 3-1).

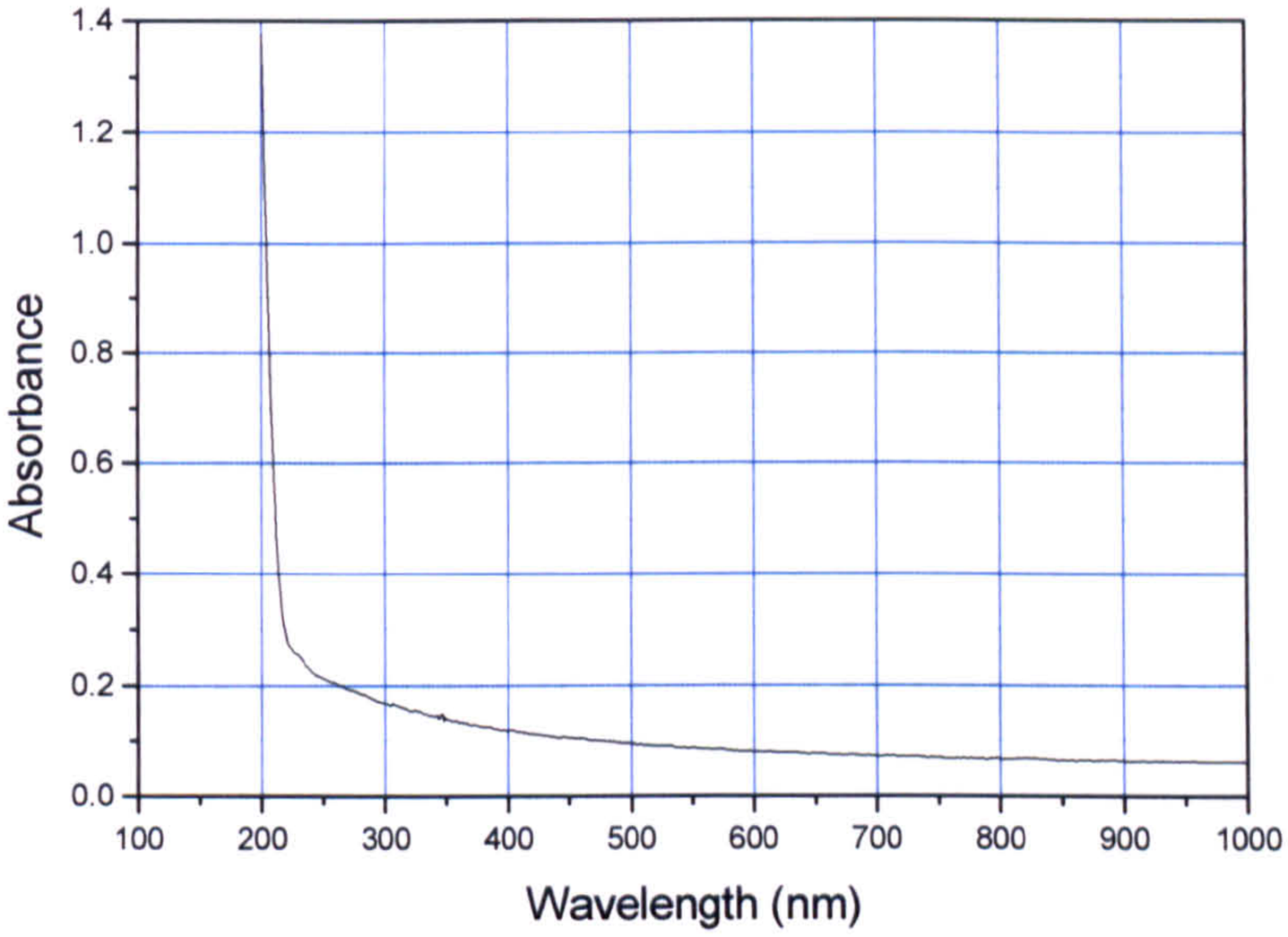

Figure 3-1 Absorbance spectrum of unpigmented 100μm PE U-1 film from 200-1000nm.

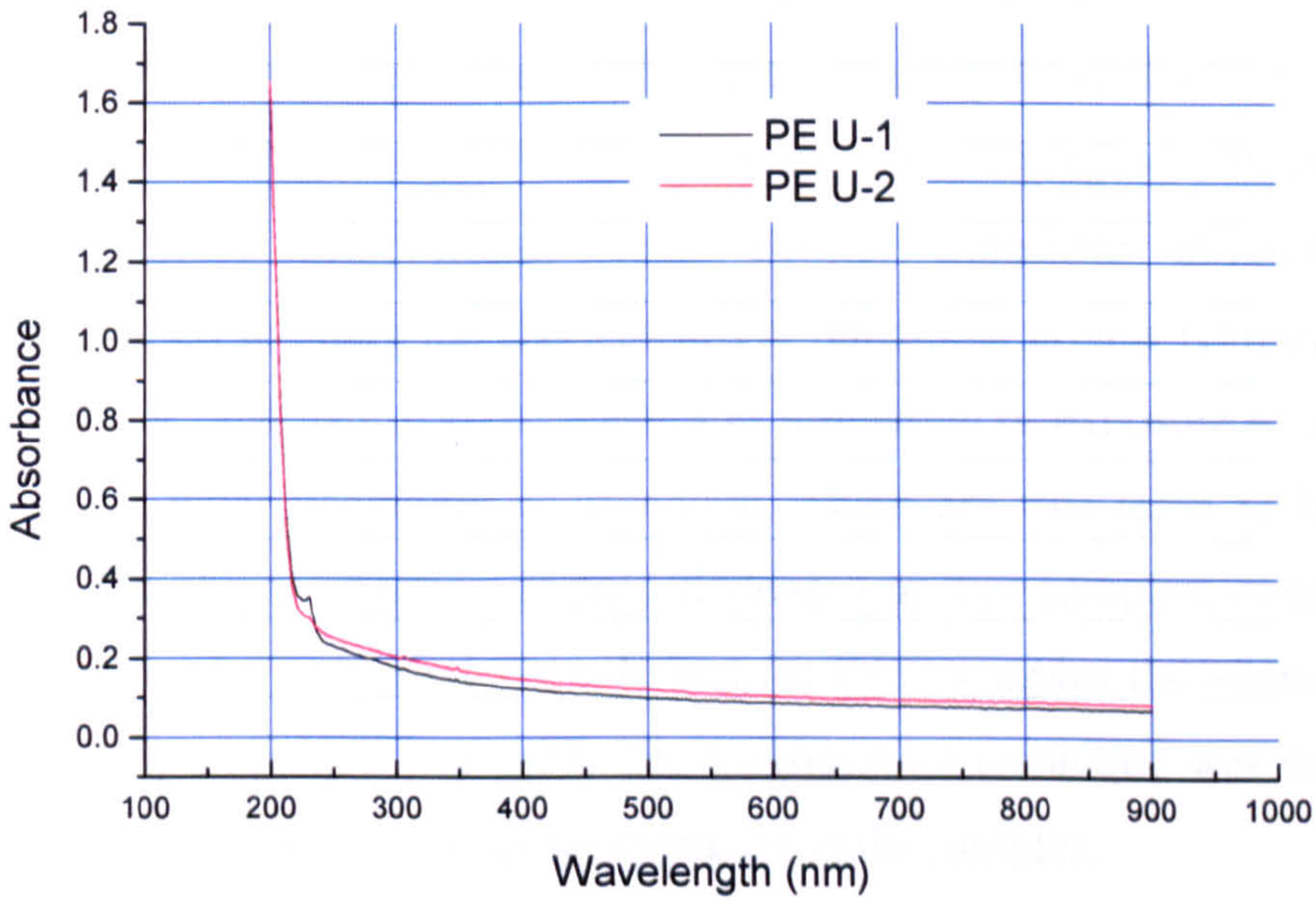

Figure 3-2 Absorbance spectra for two different batches of unpigmented 100μm PE film. PE U-1: 30 months after receipt; PE U-2: one month after receipt.

Figure 3.2 shows samples of UV-visible spectra from two different batches of unpigmented polyethylene films and demonstrates very good reproducibility. The black curve and red curve are recorded from U-1 PE film and U-2 PE film,

respectively. After nearly three years storage U-1 shows a little absorbance around 220 nm.

These results can be compared with those from an alkyd paint film which strongly absorbs throughout the UV region and into the visible [1] and photodegraded significantly. The lack of UV absorption by the PE film suggests that unpigmented polyethylene should demonstrate very low photo-activity.

3.3 CARBONYL GROUP DEVELOPMENT UNDER QUV IRRADIATION

3.3.1 Preliminary studies on unpigmented PE

The weathering of plastics can be followed by many different analytical techniques. Their validity depends on the nature of the material and the mode of deterioration. Since most of the degradation results from irreversible chemical reaction of polymer molecules, changes in molecular composition provide a logical method for measuring the course of polymer degradation. As hydrocarbon polymers degrade, many different changes in polymer composition occur. Fourier transform infrared (FTIR) spectroscopy is used to study the changes in the functional groups (carbonyl, vinyl, vinylidene , alkene, and hydroxyl) of plastics as a function of exposure to the natural weather [1-5] or other degrading environment. There are two main techniques of FTIR used in the characterization of polyethylene. For thin samples, measurements were performed in the transmission mode and for thick samples the attenuated total reflectance (ATR) technique was used. The transmission technique was used in this study to measure the carbonyl group development in the samples.

The QUV Accelerated Weathering Tester [6] was used as the source of UV light to simulate of the damaging forces of weather. Unpigmented polyethylene film was irradiated under fluorescent lamps (QUV A-340 tubes) in the QUV machine.

As explained in the introduction, the conventional method of measuring photodegradation of polyethylene (PE) is to monitor the development of carbonyl groups. In the case of oxidation, usually the carbonyl group associated with the

products of degradation is detected by the absorption bands around 1710 cm^{-1} due to the formation of ketones [7]. Figure 3-3 shows that the absorption band around 1712 cm^{-1}, which can be assigned to the C=O stretching vibration of a ketone group, grew in intensity with extended time. With continued irradiation, the new bands began to appear. These absorption bands indicate that more than one oxidation product is formed. For example, the carbonyl band at around 1733 $cm^{-1}$was assigned to C=O stretching vibration in aldehydes or esters [7]. In these studies the absorption caused by ketone group at 1712 cm^{-1} was monitored.

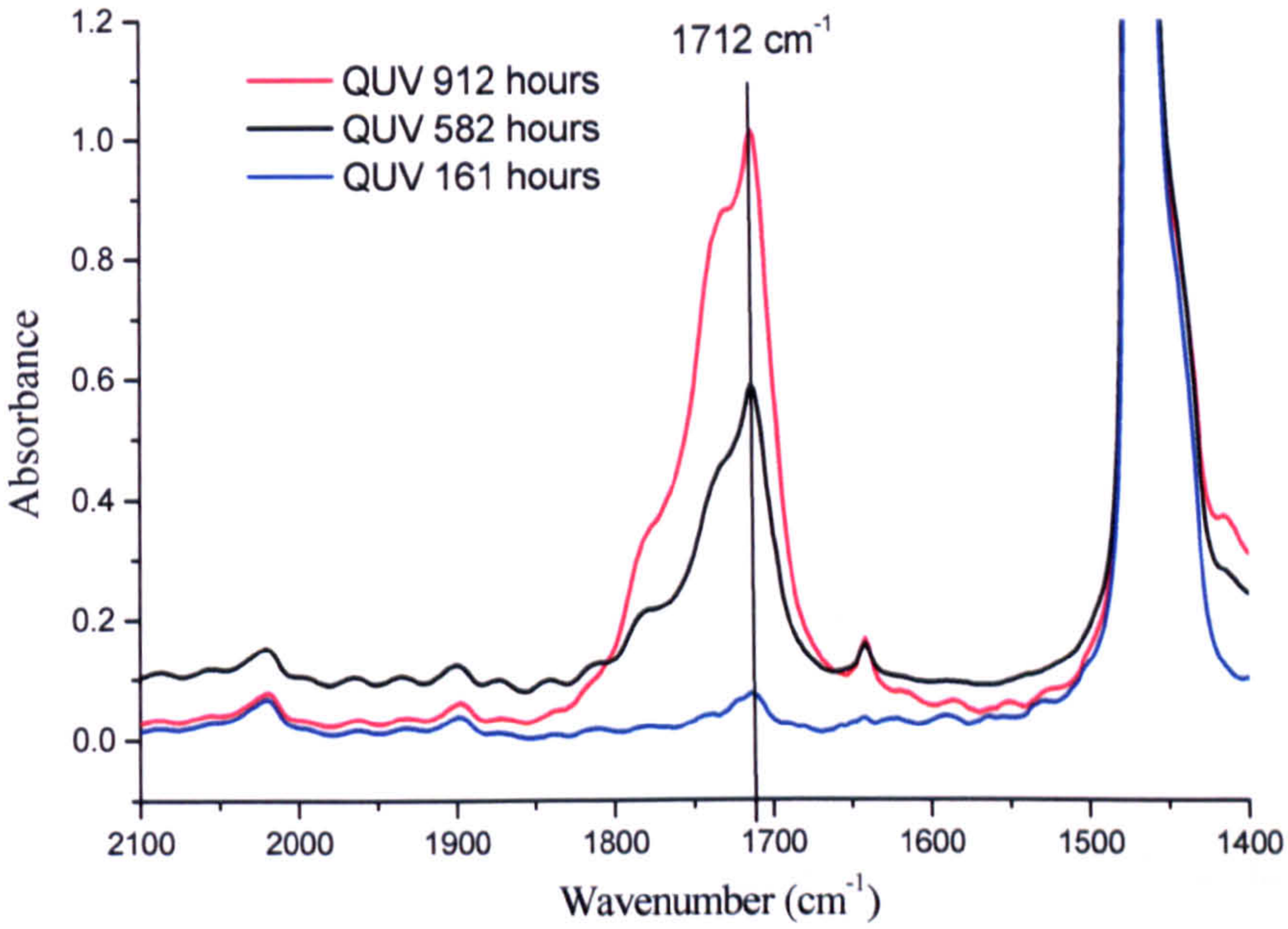

Figure 3-3 Unpigmented PE U-1, carbonyl group (1712 cm^{-1}) development after different UV exposure times.

Two discs of the same film were exposed in the QUV at the same time. Elucidation of the chemical changes that take place during photooxidation of polymer was monitored by FTIR transmission technique. Oxidation rates were determined via the well-established carbonyl index (C.I) method (see section 1.9.6.2).

$$C.I = \{[Log_{10} (I_o/I_t)]/D\} \times 100$$

where D is film thickness in μm, I_o is the initial light intensity at 1712 cm^{-1} and I_t is the transmitted light intensity at 1712 cm^{-1}. Because the samples used in these

experiments were mostly 100 μm thickness film, the C.I., in this case, was equal to the absorbance of the PE film. Therefore, in the rest of this study 'absorbance' is used instead of 'carbonyl index' for all data analysis, the thickness being 100 μm except where indicated. The variation in carbonyl intensity with time is shown in Figure 3-4.

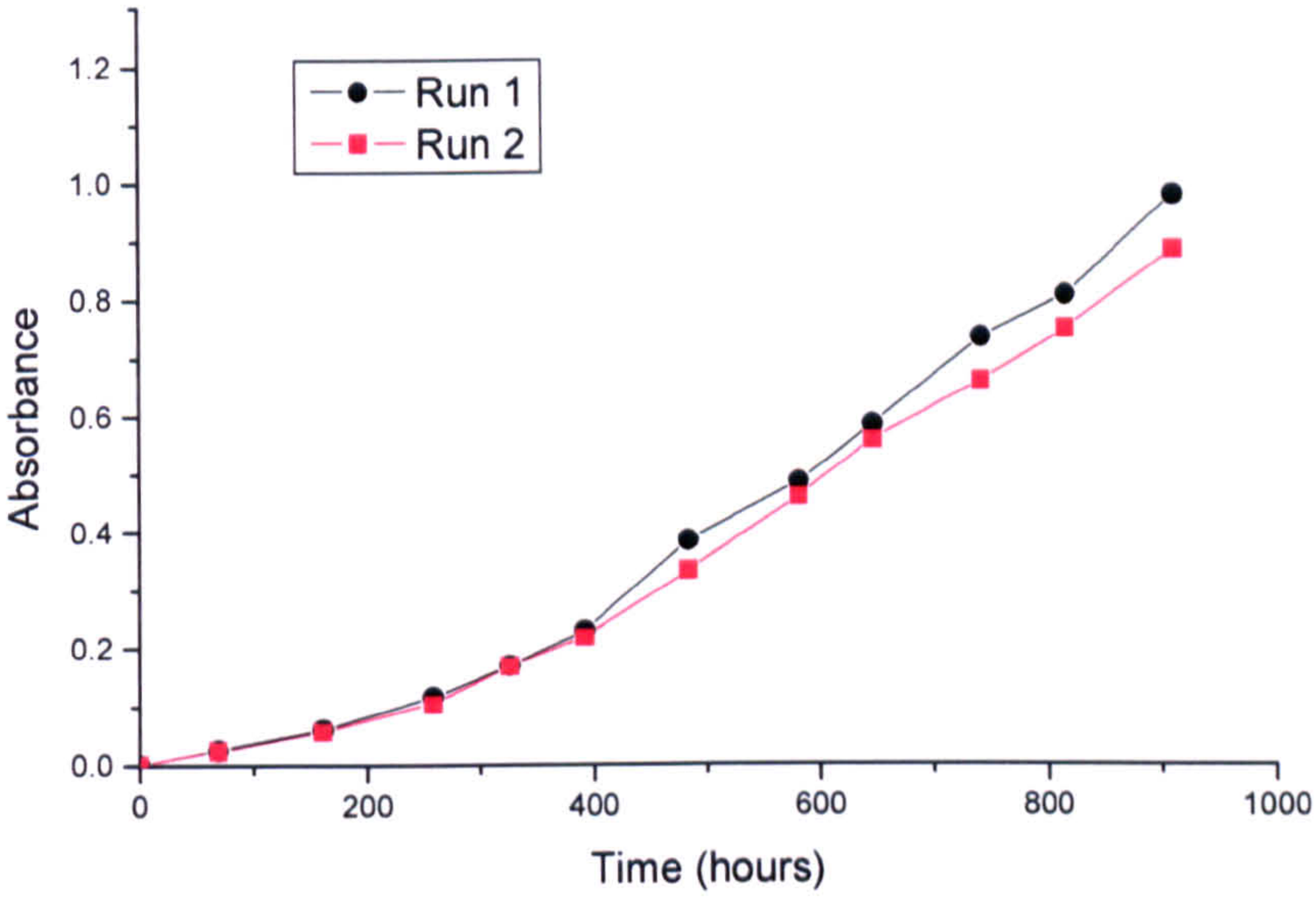

Figure 3-4 Carbonyl development in unpigmented polyethylene U-1 exposed in the QUV machine at a constant temperature of 42°C.

Reproducibility for repeat runs of the two unpigmented polyethylene samples was excellent up to 400 hours. With extended exposure (> 400 hours), the carbonyl group development appears more scattered for different samples. Under normal atmospheric conditions, moisture and carbon dioxide influenced the observed spectra. This problem was eliminated by the acquisition of reference (background) and sample spectrum (absorbance) by flushing gaseous nitrogen through the chamber for at least 10 minutes before collecting the IR spectra. All spectra were recorded for averages of 100 scans, taken over ~ 40 s, at 4 cm^{-1} resolution. A single beam reference spectrum was recorded first by flushing with gaseous nitrogen. Then the sample spectra were referenced to this with the same time nitrogen purging. The comparison was based on the ratio obtained by comparing the height of the sample absorbance peaks with this baseline.

3.4 EFFECT OF SAMPLE THICKNESS ON CARBONYL DEVELOPMENT

Carbonyl compounds are the main intermediate products of photodegradation of polyethylene. They contain the carbonyl group, which is built into the polymer chain. When dealing with photodegraded samples, it is important to recognise that the carbonyl group may not be homogeneously distributed through the sample thickness. In general, most authors assume that the photochemical process is a surface restricted phenomenon [8]. It is well established that in polyethylene, polypropylene and many other polymers a steep degradation gradient develops at a surface exposed to UV [9]. In relatively thick samples (of the order of say 2-3 mm) made from relatively (UV) transparent materials, the molecular degradation can be very considerable within the first 100 microns of the exposed surface yet be almost undetectable 0.5 mm from the surface [10]. This is primarily the consequence of oxygen-diffusion-limited reaction. Another contribution to the degradation gradient is due to the reduction in UV intensity as it penetrates deeper into the material.

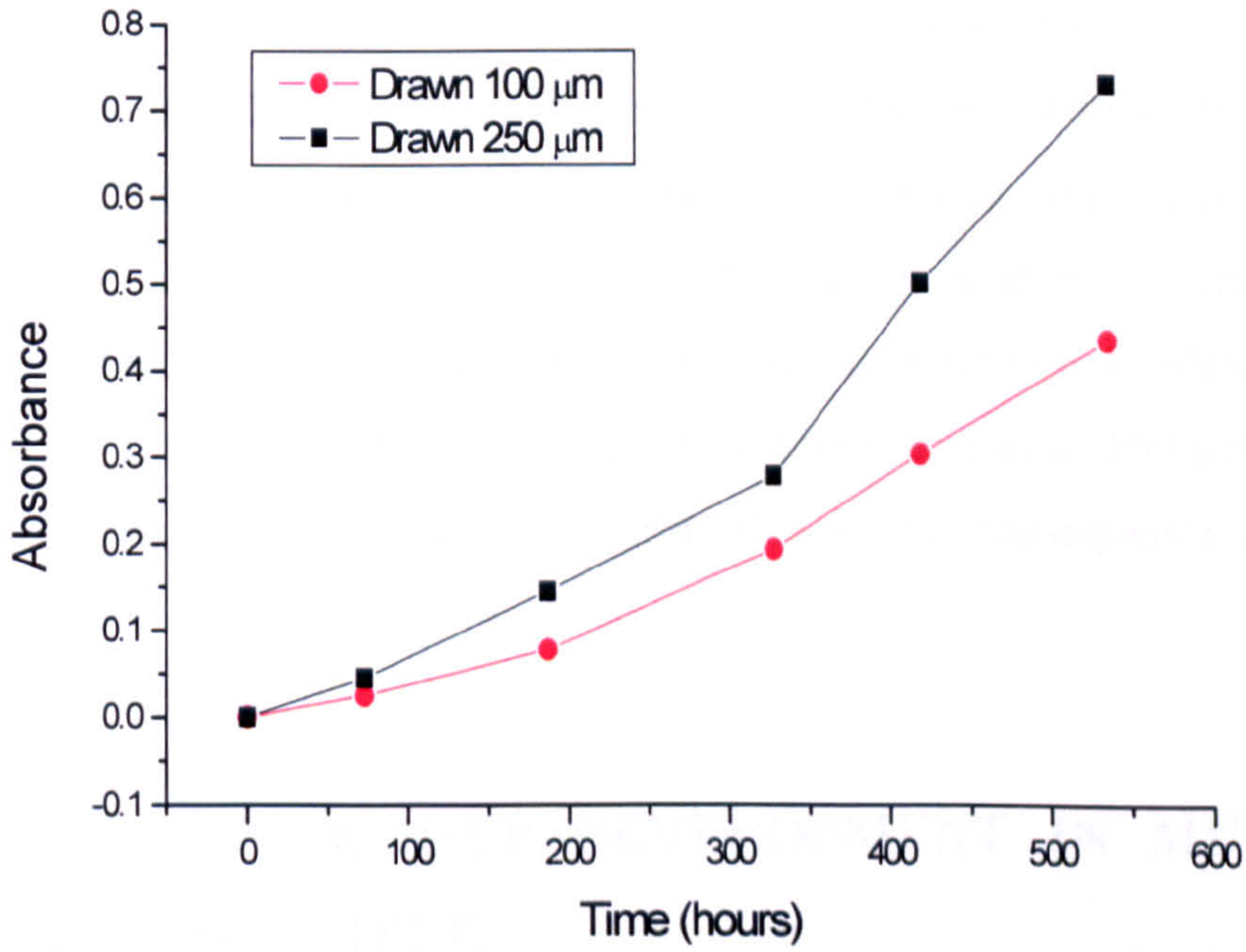

Figure 3-5 Absorbance of carbonyl group directly measured from drawn PE samples of 100 μm and 250 μm thickness respectively.

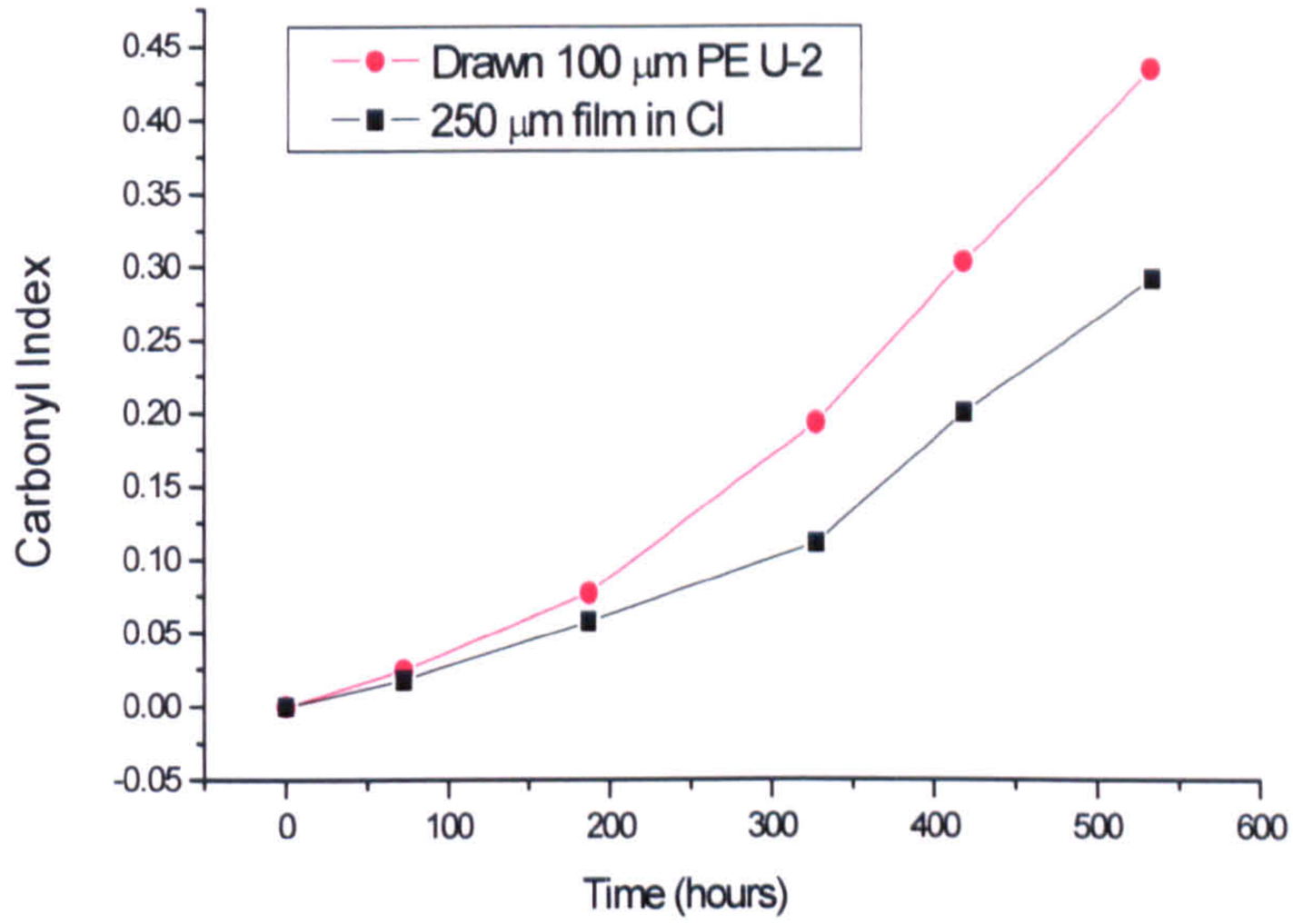

Figure 3-6 Carbonyl index development measured from drawn PE samples of 100 μm and 250 μm thickness corrected into 100μm (CI) respectively.

UV irradiation of drawn PE films produces absorption at 1712 cm^{-1} in the transmission FTIR spectrum. This absorption increases with irradiation time and is assigned to the formation of carbonyl groups. The absorbance of carbonyl groups grows faster in 250 μm drawn film than 100 μm drawn film (see Figure 3-5). This suggests that the depth of photodegradation of PE was more than 100 μm. In Figure 3-6, the absorbance of 250 μm PE film is presented as a Carbonyl Index. It is clear that the Carbonyl Index in 250 μm PE film is smaller than that in 100 μm film. This shows that the photodegradation of PE film also is the consequence of oxygen-diffusion limited reaction.

3.5 CARBONYL GROUP DEVELOPMENT IN MULTIPLE-LAYERED SAMPLE

In order to explore the cause of the variation of carbonyl group concentration with sample thickness, the following simple experiments were conducted. A set of either three layers or seven layers of unpigmented PE discs (12 mm diameter) were sandwiched together between metal rings and placed in the QUV. The samples were removed periodically and FTIR measurements were made on the individual layers

before remounting them in the same sequence and returning them to the UV exposure unit. Figures 3-7 to 3-9 show replicate results for three layer unpigmented PE films experiments. Figure 3.10 shows results obtained for seven layers of unpigmented PE films.

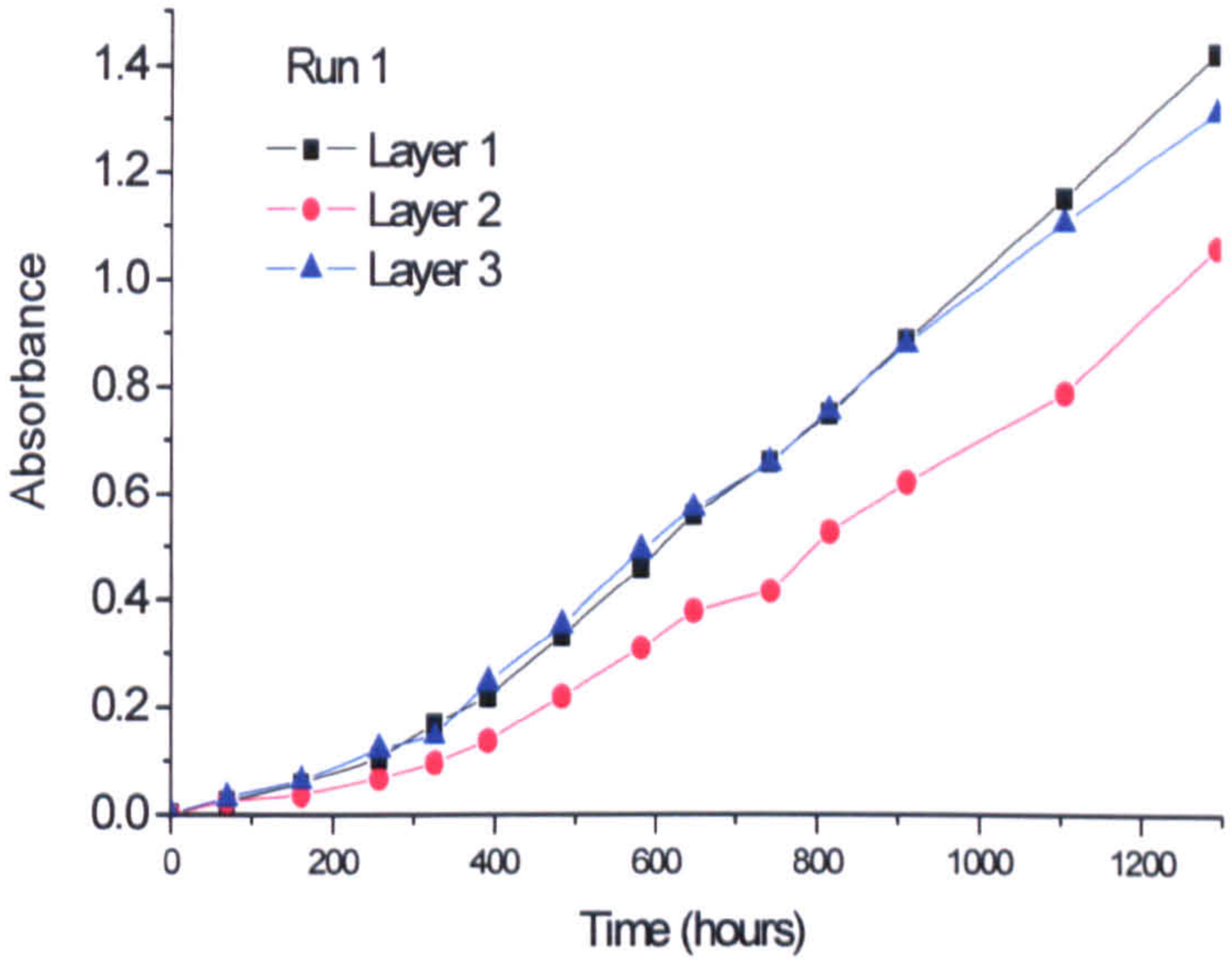

Figure 3-7 Carbonyl group development in three layers of unpigmented PE (U-1) run 1.

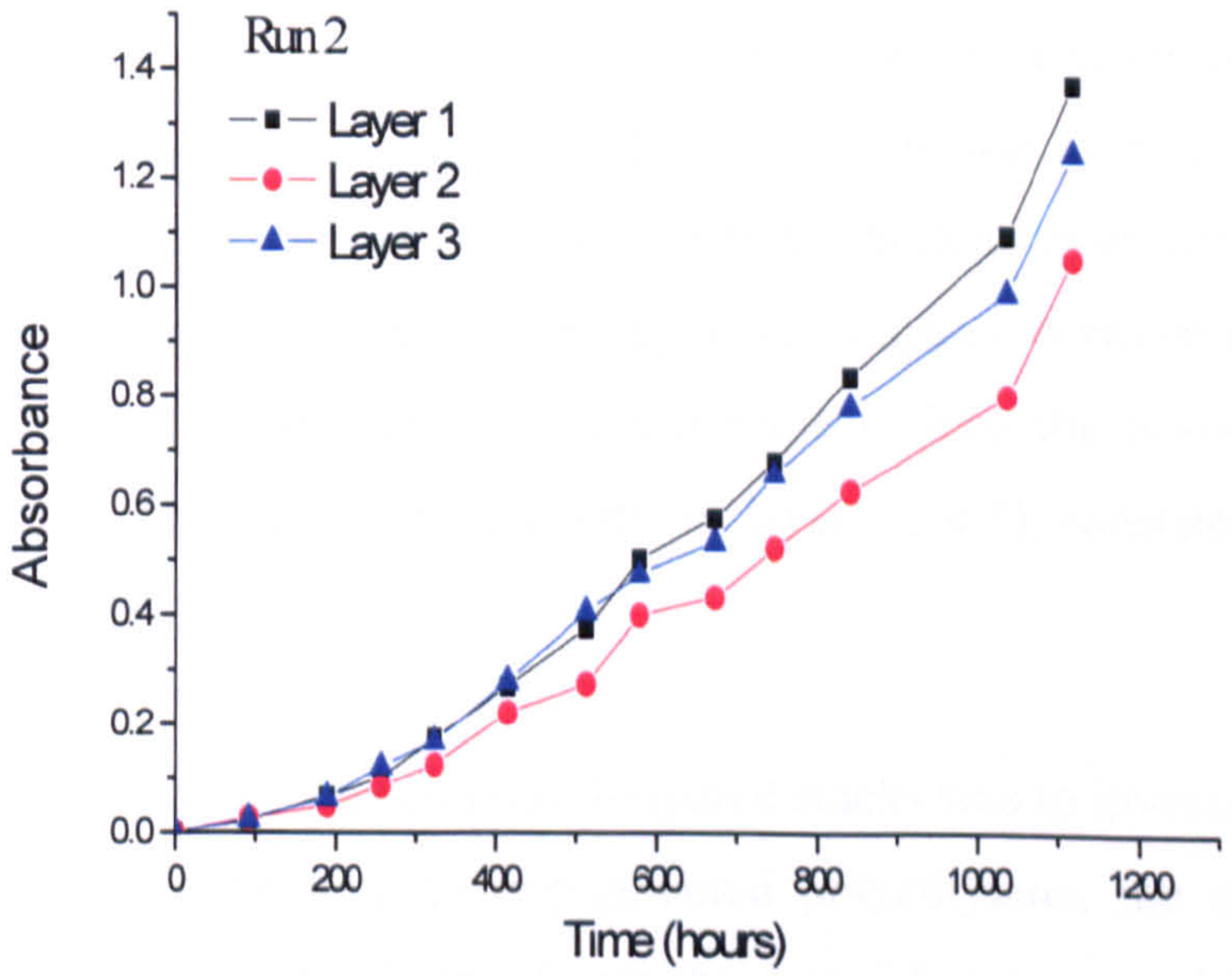

Figure 3-8 Carbonyl group development in three layers of unpigmented PE (U-1) run 2.

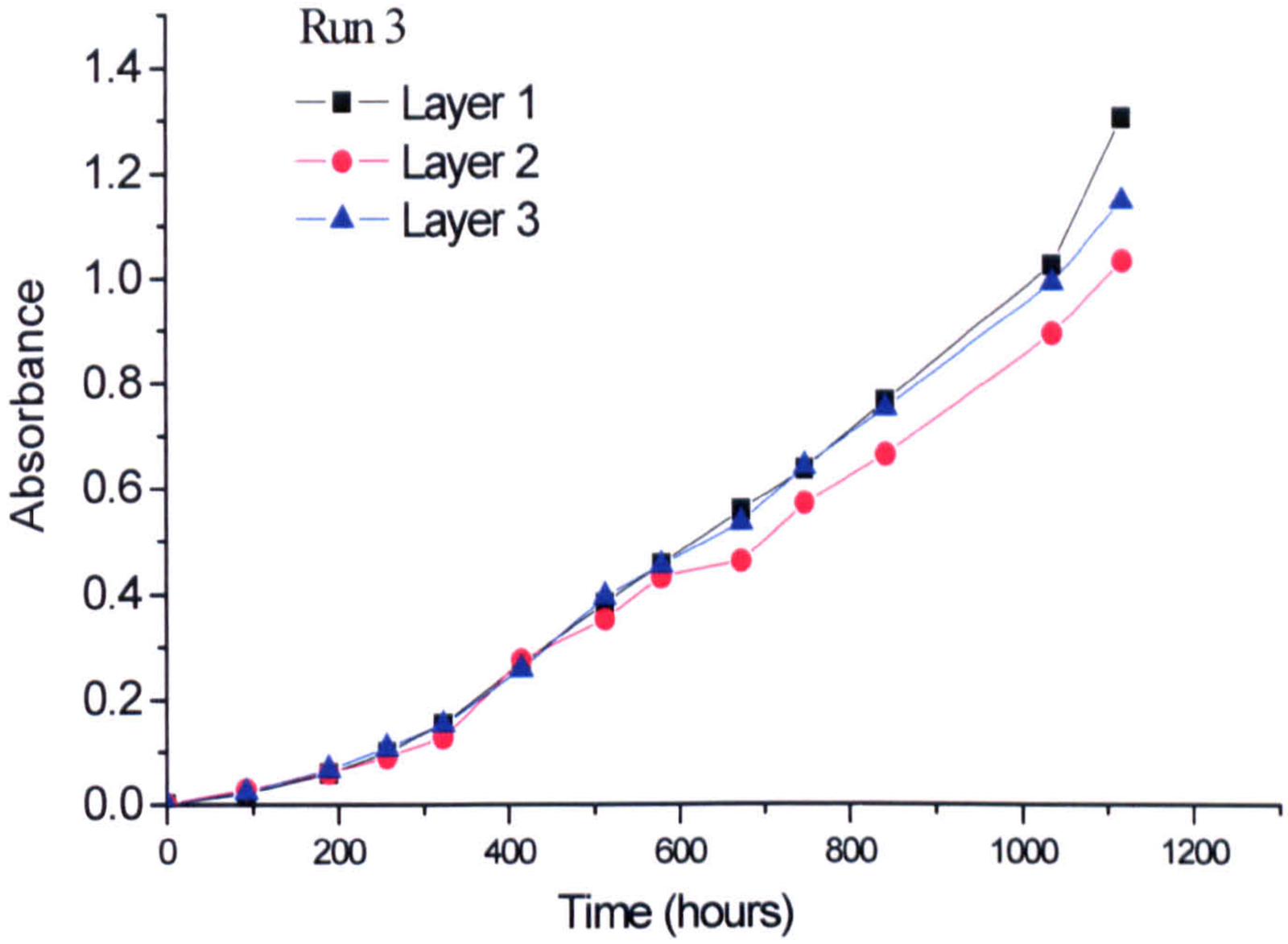

Figure 3-9 Carbonyl group development in three layers of unpigmented PE (U-1) run 3.

For the three layer experiments, the fastest rates of carbonyl group formation were observed with the top layer and the slowest rates of carbonyl group formation were obtained with the central layer, as would be expected if reaction was limited by oxygen starvation. Another reason for differences in carbonyl group development in the three layers is that the UV intensity decreases from top to bottom. This effect causes less reduction in carbonyl development in the bottom layer than the reduction caused by oxygen starvation in the centre layer. The balance between the two effects seems to be changed in the seven layer experiment since the absorbance for the bottom layer (7) is closer to that for the interior layers (3,4,5), consistent with greater attenuation distance.

The main aim of the experiments on multi-layered stacks was to investigate where the carbonyl groups are generated. In unpigmented polyethylene, the slowest rate of carbonyl group formation was observed with the central layer, as would be expected if oxygen starvation played a major part. The unpigmented PE film allows most UV to pass through the top layers then reach the next one.

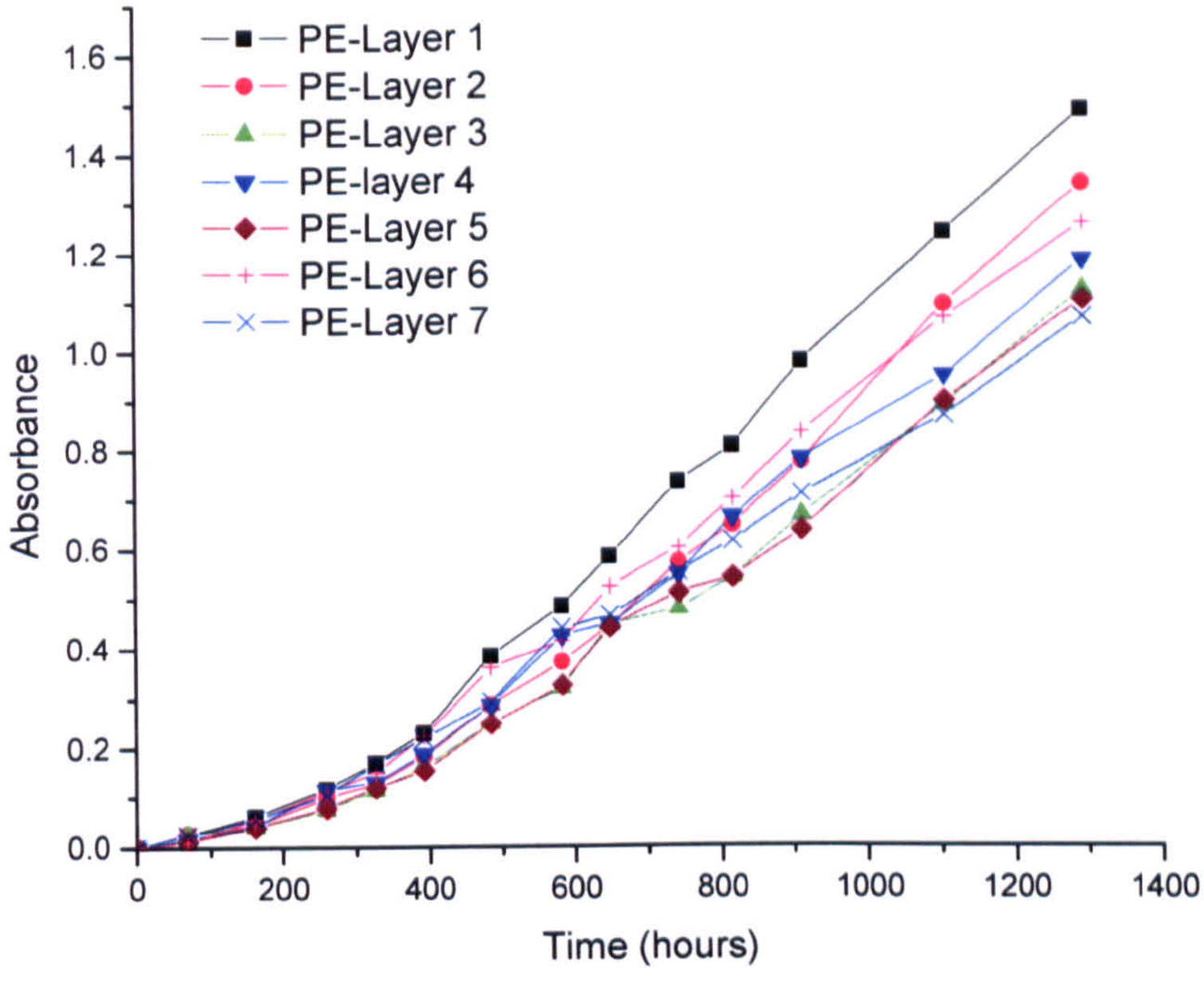

Figure 3-10 Carbonyl group development in seven layers of unpigmented PE (U-1). Layer-1 was the one closest to the source of the illumination.

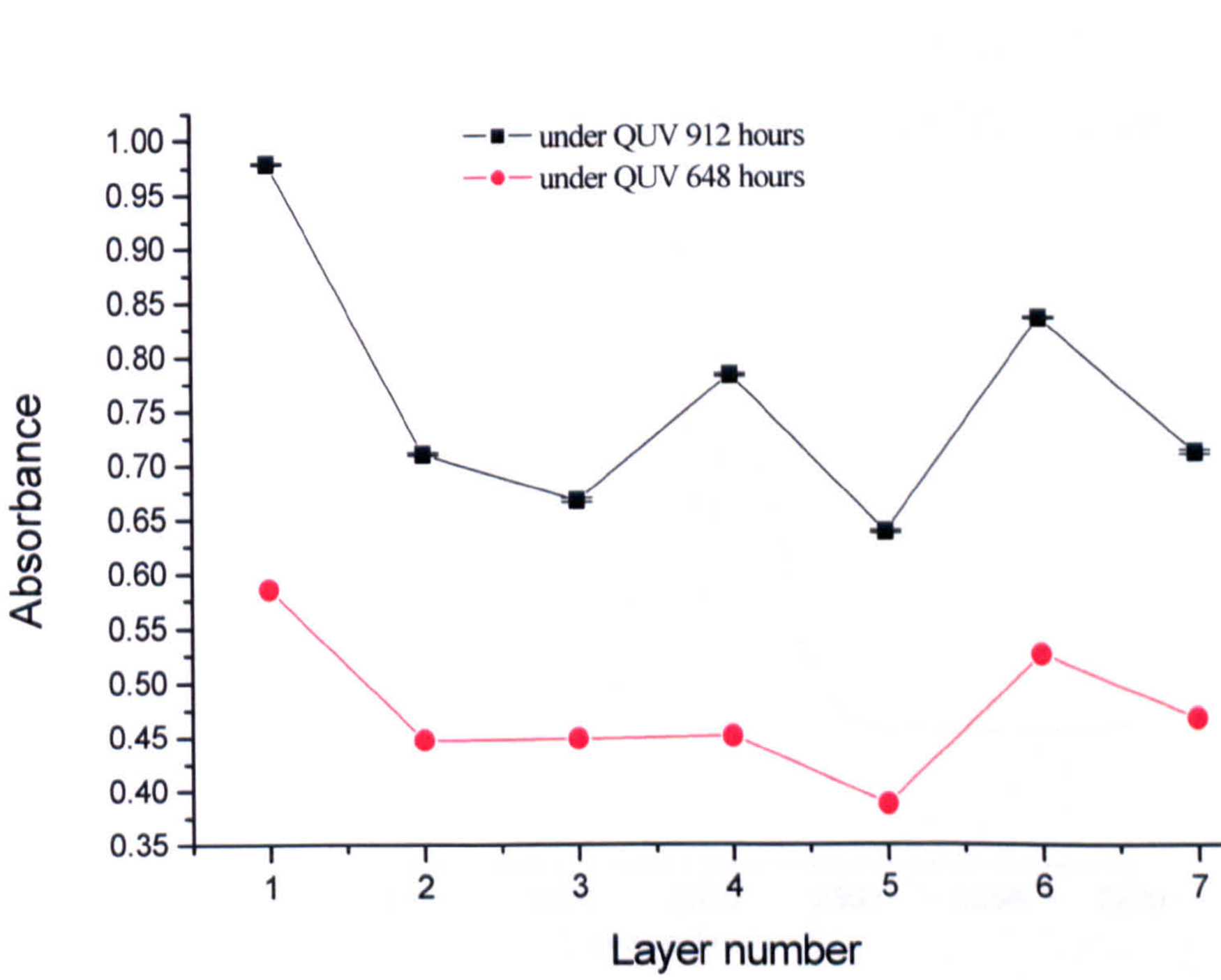

Figure 3-11 Carbonyl group Absorbance for different layers under QUV irradiation as function of layer number (U-1).

Therefore the oxygen diffusion is the dominant factor with top and bottom layers developing the greater carbonyl concentration in three-layer experiments. But with thicker samples, the effective UV intensity at different depths may become the main factor in the photooxidation of polyethylene, and then cause the bottom layer to develop carbonyl groups slower than the top ones in the seven layer stack.

3.6 *IN-SITU* METHOD ON UNPIGMENTED PE FILM

The *in-situ* FTIR method for analysis of the gas phase carbon dioxide was then used to measure the evolution of carbon dioxide during the photo-degradation of the same unpigmented polyethylene films. In order to be able to detect a vibration in the IR spectrum, it must produce a change in the dipole moment of the molecule. CO_2 has a dipole moment when asymmetric stretching or bending occurs, even though it has no dipole moment in the normal state. This asymmetric stretch of gas-phase CO_2 produces a strong doublet band around 2360 and 2340 cm^{-1} in the FTIR spectrum. The absorbance of carbon dioxide at 2360 cm^{-1} was found to be proportional to the concentration of carbon dioxide in the cell. The absorption at 2360 cm^{-1} is measured for quantitative analysis in this study. More details were described in experimental section 2.2. Figure 3-12 shows a gas-phase carbon dioxide FTIR spectrum.

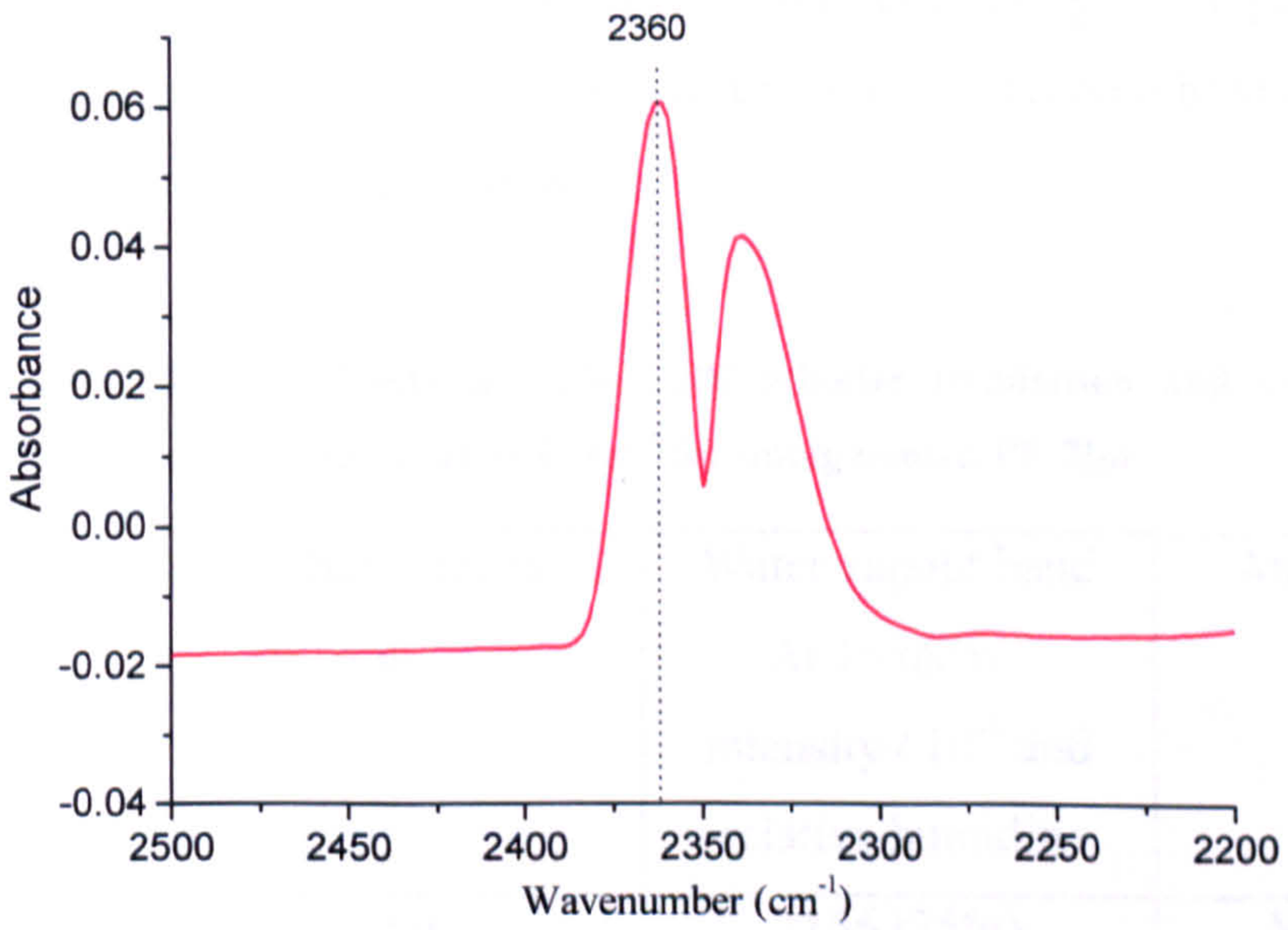

Figure 3-12 The typical gas phase carbon dioxide FTIR spectrum recorded from ca 1197 Pa CO_2 pressure filled cell .

3.6.1 Preliminary study and Reproducibility checking

Works were carried out in order to explore whether the FTIR CO_2 method can be used to measure the evolution of carbon dioxide gas generated from the degradation of the unpigmented polyethylene film. The samples were U-1 100μm film and were placed in the back position in the analysis cell [11] with moist ~ 80 % humidity oxygen atmosphere. UV light was provided by a 150 W Xenon lamp system with IR filter and Solar filter AM1.5. Although this thesis centres on the role of TiO_2 pigment, degradation of an unpigmented PE film was studied in order to subsequently assess the relative contribution of direct photochemical and TiO_2-mediated heterogeneous photocatalytic oxidation in pigmented films. Figure 3-13 shows changes in the infrared absorbance of gaseous carbon dioxide before, during and after irradiation of unpigmented PE film. It can be seen that there is no evolution of carbon dioxide in the dark. Carbon dioxide bands increase only during UV irradiation. It also shows that the rate of CO_2 evolution is constant during the course of the experiment under this condition. When the UV irradiation was switched off, the carbon dioxide evolution stopped immediately. When UV light was switched on again, the rate of carbon dioxide evolution was the same as in the previous stage. This may suggest that short time UV radiation with the experimental conditions used did not cause any significant change in the physical or chemical state of unpigmented polyethylene. The results of two duplicate samples are shown in Table 3-1 and the good repeatability is demonstrated in Figure 3-13. The numbers in brackets are relative humidities in the cell when the experiment was carried out.

Table 3-1 The CO_2 band intensity after 180 minutes irradiation and values for the intensity of the water vapour band near 1557 cm^{-1} for unpigmented PE film

Run	CO_2 band intensity / 10^{-4} a.u.	Water vapour band At 1558cm^{-1} intensity / 10^{-4} and relative humidity	Atmosphere
1	69	1156 (75%)	Moist O_2
2	66	1211 (83%)	Moist O_2
Average	67.5	1183	

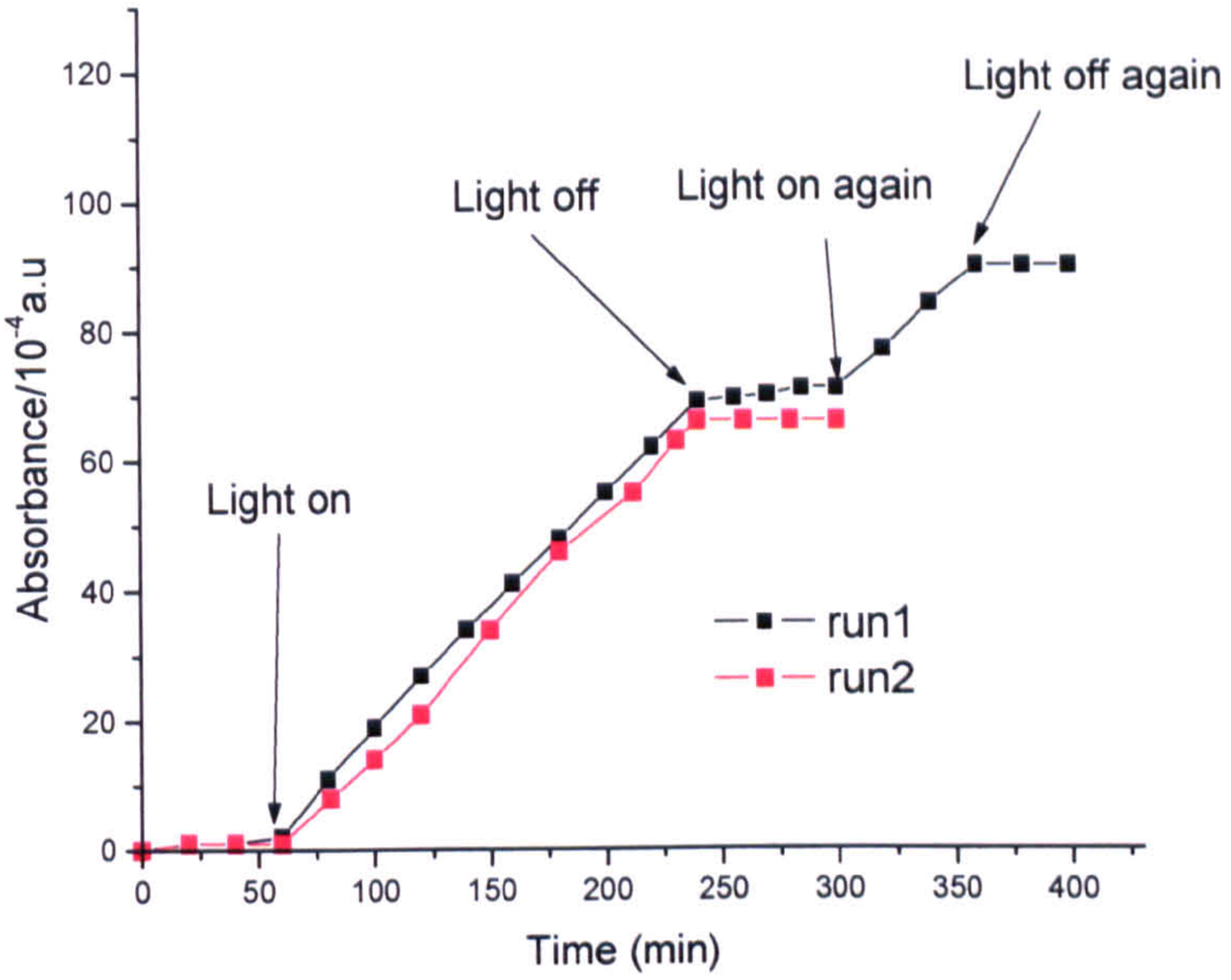

Figure 3-13 The infrared absorbance of gaseous CO_2 before, during and after UV irradiation of duplicate unpigmented PE film samples (U-1) with filter AM1.5.

3.6.2 Results for PE film (PE U-2) in front position

For the runs reported in Figure 3-13 it was shown that in the absence of UV, there was a small and neglected background carbon dioxide. However, during the course of the research it has become obvious that the CO_2 signal from an empty cell under UV irradiation is not always negligible. This signal is attributed to generation of CO_2 by UV photolysis of *e.g.* vacuum grease or 'Araldite' adhesive. The absolute amount depended on the age of the cell and, most importantly, on the amount of stray UV irradiation. As explained in the experimental section the problem of UV-induced background CO_2 was minimised by placing the sample at the front of the cell.

Figure 3-14 shows the data obtained with a sample of PE U-2 film placed in the front position. When no PE film was present, the background carbon dioxide was 12×10^{-4} a.u. after 10 hours UV illumination with AM0 filter. This carbon dioxide background is comparable with the carbon dioxide changes caused by temperature fluctuation in the course of the experiment. This means that the carbon dioxide contribution coming from UV irradiation of the sample holder and other parts of cell is small and may be neglected.

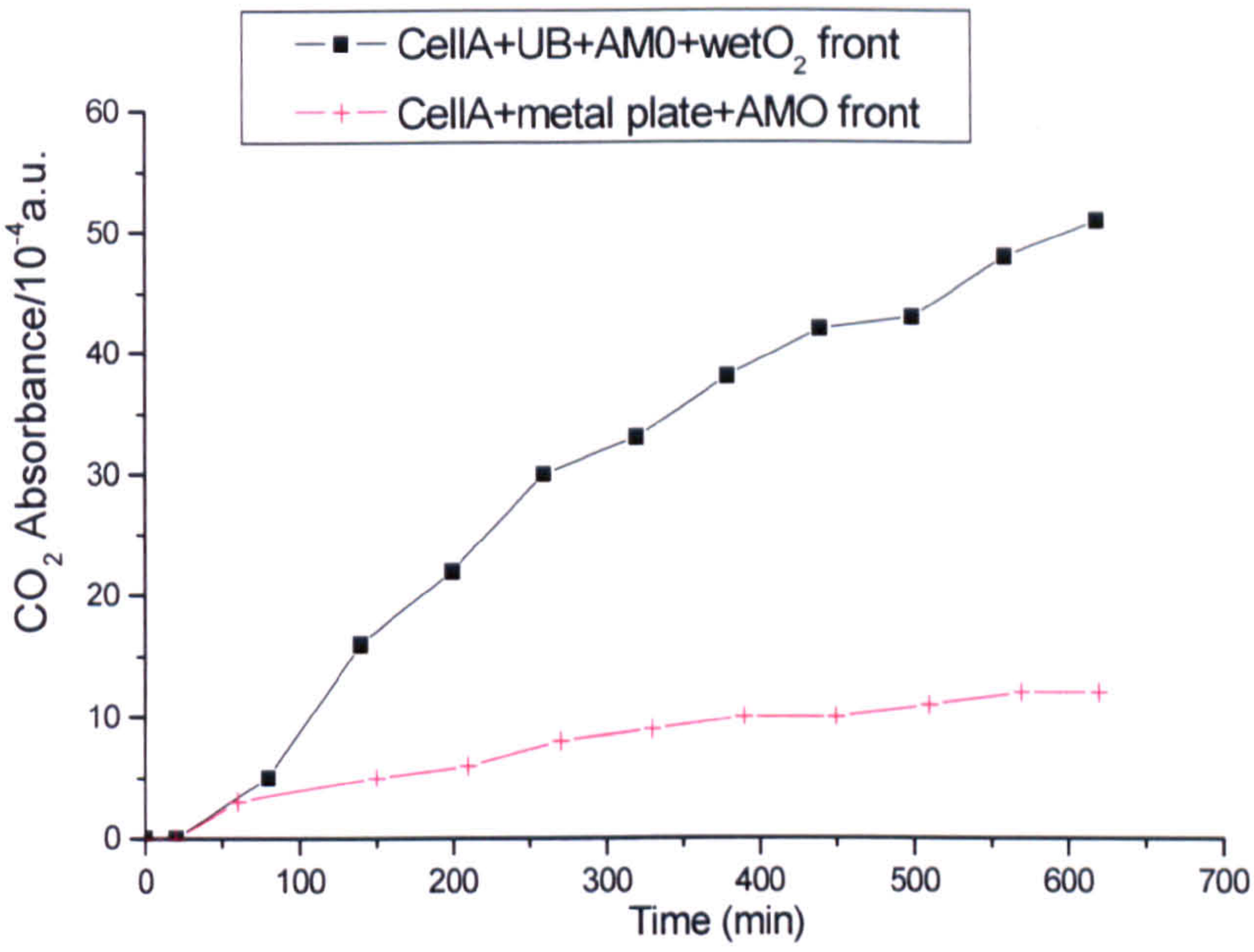

Figure 3-14 CO_2 evolution from unpigmented PE sample placed at front position.

3.7 CO_2 EVOLUTION DEPENDENCE

3.7.1 Effect of film thickness on CO_2 evolution

Pigmented films absorb UV in a very short distance but unpigmented films do not. Therefore it was desired to establish the effect of the film thickness of unpigmented films on measured rates of CO_2 evolution, with drawn polyethylene of 250 μm and 100 μm thickness. Figure 3-15 shows that, for samples placed at the front position, the carbon dioxide evolutions are different from these two samples under UV exposure. Evolution of CO_2 from the 100 μm PE sample and the 250 μm PE sample are 30 and 65 a.u. respectively, under 10 hours UV irradiation with the AM0 filter. It appears that the carbon dioxide evolved was not precisely proportional to the sample thickness. With sample thickness increase, the CO_2 evolution rate per unit thickness decreased (see Figure 3-16). Most is probably because of oxygen diffusion limitation.

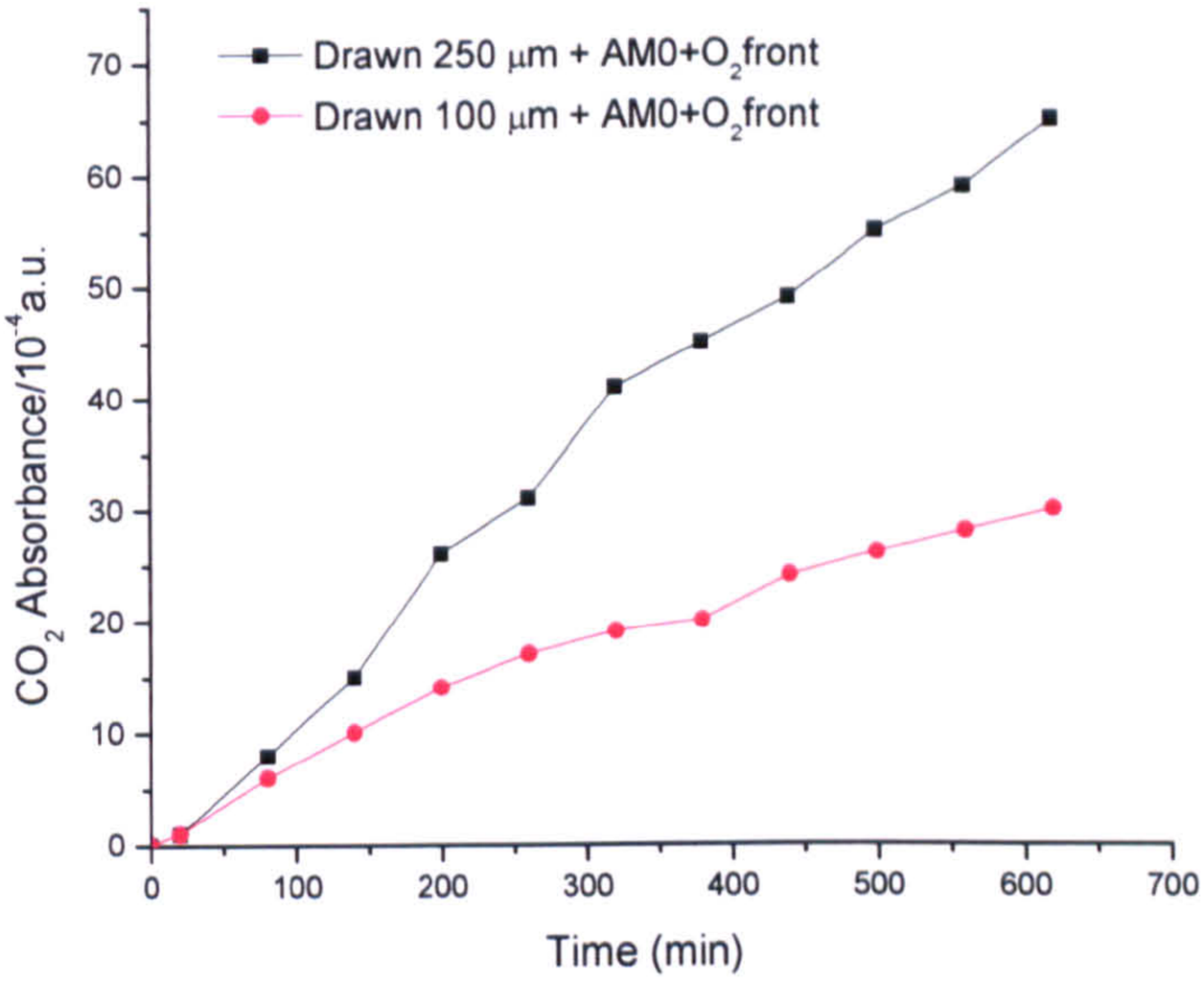

Figure 3-15 Carbon dioxide evolution from drawn polyethylene of 250 μm and 100μm thickness.

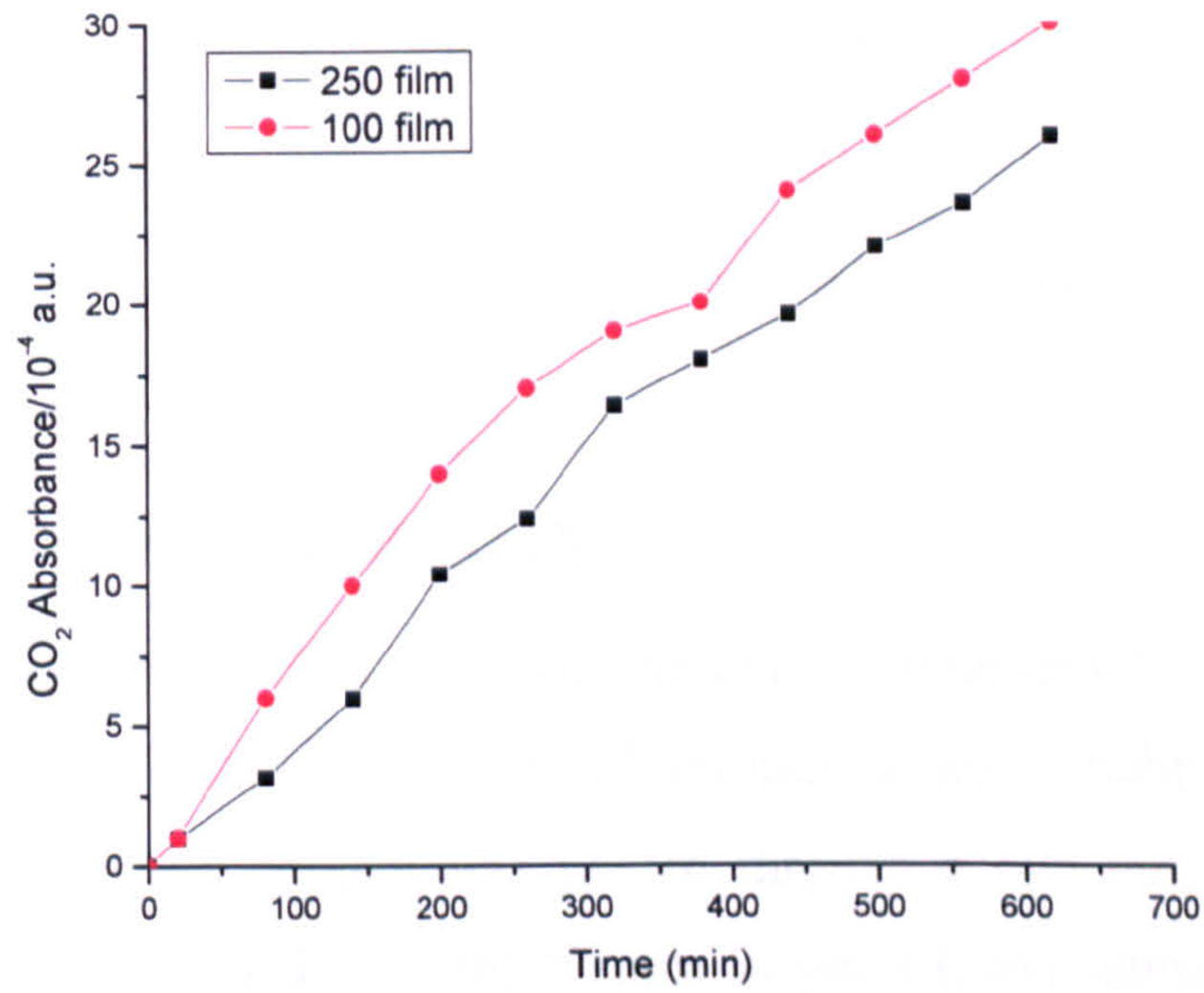

Figure 3-16 Carbon dioxide evolution from drawn 250 μm PE film divided by 2.5 for comparison with 100 μm thickness PE film.

3.7.2 Dependence of carbon dioxide evolution rate on UV intensity

The dependence of CO_2 evolution on UV intensity was measured using runs without an AM filter. The results in Figure 3-17 show that there is a direct linear relationship between the rate of carbon dioxide evolution and the UV intensity used which was

changed by putting one different neutral filter between the head of the light pipe and the cell. A U-1 sample was used and placed in the front position.

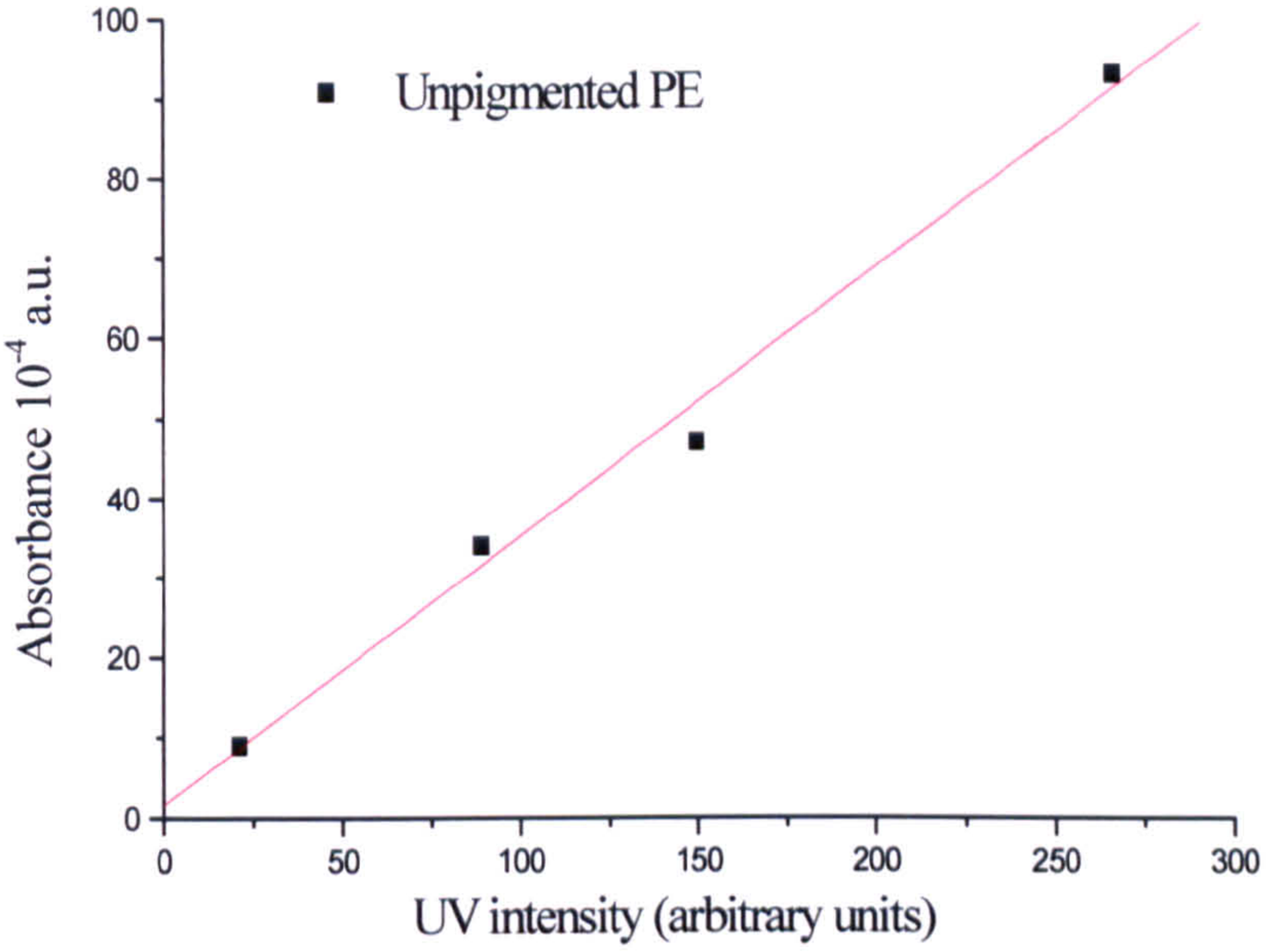

Figure 3-17 CO_2 evolution from unpigmented PE film after 240 minutes as a function of variation in incident UV intensity without AM filter.

3.8 EFFECTS OF HUMIDITY

In order to assess the effect of humidity on CO_2 evolution under UV irradiation, it was convenient to use cylinder oxygen passed through a water bubbler to get moist atmosphere gas. Cylinder oxygen was passed through a 600 mm glass tube with interior diameter 5 mm filled with fresh silica to get a lower humidity atmosphere. Surprisingly the humidity of the gas obtained direct from the cylinder was sometimes lower than that "dried" through silica, as shown by monitoring the water vapour band intensity (presented in the bracketed number on the graph) at 1557 cm^{-1}. Results for unpigmented PE film are shown in Figure 3-18. The CO_2 evolution during 3 hours UV irradiation for the sample, and water vapour band intensity are summarised in table 3-2.

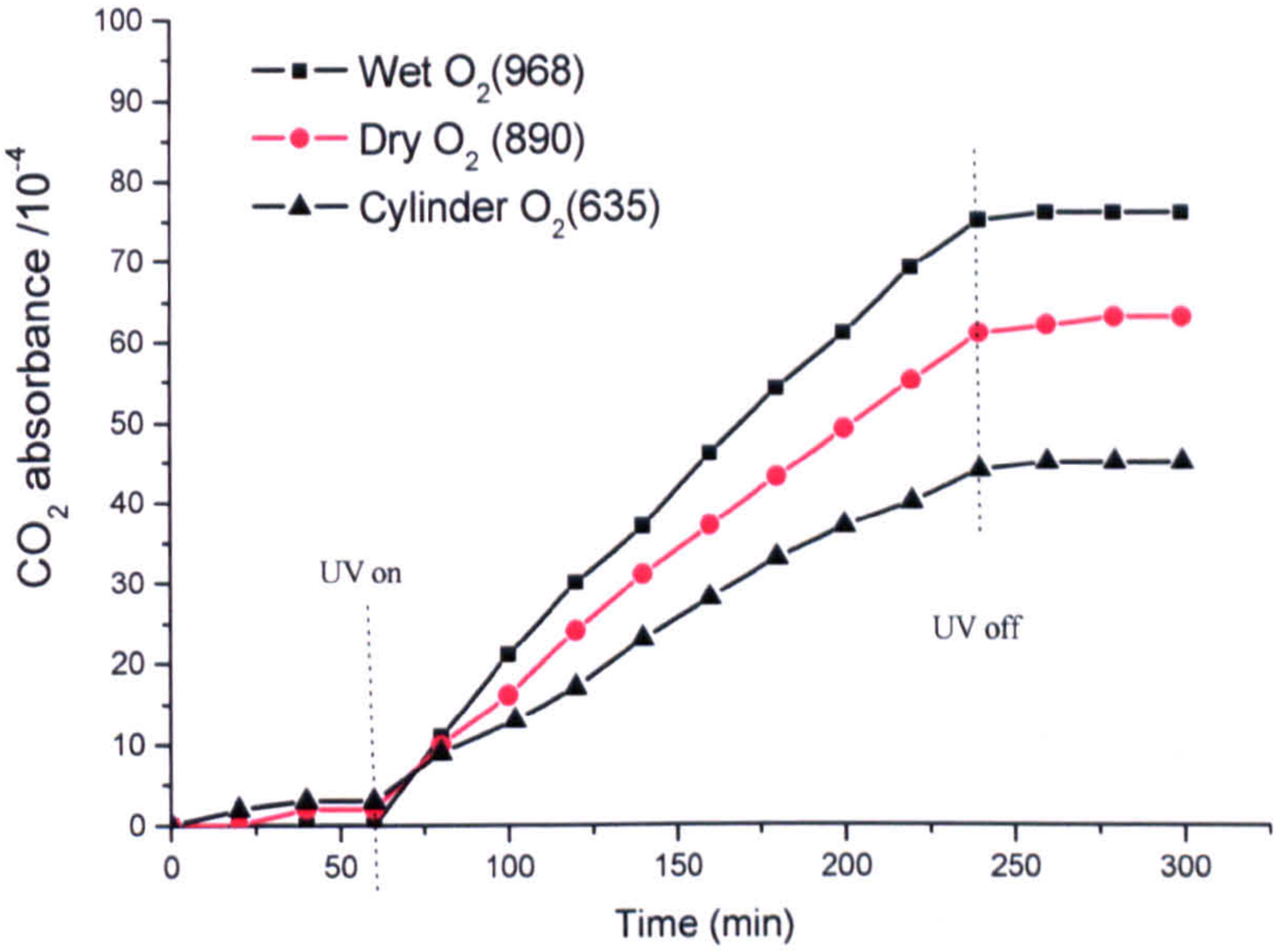

Figure 3-18 Carbon dioxide evolution from unpigmented PE film in different humidity atmospheres.

It can be clearly seen from Figure 3-18 and Table 3-2 that in the presence oxygen, water accelerates CO_2 formation as the humidity increases for unpigmented PE films. Therefore, the present results demonstrate that it is essential to control humidity if reproducible comparisons of PE films are to be made by monitoring the carbon dioxide produced during film breakdown.

Table 3-2 Dependence CO2 evolution on humidity for unpigmented PE.

Run	Water vapour band at 1557 cm^{-1} Abs×10^{-4} By background	Atmosphere	CO_2 Abs×10^{-4} After 3h irradiation	Reduction comparison with wet O_2 %
1	968	Wet O_2	75	
2	890	Dry O_2	61	81
3	635	Cylinder O_2	43	57

3.9 EFFECT OF OXYGEN CONCENTRATION

Oxygen is one of the main reactants in both direct photochemical and indirect photo-catalysed oxidation of a polymer system. The oxygen concentration is expected to play an important role in the reaction. The effect of reducing the oxygen partial pressure was therefore investigated by purging with a 20/80 (v/v):O_2/N_2 mixture using the standard procedure. All gases were bubbled through de-ionised water to give similar humidity. Results are given in table 3-3 and shown in Figure 3-19.

Table 3-3 Dependence of CO_2 evolution on oxygen concentration from unpigmented PE films quote value.

Run	Atmosphere	CO_2 Abs$\times 10^{-4}$ After 3h irradiation	Reduction comparison with Wet O_2 %
1	Wet O_2	75	
2	20% O_2	68	90
3	Wet N_2	43	57

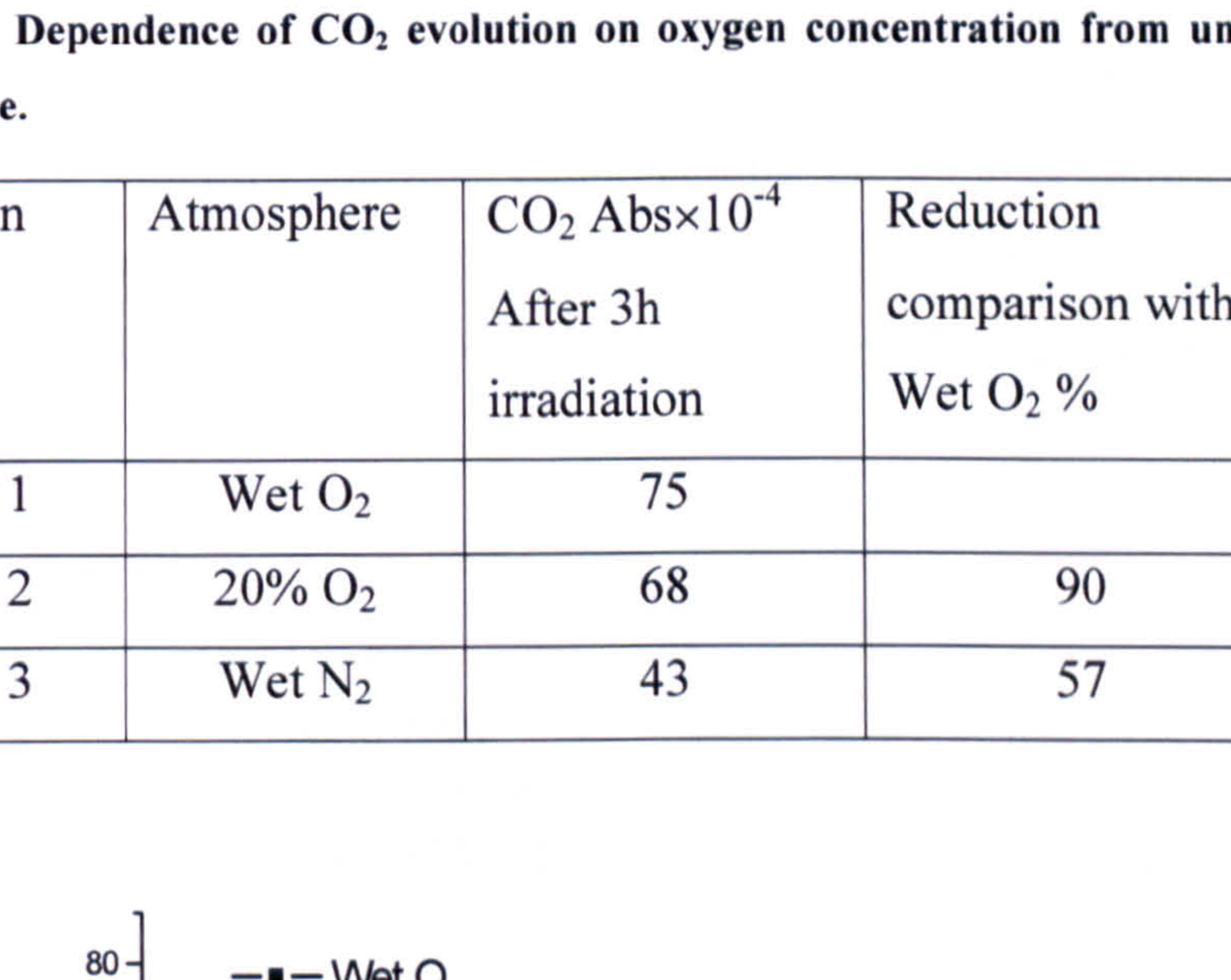

Figure 3-19 Carbon dioxide evolution in different oxygen concentration atmospheres from Unpigmented PE film.

It can be seen from table 3-3 that the difference in CO_2 evolution between pure oxygen and 20 % oxygen is small. The oxygen concentration difference between them is 80 %, but this just causes a carbon dioxide reduction of 10 %.

3.10 EFFECT OF AM FILTERS - DIFFERENT SPECTRAL DISTRIBUTION

In these experiments, different filters were used to select defined portions of the UV spectrum and the effect on carbon dioxide evolution rates was monitored. Figure 3-20 shows spectroradiometer results for the intensity and spectral distribution of UV falling on the cell with different filter combinations. Figure 3-21 shows the results for unpigmented PE film irradiated with different UV distributions caused by no filter or different filter combinations. The rate of the CO_2 evolution depended on the filters which were used.

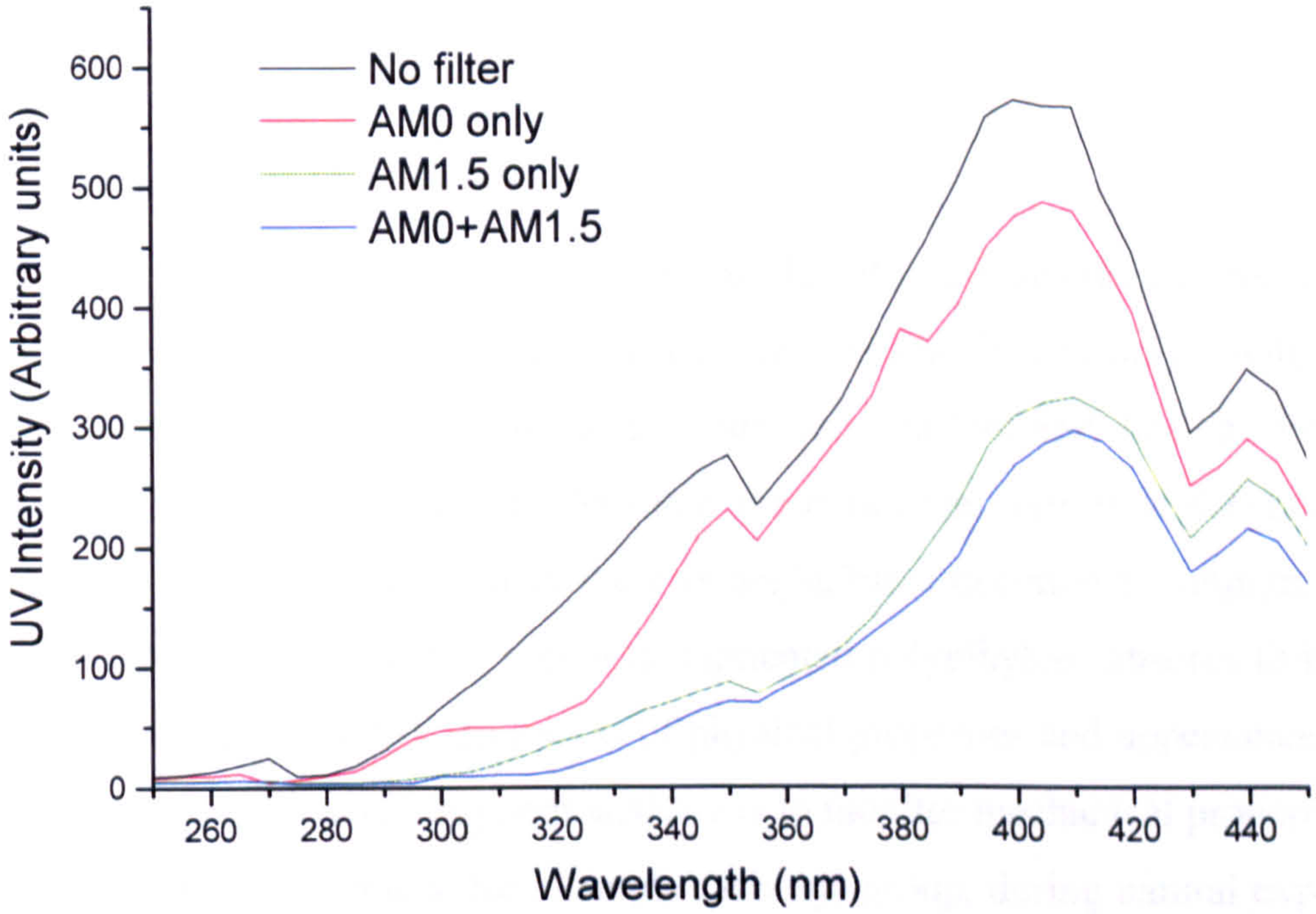

Figure 3-20 Spectroradiometer results for the intensity and spectral distribution of UV falling on the cell with different filter combinations.

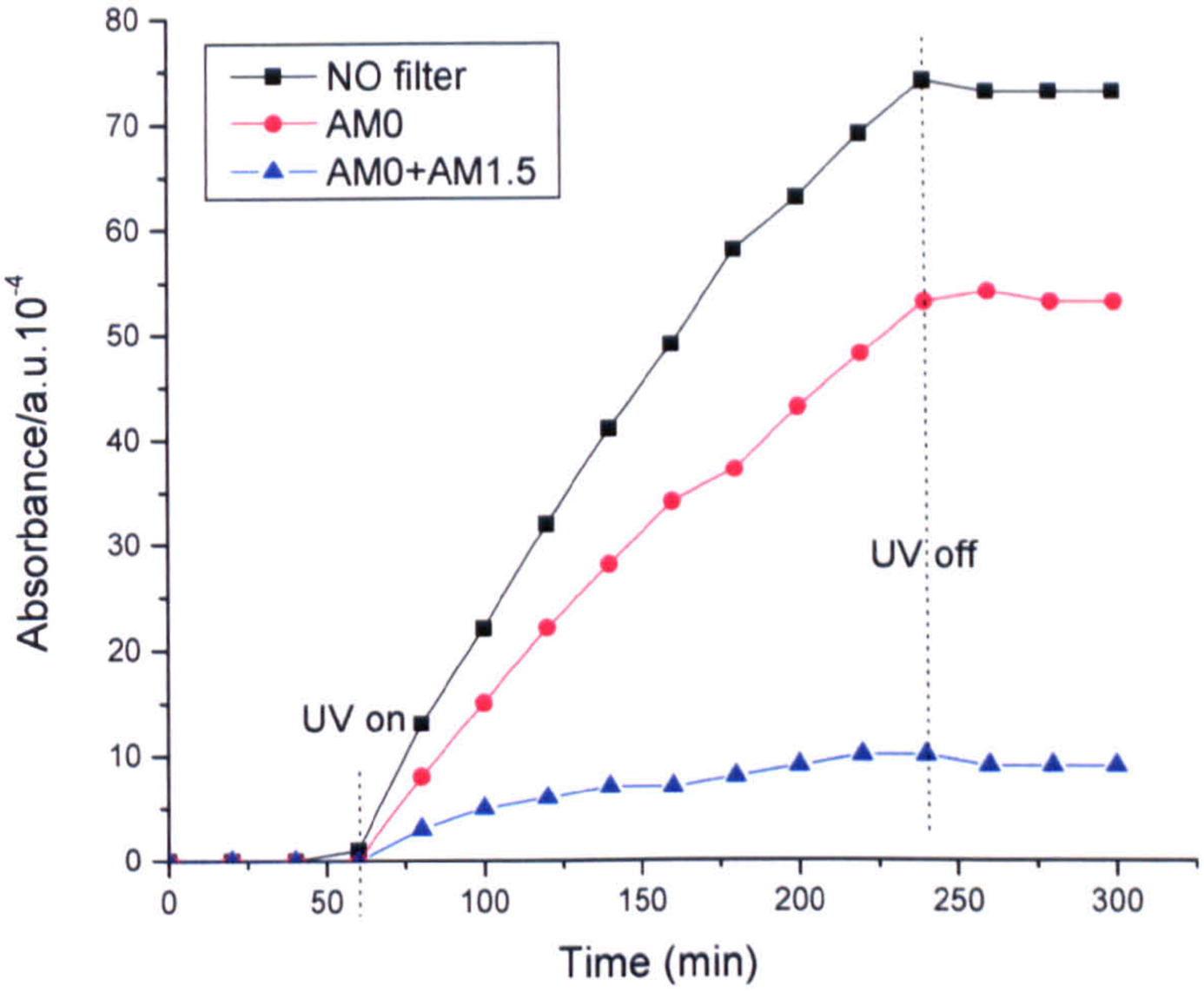

Figure 3-21 Unpigmented PE film CO_2 evolution with different filter combinations. All the measurements were made with the samples in the front position.

3.11 DISCUSSION

The results in Figure 3-1 and Figure 3-2 show that the unpigmented polyethylene starts strongly absorbing UV light at very low wavelengths (< 225 nm). Sunlight or common artificial UV lamps produce a spectrum between 290 and 400 nm. For the Xe lamp used in this study without AM filter, the major emission is at 400 nm (see Figure 3-20) - a wavelength at which there is negligible absorption by unpigmented polyethylene. Although in the UV region unpigmented polyethylene absorbs little UV light, this causes significant deterioration of physical properties and appearance. The current FTIR method of assessing photoactivity is to monitor mechanical properties of some kind of functional groups, for example carbonyl group, during natural exposure in areas of high sunlight intensity. This can take upwards of years to obtain satisfactory results [12]. Even with accelerated artificial UV sources, it can still take months to obtain suitable data. Sections 3.3-3.5 in this chapter show that the carbonyl group development method took hundreds of hours to build up detectable signals in the samples.

A new technique - *in-situ* FTIR spectroscopy has been developed for the study of photo-degradation of polyethylene that is sufficiently sensitive to detect the CO_2 evolution under UV irradiation in hundreds of minutes. The results in Figure 3-13 show that the evolution of carbon dioxide from unpigmented polyethylene increased significantly above the background value (~12×10^{-4} absorbance per-run) when the samples were irradiated. The comparison, in Figure 3-5 and Figure 3-15, of relative rates of photo-degradation of unpigmented polyethylene by these two methods shows a similar pattern. This confirms that the FTIR assay of carbon dioxide evolution provides information that is relevant to conventional accelerated testing of polyethylene photoactivity but the carbonyl accumulation method needs much more time than the CO_2 method.

All of the above analysis has demonstrated that CO_2 evolution from unpigmented polyethylene can be measured using *in-situ* FTIR spectroscopy. The results of the FTIR CO_2 method are relevant to practical polyethylene durability. Therefore, the method may be usefully exploited to probe details of the mechanism of the photo-degradation of polyethylene and results described in sections 3-7 → 3-12 show that the CO_2 method is a versatile technique for evaluation of the effect of different factors on unpigmented polyethylene photodegradation. Firstly it is easy to use it to determine the effect of the UV intensity and wavelength. The results of Figure 3-17 illustrate that the FTIR method can directly monitor changes in unpigmented polyethylene degradation rates when UV intensity changes are made. A linear relationship was found to exist between CO_2 evolution and UV intensity. This result is different from that obtained with the unpigmented acrylic paint which has a degradation rate proportional to the square root of the UV intensity [4]. The results in Figure 3-21 show that the incident UV spectral intensity distribution affects the CO_2 evolution. This enables meaningful understanding of the effect of wavelength on polyethylene photodegradation. In particular, there is negligible CO_2 generation if AM0 and AM1.5 filters are combined to remove wavelengths below 290 nm from the output of the xenon lamp. Figure 3-18 and Figure 3-19 show that the rate of CO_2 evolution increases both with humidity and with the oxygen content.

3.12 CONCLUSION

The results and discussion above have shown that, although the unpigmented polyethylene appears to the quite stable in comparison with the paints systems studied previously [4, 11, 13], the UV stability of unpigmented polyethylene can be monitored by an FTIR measurement of the UV-generated carbon dioxide. There is a good correlation between the traditional FTIR carbonyl method and the CO_2 method, which is easy to conduct, versatile, and permits fairly rapid assessment of the relative photodegradability of unpigmented polyethylene affected with many factors - UV wavelength, humidity, oxygen content *etc.*

3.13 REFERENCES

1. Christensen, P.A., A. Dilks, T.A. Egerton, E.J. Lawson, and J. Temperley, *Journal of Materials Science,* 2002. **37**(22): p. 4879-4887.
2. Allen, N.S. and H. Katami, *Polymer Degradation and Stability,* 1996. **52**(3): p. 311-320.
3. Gulmine, J.V., P.R. Janissek, H.M. Heise, and L. Akcelrud, *Polymer Testing,* 2002. **21**(5): p. 557-563.
4. Christensen, P.A., A. Dilks, T.A. Egerton, and J. Temperley, *Journal of Materials Science,* 2000. **35**(21): p. 5353-5358.
5. Christensen, P.A., A. Dilks, T.A. Egerton, and E.J. Lawson, *Journal of Materials Science,* 2002. **37**: p. 1-9.
6. COMPANY, T.Q.-P., Operating Manual Q.U.V. Accelerated Weathering Tester.
7. Gulmine, J.V., P.R. Janissek, H.M. Heise, and L. Akcelrud, *Polymer Degradation and Stability,* 2003. **79**(3): p. 385-397.
8. Shlyapintokh, V. and Ya., *Chem.,,* 1983. **55**: p. 1661.
9. O'Donnell, B. and J.R. White, *Polymer Degradation and Stability,* 1994. **44**: p. 211-222.
10. Giesse, R. and M.A. Depaoli, *Polymer Degradation and Stability,* 1988. **21**(2): p. 181-187.
11. Christensen, P.A., A. Dilks, T.A. Egerton, and J. Temperley, *Journal of Materials Science,* 1999. **34**(23): p. 5689-5700.
12. Johnson, B.W. and R. McIntyre, *Progress in Organic Coatings,* 1996. **27**: p. 95-106.
13. Christensen, P.A., T.A. Egerton, E.J. Lawson, and J. Temperley, *Journal of Materials Science,* 2002. **37**(17): p. 3667-3673.

CHAPTER 4

PIGMENTED POLYETHYLENE

4.1 INTRODUCTION

In Chapter 3, the methods used to characterize the photodegradation of unpigmented polyethylene (PE) film were outlined. A new method for gas-phase monitoring of the evolution of CO_2 was introduced and conventional measurement of carbonyl group development by FTIR was described. These techniques can be used to characterize pigmented polyethylene photodegradation under UV exposure and it is important to establish whether there is a good correlation between them. The work reported in this chapter represents an extension to the preliminary studies, discussed in chapter 3, designed to establish an increased understanding of the mechanism of the photo-oxidation of practical films pigmented with different grades of pigments. The chapter reports studies on all aspects described in Chapter 3 for unpigmented polyethylene films and the comparison of unpigmented polyethylene films and pigmented polyethylene films.

A new approach to *in-situ* monitoring of photo-oxidation of polyethylene was driven by the desire to evaluate whether a simple *in-situ* FTIR gas-phase rapid photo-oxidation technique could be employed in order to establish, the relatively long term weathering performance of commercial grade pigments in a matter of hours, thus facilitating (for obvious commercial advantages) the development of new pigment grades. It was essential to ensure that the gas-phase FTIR procedure has with sufficient sensitivity to distinguish between durable commercial pigment grades and to rank the commercial grades in the same order as that seen from conventional weathering tests.

4.2 EXPLORATORY EXPERIMENTS

4.2.1 *In-situ* method on pigmented PE film

4.2.1.1 PE film pigmented with anatase TiO_2 (PE A-1)

The preliminary experiments were undertaken in order to explore whether the gas-phase FTIR method can be used to measure the evolution of carbon dioxide from the degradation of the pigmented polyethylene film. This is necessary in order to assess subsequently the relative contribution of direct photochemical and TiO_2-mediated heterogeneous photocatalytic oxidation in pigmented films.

Firstly, the effects of anatase (A-1) titanium dioxide pigment on CO_2 evolution under UV irradiation and experiment reproducibility were explored. The experimental conditions were the same as those for the unpigmented PE film experiments described in section 3.6.1. UV light comes from a 150 W Xenon lamp system with IR water filter and Solar filter AM1.5. The results reported here are from the batch-1 sample, which was supplied in September 2000 by Huntsman Tioxide. The samples were placed in the back position in the cell. Normally, a blank experiment, for checking that the CO_2 background-level was lower than 10-12×10^{-4} a.u. took place before trial experiments were run. The results for two runs are shown in Table 4-1 and plotted in Figure 4-1. The numbers in brackets are the relative humidity in the cell when the experiment took place, obtained from the IR signal.

Table 4-1 The CO_2 band intensity after 180 minutes irradiation and values for the intensity of the water vapour band near 1557 cm^{-1} for A-1 pigmented PE film.

Run	CO_2 band intensity / 10^{-4} a.u.	Water vapour band intensity/10^{-4} a.u.	Atmosphere
1	92	1175 (78%)	Moist O_2
2	93	1222 (86%)	Moist O_2
Average	92.5	1198	

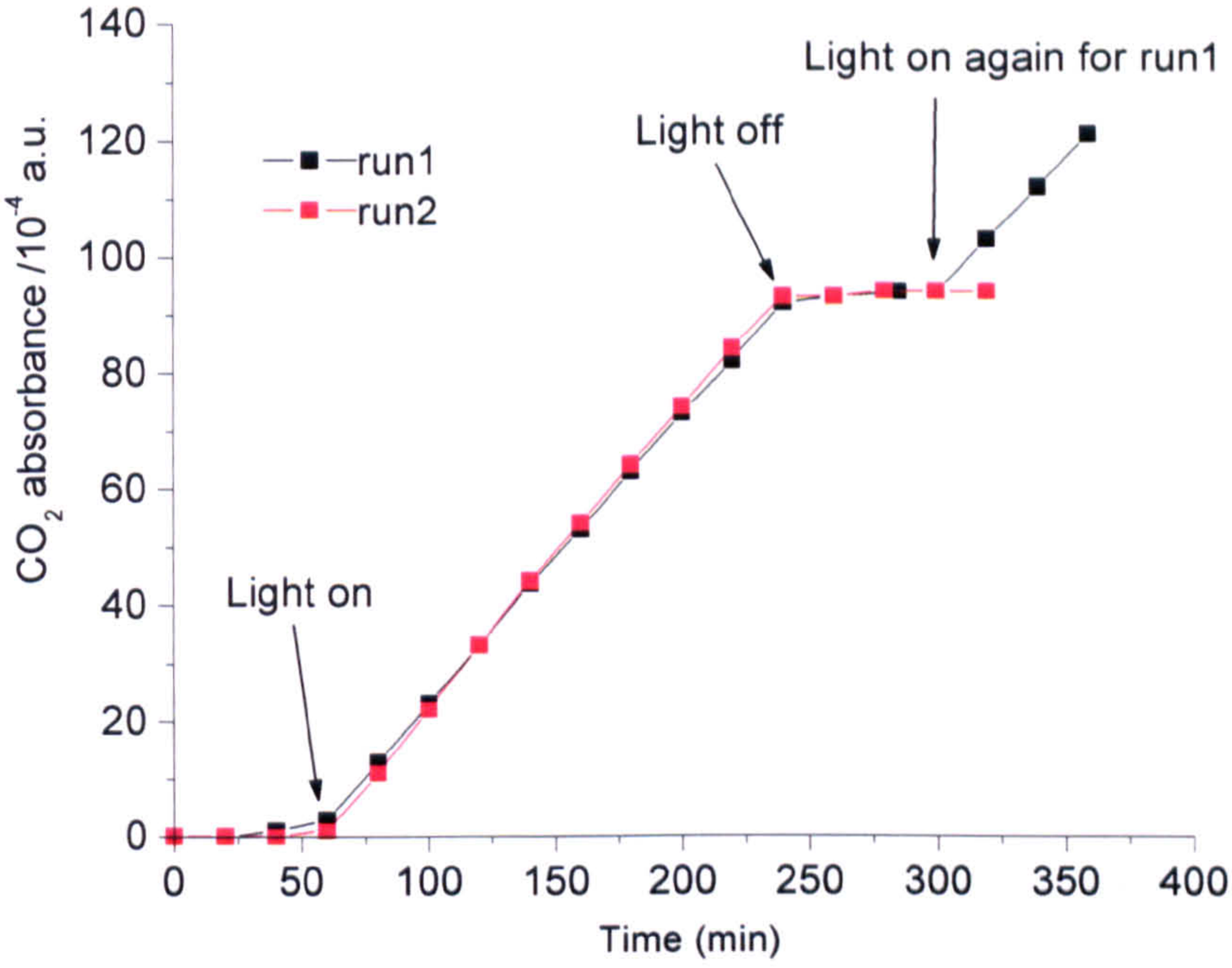

Figure 4-1 The infrared absorbance of gaseous CO_2 before, during and after UV irradiation of replicate A-1 pigmented PE films.

From Table 4-1 and Figure 4-1 it can be seen that, as with unpigmented PE film, CO_2 evolution from PE A-1 occurs only during UV irradiation. The rate of carbon dioxide generation for PE A-1 film was significantly faster than for unpigmented PE film. For the PE A-1 films, the average CO_2 absorbance observed was *ca.* 92×10^{-4} a.u. and for the unpigmented PE films was *ca.* 67×10^{-4} a.u after 3 hours irradiation. Reproducibility for repeat runs of the two PE A-1 samples was excellent. It also shows that the rate of CO_2 generation was constant during irradiation. This shows that photoreaction of PE A-1 film was very stable in the course of 3 hours UV irradiation. If the same sample was irradiated again following an hour interval after the light was switched off, the same rate of CO_2 evolution was observed (Figure 4-1). It is shows below that PE A-1 also gave more carbon dioxide than any rutile containing pigment PE film. This also suggests that the ability of strong photocatalytic activity of A-1 pigment is more important than the ability to reduce photochemical rate by absorption of UV light, even though, as will be shown later, the UV absorption restricts the depths of film in which photochemical reactions take place.

4.2.1.2. PE film pigmented with rutile TiO_2

PE A-1 gave significantly higher CO_2 emission than unpigmented polyethylene (PE u-1) and the *in-situ* test method is sufficiently sensitive to distinguish anatase pigmented polyethylene from unpigmented polyethylene. However, an accelerated weathering test must be able to distinguish between samples which are more closely similar in their level of photoactivity *i.e.* commercial pigment grades with similarly low photoactivies. Studies were therefore carried out on a set of rutile pigment containing PE films. The samples used were denoted as PE R1-1, PE R2-1 and PE R3-1 and are described in detail in section 2.1.1, Table 2-1. As can be seen from table 2-1 the three rutile pigmented films have coatings consisting of inorganic hydrous/hydrated oxides: alumina, zirconia, and silica which encapsulate the pigment, in order to reduce the photocatalytic degradation possibly by preventing the highly oxidizing hydroxyl radicals $OH^{\bullet}$ migrating into the coating layer, thus preventing oxidation of the organic resin [1]. The samples were in back position.

Table 4-2 The CO_2 band intensity after 180 minutes irradiation and values for the intensity of the water vapour band near 1557 cm^{-1} for PE R1-1, PE R2-1 and PE R3-1.

Run	CO_2 band intensity / 10^{-4} a.u.	Water vapour band intensity	Atmosphere
PE R1-1			
1	54	1219(85%)	Moist O_2
2	59	1164(77%)	Moist O_2
Average	56.5±2.5	1191	
PE R2-1			
1	43	1183(79%)	Moist O_2
2	46	1151(74%)	Moist O_2
Average	44.5±3.0	1167	
PE R3-1			
1	38	1181(78%)	Moist O_2
2	30	1095(65%)	Moist O_2
Average	34±4.0	1138	

Figure 4-2 shows the results obtained for the UV-induced photo-oxidation of the three coated rutile pigment containing PE R1-1, PE R2-1 and PE R3-1 films using the same experimental condition as for the anatase pigmented samples. It can be seen from Figure 4-2 that the gas-phase FTIR method is able to distinguish between these three rutiles pigmented PE films. The repeat runs on the samples were reasonably reproducible as shown in table 4-2. From these studies it was shown that PE R1-1 from alumina-coated rutile pigment PE film, was the most photoactive of the three samples, and PE R3-1 (pigment coated with alumina and silica) was the least photoactive sample (most durable), with mean average CO_2 band intensities of 56.5×10^{-4} a.u. and 34×10^{-4} a.u. respectively, after 180 minutes irradiation. PE R2-1 (also alumina coated but with the different coating layers to R1-1 pigment) showed intermediate photo activity. It gave an average of the 44.5×10^{-4} absorbance for the CO_2 band intensity. The rates of carbon dioxide generation for these three films pigmented with coated-rutile were less than for the anatase A-1 pigmented PE film and the unpigmented PE film U-1.

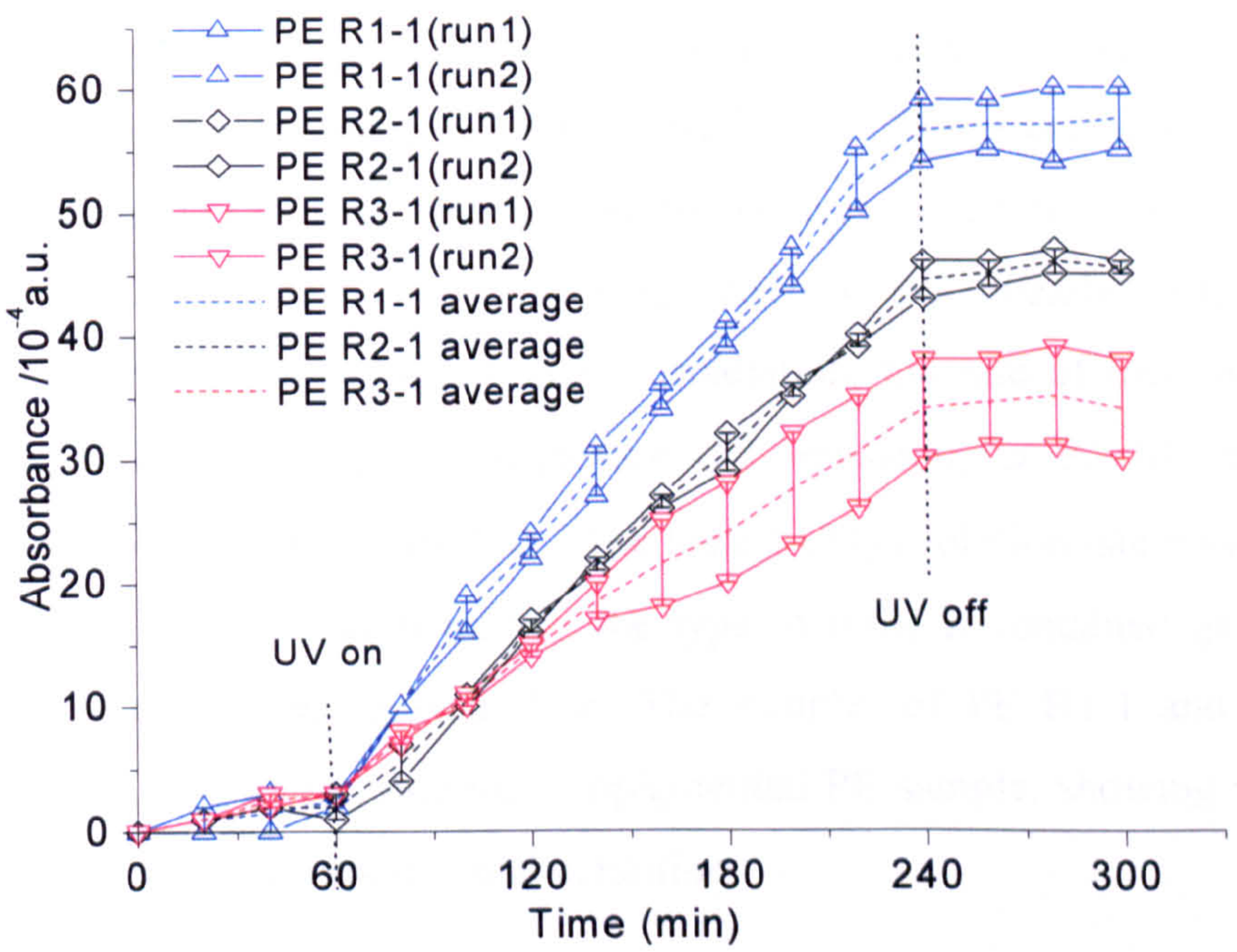

Figure 4-2 The infrared absorbance of gaseous CO_2 before, during and after UV irradiation of replicate films containing R1-1, R2-1 and R3-1 rutile pigment. Repeats were carried out 'immediately' *i.e.* within a few days of the first measurement but on different discs cut from the same film.

The lower the photoactivity of the pigment, the more the relative fluctuations in the rate of CO_2 evolution. This may be attributed to the effect of the background CO_2 evolution on the rate of CO_2 evolution becoming a considerable factor in the course of experiment. This is because the rutile TiO_2 pigments absorb the UV light to reduce the photochemical process to a greater extent than it is accelerated by the residual photoactivity of the coated pigments.

4.2.1.3. Comparison of CO_2 evolution during and after UV irradiation

The object of the exploratory work was to evaluate the use of the gas-phase FTIR method as a quick, reliable test with sufficient sensitivity to rank TiO_2 photocatalyts and to compare the ranking with that seen from conventional weathering tests. Figure 4-3 summarizes the mean rates of CO_2 evolution for PE U-1, PE A-1, PE R1-1 PE R2-1 and PE R3-1, irradiated with Xe lamp UV light filtered by AM1.5 which gives a spectral distribution in the UV-visible range approximately simulating sunlight. For the first hour, prior to switching on the UV source, CO_2 build up was negligible. The fluctuations of the CO_2 intensity at this stage were considered to be caused by the temperature changes in the cell and spectrometer caused by adding liquid nitrogen to the detector. As soon as the samples were exposed to UV, CO_2 was emitted and the IR absorption within the cell rose. The CO_2 emission rates for different materials were different. For PE A-1, the CO_2 evolution increased almost linearly with time. On disconnecting the UV source after 3 hours irradiation, the rate of increase in CO_2 concentration leveled off. It gave the greatest CO_2 emission, *ca.* 92×10^{-4} a.u., much higher than *ca.* 67×10^{-4} a.u. for PE U-1. The lowest CO_2 evolution rate was observed with the sample PE R3-1, showing that the type of rutile it contained gave a high degree of protection to the polyethylene. The samples of PE R1-1 and PE R2-1 emitted lower CO_2 evolution rate than unpigmented PE sample, showing protective activity as well under this experimental condition.

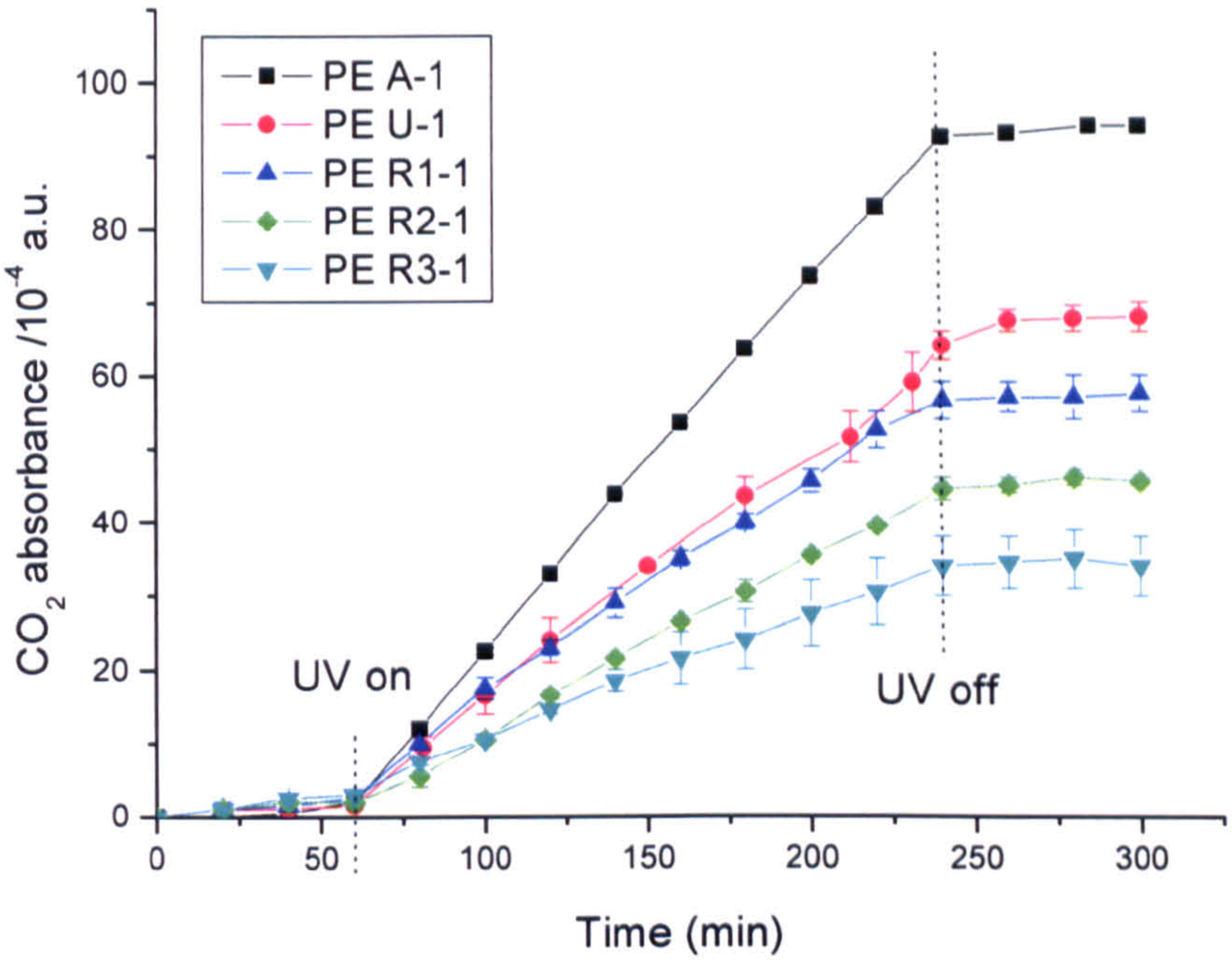

Figure 4-3 CO_2 evolution from the photo-oxidation of different PE films (PE A-1, PE U-1, PER1-1, PE R2-1 and PE R3-1) during preliminary experiments.

The overall order of photoactivity of the films was PE R3-1 < PE R2-1 < PE R1-1 < unpigmented PE U-1 < PE A-1. This suggests that the technique is able to distinguish between the different PE samples according to the different photoactivities of their pigments on the basis of the amount of CO_2 evolved under UV irradiation. Whether the results of this method are consistent with other weathering tests for all unpigmented or pigmented PE films is a key point of this research and will be dealt with in section 4.2.3.

4.2.2 Carbonyl group Development under QUV irradiation

4.2.2.1. Long term exposure sample with QUV-A

The next stage of this work was to compare the results of the CO_2 evolution measurements with measurements of carbonyl group development - the conventional measure of polyalkene degradation [2-6]. In order to test the correlation between the two methods, it is necessary to use samples extracted from adjacent locations in the films to measure the photooxidation by conventional carbonyl group development method.

As for PE U-1, the carbonyl group peak height at 1712 cm^{-1}, which is assigned to ketone, was measured with increasing exposure times. For the blown films used in this study, the thickness, is again, 100 μm and the carbonyl index equals their carbonyl group absorbance at 1712 cm^{-1}.

All batch 1 PE films were illuminated using two fluorescent tubes (QUV A-340) in a constant temperature (30 ± 1.5 °C) room described in chapter 2.3. Formation of carbonyl groups, which absorb at 1712 cm^{-1}, was monitored by removing the samples at regular intervals, measuring their spectrum (see Figure 4-4) and then returning the samples for further UV exposure. Figure 4-4 presents the FTIR transmission spectra of carbonyl group development after 1090 hours under QUV irradiation. The absorbance peaks were measured by taking top minus the baseline value at 1712 cm^{-1}. This figure was used as absorbance of the carbonyl group in Figure 4-5 and Figure 4-6.

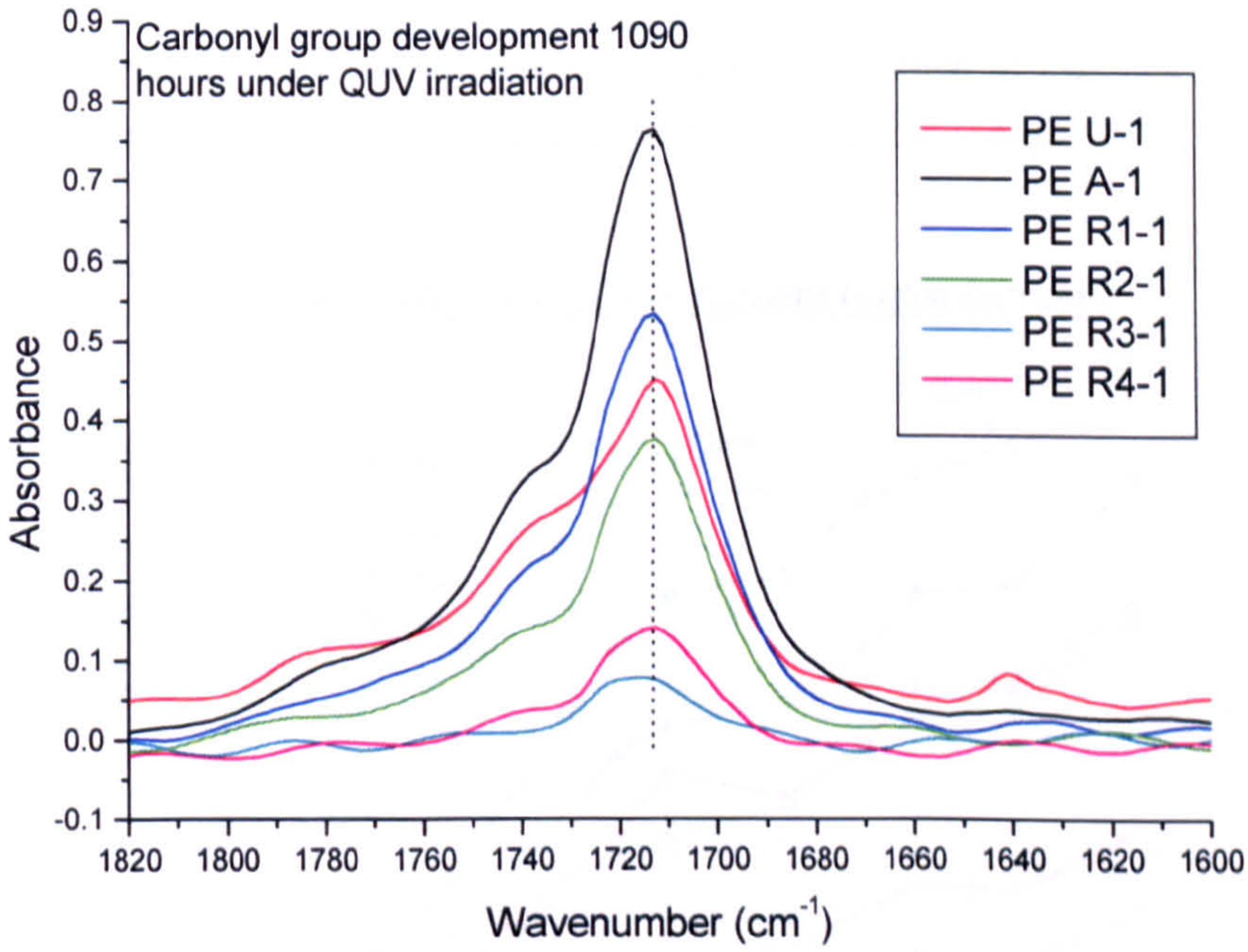

Figure 4-4 FTIR transmission spectra of carbonyl group development at 1090 hours under QUV irradiation. The data were taken from one-disc samples used in fig4.6.

Figure 4-5 shows the carbonyl group development in the batch 1 PE films. For each film sample, separate discs were cut from the initial mother film (6 mm × 6 mm sheet

exposed under UV light in a constant temperature room), exposed for the time indicated, measured and then discarded.

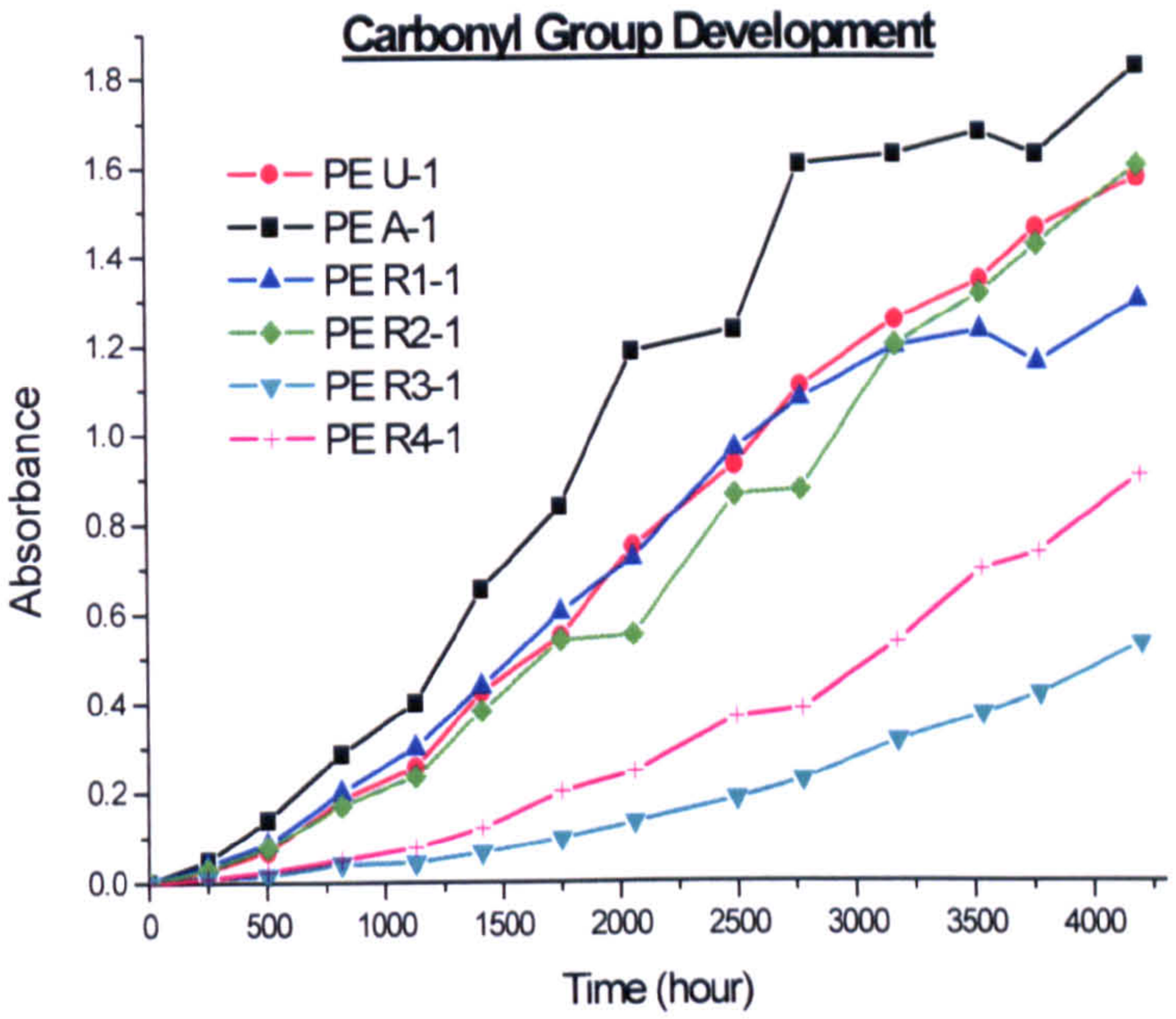

Figure 4-5 Carbonyl group absorbances are plotted as a function of exposure time. For these experiments, the IR spectrum was measured and the discs were then discarded.

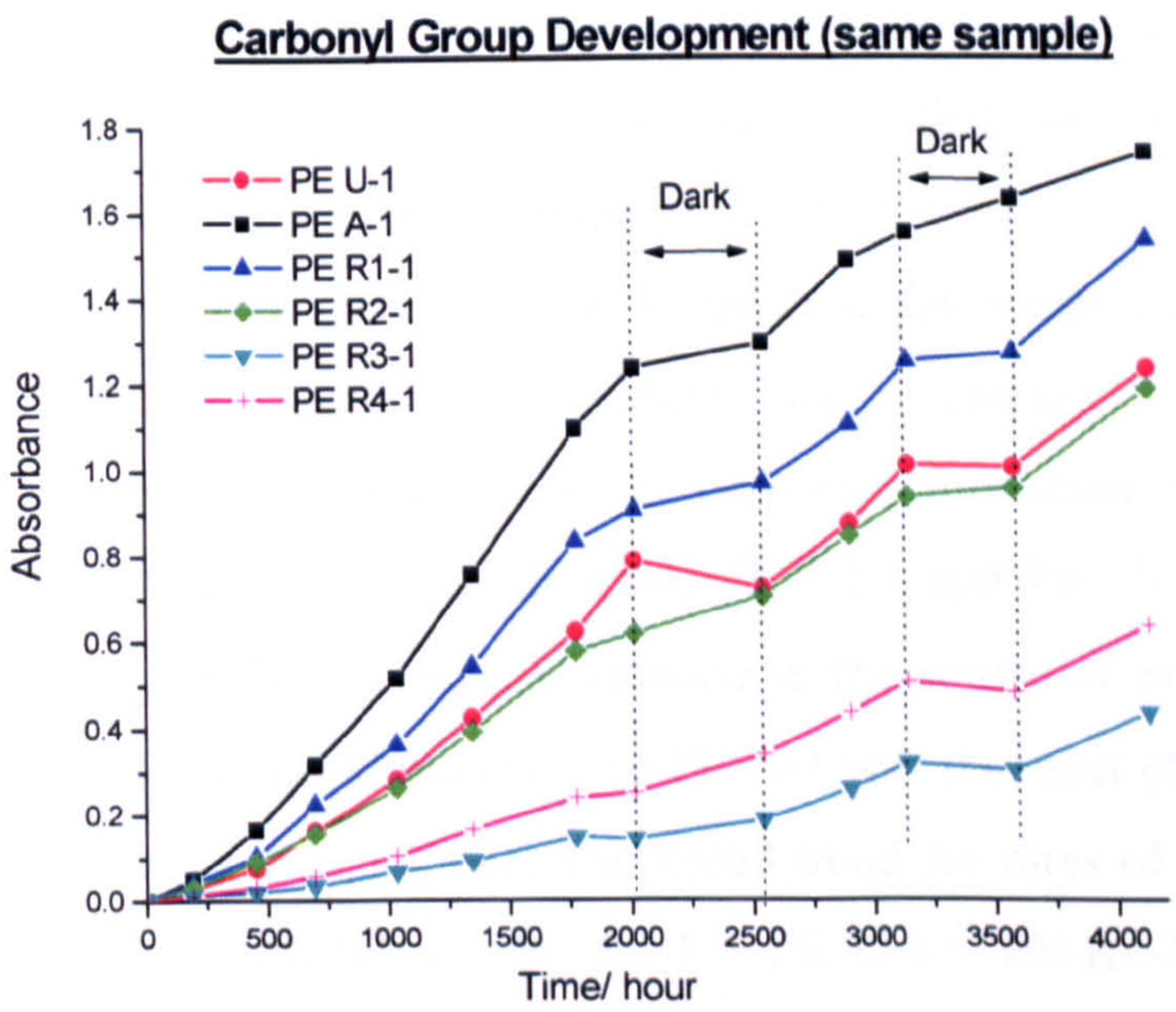

Figure 4-6 Carbonyl group absorbances, obtained from the same disc which was exposed under UV light in room at 30°C. For these experiments, the IR spectrum was measured periodically and the disc was then returned to the exposure unit and UV exposure was recommenced.

Figure 4-6 shows a corresponding exposure series. However for this series measurement on a particular material composition were all made with the same disc, which was removed from UV exposure, measured and then returned to the exposure unit. Finally all samples were irradiated over 4000 hours. PE A-1 and PE R1-1 were observed curling and damaged to fracture by UV light. PE R2-1 and PE U-1 were not visibly damaged to fracture but curled. The direction of curl was towards the UV irradiated surface, presumably due to material near the surface shrinking due to secondary crystallization. The same phenomenon were not observed for PE R3-1 or PE R4-1, these films remained flat.

The results in Figure 4-5 and Figure 4-6 follow the same trend of carbonyl peak development during QUV irradiation in the constant temperature room, although in Figure 4.5, the carbonyl group development showed slightly more scatter than that in Figure 4.6, probably because sample to sample variation. The data for each line in Figure 4-5 were obtained from the different sample disks. In both experiments, for example, the PE A-1 took nearly 2000 hours to reach an absorbance of 1.2. In a separate experiment, duplicate samples were exposed in a QUV machine and will be reported in 4.3.3. The same samples were exposed in parallel in this QUV machine at the same time and temperature (42°C) but covered with aluminum film. No carbonyl peaks were observed in these samples. This suggests that no thermal oxidation happened within these samples at a temperature (42°C) even higher than above mentioned room temperature (30°C). It can be inferred that under this experimental condition the carbonyl group development was completely attributed to photodegaradation reaction. The rates of carbonyl formation represented an autocatalytic oxidation with PE A-1, PE R1-1, PE R2-1 and PE U-1. This may be attributed to the concentration of radicals increase in the course of experiments. On the basis of carbonyl group development, also PE A-1 was the most photodegradable; PE R3-1 was the least photodegradable. The broad trend for rates of carbonyl group development is PE A-1 > PE R1-1 > PE R2-1 > PE U-1 > PE R4-1 > PE R3-1 in beginning *ca.* 500 hundreds. But unpigmented PE film showed that its carbonyl group grew faster than PE R1-1 and PE R2-1with irradiation time. It is clear that with longer term exposure, all rutile pigment gave protestation to polyethylene film.

Figure 4-6 also shows the consequence when the room QUV irradiation was stopped and then the samples were kept in the dark. The carbonyl group height appeared to decrease with time for unpigmented PE film. For PE A-1, PE R1-1 and PE R2-1, the carbonyl group height appeared to continue increasing a little in dark time after switching off the UV light. For PE R3-1 and PE R4-1, the carbonyl group height appeared to increase slightly in the first dark period and appeared to decrease slightly in dark time in the second dark period.

4.2.3 The correlation between CO_2 evolution and Carbonyl group

The '*in-situ* CO_2 method' results for PE films are shown in Table 4-2. Obviously the CO_2 data from the *in-situ* method represent the initial stage of photodegradation. In order to assess the correlation between the CO_2 method and the conventional carbonyl method, it is preferable to choose carbonyl data from the initial period of exposure. The carbonyl group absorbances after 426 hours UV were judged to be a reasonable basis of comparison and are tabulated in Table 4-3 with *in-situ* data and are plotted in Figure 4-7.

Table 4-3 Table shows the CO_2 band intensity after 3 hours Xe UV illumination in the *in-situ* cell and the carbonyl group absorbance for the conventional method after 426 hours UVA exposure.

Sample	CO_2 absorbance/10^{-4}	Carbonyl absorbance
PE A-1	92	0.1642
PE U-1	67	0.0733
PE R1-1	56.5	0.1004
PE R2-1	44.5	0.0899
PE R3-1	34	0.0169

The CO_2 absorbance values are plotted in Figure 4-7 against carbonyl group intensity, measured after 426 hours exposure under UV light, for polymers from the same batch. There is a reasonable correlation, R^2=0.76, between the two methods.

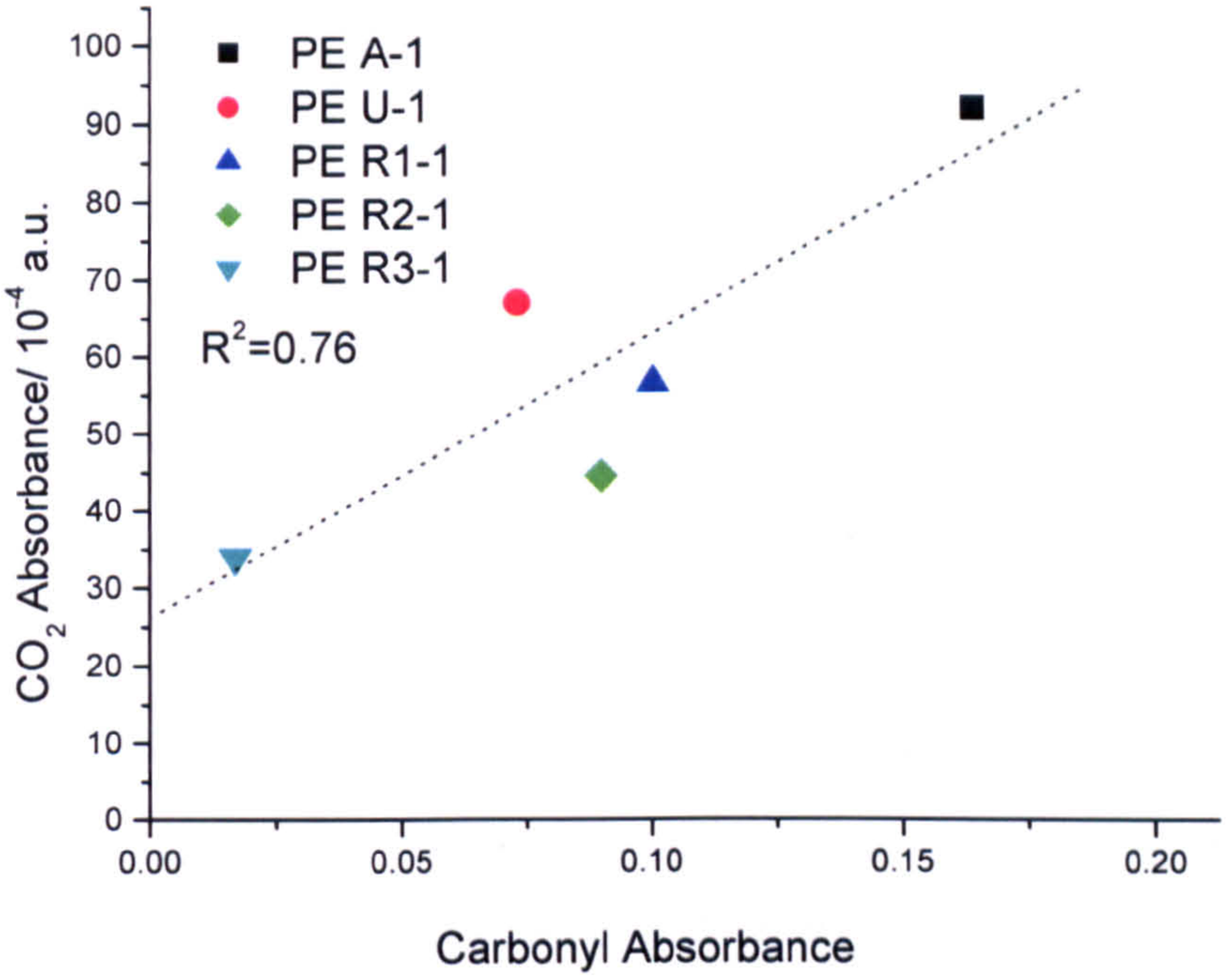

Figure 4-7 The correlation between CO_2 evolution in the FTIR cell and carbonyl group development for all samples.

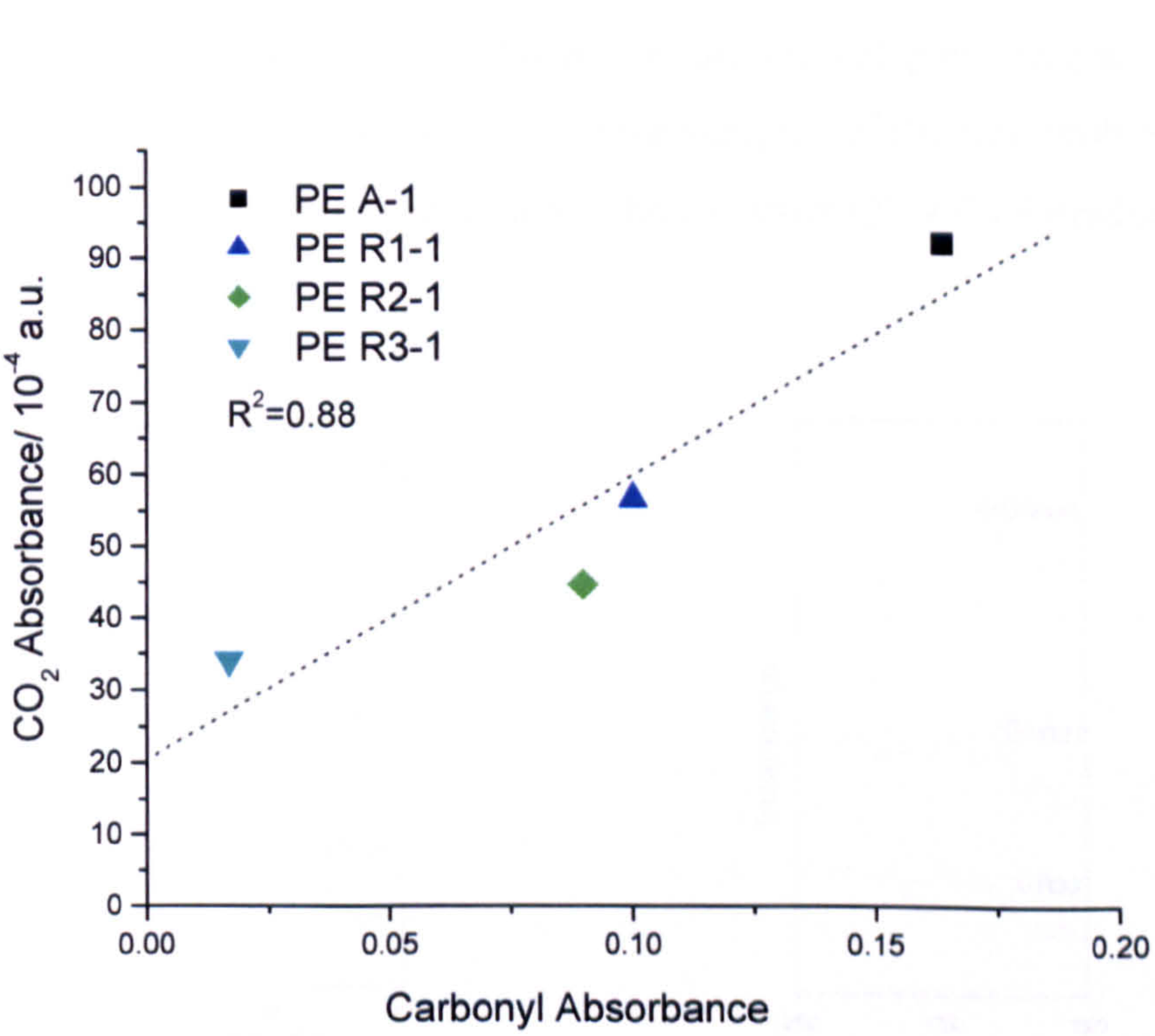

Figure 4-8 The correlation between CO_2 evolution in the FTIR cell and carbonyl group development, omitting result for unpigmented PE film.

Because the UV radiation used in these experiments is provided from different lamps and filtered with different optical filters, the effects of these differences are expected to be particularly significant for unpigmented PE film which absorbs only at $\lambda < 290$ nm and whose oxidation is therefore particularly sensitive to the wavelength of the incident radiation. These reasons make a good correlation between the two methods less likely. For pigmented films there is a much better correlation between the two methods (R^2=0.88) because pigmented PE film are less sensitive to UV light wavelength than unpigmented PE.

4.2.4 Preliminary studies on the dichroic behaviour of PE

In order to detect any effects of film anisotropy on the behaviour of the carbonyl group, PE A-1, PE U-1 and PE R3-1 films were illuminated using fluorescent lamps (QUV-340) and measurements made using polarized IR beams. The rates of photooxidation of the polymer films were monitored by measuring the build-up in the concentration of the non-volatile carbonylic oxidation product absorbing at the region around 1712 cm^{-1} using infrared dichroism measurements. The IR beam was polarized by employing a KRS-5 wire grid polarizer in the optical path before the sample holder. Figure 4-9 shows FTIR spectra of three samples of PE film with S-polarized and P-polarized IR after 0, 80 hours and 910 hours under QUV-340 irradiation in the constant temperature room.

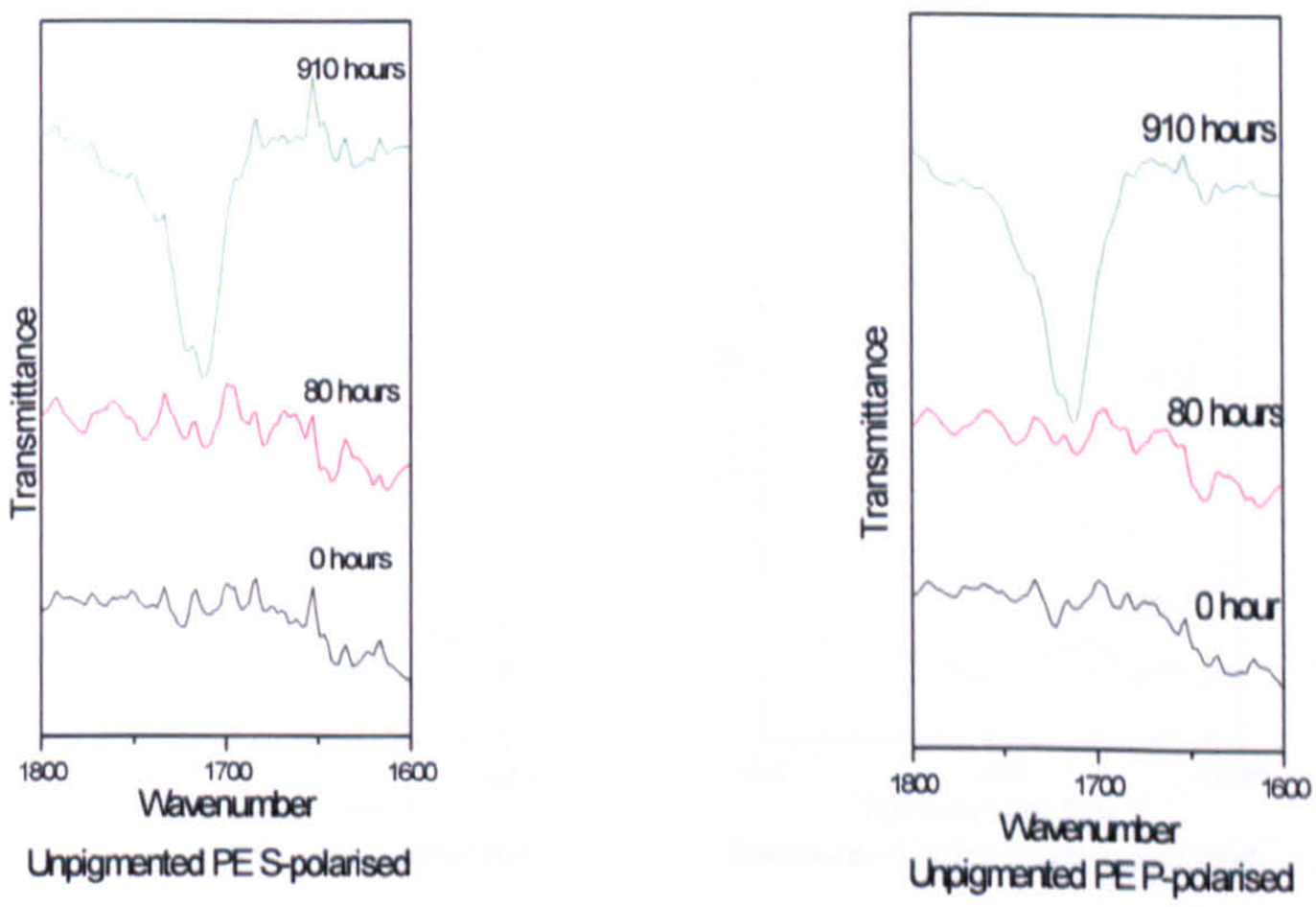

Figure 4-9 (continued next page)

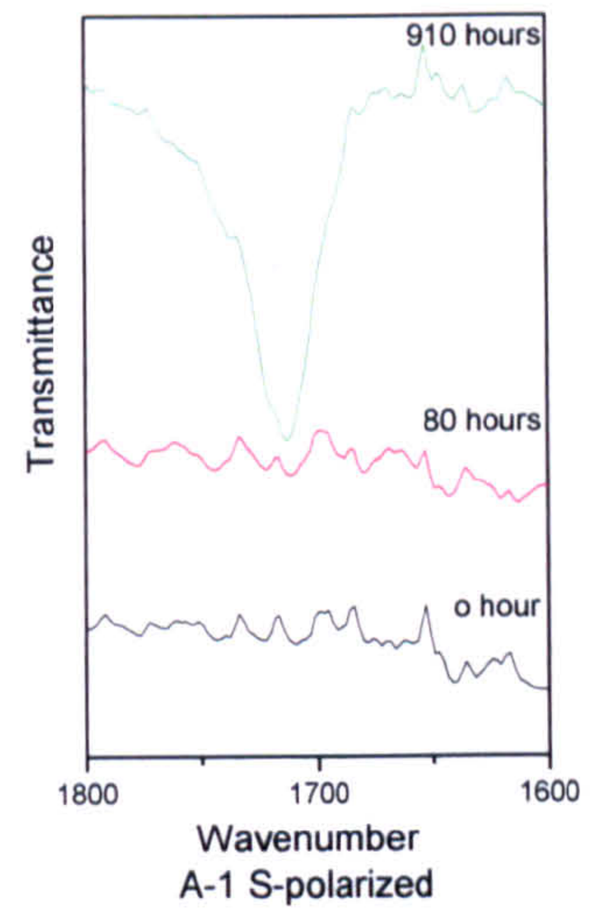

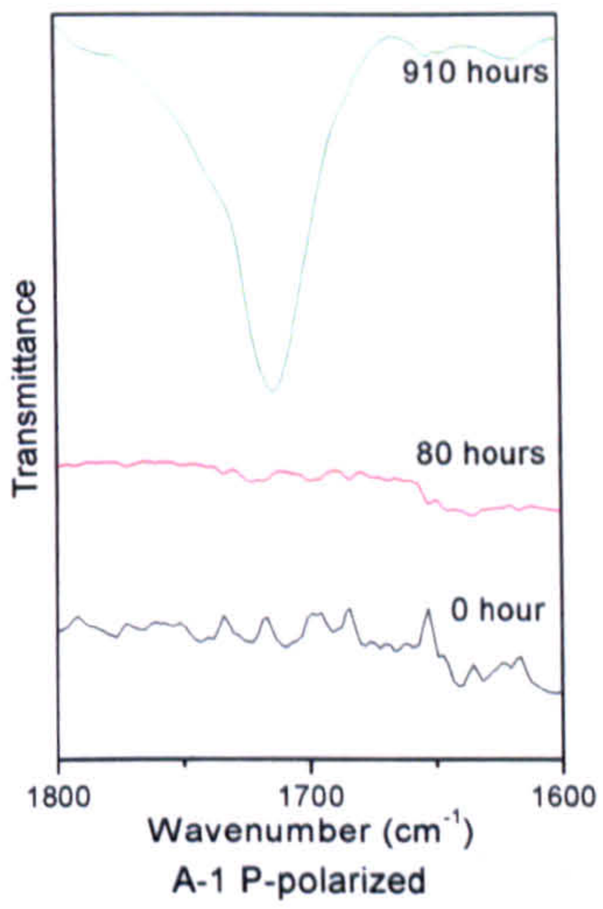

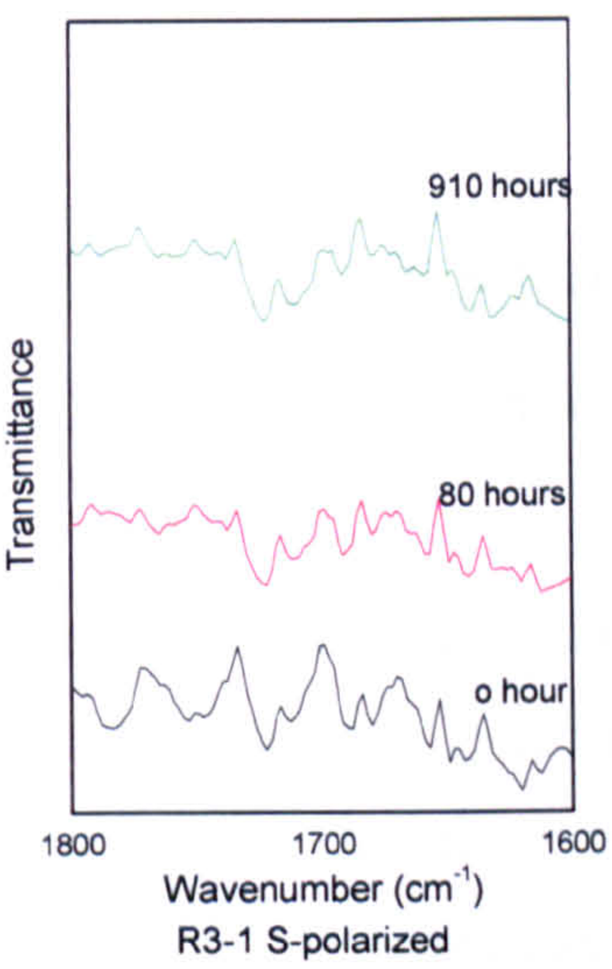

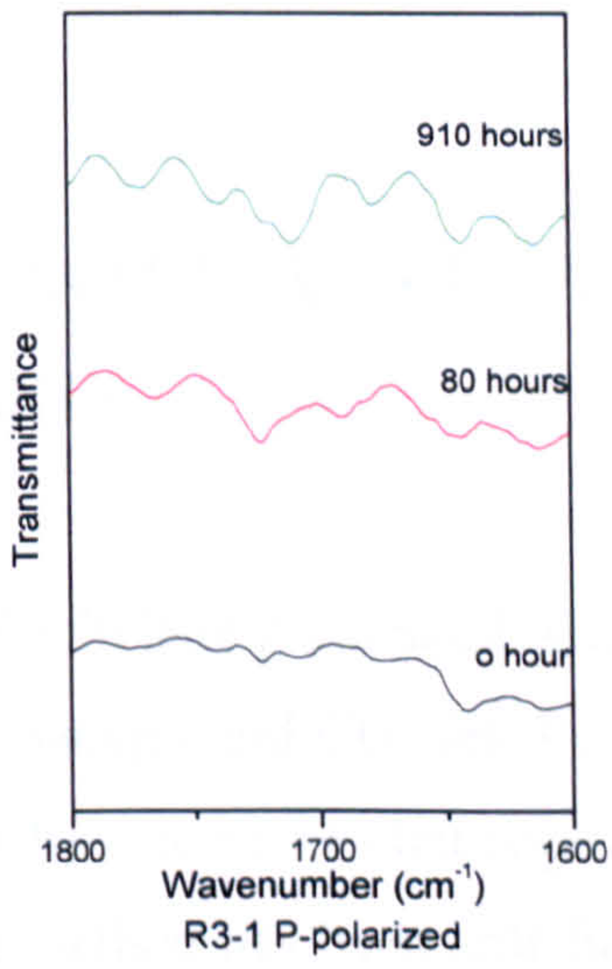

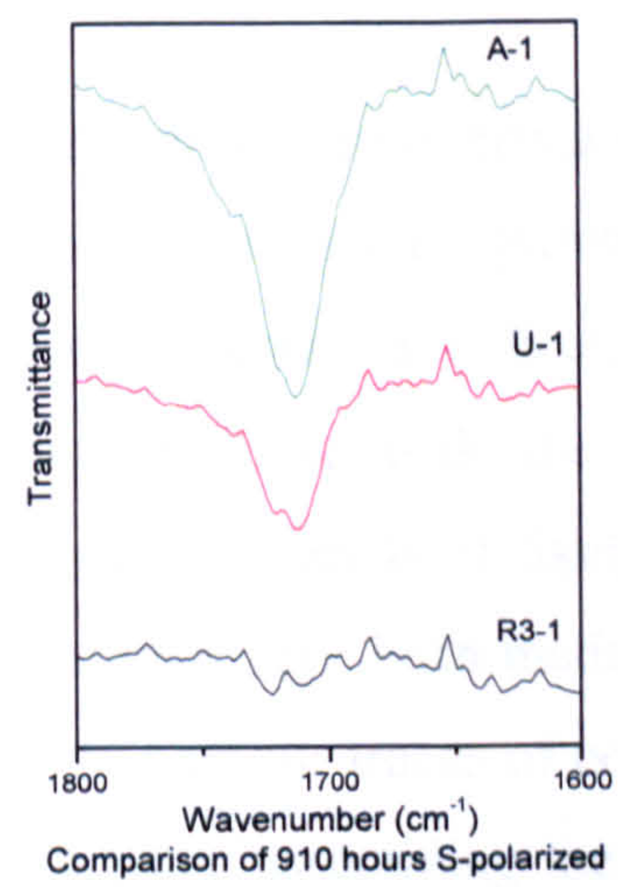

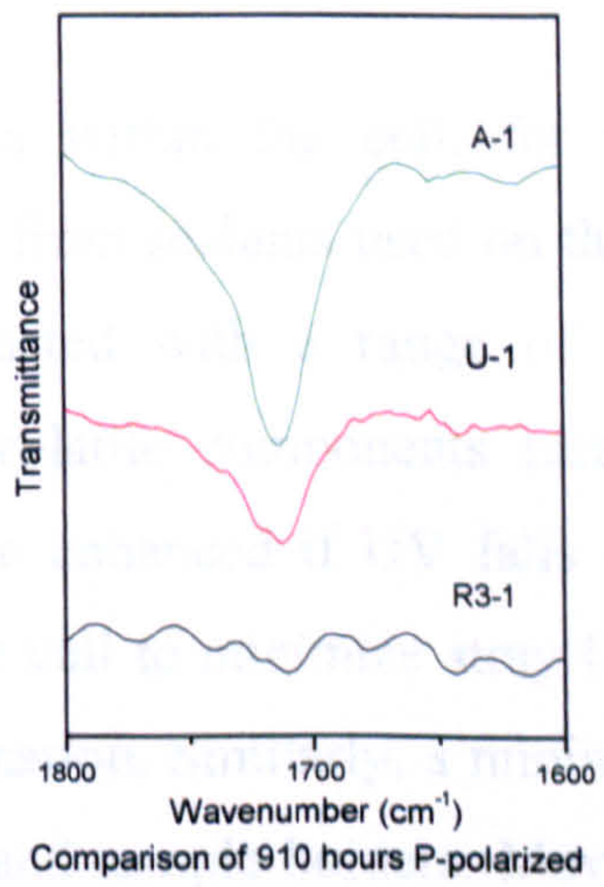

Figure 4-9 Carbonyl developments show in FTIR spectra S-polarized and P-polarized with PE U-1, PE A-1 and PE R3-1.

From Figure 4-9 it can be seen that there are no big differences between S-polarized and P-polarized FTIR spectra for the carbonyl peak development during QUV irradiation in a constant temperature room. The carbonyl peaks were not observed for unexposed samples or for those exposed for 80 hours. After 910 hours irradiation, strong carbonyl absorption peaks appeared at around 1712 cm^{-1} for PE A-1 and unpigmented PE films. For PE R3-1, no clear absorption peak can be detected at this position in FTIR spectra after 910 hours irradiation. It also can be seen that the carbonyl absorption peaks for PE A-1 were bigger than those for the others. The results confirmed that PE A-1 degraded faster than unpigmented PE film, unpigmented PE film degraded faster than PE R3-1. Significant differences in dichroism behaviour from these three type PE films for carbonyl group development were not observed.

4.3 THE EFFECT OF SAMPLE BATCH AND OF VARIATION IN THE CELL ARRANGEMENT

When the CO_2 method is used to evaluate polyethylene pigmented with durable rutile TiO_2, it is especially important to reduce the background CO_2 level or to maintain it constant. As described in Chapter 2, this has been a major challenge. Therefore, for the most recent studies, the sensitivity of the method has been still further improved by reducing the background signal.

The background comes from contamination within the cell, for example from adhesives used to assemble the equipment or from sealants used on the demountable components. Experiments have been conducted with a range of adhesives and sealants, to identify those with the least volatile components (see section 2.6). Emission from such materials is likely to be enhanced if UV falls onto them and detailed modifications have been made to the cell to minimize stray UV falling onto regions that might harbour traces of contamination. Similarly, a minimum amount of adhesive is used when assembling the cells and sample holders. Moving the sample nearer to the UV light port at the front of the cell has increased the UV radiation intensity on the sample, and shielded any organic cell contaminant such as grease and

glue from UV irradiation. This has greatly decreased the background CO_2 concentration and hence improved the sensitivity of the test. Blank experiments were carried out, in which a clean metal plate of the same size as the sample, was irradiated under the same condition as the test samples. Reduced amounts of background CO_2 were observed during the irradiation of the blank cell, with CO_2 levels of *ca.* 10×10^{-4} absorbance units (a.u.) after 600 minutes irradiation being typically observed. With these improvements (and the resulting reduced contribution of the background to the measured signal), the observed rate of CO_2 emission for the anatase-pigmented polyethylene was an order of magnitude greater than for the rutile-pigmented polyethylene with the lowest rate of emission (see table 4-4).

4.3.1 CO_2 evolution results with sample placed at the front position

After the attempts described above to develop a more reliable gas cell for measurement of CO_2 evolution, samples were placed nearer to the UV light port at the front of the cell. To quickly obtain some information about CO_2 signal response under different experimental conditions, several experiments were conducted to test sensitivity with samples (batch 1) PE A-1, PE U-1 and PE R2-1. This work was mainly focused on the different filter effects on CO_2 evolution in order to understand the mechanism of UV induced photoreaction and to find optimum experimental conditions when the sample is put at the front position. The CO_2 emission results for several experimental conditions are shown in Table 4-4 below.

These studies demonstrated that after moving the sample nearer to the UV light port at the front of the cell the reproducibility was good. For PE A-1, there was detectable CO_2 evolution with all filter combinations. The amount of the CO_2 evolution is more than that when the sample is placed at the back position. For example, PE A-1 with AM0+AM1.5 filters in combination gave *ca.* ~130×10^{-4} a.u. CO_2 evolution after three hours UV irradiation when the samples were at the front position, whereas the greatest CO_2 evolution for the PE A-1 in back position was less than 107×10^{-4} a.u. Another benefit for the sample at the front position is that the CO_2background is lower and more stable than when the sample is in back position.

Table 4-4 Table showing the band intensity of the CO_2 produced from PE A-1, PE R2-1 and PE U-1 under UV-induced photo-oxidation using different filter combinations. All are in the front position.

Sample	CO_2 emission after 3 hr (10^{-4} a.u.)	Average CO_2 emission (10^{-4} a.u.)	Filters	UV intensity at 350nm(Arbitrary Units)
PE A-1(1)	126		AM0+AM1.5	69
PE A-1(2)	134	130	AM0+AM1.5	69
PE U-1(1)	10		AM0+AM1.5	76
PE U-1(2)	8	9	AM0+AM1.5	67
PE R2-1(1)	10		AM0+AM1.5	67
PE R2-1(2)	11	8.5	AM0+AM1.5	63
PE A-1(1)	254		None	275
PE A-1(2)	244		AM0	217
PE U-1(1)	74		None	267
PE U-1(2)	53		AM0	206
PE R3-1(1)	29		None	265
PE R3-1(2)	31		AM0	216

The AM0 filter did not greatly reduce the amount of CO_2 evolved for PE A-1 and PE R3-1. Both pigmented PE films show the CO_2 reduction less than 5% caused by AM0 filter. A large decrease in CO_2 evolution was obtained when the AM0 and AM1.5 filters were used in combination. With no filter, the absorbance was 254×10^{-4} a.u. after three hours UV exposure for PE A-1; with AM0 filtered UV exposure, the absorbance was 244×10^{-4} a.u. after three hours UV exposure for PE A-1; but when using the AM0+AM1.5 combination UV light to irradiate the same type PE A-1 sample, the absorbance of CO_2 was 130×10^{-4} a.u. after three hours UV exposure. However AM0 filter did have a significant effect on unpigmented PE film. The CO_2 intensity reduced from 74 a.u. to 53 a.u. when the AM0 filter was used, which reduced more than 20% CO_2 evolution compared to the absorption when no filter was used.

For unpigmented PE film, the amount of CO_2 evolved was reduced as the UV intensity was reduced and the spectral distribution modified by the use of AM0 and AM1.5 filters. The AM0 filter had greater effect on the rate of CO_2 evolution than with pigmented PE films. For PE R3-1, less CO_2 was evolved than for non-pigmented PE. The AM0 filter had little effect on the rate of CO_2 evolution. For PE R3-1 and unpigmented PE, use of the AM0 and AM1.5 filters in combination resulted in no evolution of CO_2 above the background, whereas PE A-1 continued to produce CO_2. The differences observed for the three PE film samples agreed with the expected order of photoactivity as deduced from conventional accelerated weathering data *i.e.* PE A-1>PE U-1>PE R3-1. In order to obtain significant amounts of CO_2 evolution for comparison of different PE films, the AM0 filter was selected.

On the basis of these preliminary results the measurements of all second batch samples were conducted with samples placed at the front position in the cell and with UV light filtered with an AM0 filter only.

4.3.2 Measurements on batch 2 polymer films

The batch 1 (old) of 100 μm thick PE films was supplied by Huntsman Tioxide in Sept 2000 – for details see Table 2-1 in section 2.2.1. These films were stored in the dark at room temperature and samples were taken for testing as required over the next 2.5 years. From the results obtained over an extended test period (~2 years), it was suspected that an ageing process was changing the photoreactivity as time went on. The experiments described below were designed to investigate a (new) batch 2 of samples supplied by Huntsman Tioxide in January 2003 to the same original specification (compression, thickness, production route *etc*). Additional films made with other grades of TiO_2 pigmented polyethylene film and two different thicknesses of 250 and 100 μm unpigmented PE film, as detailed in Chapter 2 (Table2-2), were also supplied at the same time. The experiments concerned with both 'old' and 'new' samples will be reported in this section.

Because of experimental condition changes (UV intensity, samples holder *etc*) for the batch 2 samples, CO_2 emission was quite slow except for the PE A-2. Therefore the

irradiation time was expanded to ten hours for the batch 2 samples. Figure 4-10 summarizes the rates of carbon dioxide evolution for samples of PE U-2, PE A-2, PE R1-2, PE R2-2, PE R3-2 and PE R4-2.

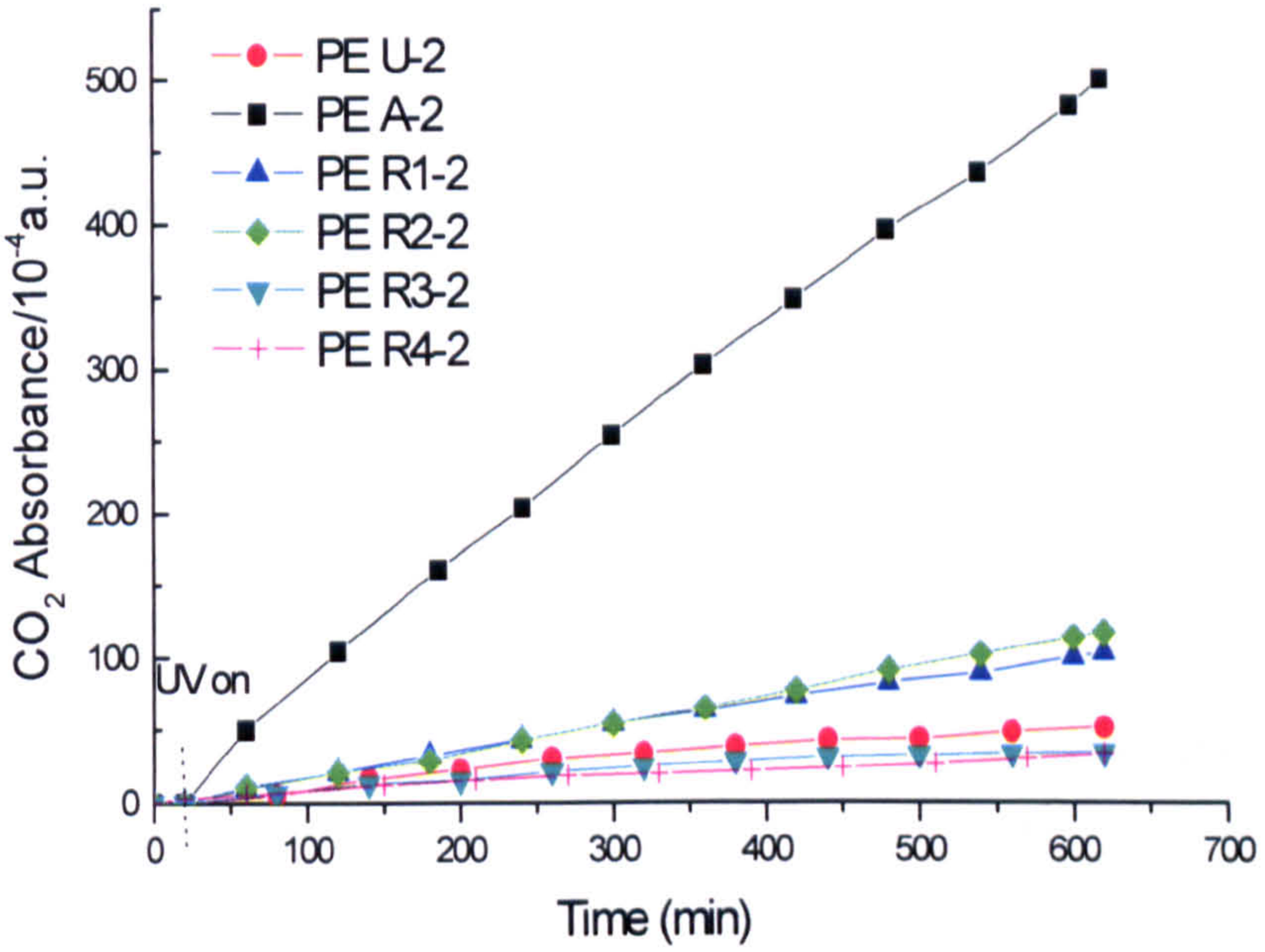

Figure 4-10 CO_2 evolution was obtained from the batch II PE films at front position. Results were obtained about two months after manufacture.

Figure 4-10 shows the CO_2 evolution profiles for the batch 2 samples. The behaviour of anatase pigmented PE film (PE A-2) was similar to PE A-1. But there was a big gap between PE A-1 with others. The amount of CO_2 evolution was faster and at least 5 times greater from anatase pigmented PE than from the other samples. When the samples were placed in the back-position, the CO_2 evolution from anatase pigmented PE film was less than twice that for the other samples (see Figure 4-3). It is quite clear that the detection of the relative photocatalytic effect was enhanced very much for anatase pigmented PE film when the samples were placed in the front position. As soon as the samples were exposed to UV light, CO_2 was emitted and the concentration within the cell rose almost linearly with time for PE A-2, PE R2-2 and PE R1-2. For PE U-2, PR R3-2 and PE R4-2, the concentration of CO_2 within the cell rose more slowly with time. The lowest emission rate was produced by the sample PE R4-2 and PE R3-2, showing that they gave some degree of protection to the polyethylene. The PE R1 and PE R2-2 gave higher CO_2 emission rates than PE U-2, showing pro-degradation activity. But PE R2-2 gave more CO_2 evolution than PE R1-2 for batch 2

samples. In other words, the ranking is changed compared to the first batch samples, for which PE R1-1 gave higher CO_2 emission.

Because anatase pigmented film gave nearly five times more carbon dioxide emission than other films (rutile pigmented films and unpigmented film) under the conditions using in these experiments, for a convenient comparison Figure 4-11 shows the results for all of the films except the anatase pigmented one. Here R5-R9 is a code which expresses different grade rutile TiO_2 pigments. The results used in Figure 4-1 were the average of two runs. The reproducibility of experiments was good.

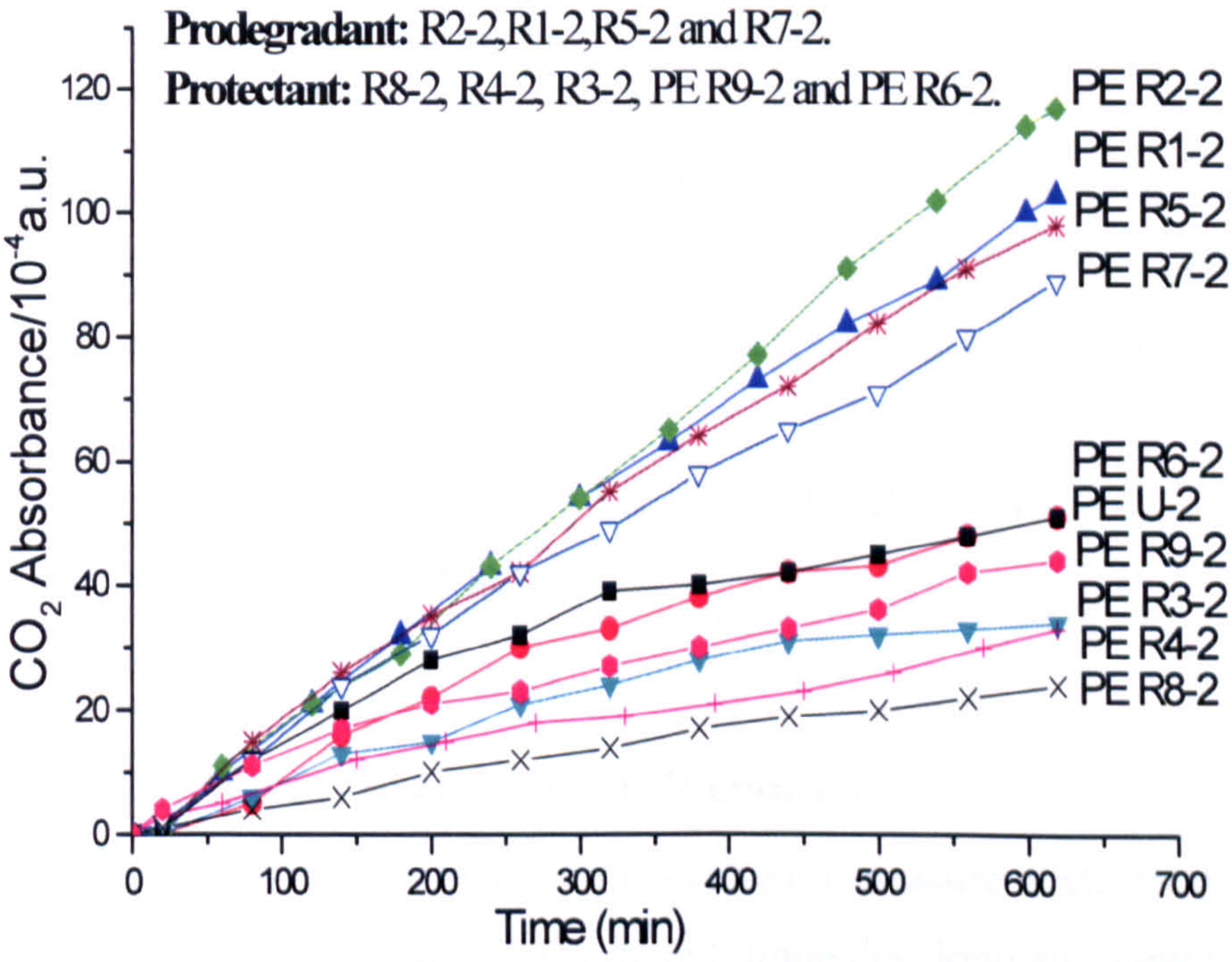

Figure 4-11 **CO_2 evolution from (new) PE films pigmented with different grades TiO_2.**

As can be seen from Figure 4-11, the gas cell technique was able to differentiate between all rutile pigmented films even though some samples gave closely similar results. PE R6-2 gave the same CO_2 emission as the unpigmented polyethylene. This means that the effect of the rutile pigment in PE R6-2 balanced the reduced direct homogeneous photochemical oxidation of the organic medium and enhanced heterogeneous photo-catalytic oxidation caused by the R6 pigment. The final

influence of the R6 pigment is neutral as far as its effect on photodegradation is concerned.

It is quite clear that the rutile pigmented polyethylenes either gave reduced CO_2 emission or enhanced emission depending on the surface treatment of the rutile. One group, including R2, R1, R5 and R7 pigments, appear as pro-degradants. The increases in CO_2 with irradiation time exhibit almost linear behaviour. It may be suggested that this is due to photo-catalytic oxidation dominating the whole reaction. Another group, including, R3, R4, R8 and R6 pigments acted as protectants, giving reduced carbon dioxide evolution compared with PE U-2. In addition, the rate of CO_2 evolution for this set of films decreased during the course of the experiments. Both sets of pigments absorb UV, however, for the second set electron-hole recombination is probably the dominating reaction compared to their photo-catalytic reaction because of surface treatment. The ranking of the photo-activity of polyethylene pigmented with the different pigments in terms of CO_2 evolution rate was:

PE R2-2 > PE R1-2 > PE R5-2 > PE R7-2 > PE R6-2 ≅ PE U-2 > PE R9-2 > PE R3-2 > PE R4-2 > PE R8-2

4.3.3 Carbonyl group development in QUV machine

In order to compare the results of the CO_2 evolution measurements for the second batch of samples with measurements of carbonyl group development, samples of each film were exposed in a QUV machine in which the ultraviolet illumination was provided by QUV340 fluorescent tubes (the same type as in the constant temperature room). The QUV machine was operated as a simple constant temperature enclosure set at around 42°C±1.5 (no temperature or humidity cycling). The details of the QUV machine have been described in section 2.3.4. It provides high UV light intensity on the samples, with the tubes at short distance to the samples, but the UV distribution is the same as in the room UV exposure. For this series, repeat measurements were made on the same disc, which was removed from UV exposure, measured, and then replaced. For the purpose of comparison, all the first batch samples were also exposed

in the QUV machine at the same time as the second batch samples. The measurement of the carbonyl group development was as described in section 4.2.2.

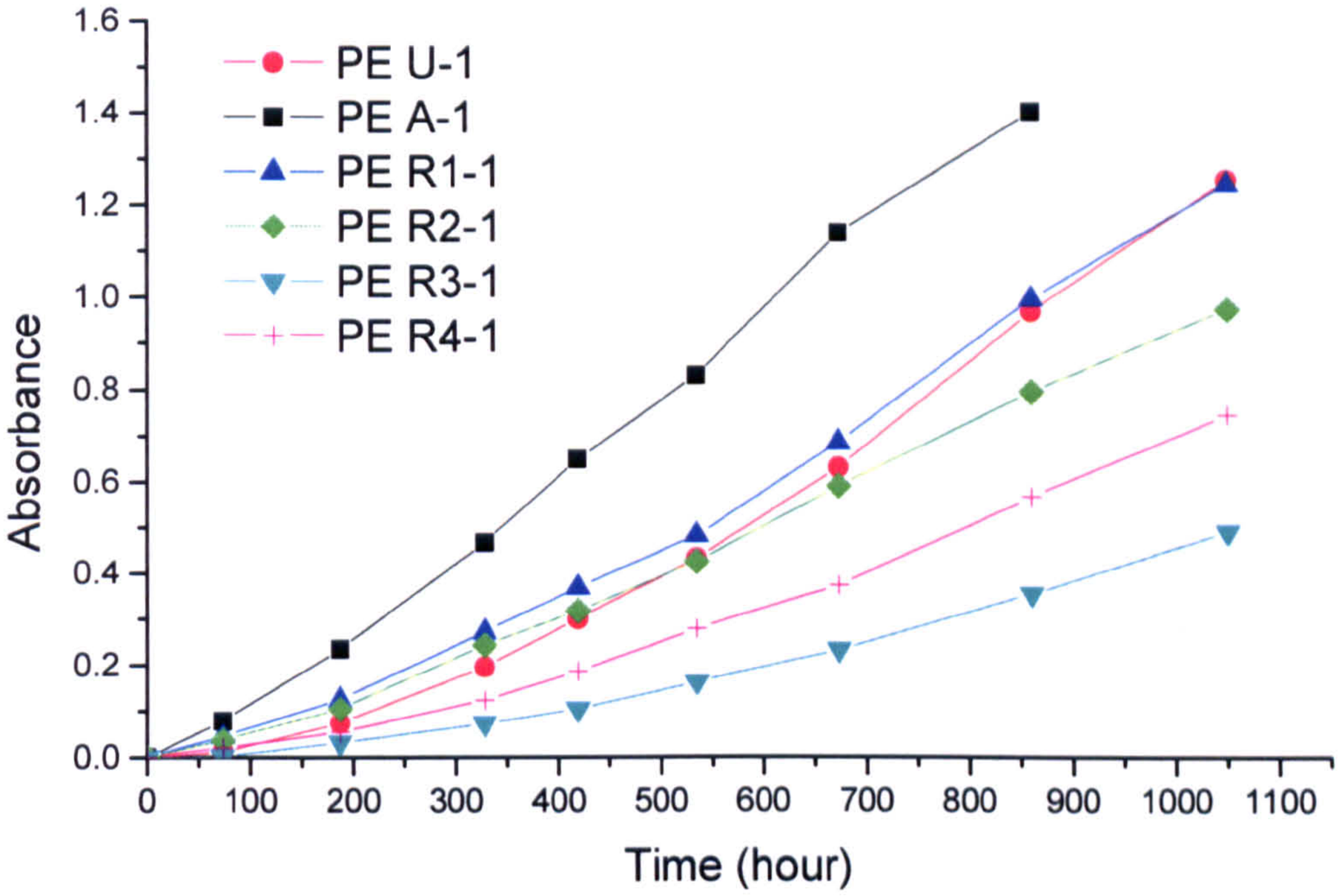

Figure 4-12 Results using conventional method, monitoring carbonyl group development under QUV irradiation (old samples). Ageing time: 2.5 years.

Figure 4-12 shows an exposure series for batch 1 samples. It can be seen from Figure 4-12 that the trend of carbonyl group development is the same as for the samples exposed in the constant temperature room (see Figure 4-6). The ranking of photoactivity in terms of carbonyl group growth rate was similar to that of the samples exposed in the constant temperature room. However in the QUV machine the carbonyl growth is very much faster than in the samples illuminated in the room. For example, with PE A-1 the carbonyl group development from 0 to 1.2 a.u. needed *ca.* 700 hours in the QUV machine, whereas it needed *ca.* 2000 hours when exposed in the constant temperature room. This is because when the carbonyl group growth reached more than 1.4 a.u., the sample was destroyed by UV light due to molecule bond scission throughout film. This caused that no further transmission measurements could be made. The same behaviour was observed for rutile pigmented PE films and unpigmented PE film. The IR carbonyl peak growths for unpigmented PE film increased faster than for PE R1-1 and PE R2-1. After about 470 hours QUV

irradiation, the absorbance of the unpigmented sample carbonyl group overtook R2-1 and was approaching that for PE R1-1. For all of them, the carbonyl group growth in the QUV machine was at least three times faster than in the constant temperature room.

Figure 4-13 shows carbonyl group development for the batch 2 samples, coded as PE U-2, PE A-2, PE R1-2, PE R2-2, PE R3-2 and PE R4-2, which were irradiated same time with batch1 samples.

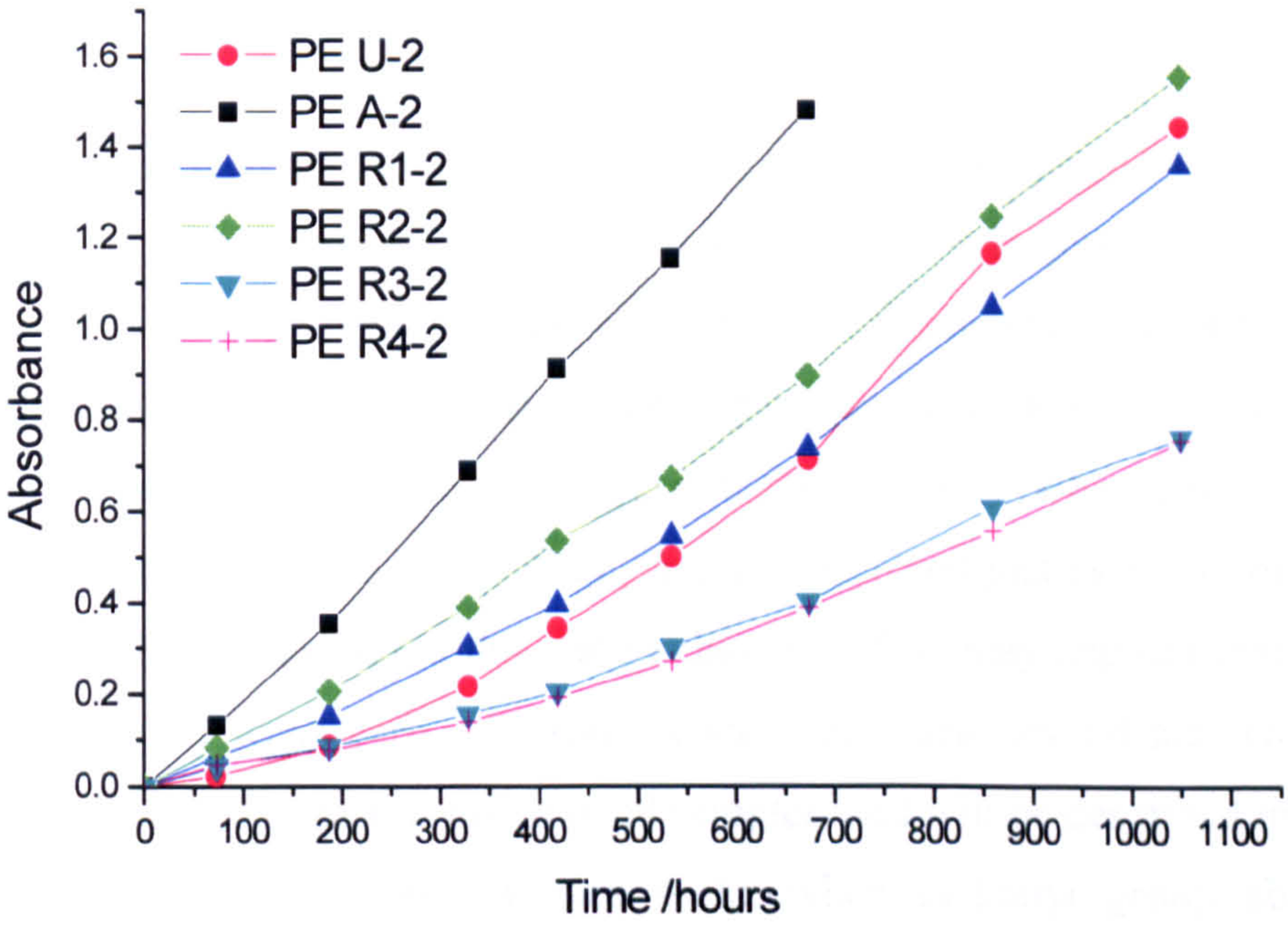

Figure 4-13 Carbonyl group development under QUV irradiation (new samples). Ageing time: two months.

The rates of carbonyl group development were little different from the first batch samples. Anatase pigmented PE film still demonstrated the greatest carbonyl growth. Only a marginal difference in the oxidation rates of the PE R3-2 and PE R4-2 was seen in the course of the experiment. But PE R3-2 carbonyl group development was little faster than in PE R4-1.

The evident difference for carbonyl group development with R1-2 and R2-2 was observed. For batch 1, carbonyl group growth in the PE R1-1 was faster than in PE

R2-1 film. For batch 2 samples, the ranking was not same as PE R1-1 and PE R2-1. The carbonyl group development in PE R2-2 was clearly faster than that in PE R1-2.

For unpigmented PE sample PE U-2, the carbonyl group development behaviour was the same as for the batch 1 sample PE U-1 *i.e.* the peak growth rates for unpigmented PE film was greater than those in PE R1-2 and PE R2-2. After about 730 hours irradiation in the QUV machine, the absorbance of the unpigmented sample carbonyl group overtook PE R1-2 and was approaching that for PE R2-2. The curves of carbonyl formation are concave upward, indicating autocatalytic reaction for all samples.

Because the experimental condition is same for the results displayed in Figure 4-12 and Figure 4-13, a comparison can be made between them. It is quite clear that for the batch 2 samples the carbonyl group development was faster than that for the batch 1 samples. In the PE A-2 samples, the carbonyl peak reached absorbance 1.4 after *ca.* 700 hours, whereas it needs *ca.* 850 hours in the PE A-1. When carbonyl group development achieved more than 1.4 a.u, fracture occurred just as with both PEA-1 and PE A-2. PE R2-2 exhibited the same behaviour. This may suggest that the film will fail completely when carbonyl group concentration reaches 1.4 a.u. The similar phenomenon was also observed for strained samples, and will be described in the next chapter. For strained samples, samples broke when carbonyl group absorbance reached *ca.* 0.5 a.u.

The most important fact is that the ranking of photoactivity for sets of films obtained by measuring carbonyl group development is consistent with the results obtained by the gas-phase method - monitoring CO_2 evolution. Although different batch samples caused little difference in carbonyl group development, the ranking of carbonyl group development was reversed between R1 and R2 or R3 and R4 pigmented PE films from different batches, but the same rankings were observed with these two methods for a given batch samples. This is a convincing demonstration that the gas cell technique can be used to assess photoactivity in polymers pigmented with different grades of titanium dioxide with confidence. Since experience has shown that the

conventional carbonyl index method correlates reasonably well with service performance.

For the batch 2 samples except PE A-2, the carbonyl group developments are shown in Figure 4-14. The results clearly show that the ranking of unpigmented PE film in carbonyl method was different as the ranking in the CO_2 method. Apart from PE R2-2, the carbonyl group intensities for the rutile pigmented PE films were less than unpigmented PE film at the longer exposure times. At the beginning, the carbonyl group intensity of unpigmented PE was lower than that for most of the rutile pigmented PE films. With time irradiation, the carbonyl group rate for unpigmented PE film grew faster than that for rutile pigmented samples. When fracture occurred in the PE R2-2, the carbonyl intensity build-up in the unpigmented PE sample had not reached the carbonyl intensity in the PE R2-2. In other words, all rutile pigments tested except for the PE R2-2 in those experiments gave protection to PE film. The same phenomenon was not observed in CO_2 method. This is not surprising because the CO_2 method gives information about the very short (3 hours) and beginning stage of UV-induced photoreaction.

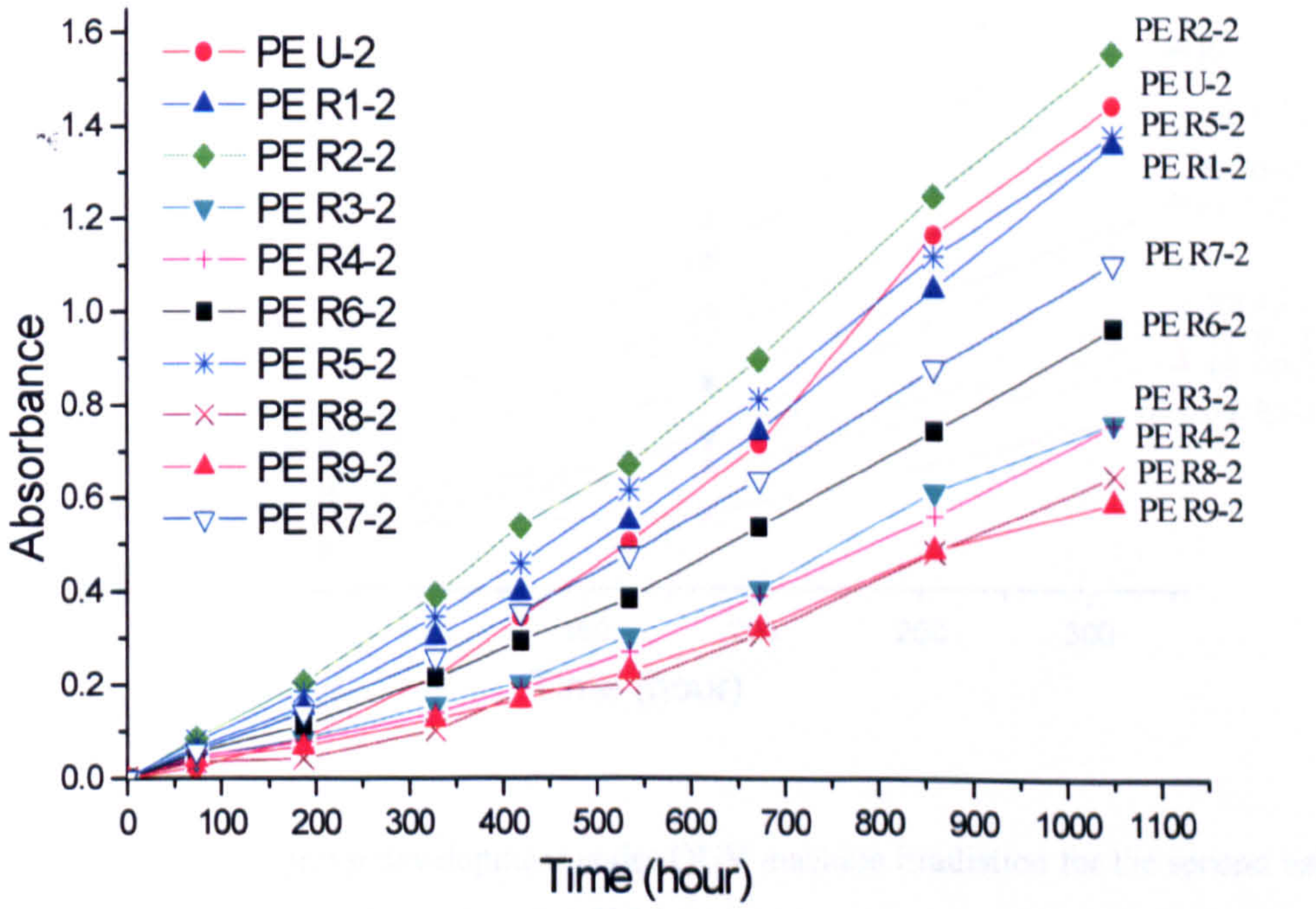

Figure 4-14 Carbonyl group development under QUV machine irradiation for the second batch of unpigmented and rutile pigmented samples.

Figure 4-15 shows carbonyl group development results recorded after exposure under UV light for 328 hours. The order of photoactivity in terms of carbonyl group development behaviour was similar to the results from the CO_2 method (see figure 4-11). The fact is that the ranking of the carbonyl group development for all rutile pigmented PE films was the same in the course of the experiments for both methods. For the detectable carbonyl data obtained at 328 hours, the absorbance divided into two groups like with the CO_2 method. One group, which included PE R1-2, PE R2-2, PE R5-2 and PE R7-2, exhibited pro-degradant behaviour compared to unpigmented PE. The other group included PE R3-2, PE R4-2, PE R8-2 and PE R6-2 demonstrated protection against UV degradation. There was a slight change in the order of photoactivity in each group. For the pro-degradant group, PE R5-2 gave a little higher intensity than PE R1-2, whereas in the CO_2 method the order was reversed; for the protectant group, PE R9-2 gave a smaller intensity than PE R3-1 and PE R4-2, whereas the CO_2 evolution of the PE R9-2 was faster than with PE R3-2 and PE R4-2.

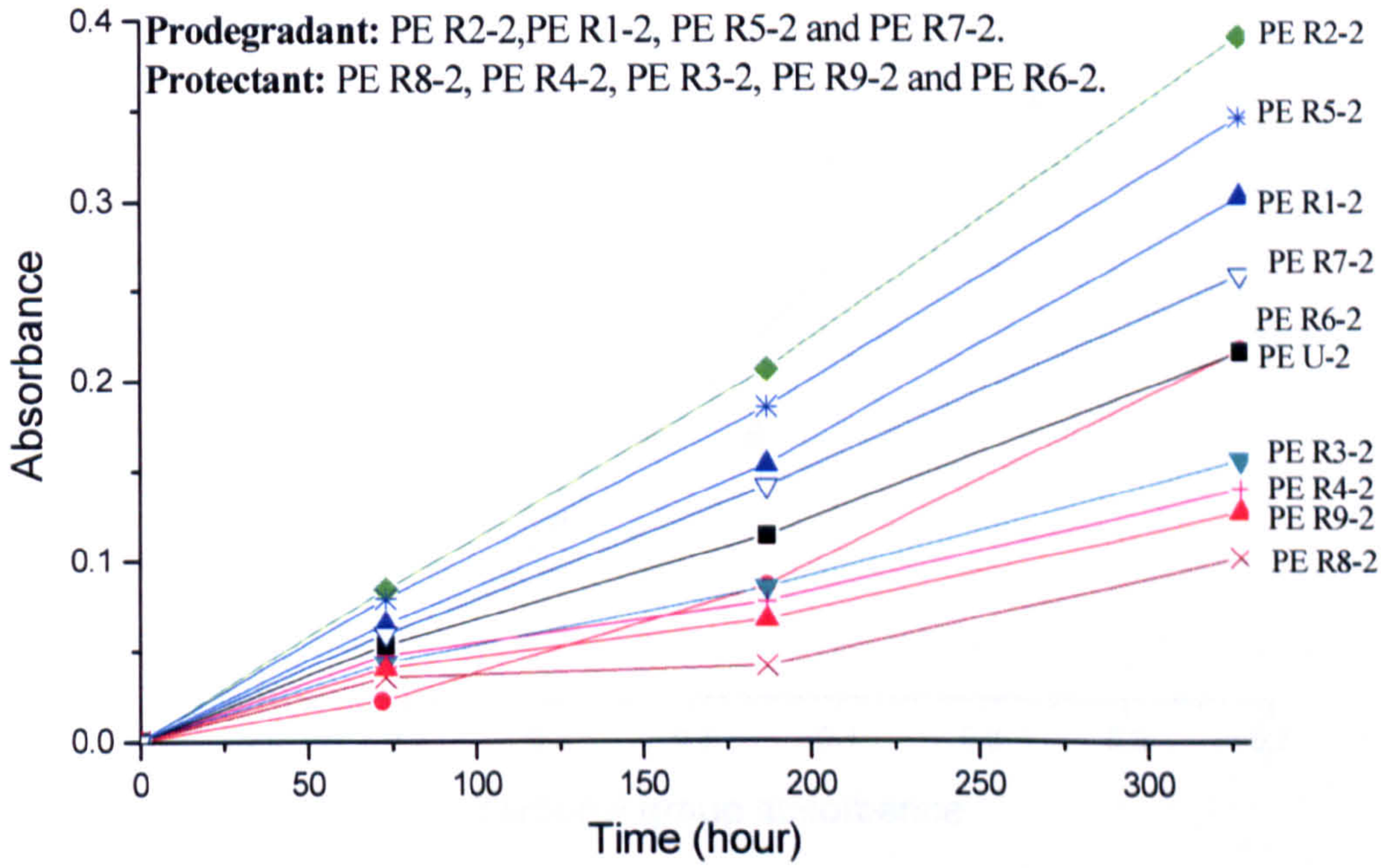

Figure 4-15 Carbonyl group development under QUV machine irradiation for the second batch of unpigmented and rutile pigmented samples after 328 hours exposure.

Nevertheless, it is clear that different rates of carbonyl group development were obtained at the same phr pigment loading with different grade rutile TiO_2 pigments. The ranking of rutile pigmented PE films and unpigmented PE film photoactivity, from the carbonyl group development rate at 328 hours, was as follows:

PE R2-2 > PE R5-2 > PE R1-2 > PE R7-2 > PE R6-2 ≅ PE U-2 > PE R3-2 > PE R4-2> PE R9-2> PE R8-2

4.3.4 Comparison between these two methods for batch 2 samples

For the batch 2 samples, the conventional method of measurement of carbonyl group development again gave similar results to the CO_2 method. To explain the sensitivity of the CO_2 method, it is more testing if attention is concentrated on the rutile pigmented PE and unpigmented PE, leaving aside the anatase pigmented PE film.

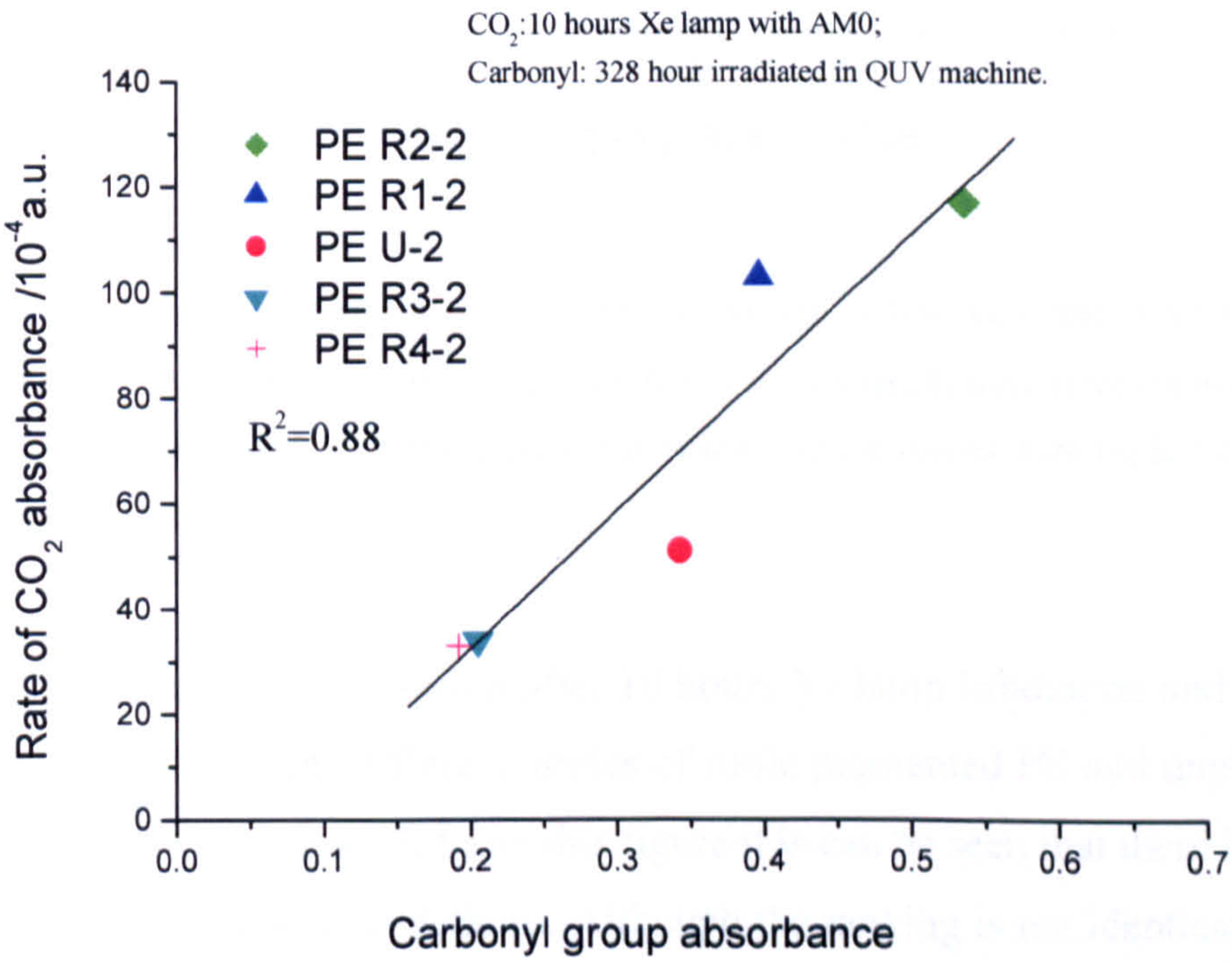

Figure 4-16 Correlation between CO_2 evolution in the FTIR cell and Carbonyl group growth measurement for same pigmentation as first batch samples. The CO_2 results were recorded from samples in the front position with AM0 filtered UV light and carbonyl group development results were made from samples irradiated in QUV machine.

Figure 4-6 shows the CO_2 absorbance rates obtained in the front position using AM0 filter, plotted against the carbonyl group concentration measured after 328 hours in the QUV machine. From this figure it is clear that the ranking is identical, and there is a good correlation, R^2=0.88, between the two methods.

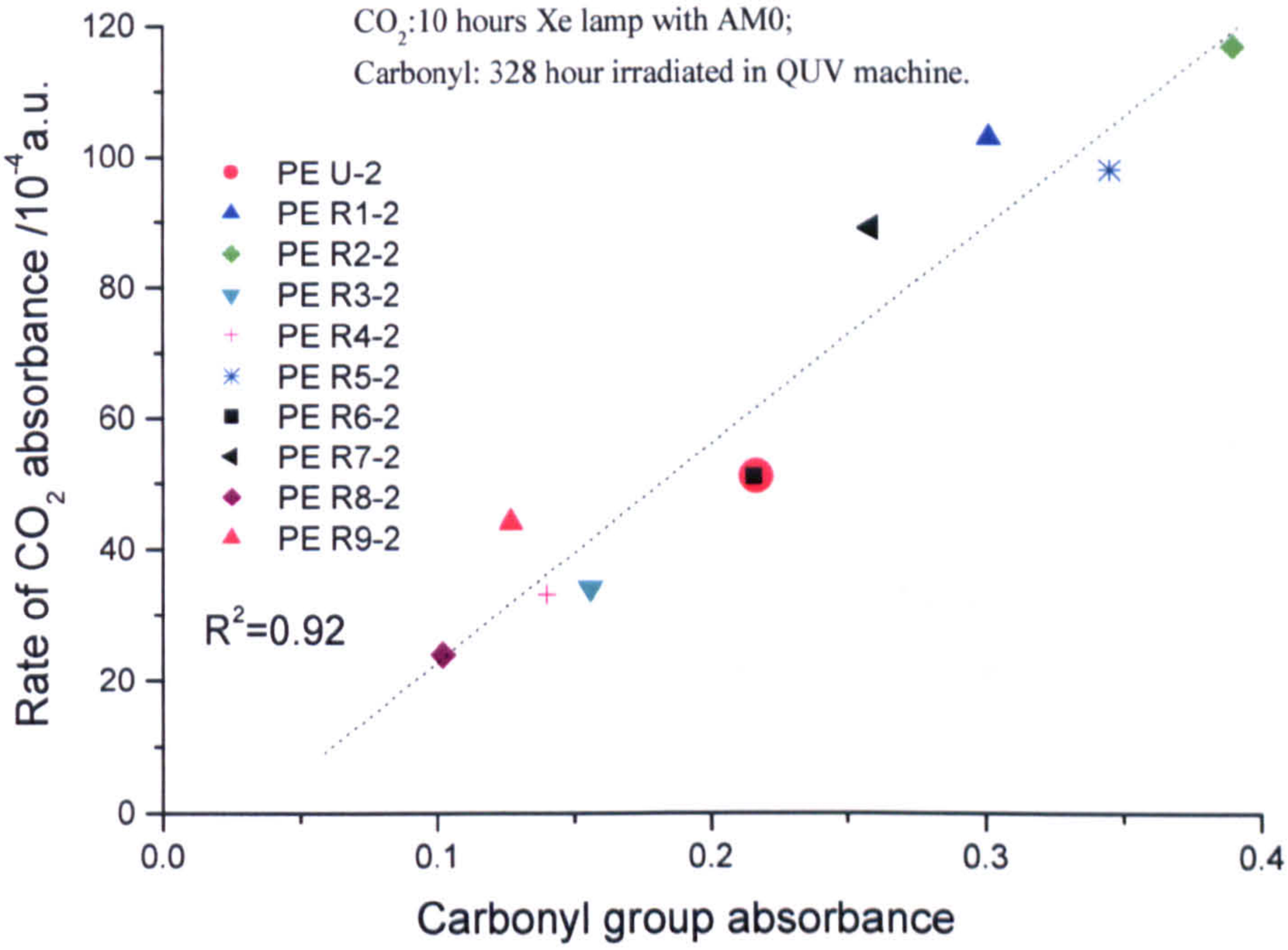

Figure 4-17 Correlation between CO_2 evolution in the FTIR cell and Carbonyl group measurement for all second batch samples except PE A-2. The CO_2 results were recorded from samples in the front position with AM0 filtered UV light and carbonyl group results were made from samples irradiated in the QUV machine.

The relation between CO_2 evolutions after 10 hours Xe lamp irradiation and carbonyl group development for nine different grades of rutile pigmented PE and unpigmented PE film is shown in Figure 4-17. From this figure it is can be seen that there is slightly changed ranking for these two methods. Although the ranking is not identical, there is an excellent correlation, R^2=0.92, between the two methods.

4.4 WATER AND OXYGEN EFFECT ON CO_2 EVOLUTION

One of the main advantages of the gas-phase FTIR method measurements of CO_2 evolution is that a change of atmosphere in the cell is easily achieved by changing the

composition of the flushing gas flowed through the cell. The work reported in this section represents an extension to pigmented polyethylene films of the preliminary study, discussed in Chapter 3, on the effects of atmosphere on photodegradation. Water and oxygen concentration are two dominating parameters studied on the effect of the composition of the gaseous atmosphere on the photodegradation rate of pigmented PE film.

The importance of water and oxygen and their role in the photocatalytic reaction mechanism of semiconductor TiO_2 has been well studied and has been described in more detail in section 1.6. Although it is widely accepted that UV, oxygen and moisture are essential for the photo-oxidation processes to occur, the *in-situ* FTIR method described in this study allows for fast, simple evaluation of the influences of oxygen and humidity on the photodegradation of unpigmented PE film and, more importantly, pigmented practical PE films which has not been possible previously, using other methods.

4.4.1 Effect of humidity on the CO_2 evolution

In order to elucidate the effect of humidity on CO_2 evolution under UV irradiation for pigmented PE films, PE A-1 and PE R2-1 were selected which were tested under the same experimental conditions as described in section 2.5.6, *i.e.* the films were placed at the back position in the gas cell. The background of CO_2 absorbance ($\sim 12\times10^{-4}$ a.u.) is stable in these experiments when filtered with AM0+AM1.5 filters together, the relatively high activity samples (PE A-1, PE R2-1 and unpigmented films) were selected to ensure that the CO_2 background is quite small compared to CO_2 evolution from these samples. PE A-1 contained a coated anatase-based TiO_2 pigmented PE film (see table 2.1) and was found to be highly photoactive and was used here for studying the effect mainly on the PCD process. PE R2-1, although it was more durable than PE A-1, was found to be the most photoactive rutile-based PE film and was used to elucidate any differences in activity between the different pigment crystal forms due to changes in the humidity condition. The different humidity atmospheres in the gas cell were obtained by passing cylinder oxygen (BOC) through a water bubbler to get moist gas; passing cylinder oxygen through a 600 mm tall interior

diameter 5mm-glass tube filled with freshly dried silica gel was used to get a lower humidity atmosphere. A third option was to use cylinder oxygen directly, with no humidifying or drying treatment. The actual humidity in the cell for the respective runs was characterized by the absorbance of the IR water band at 1557 cm^{-1} (as in the experiments with the unpigmented PE film in Chapter 3). Difficulties were experienced with controlling the humidity in the cell. It was found that the humidity was sometimes higher when the silica gel column was used than when cylinder oxygen was used directly, presumably because water was picked up from the silica gel. Although an absolute humidity atmosphere could not be set, reasonably varied humidities were obtained by using the methods described above. With the IR water band at 1557 cm^{-1} to monitor the water concentration in the cell, satisfactory results were observed for anatase and rutile based PE films. All experiments were performed in the same glass gas cell, and to eliminate the effects of cross contamination, the water in the water bubbler was replaced before each experiment with freshly drawn Millipore water.

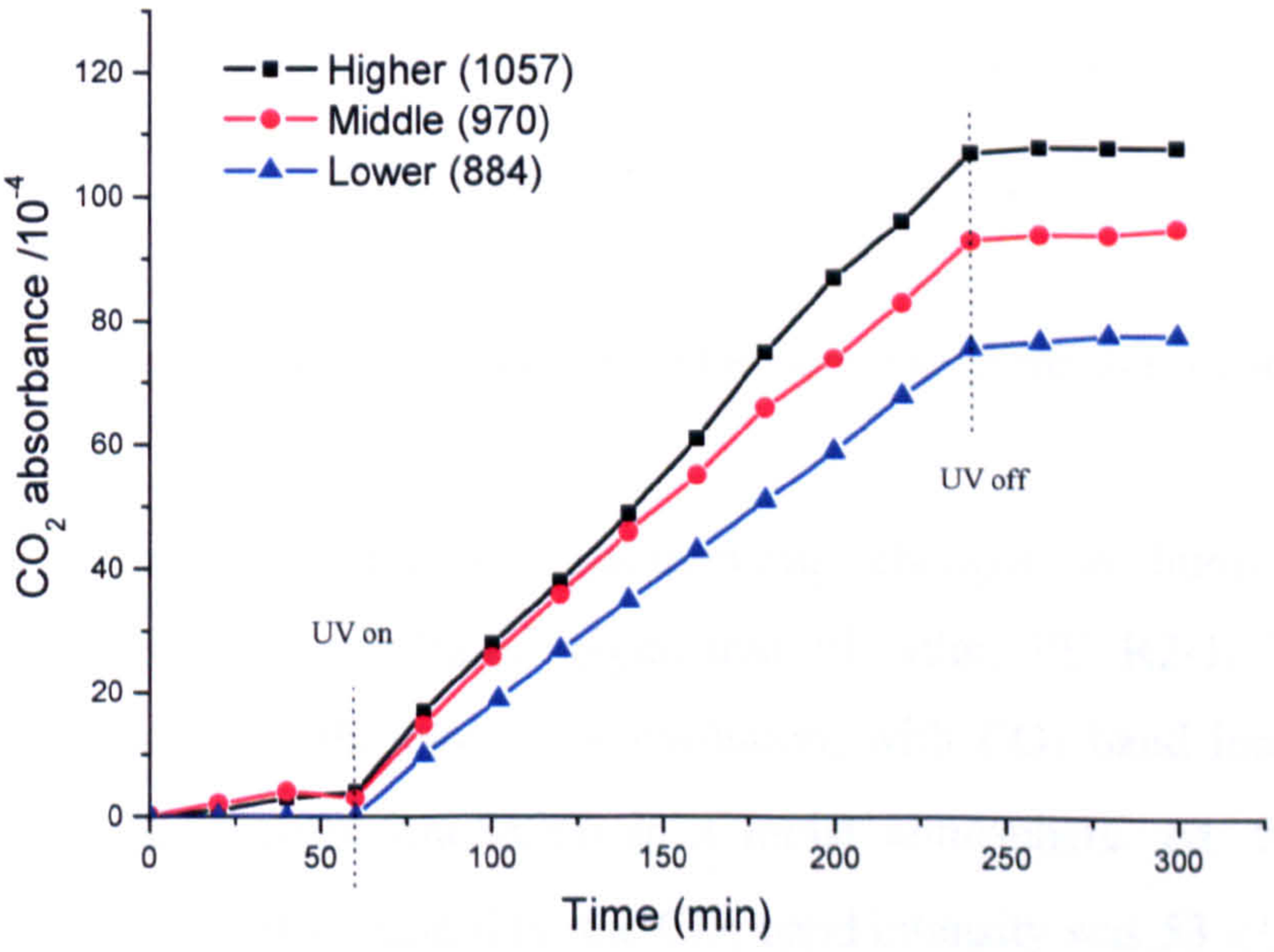

Figure 4-18 Carbon dioxide evolution in different humidity atmospheres from PE A-1. The number in bracket is relative humidity in the cell.

Figure 4-18 shows the effect of changing humidity in the reaction cell on PE A-1. As can be seen, the highest rate of CO_2 evolution was observed with the atmosphere with the highest moisture content (*ca.* 60 % relative humidity), with CO_2 band intensity of

107×10^{-4} a.u. after 180 minutes irradiation. A change in humidity from higher level to middle level *i.e.* relative humidity from 60 % to 45 % resulted in a decrease in CO_2 evolution from 107 to 93 (14 a.u.): a further drop in humidity to 15 % caused CO_2 evolution to decrease by 17 a.u. It seems that the decreases in CO_2 evolution were proportional to the reduction in humidity for anatase pigmented PE film (see Figure 4-20).

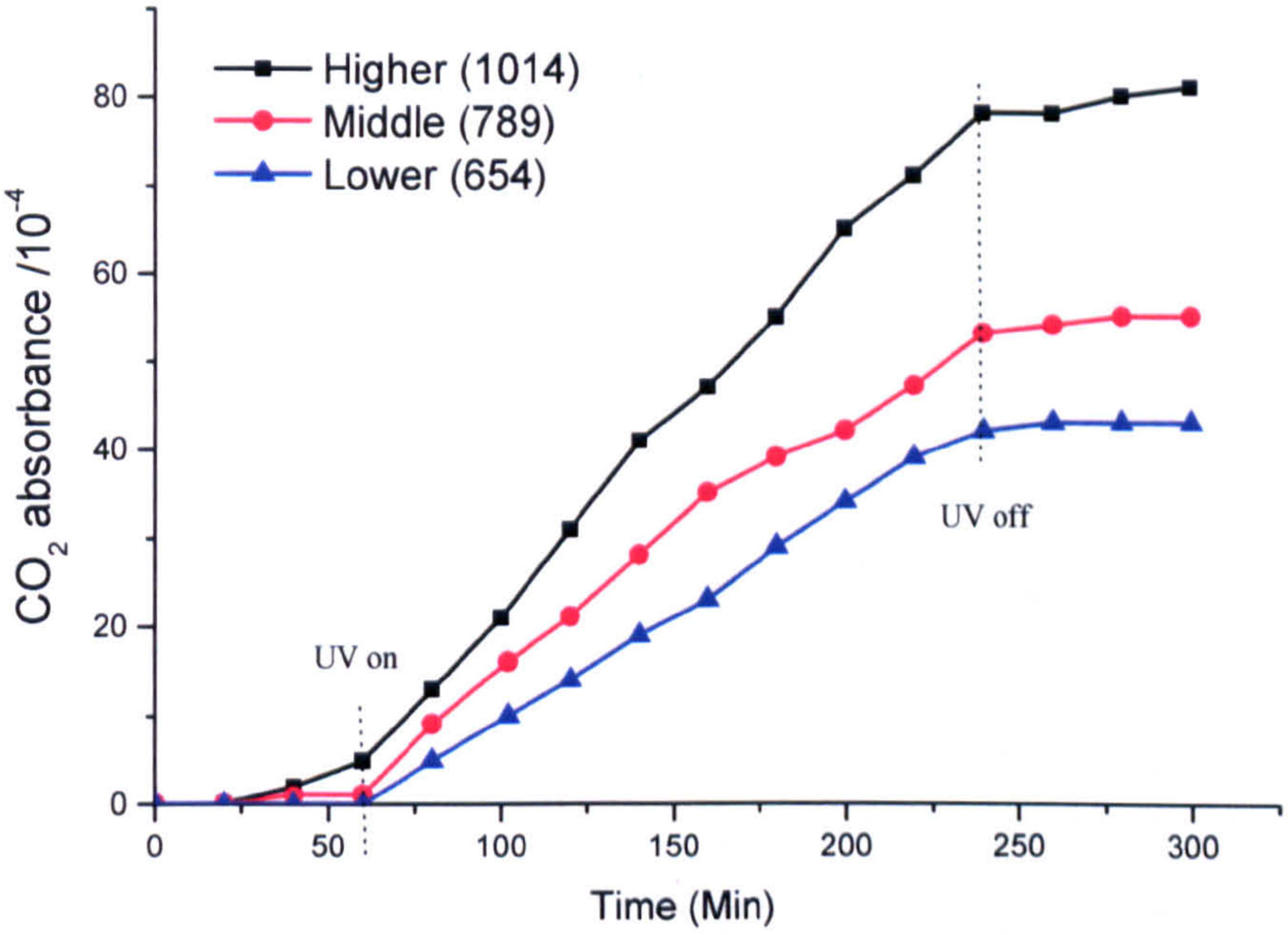

Figure 4-19 Carbon dioxide evolution in different humidity atmospheres from PE R2-1.

Figure 4-19 shows the effect of corresponding changes in humidity on the photodegradation of the rutile-based pigmented PE film, PE R2-1. The highest moisture atmosphere gave the most CO_2 evolution, with CO_2 band intensity of 78 $\times 10^{-4}$ a.u. after 180 minutes irradiation in a moist atmosphere, *ca.* 53% relative humidity. At *ca.* 16% relative humidity, the CO_2 band intensity was 53 $\times 10^{-4}$ a.u. after 180 minutes exposure. The lowest level humidity atmosphere was quite low, with relative humidity near to 0, the CO_2 band intensity was 42 $\times 10^{-4}$ a.u. after 180 minutes irradiation. Hence, a similar comparison was obtained to PE A-1; for PE R2-1 a change in relative humidity from 53 % to 16 % resulted in a decrease in CO_2 evolution from 78 to 53 (25 a.u.); and further reduction from 16 % to 0 (16 %) caused CO_2 evolution to decrease from 53 to 42 (11 a.u.). From these data the humidity

decrease from moist to middle divided by decrease of CO_2 band intensity; =37/25 = 1.48 compared with 16/11=1.45, for corresponding results from middle level to low humidity. As for A-1 film, decrease in CO_2 evolution seems to be proportional to the fall in humidity. Table 4-5 summarizes results of CO_2 evolution in different humidity atmospheres for PE A-1, PE U-1 and PE R2-1.

Table 4-5 Dependence humidity atmosphere on CO_2 evolution from five samples

Pigment	Water vapour band at 1557 cm^{-1} Abs×10^{-4} by background	Atmosphere Moist oxygen In RH	CO_2 Abs×10^{-4} After 3h irradiation	Reduction Rate % (reduce account/ Moist value)
A-1	1057	60 %	107	
A-1	970	45%	93	87
A-1	884	15%	76	71
U-1	968	45%	75	
U-1	890	33%	61	81
U-1	635	~0%	43	57
R2-1	1014	53%	78	
R2-1	789	16%	53	68
R2-1	654	~0%	42	54

It can be clearly seen from Table 4-5 that in the presence of oxygen, the rate of carbon dioxide generation was sensitive to humidity for the different PE films. Carbon dioxide generation was greatest in the highest moisture oxygen atmosphere *i.e.* in the presence of oxygen, increased humidity accelerated CO_2 formation for all PE films.

The effect of humidity for all of these three PE films have been summarized in Table 4-5. Figure 4-20 shows plots of the CO_2 band intensity observed after 180 minutes irradiation against the measured water vapour band intensity at 1557 cm^{-1} under different humidity atmospheres. It can be clearly seen that the CO_2 evolution for both

the pigmented and unpigmented PE films increases with humidity. This observation is fully consistent with practical experience and the known importance of humidity in the natural weathering of polymer films. From Figure 4-20, although the photodegradation rates of all the PE films are affected by changes in humidity the PE A-1, showed a significantly greater sensitivity (sharp slope) to humidity changes in the oxygen cell atmosphere than the rutile-based PE film (PE R2-1) and the unpigmented PE film PE U-1. This may be because for anatase PCD dominates. Therefore, the results confirm that it is essential to control humidity if reproducible comparisons of PE films are to be made by monitoring the carbon dioxide produced during film breakdown.

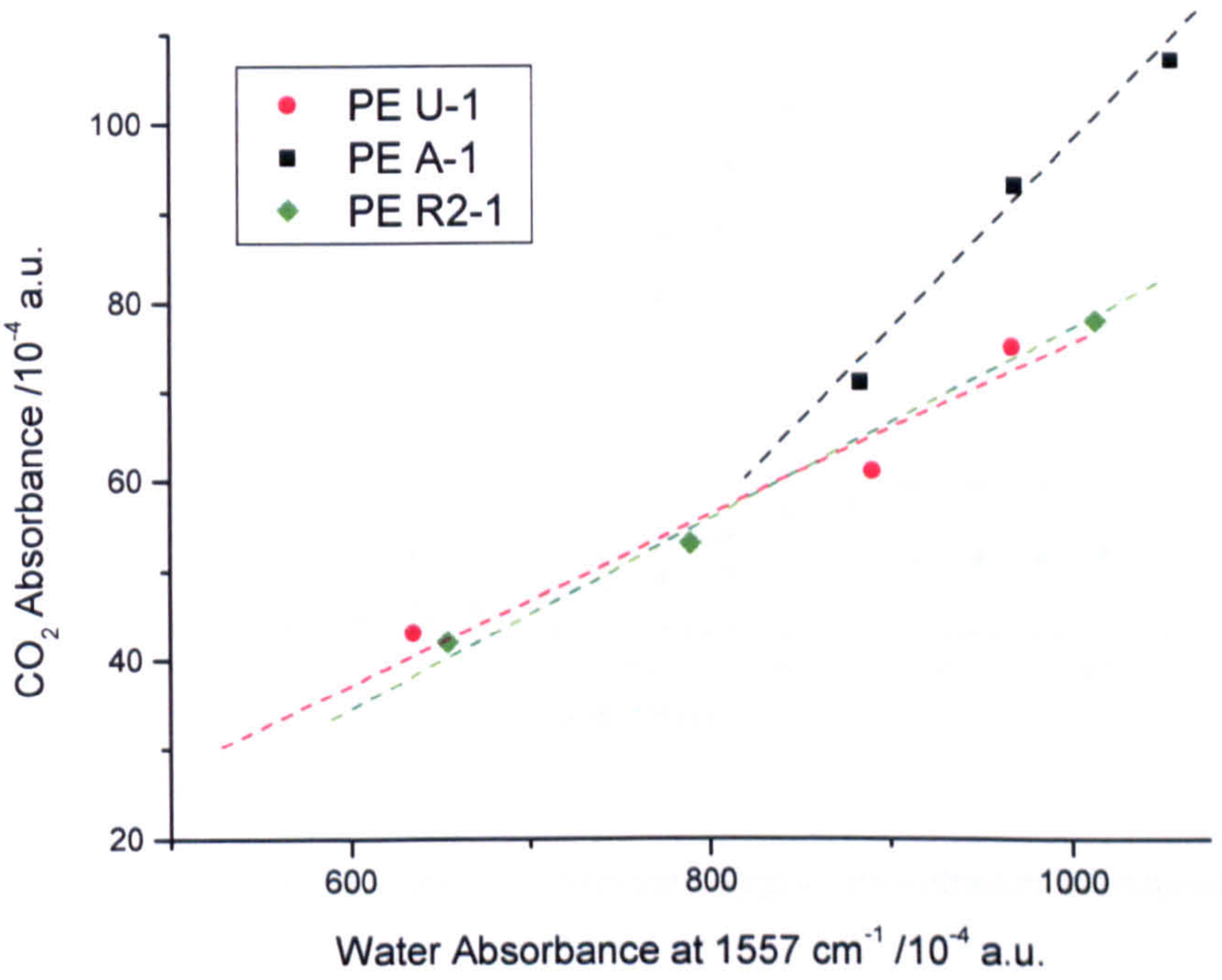

Figure 4-20 The effect of varying humidity on the FTIR cell CO_2 absorbance rate against initial H_2O absorbance peak height for pigmented and unpigmented films.

4.4.2 Effect of oxygen concentration on the CO_2 evolution

Oxygen is a key reactant in both direct photochemical and indirect photo-catalysed oxidation of polymer systems. The presence of oxygen in the atmosphere enhances the effects of photodegradation. The role of oxygen in indirect photo catalysed

oxidation of polymer systems is different compared to direct photochemical reaction. Oxygen is a necessary agent for the heterogeneous photocatalytic reaction because it suppresses the recombination of photogenerated electrons (e^-) and (h^+). The effect of reducing the oxygen partial pressure was therefore investigated by purging the cell either with a 20:80 volume % O_2:N_2 mixture or nitrogen instead of (wet) oxygen, again using the water bubbler. All gases were bubbled through freshly drawn Millipore water. PE A-1 and PE R2-1 films were selected and were studied under the same experimental conditions as for the unpigmented PE experiments reported in Chapter 3. Results are shown in Figure 4-21 and Figure 4-22.

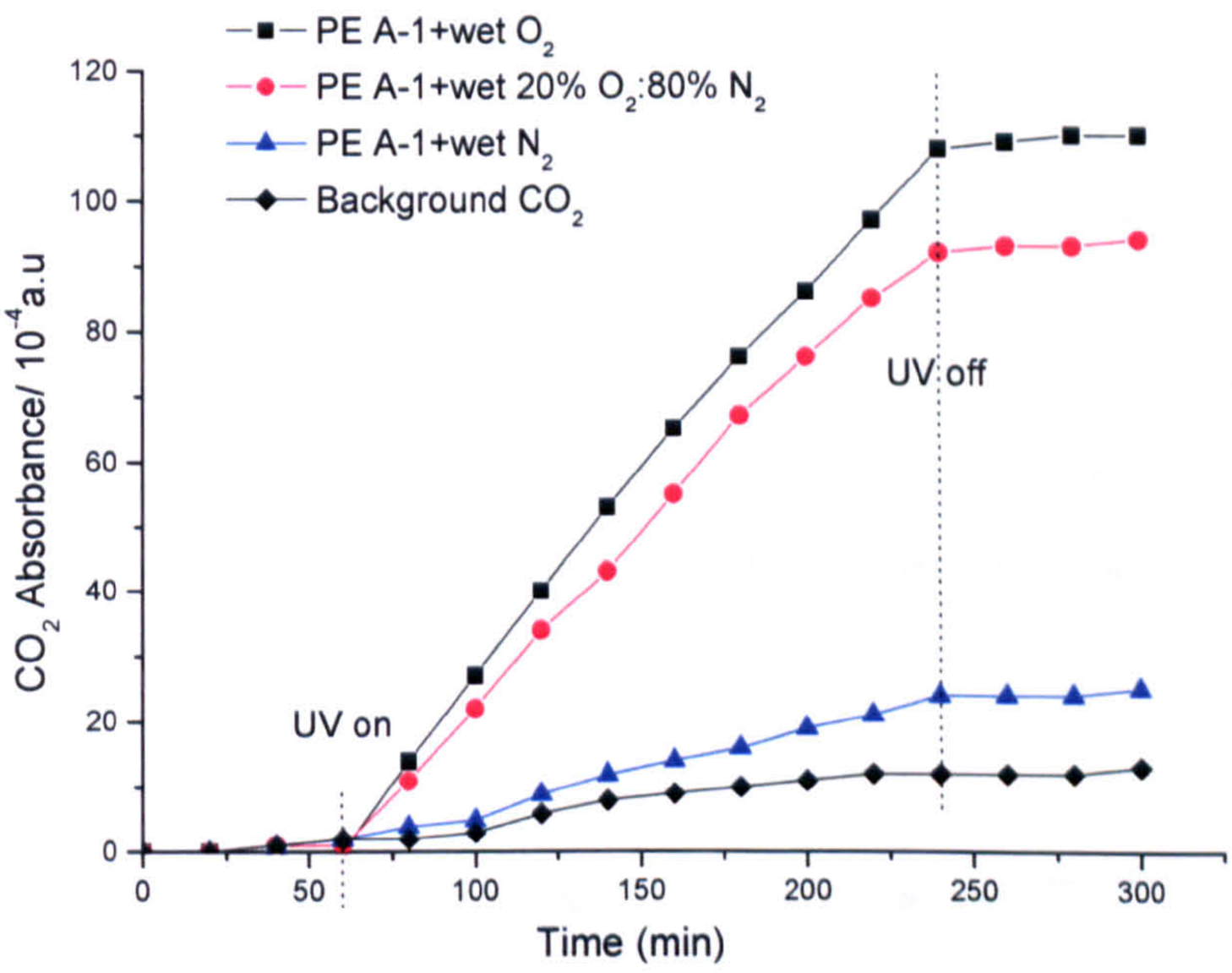

Figure 4-21 Carbon dioxide evolution in different oxygen concentration atmospheres from A-1 film.

Figure 4-21 shows the effect of oxygen concentration on CO_2 evolution for PE A-1. It can be seen that changing the gaseous atmosphere from oxygen to nitrogen caused a dramatic decrease in the rate of CO_2 evolved from the PE A-1. The highest rate of CO_2 evolution was observed with 100% oxygen in a moist atmosphere (*ca.* 60% relative humidity), the CO_2 band intensity was 107 $\times 10^{-4}$ a.u. after 180 minutes irradiation. Wet nitrogen gave the lowest rate of CO_2 evolution, with CO_2 band intensity of 37 $\times 10^{-4}$ a.u. after 180 minutes irradiation. The CO_2 evolved with the PE

A-1 under a moist nitrogen atmosphere was a factor of 3 less than that seen in a moist oxygen atmosphere. The rate of CO_2 evolution for the 20:80 volume % O_2:N_2 mixture was intermediate between those for wet oxygen and wet nitrogen, with CO_2 band intensity of 89 $\times 10^{-4}$ a.u. after 180 minutes irradiation. However, the CO_2 evolved under a moist 20:80 volume % O_2:N_2 mixture atmosphere represents just a factor of 1.2 decrease in the photodegradation rate with the PE A-1 from that seen in a 100 % moist oxygen atmosphere. Thus 80 % oxygen concentration reduction caused just *ca.* 17% reduction in the rate of CO_2 evolution decrease compared to the higher oxygen concentration atmosphere whereas a further 20 % oxygen concentration decrease, from 20:80 volume % O_2:N_2 mixture to nitrogen atmosphere caused *ca.* 58 % decrease in the rate of CO_2 evolution. The above results suggest that anatase pigmented PE film (PE A-1) is more sensitive to oxygen at low oxygen concentrations. The phenomenon of the sensitivity decrease with oxygen concentration increase may be attributed mainly to the CO_2 evolution coming from the photocatalytic reaction for anatase pigmented PE film *i.e.* the rate of photocatalytic reaction increases faster when oxygen concentration rises at low level oxygen concentration. With the oxygen concentration rise, the enhancement on the rate of photocatalytic reaction decreased.

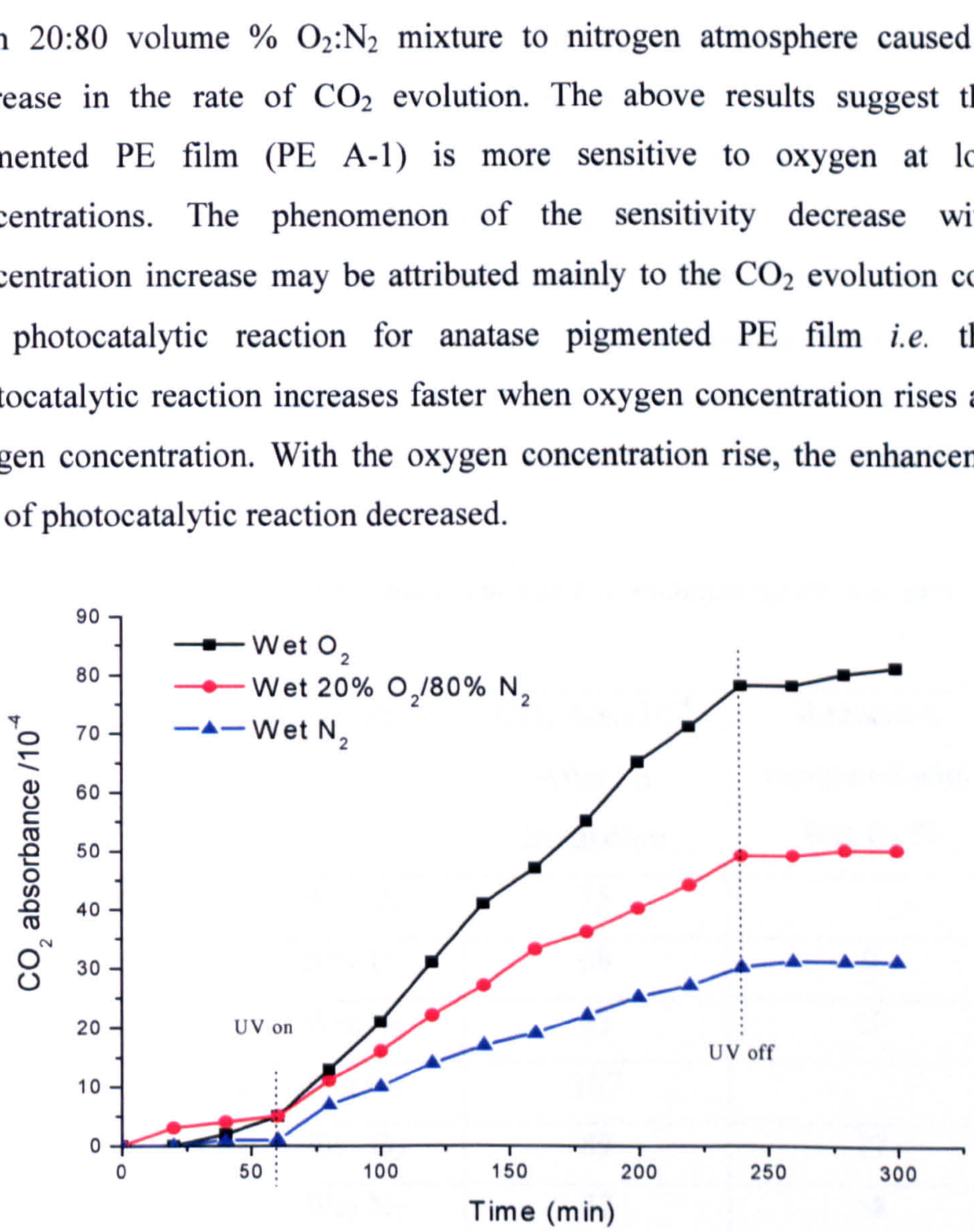

Figure 4-22 Carbon dioxide evolution in different oxygen concentration atmosphere from R2-1 film. Background CO_2 as in Fig 4-21.

Figure 4-22 gives the data for the PE R2-1 sample. Wet nitrogen gave the lowest rate of CO_2 evolution with absorbance of 30×10^{-4} a.u. after 180 minutes UV irradiation; the CO_2 absorbance 49×10^{-4} a.u. after 180 minutes UV irradiation in the moist 20:80 volume % O_2:N_2 mixture was intermediate between those for wet oxygen and wet nitrogen respectively. The behaviour of the PE R2-1 was slightly different compared to the PE A-1. The CO_2 evolved under a moist nitrogen atmosphere was less by a factor of 2.6 from that seen in moist oxygen atmosphere. The rate of CO_2 evolution for the 20:80 volume % O_2:N_2 mixture was a factor of 1.6 less than that seen in a moist oxygen atmosphere. This shows that 80 % oxygen concentration reduction caused just *ca.* 37 % decrease in the rate of CO_2 evolution compared to that in the higher oxygen concentration atmosphere, and with a further 20 % oxygen concentration decrease from a moist 20:80 volume % O_2:N_2 mixture to nitrogen atmosphere caused *ca.* 39 % decrease in the rate of CO_2 evolution for PE R2-1. Therefore, the sensitivity to oxygen concentration of the PE R2-1 was less than that for PE A-1 which was more sensitive at low oxygen concentrations. This correlated with the fact that the pigment used in PE R2-1 has lower photoactivity compared to the pigment used in PE A-1. Table 4-6 summaries the result for the three different types of PE film.

Table 4-6 Effect of oxygen concentration on CO_2 evolution for PE A-1, PE U-1 and PE R2-1films

Sample	Atmosphere	CO_2 Abs$\times10^{-4}$ After 3h irradiation	Reduction compared with Wet O_2 %
PE U-1	Wet O_2	75	
PE U-1	20% O_2	68	9
PE U-1	Wet N_2	43	37
PE A-1	Wet O_2	107	
PE A-1	20% O_2	89	17
PE A-1	Wet N_2	37	58
PE R2-1	Wet O_2	78	
PE R2-1	20% O_2	49	37
PE R2-1	Wet N_2	30	39

The above results in table 4-6 were plotted using CO_2 absorbance as a function of oxygen concentration in Figure 4-23.

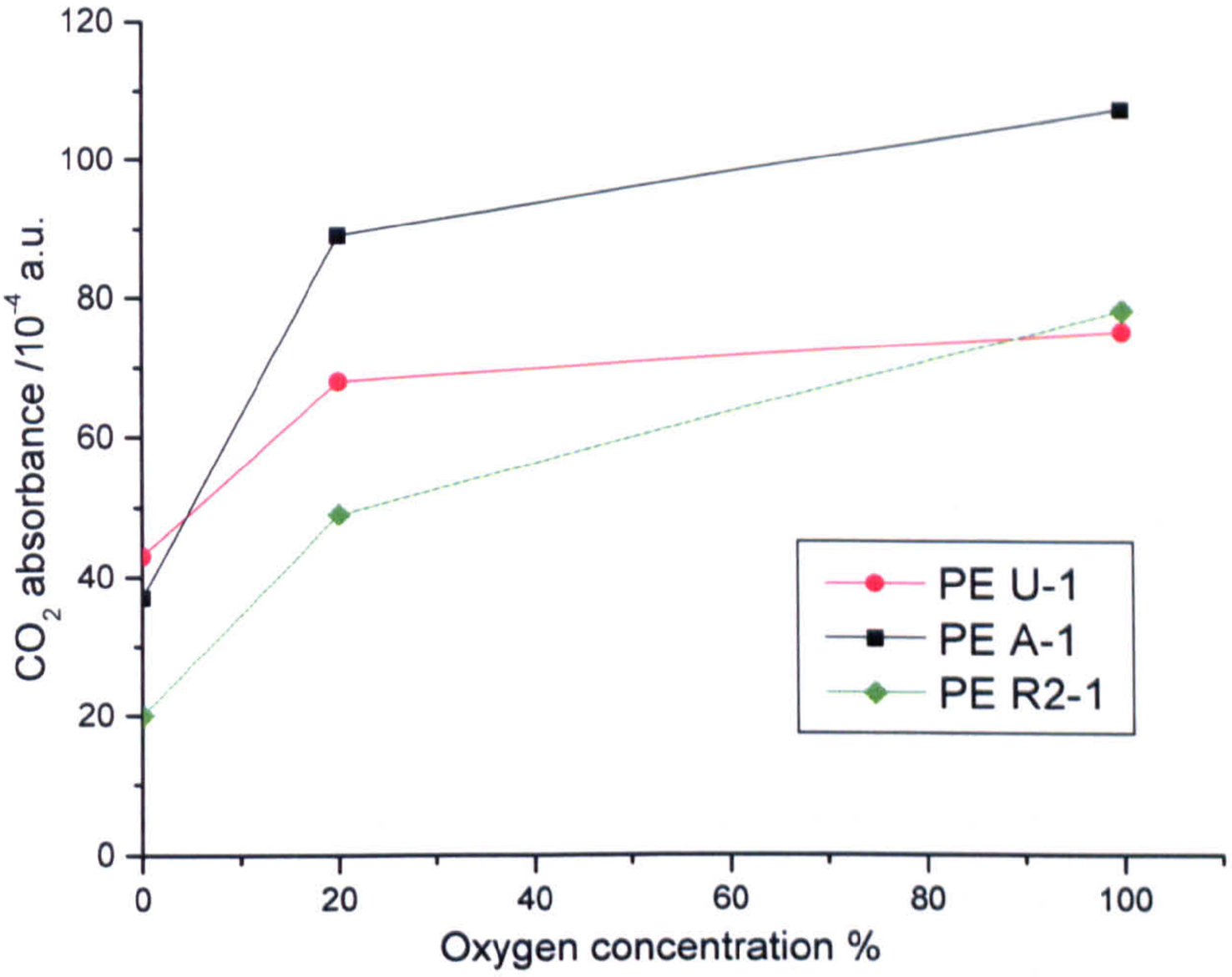

Figure 4-23 The effect of varying oxygen concentration on the FTIR cell CO_2 absorbance rate for pigmented and unpigmented films.

As expected, the PE A-1 has the strongest sensitivity at low oxygen concentration in the cell; the next was PE R2-1. The Unpigmented PE film seems relatively insensitive to oxygen concentration, and oxygen concentration has a stronger effect on pigmented PE film than unpigmented PE film. With the nitrogen atmosphere, unpigmented PE film gave more CO_2 evolution even than anatase pigmented PE film PE A-1.

These observations are consistent with a mechanism in which electrons reaching the pigment surface react with adsorbed oxygen to form the O_2^- radical ion, which is able to react with water to form the $OH_2^\bullet$ radical. Formation of O_2^- reduces surface recombination of electrons and holes. This mechanism would cause oxygen concentration to have a strong effect on photocatalytic oxidation when TiO_2 pigment is present in the film. In contrast to TiO_2 pigmented PE films, unpigmented PE film was less affected by oxygen concentration.

Rather more surprisingly, CO_2 formation was observed after purging with nitrogen for an hour under UV irradiation. The small CO_2 evolution in wet nitrogen may be the

result of oxygen absorbed in the polymer, or of pre-existing CO_2 diffusing out during UV exposure. This work was carried out in parallel with studies by E.J. Lawson [7] on paint film. As part of these studies the cell was purged for an hour and then the sample was left under nitrogen for three days before being purged again for an hour. In E.J. Lawson's studies there was a marked reduction in CO_2 evolution but CO_2 evolution was still observed. It is not possible to remove solute or percolated residual oxygen totally to gain an oxygen free atmosphere in the cell under the current experimental conditions.

4.5 UV INTENSITY AND WAVELENGTH DEPENDENCE STUDIES

The studies discussed in section 4.4 focused on the use of the gas-phase CO_2 method as an easy and convenient means of studying the photo-oxidation of pigmented PE films affected by a changing humidity or oxygen concentration in the gas cell. Because the experimental procedure allows the ready interposition of suitable optical filters, the method is well suited to studies of *e.g.*, incident wavelength and intensity. This section describes the use of the gas-phase CO_2 method to study the effect of changing irradiation intensity and wavelength on the photo-oxidative formation of carbon dioxide from pigmented PE films. The behaviour of the unpigmented PE film is contrasted with films pigmented with both relatively inert (coated rutile) and catalytically active (anatase) varieties of titanium dioxide pigment.

As in the previous studies, photooxidation of the PE film was measured by an I.R. spectrometric determination of the amount of CO_2 emission to the gas phase as a result of the oxidation. The effect of incident wavelength on film breakdown was studied by using different optical air-mass (AM) filters or their combination to modify selected spectral portions of the Xenon lamp output. It is not practical to keep the same UV intensity when AM filters are used to change wavelength in different experiments. Since the use of different AM filters entails a change in both the intensity and wavelength of the incident radiation, the effect of UV intensity on the rate of carbon dioxide evolution was monitored by using neutral density filters to reduce the output from the xenon lamp. By combining the two sets of measurements it was possible to comment on two issues:

(i) Intensity dependence: the effect of increased intensity of light, particularly UV radiation, on the degradation of pigmented PE films.

(ii) Spectral sensitivity of the unpigmented and pigmented PE film: this is the relative effectiveness of different wavebands of the UV-light spectrum in bringing about photodegradation.

It is convenient at this time to deal also with the effect of ageing of the Xenon lamps, which causing gradual reduction in intensity and changes in spectral distribution throughout the duration of this project. Output levels were checked regularly and the lamp was changed whenever such changes were deemed unacceptable.

4.5.1 Effect of lamp age on CO_2 evolution

The UV intensity of the 150 W high-pressure Xenon bulb output was observed to decrease with the lamp ageing. The output of one 150 W Xenon bulb was shown to fall from 51900 lux to 33500 lux over a period of 6 months (actual use time around 1000h) by Dilks [8]. The day-to-day variation in intensity was monitored. For a new bulb the variation was ~ 4 % but it was ~7 % for an old lamp. Two groups of experiments, using the 'old' or a 'new' bulb (used after stabilizing treatment) as UV source respectively were compared (see Figure 4-24 and Figure 4-25).

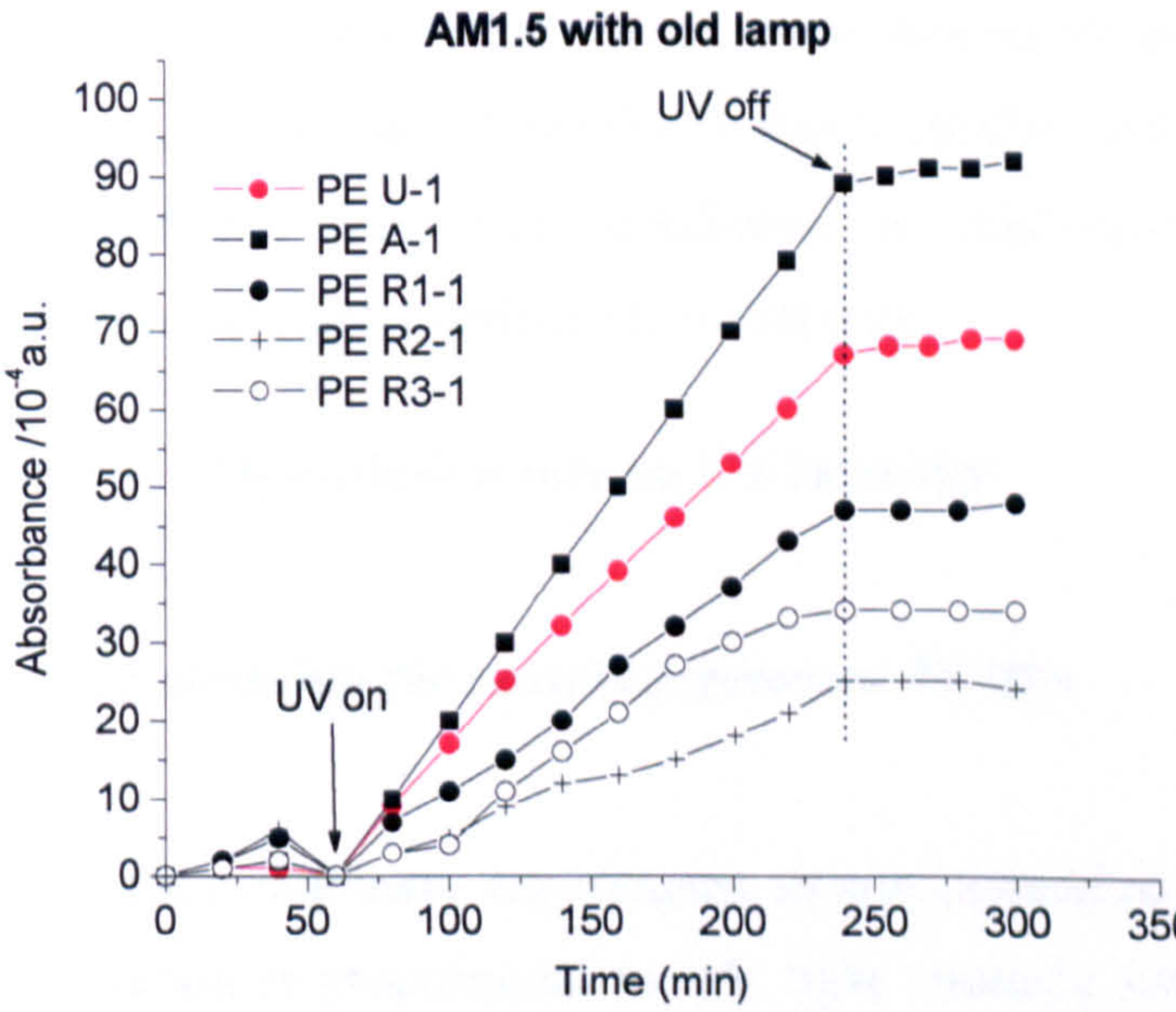

Figure 4-24 CO_2 evolution from the photo-oxidation of different films with AM1.5 using 'old' lamp.

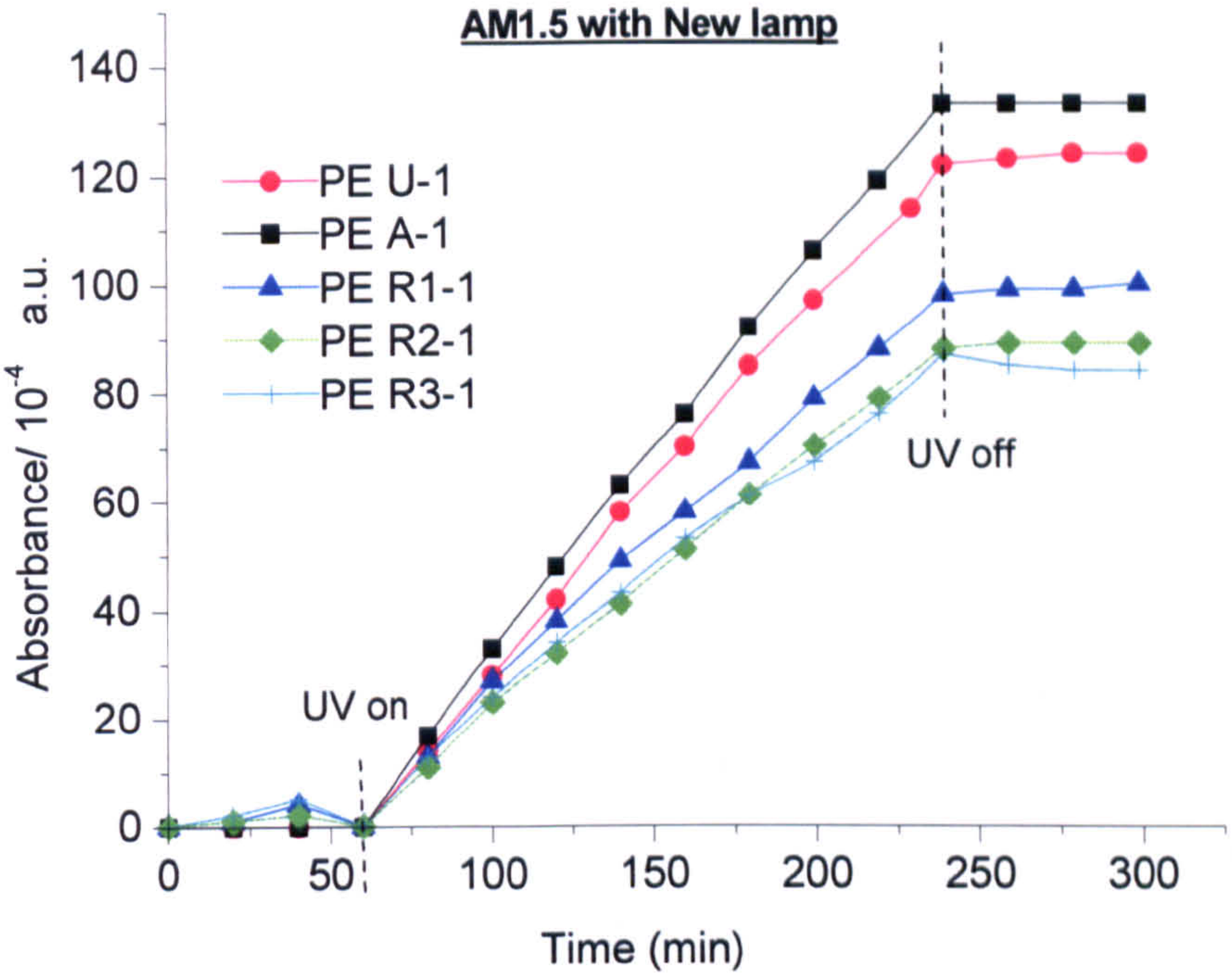

Figure 4-25 CO_2 evolution from the photo-oxidation of different films with AM1.5 and new lamp.

It can be seen from Figure 4-24 and Figure 4-25 that with the new lamp, more carbon dioxide was evolved than when using the old lamp. But the lamp age seems to have less effect on the distribution of its output because the ranking for different pigments is the same. However, the spread of results is much smaller with the new, more intense lamp. Experiments were next conducted to determine whether these differences are due to wavelength distribution or intensity.

4.5.2 Dependence of CO_2 evolution rate on UV intensity

4.5.2.1 Square root relationship for anatase pigmented PE film

The conclusion from the preliminary experiments on non-pigmented PE film was that the rate of CO_2 evolution is proportional to UV light intensity when using the Xe lamp source without AM filters. This is different from the results observed for unpigmented acrylic-emulsion paint films [9]. The mechanism of degradation of anatase TiO_2 pigmented PE film is expected to be different to that with unpigmented PE film because only the photochemical reaction occurs with unpigmented PE film.

For anatase TiO_2 pigmented PE film, the main photoreaction comes from indirect photo-catalysed oxidation. A square root relationship ($r \propto I^{1/2}$) for TiO_2 induced photocatalytic degradation reaction between the rate of oxidation r and UV intensity I was reported by Egerton and King [10].

One objective was thus to determine whether anatase TiO_2 pigmented PE film follows this mechanism of PCD process. Experiments to test this theory were carried out with AM0+AM1.5 filters as the UV source, because as demonstrated for PE U-1, the combination of two AM filters cut off short wavelength UV to reduce PD process. In order to facilitate subsequent normalization of results from different filter combinations, the UV intensity was changed using one neutral filter between the head of the light pipe and the cell. Neutral density filters (Oriel) of known transmittance (see figure 2.5) were used to produce different intensities but the same relative spectral UV distribution. PE A-1 were used and placed in the front position of the cell and irradiated for 240 minutes. The results for the UV intensity-dependence studies for the anatase pigmented PE films are shown in Table 4-7.

Table 4-7 Table showing the CO_2 absorbance measured after 240 minutes irradiation of PE A-1under different UV intensities.

Trans. %	$(Trans. \%)^{0.5}$	CO_2 Abs/ 10^{-4}a.u.	H_2O Abs/ a.u.
100	10	186	0.118
55	7.5	147	0.119
30	5.7	113	0.121
7	2.7	58	0.115

It can be seen from the tabulated results in table 4-7 that the rate of CO_2 evolution decreases with decrease in UV intensity. It seems that a relationship exists between the CO_2 evolved after 240 minutes irradiation and the amount of light illuminating the sample. Figure 4-26 shows the CO_2 band intensities plotted against the square root of the light transmission. The linear relationship between the rate of carbon dioxide evolution and the square root of intensity demonstrates the degradation rate varies as the square root of the intensity of the incident radiation. The variation of rate with $I^{0.5}$

occurred only with the anatase pigmented PE film whereas for unpigmented PE film the variation of rate degradation was directly proportional to UV intensity, as reported in section 3.7.5. This suggests that the unpigmented PE film degradation follows a different mechanism route comparing to anatase pigmented PE film. Photolytic reaction rates depending on the square root of light intensity and of low quantum yield are well known in photochemical studies, and are usually the result of a high bimolecular recombination rate of the species produced in the primary photochemical act. Also it can be seen from Figure 4-26 that the fitted line extrapolated to cut the y-axis, ordinate *i.e.* x=0, the intercept (*ca.* 12 Abs a.u.) at the background carbon dioxide level.

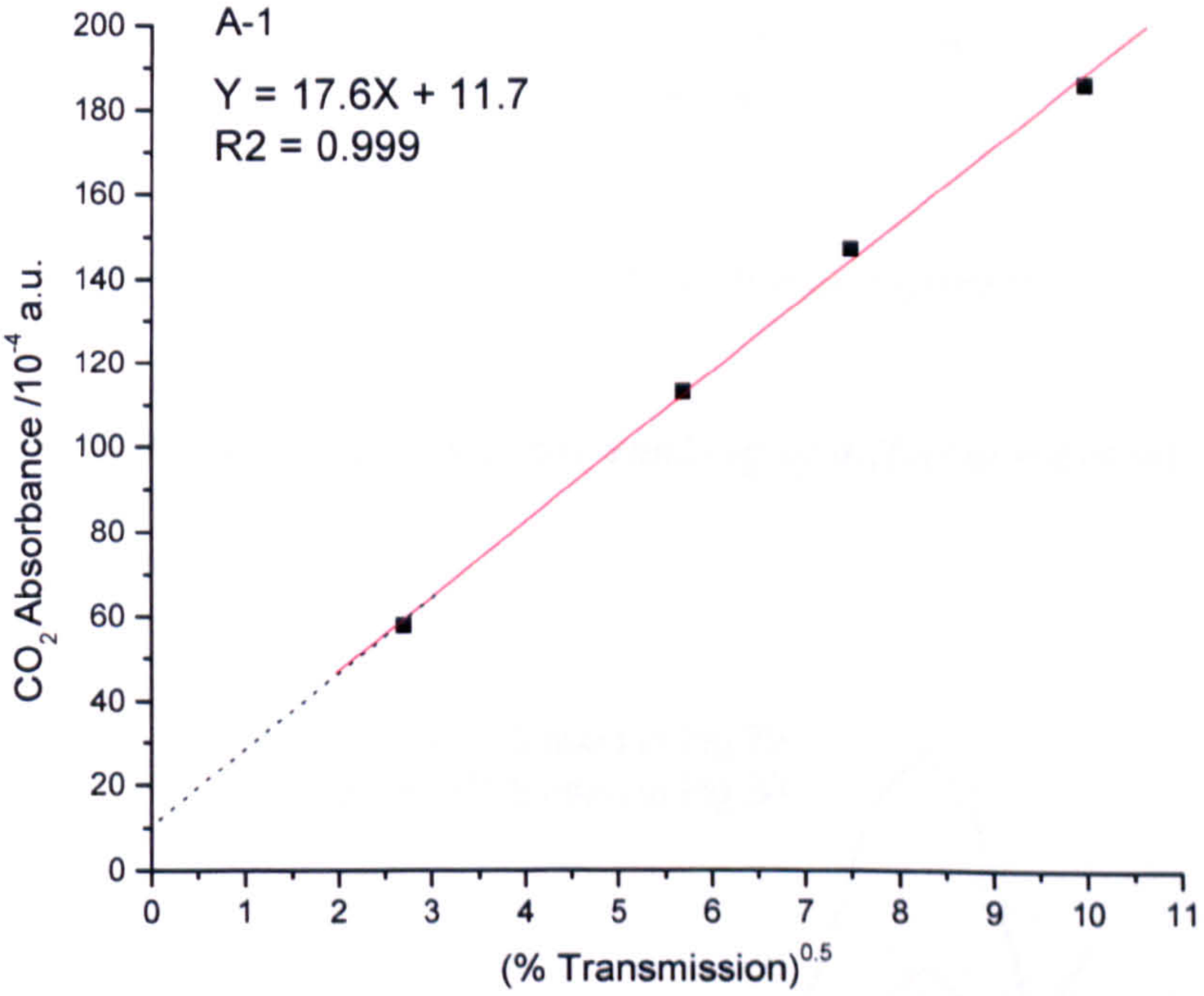

Figure 4-26 Graph showing the CO_2 evolution from Anatase pigmented PE as a function of the square root of the transmission through the neutral density filters.

Figure 4-27 shows a plot of the CO_2 evolution from anatase pigmented PE as a function of the UV intensity. It is clear that the relationship between the rate of carbon dioxide evolution and the UV intensity is not linear. But it was a clear parabolic relationship between the CO_2 evolutions with the UV intensity.

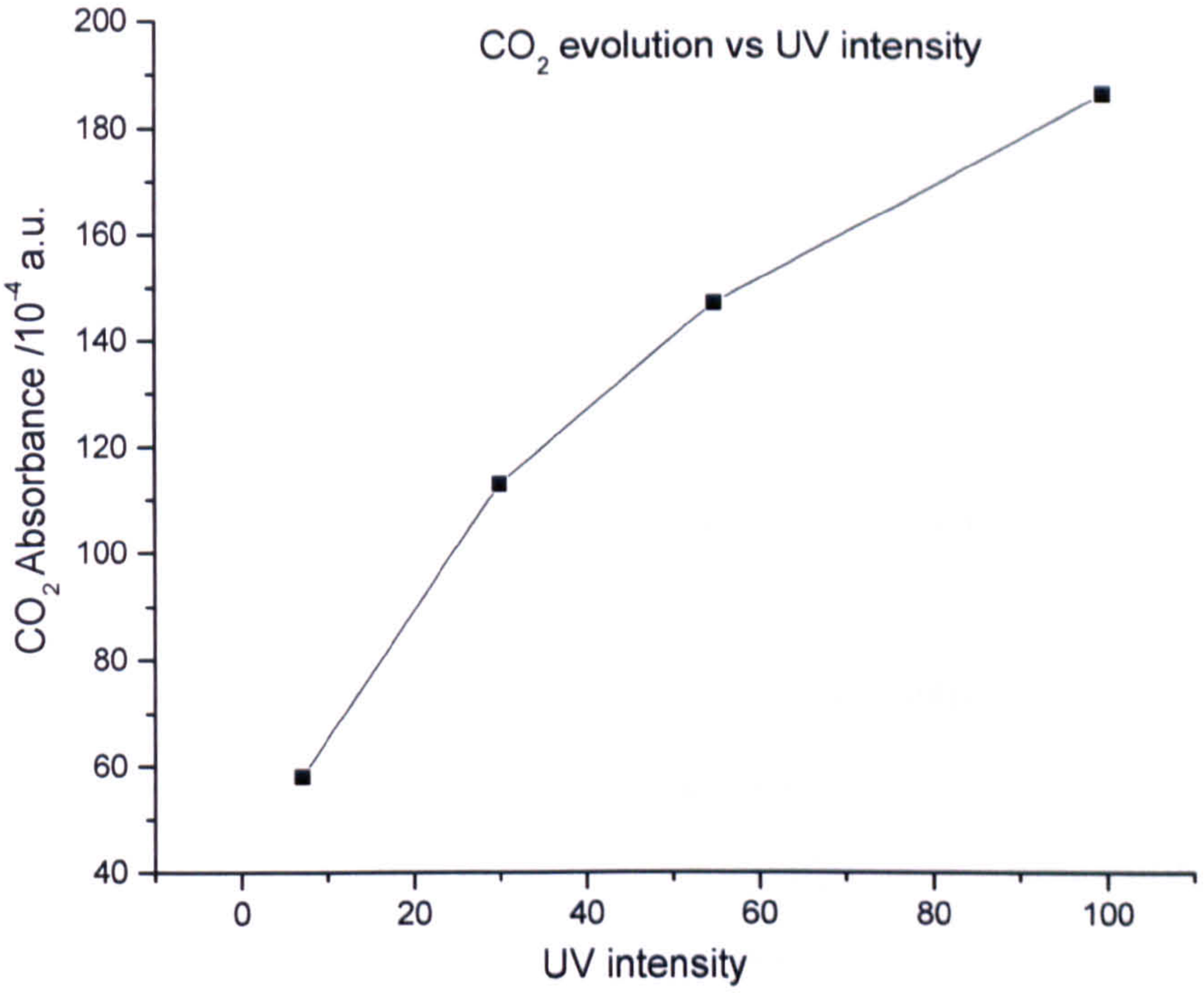

Figure 4-27 Graph showing the CO_2 evolution from Anatase pigmented PE as a function of the UV intensity.

4.5.2.2 The effect of intensity comparative ranking of different pigment

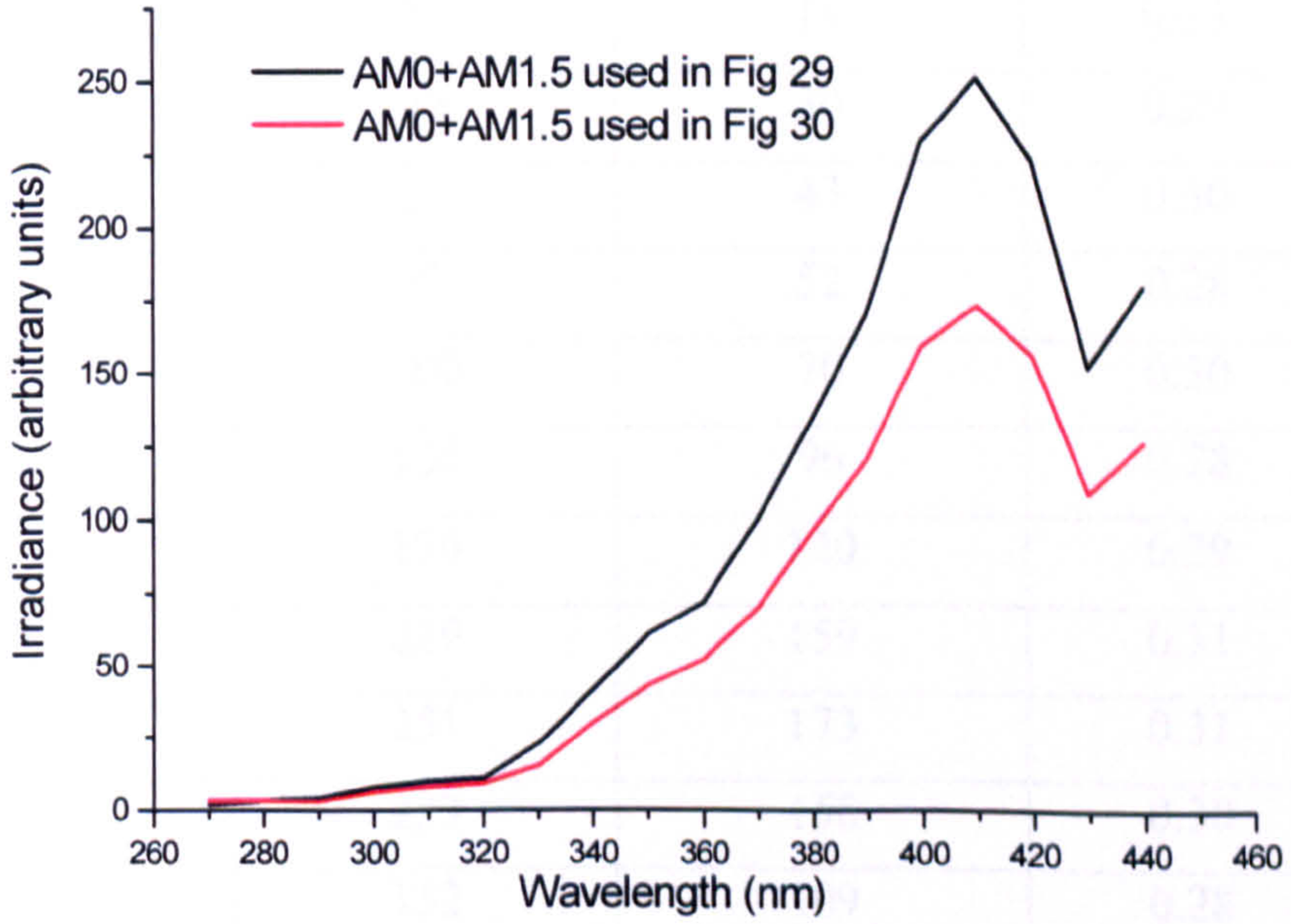

Figure 4-28 UV intensity changed by adjustment with AM0+AM1.5 optical filters (Oriel).

To explore further the effect of UV intensity, two different UV outputs were obtained by lamp adjustment. The black curve of Figure 4-28 (higher UV intensity) was used for the group experiments shown in Figure 4-29 and the red curve (lower UV intensity) was used for the group of experiments shown in Figure 4-30. Within measurement error, adjustment of UV intensity does not change the spectral distribution of the UV light and produces a proportional decrease or increase for all portions of the UV wavelength range (see table 4-8). For all experiments both AM0+AM1.5 filters were used and the sample was in the back position.

Table 4-8 A comparison of UV intensity changed by adjustments

Wavelength (nm)	UV Intensity (arbitrary) (black)	UV Intensity (arbitrary) (red)	Fractional Reduction
270	3	3	0
280	3	3	0
290	4	3	0.25
300	8	6	0.25
310	10	8	0.20
320	11	9	0.18
330	23	15	0.35
340	42	30	0.29
350	61	43	0.30
360	72	52	0.28
370	100	70	0.30
380	134	96	0.28
390	170	120	0.29
400	229	159	0.31
410	251	173	0.31
420	223	156	0.30
430	152	109	0.28
440	180	126	0.30

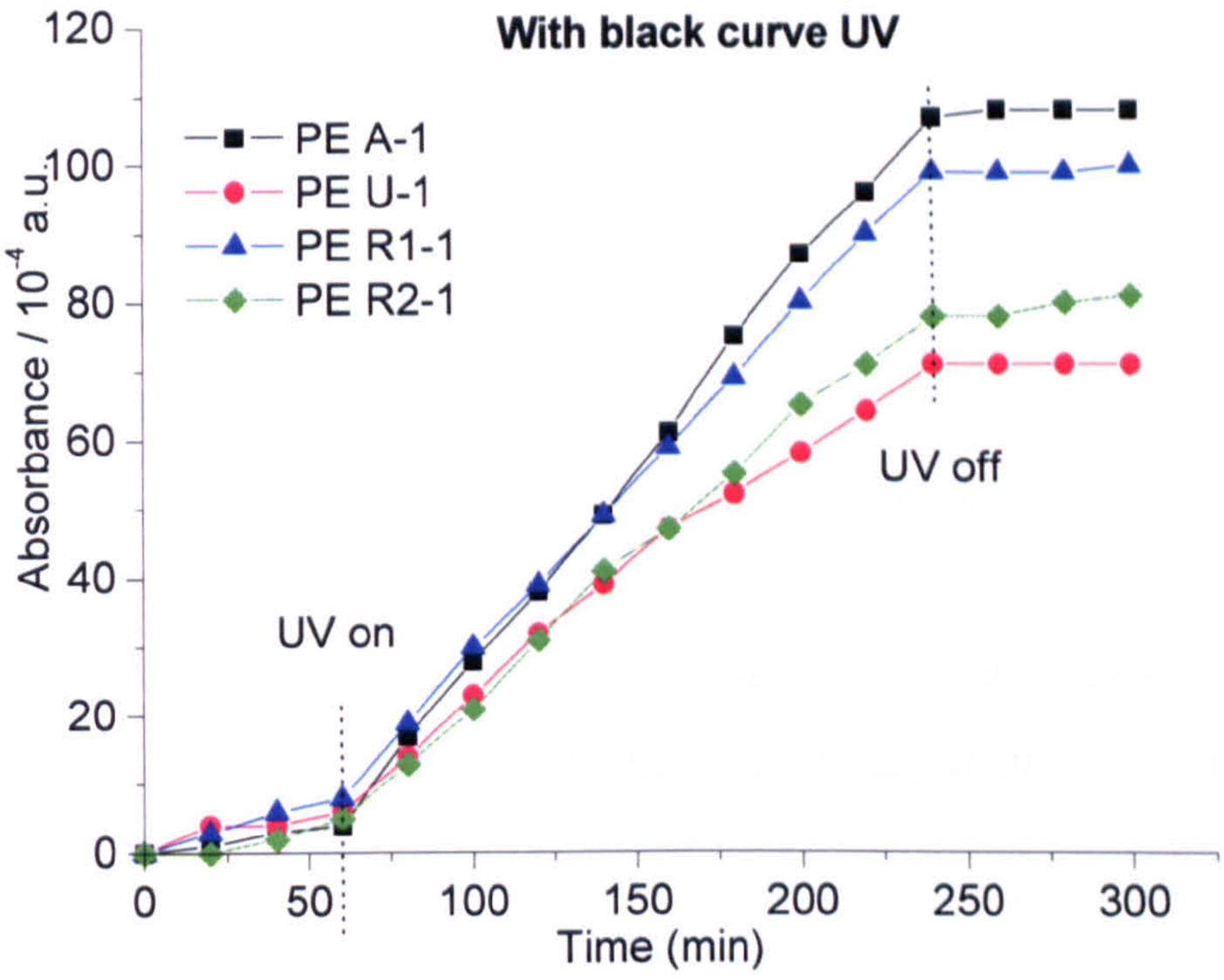

Figure 4-29 CO_2 evolution from the photo-oxidation of different PE films under irradiation defined by the black curve (high) UV of Fig 4-28.

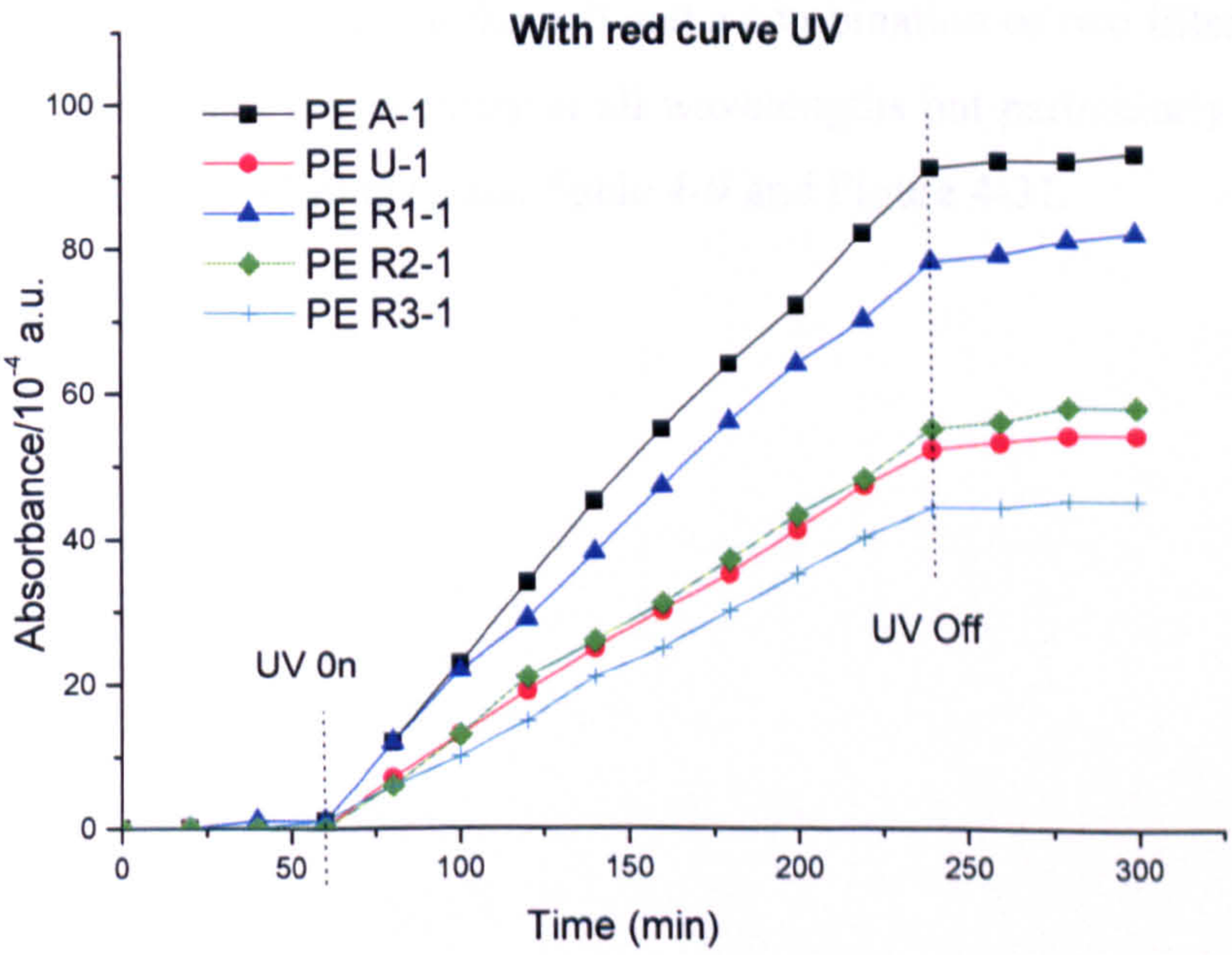

Figure 4-30 CO_2 evolution from the photo-oxidation of different PE films under irradiation defined by the red curve (low UV) of Fig 4-28.

Figure 4-29 and Figure 4-30 show the effect of UV light intensity change on the rate of CO_2 evolution for pigmented PE films and unpigmented PE film. The UV intensity for the two sets of measurements differed by ~ 4/3. It clearly demonstrates that the rate of CO_2 evolution decreases with UV intensity decrease. If in the TiO_2 pigmented PE films photoreaction follows the square root relationship with UV intensity and in unpigmented PE film CO_2 evolution is proportional to UV intensity, the unpigmented PE film would be more sensitive to UV intensity. However, with *ca.* 30 % UV intensity change, the rate of CO_2 evolution ranking is the same. In other words, the change in intensity within a relatively small range is not large enough to affect the relative ranking of CO_2 evolution for pigmented and unpigmented PE films.

4.5.3 Effect of the UV Wavelength

The effect of the Air-Mass Filter

To understand the dependence on incident UV wavelength of the photo-oxidation of the pigmented films, studies were carried out using the air-mass filters to change the distribution of UV output from the light pipe. In preliminary experiments the samples were placed in the back position in the cell and a combination of two filters was used. This combination reduces the intensity at all wavelengths but particularly reduces the shorter wavelengths (290-330 nm); see Table 4-9 and Figure 4-31.

Table 4-9 A comparison of UV Intensity with AM0, AM0+AM1.5 optical filter.

Wavelength (nm)	UV Intensity (arbitrary) (black with AM0)	UV Intensity (arbitrary) (red with AM0+AM1,5)	Fractional Reduction
270	6	0	1
280	3	0	1
290	5	2	0.60
300	13	9	0.31
310	30	11	0.63
320	51	18	0.65
330	72	35	0.51
340	100	69	0.31
350	116	99	0.15
360	133	114	0.14
370	175	162	0.07
380	259	217	0.16
390	340	276	0.19
400	430	363	0.16
410	433	399	0.08
420	392	353	0.08

The wavelength distribution cannot be changed without changing the intensity, but the results in the previous section suggest that the effect of intensity on relative performance of different samples is small.

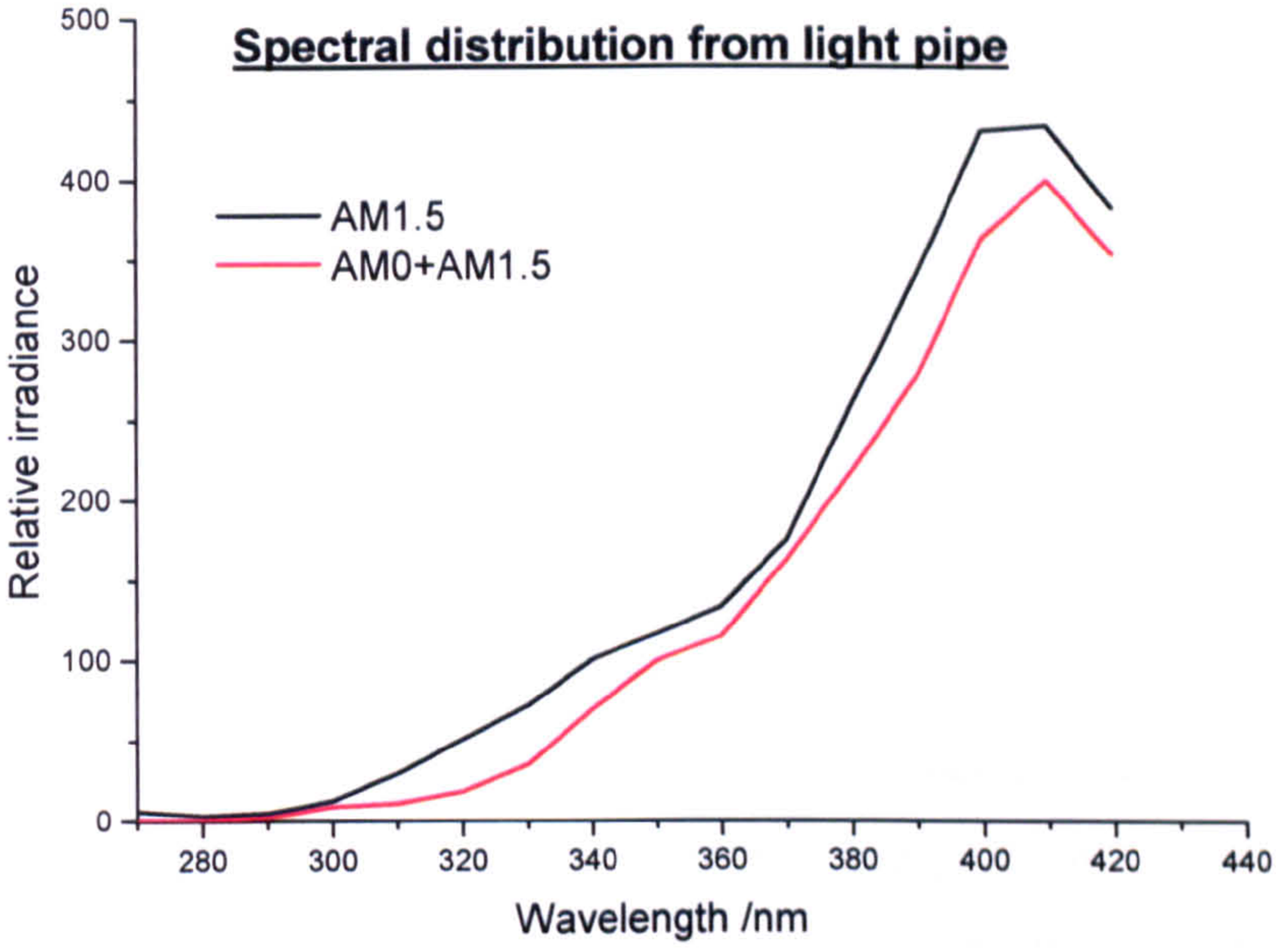

Figure 4-31 UV Intensity with AM0, AM0+AM1.5 optical filter

For the results shown in Figure 4-25, an AM1.5 filter was used. For the results shown in Figure 4-30 two filters (AM0+AM1.5) were combined. The combination of (AM0+AM1.5) changes the intensity especially at short (290-330) wavelengths, *i.e.* the AM0 filter by itself admits more irradiation in the UV range < 340 than when AM0 and AM1.5 are used in combination. The overall effect is to increase the rate of CO_2 evolution for all of the films when AM1.5 used only compared to AM0+AM1.5 used together. The main difference between Figure 4-25 and Figure 4-30 is that in Figure 4-25 the rate of CO_2 evolution is greater for PE U-1 than for any of the rutile-pigmented PE films. It suggests that removal of the shorter wavelengths caused changes in the ranking of the CO_2 evolution results. The photo-oxidation of unpigmented polymer was very much less when both filters were used to remove the last traces of short wavelength UV. This is because the unpigmented PE does not absorb the longer wavelength radiation (see section 3.2). Unpigmented PE film gave less CO_2 evolution than PE R1-1 and PE R2-1 with two filters. These results correspond to unpigmented PE absorbing shorter wavelength UV light. These results also show that neither the wavelength nor the intensity of UV light can be observed to affect the ranking of CO_2 evolution from TiO_2 pigmented PE films under UV irradiation. This can be explained by assuming that TiO_2 pigment can absorb most of

the UV light below 400 nm. The photocatalytic reaction is important and the reduced photochemical rate cannot cause the apparent change of CO_2 evolution in TiO_2 pigmented PE films. Therefore the activity sequence for both wavelength distributions, PE A-1 > PE R1-1 > PE R2-1 > PE R3-1, remains the same but with one filter (more short wavelength UV) the PE R2-1 appeared to be nearly as good as PE R3-1; with two filters the PE R2-1 is noticeably less good than PE R3-1.

In the most recent studies, the sensitivity of the method has been still further improved by moving the sample from the back position to one nearer to the UV light source at the front position, hence reducing the background signal. In these experiments different filters were used to select defined portions of the UV spectrum and the effect on carbon dioxide evolution rates were monitored. Figure 4-32 shows spectroradiometer results on the intensity and spectral distribution of UV falling on the cell with different filters, and relate to the experiments described next. Figure 4-33 to Figure 4-35 show the results for these three films (PE U-1, PE A-1 and PE R2-1), respectively.

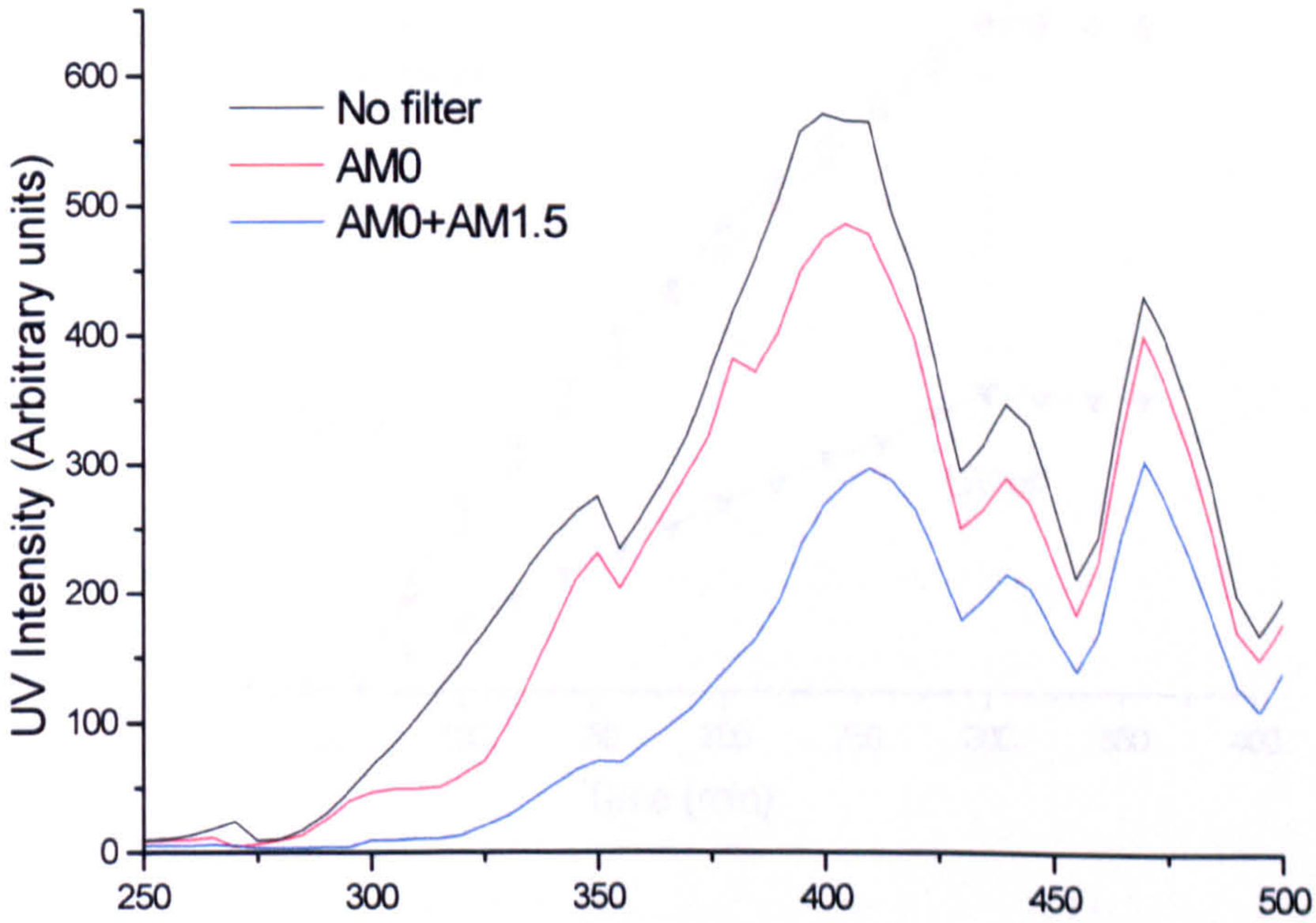

Figure 4-32 Spectroradiometer results for the intensity and spectral distribution of UV falling on the cell with different filter combinations.

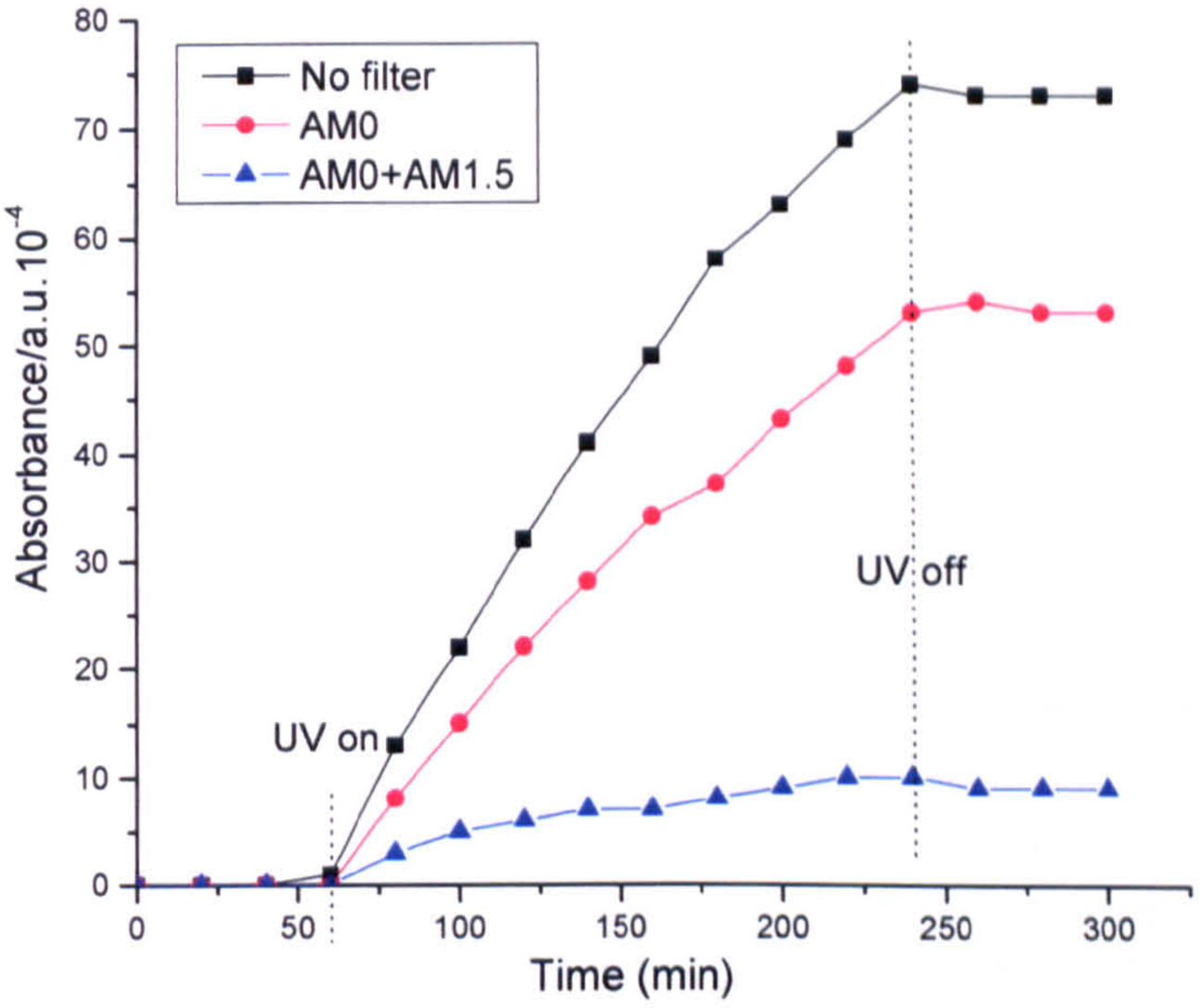

Figure 4-33 CO_2 evolution with different AM filter combinations comes from PE U-1. All the measurements were made with the samples in the front position.

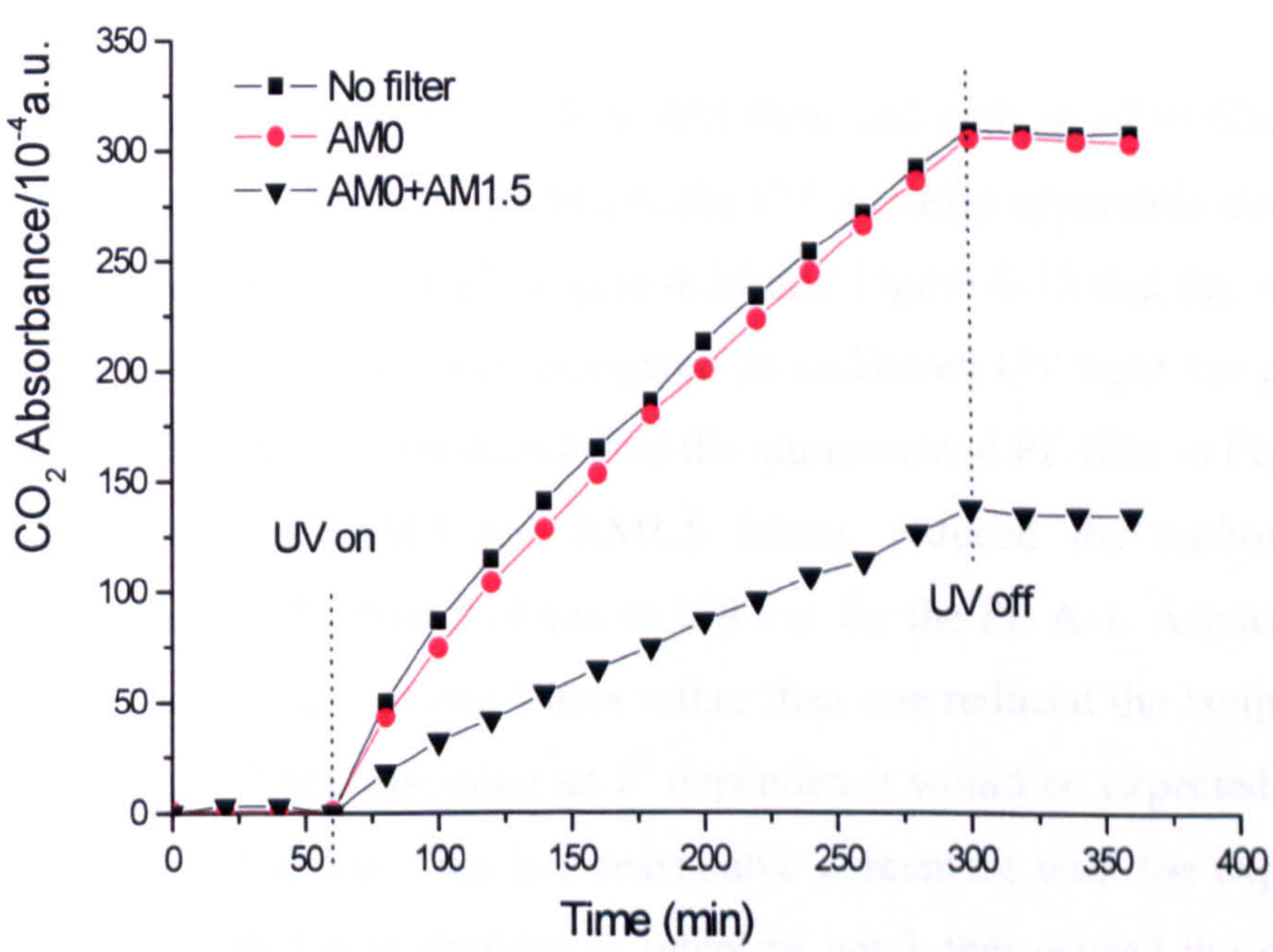

Figure 4-34 CO_2 evolution with different AM filter combinations comes from PE A-1. All the measurements were made with the samples in the front position.

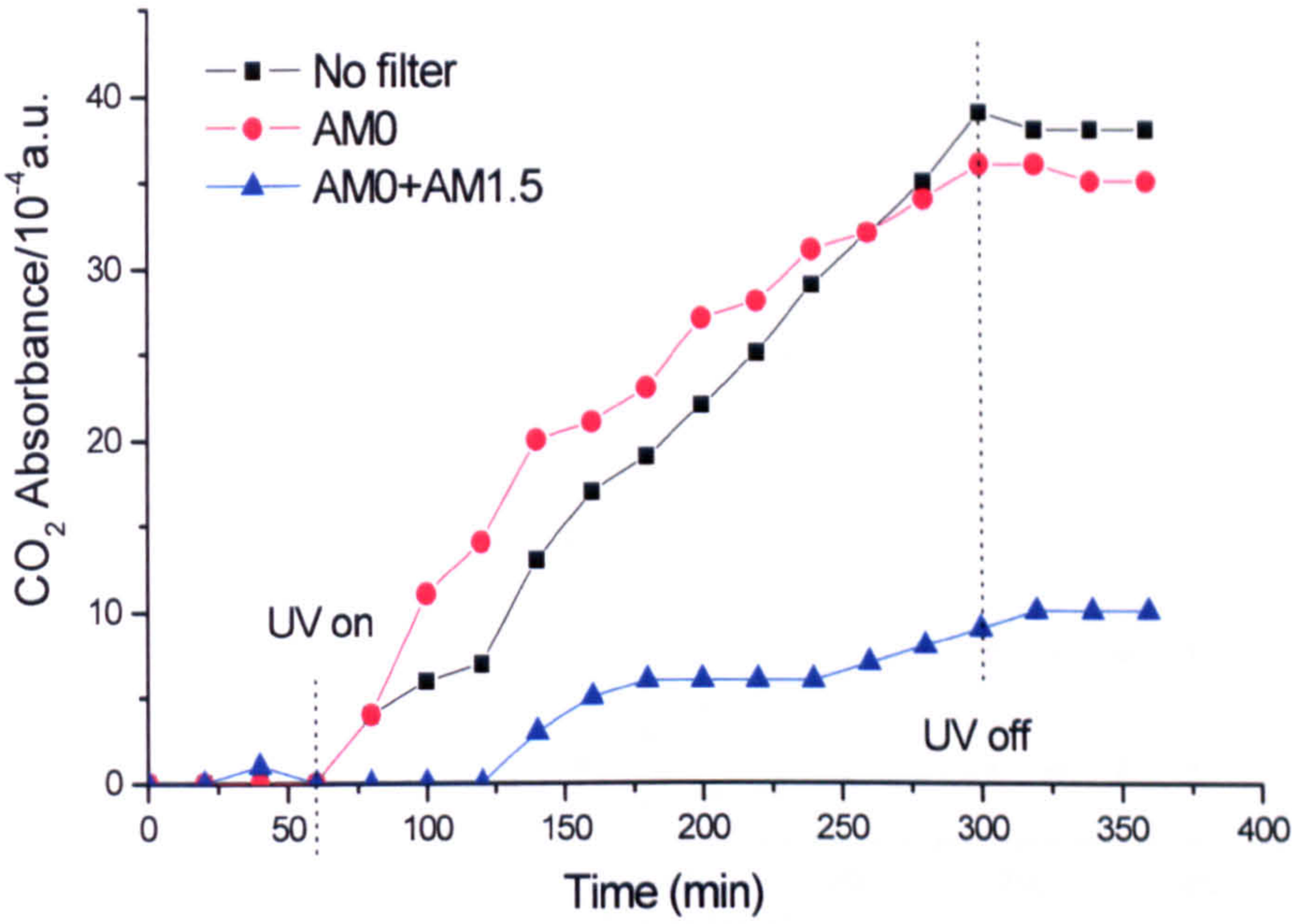

Figure 4-35 CO_2 evolution with different AM filter combinations comes from PE R2-1. All the measurements were made with the samples in the front position.

The UV intensity at 350 nm is 275 without AM filter and with an AM0 filter reduces to 230. With the AM0+AM1.5 combination, the UV intensity apparently decreases to 67. It can be seen from Figure 4-33, Figure 4-34 and Figure 4-35 that the AM0 filter hardly affected CO_2 evolution when compared to unfiltered UV light for pigmented PE films, whereas the AM0 filter does affect the unpigmented PE film in Figure 4-33. The combination of the AM0 and AM1.5 filters, reduced the carbon dioxide generation more than 55 % from 309 a.u. to 138 a.u. for the PE A-1. Anatase absorbs below 385 nm. Thus the use of two filters rather than one reduced the lamp output at 350 nm from 275 to 67 and assuming an $I^{½}$ dependence would be expected to reduce the rate from 309 to 152 a.u. This is a reasonable agreement with the experimental result. This suggests that it is changes in intensity not λ that caused the difference. With AM0 +AM1.5 filters combination and samples in the front position, near-background-level carbon dioxide evolution was observed for PE R2-1. It suggests that with both anatase and rutile pigmented PE film, CO_2 evolution is sensitive to the UV intensity change, but are less sensitive to short wavelength UV light. Unpigmented PE film is more sensitive to short wavelengths than TiO_2 pigmented films.

4.5.4 The effect of Air-Mass filters on PE A-1, PE U-1 and PE R2-1

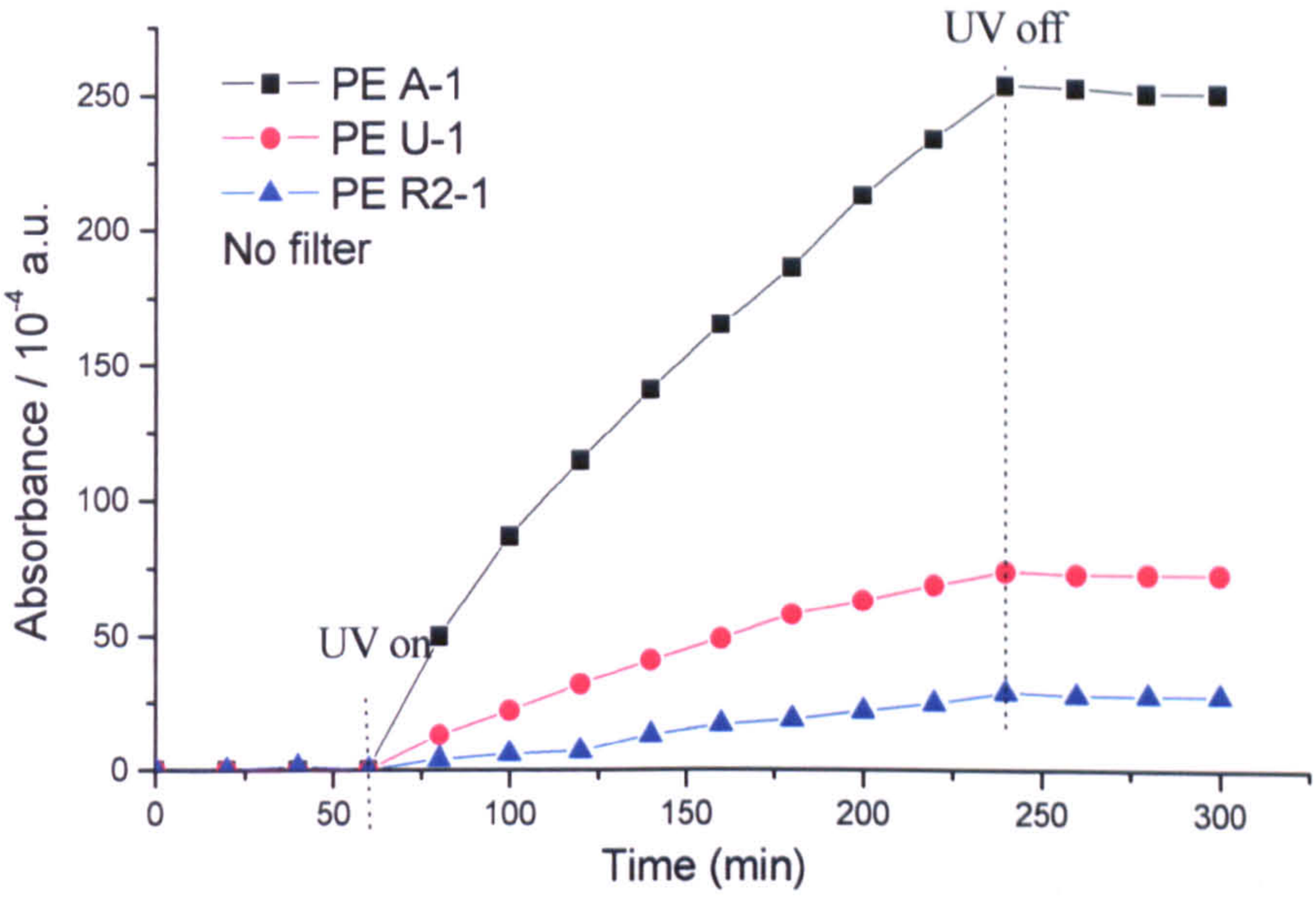

Figure 4-36 CO_2 evolution with no AM filters for PE A-1, PE U-1 and PE R2-1. All the measurements were made with the samples in the front position.

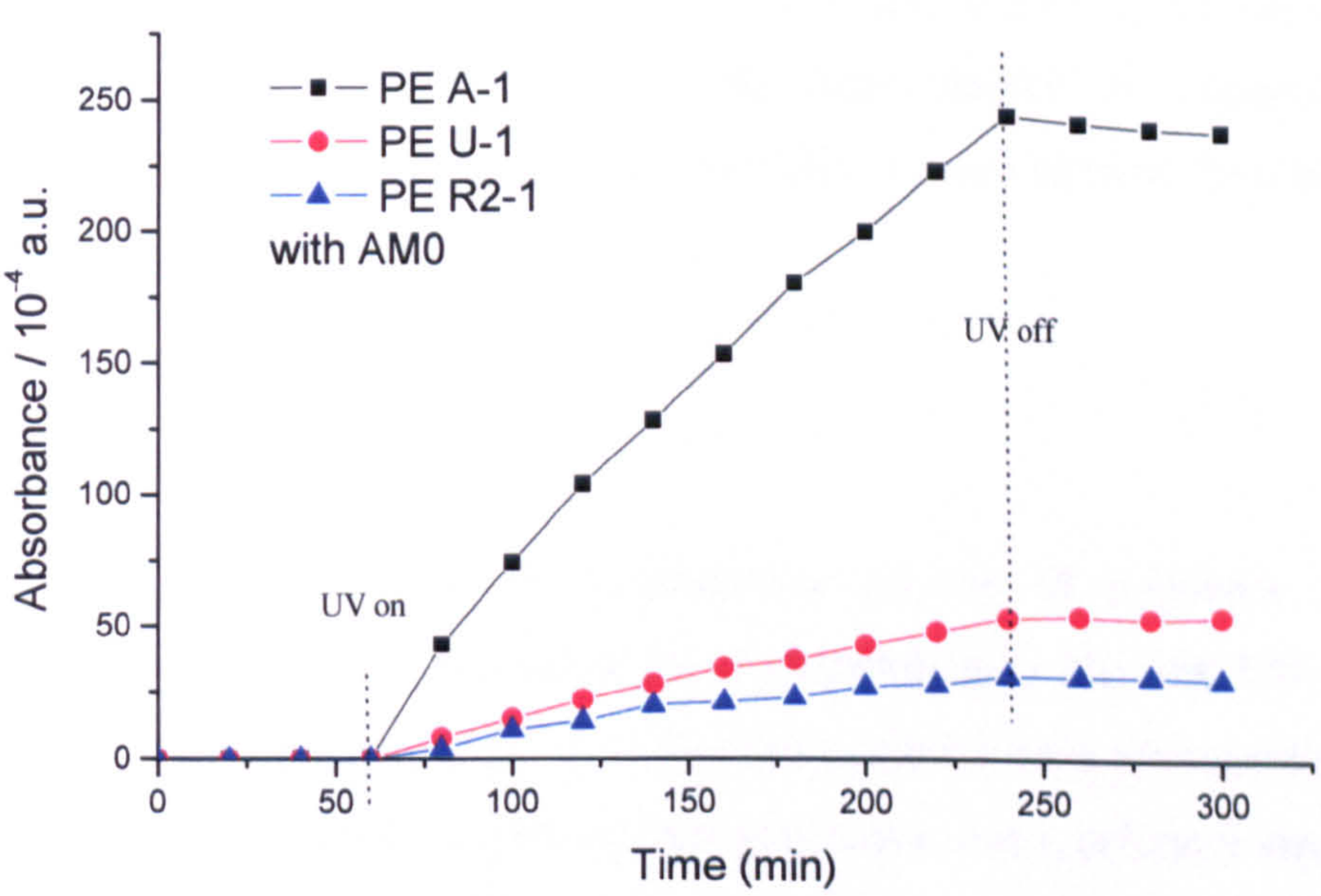

Figure 4-37 CO_2 evolution with AM0 filters for PE A-1, PE U-1 and PE R2-1. All the measurements were made with the samples in the front position.

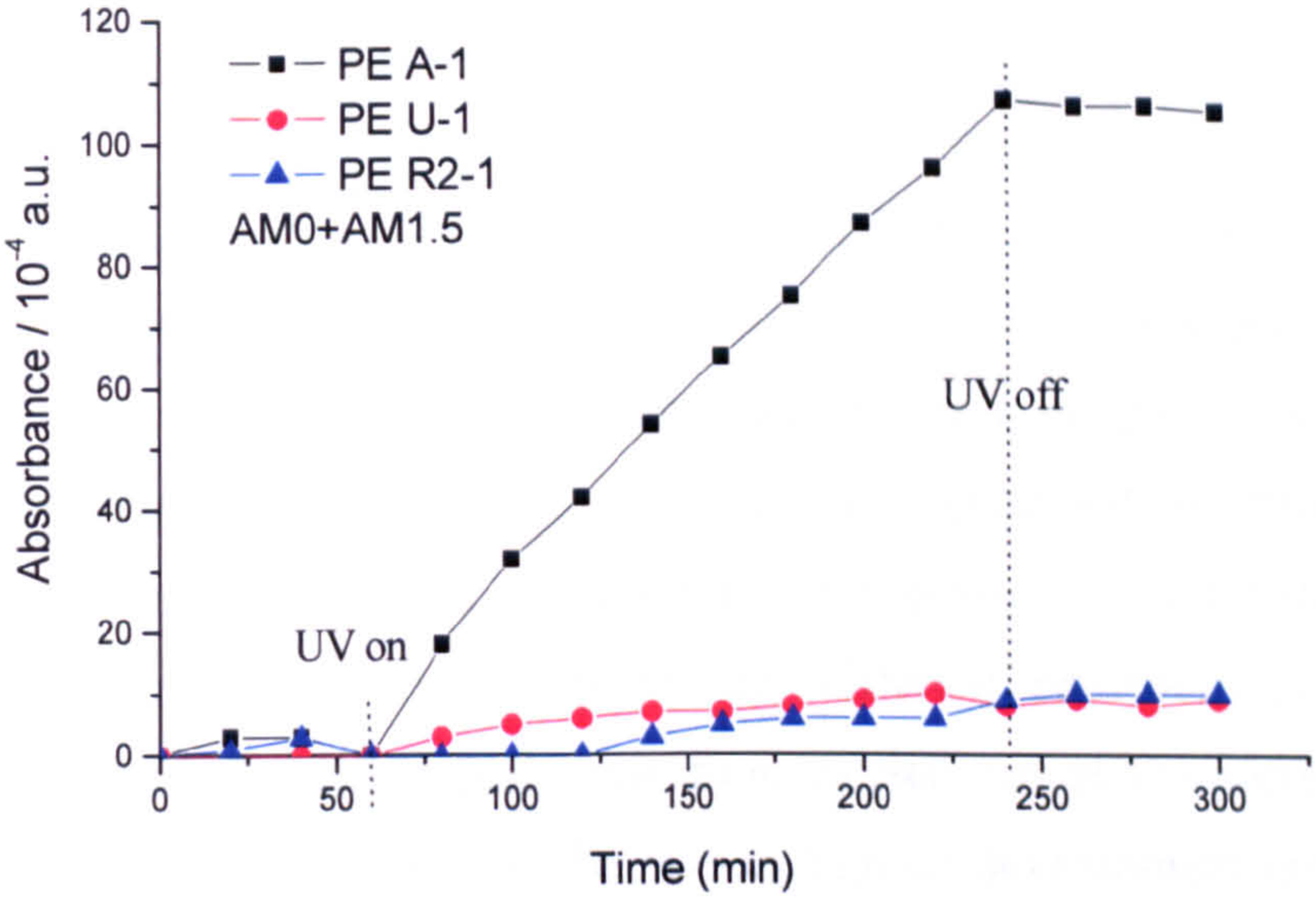

Figure 4-38 CO_2 evolution with AM0+AM1.5 filters for PE A-1, PE U-1 and PE R2-1. All the measurements were made with the samples in the front position.

It can be seen from Figures 4-36 to Figure 4-38 that PE A-1 gave significantly higher CO_2 emission than either unpigmented polyethylene film or PE R2-1at any condition. With AM0 filtered UV light, CO_2 evolution decreased quickly for unpigmented PE film. If AM0 and AM1.5 filters were used together in experiments, they killed CO_2 evolution for unpigmented and PE R2-1 films.

4.6 DISCUSSION

The role of TiO_2 pigments in the degradation process of polymers has been investigated well [9, 11-16]. TiO_2 can act predominantly as a physical UV absorber, and then protects polymer materials, or it may act primarily as a photocatalyst that is activated by UV in combination with oxygen and water and accelerates degradation. Which of these effects predominates depends on the TiO_2 crystalline structure and on TiO_2 surface modification. In this study, the TiO_2 pigments used included anatase and rutiles with different surface treatments. Anatase pigmented polyethylene gave significantly higher CO_2 emission than unpigmented PE. The rutile-pigmented PEs either gave less CO_2 emission or more emission than unpigmented PE, according to

the surface treatment. The ranking of the pigments as protectants or pro-degradants coincided with that expected from much more time-consuming laboratory testing.

It can be concluded from the results in section 4.2 that CO_2 evolution from pigmented PE film can be measured using *in-situ* FTIR spectroscopy with a good degree of accuracy. As expected, the anatase-pigmented polyethylene sample showed a higher photoactivity in terms of CO_2 evolution than the rutile-pigmented polyethylene films, consistent with the known higher photoactivity of anatase. It is clear that the CO_2 method is sufficiently sensitive to detect the different photoactivities of rutile pigmented PE films. Parallel experiments were carried out at the same time with samples of the same film assessed by the carbonyl group development method, using the growth of the IR absorption bands for >C=O around 1712 cm^{-1}. The key conclusion is that the results obtained by the CO_2 method were consistent with the carbonyl method.

The CO_2 method measures the consequence of reaction occurring at the very beginning of the photodegradation of samples; the conventional method of carbonyl group method needs time to build up a measurable signal. Therefore, it would not be surprising to observe a difference in the results obtained by these two methods. The CO_2 evolution experiments show the rate of CO_2 evolution keeping reasonable constant in the course of the experiments. For experiments relevant to carbonyl group development with the same samples, the photooxidation rates of TiO_2 pigmented or unpigmented polyethylene films, carbonyl formation was found to be consistent with an autocatalytic reaction mechanism. The CO_2 evolution rates from sample pigmented with different grades of TiO_2 have highlighted the excellent correlation with the conventional carbonyl group method.

From section 2.5.7, in a typical experiment with unpigmented PE, the CO_2 evolution was 60×10^{-4} a.u. in three hours UV irradiation with an AM1.5 filter. This is equivalent to $0.48\mu g \times 60 = 28.8\ \mu g = 2.88 \times 10^{-5}$ g carbon dioxide emission from the photodegradation. The 2.88×10^{-5} g CO_2 includes 2.88×10^{-5} g $\times$ 12/44 = 0.785×10^{-5} g carbon atoms. It is equal to 0.785×10^{-5} g $\times$14/12 = 0.916×10^{-5} g CH_2 units of PE. The effective weight of the sample was ~11 mg *i.e.* 0.011 g. So the film thickness lost

is about 0.916×10^{-5} g × 100μm/0.011g = 0.08 μm during three hours irradiation. This compares with the pigment crystal diameter of ~ 0.2 μm. At least 3 × 100/0.08 = 3750 hours *i.e.* ~ 156 days would be needed to destroy all the film under the UV light used in experiment.

In the experiments reported here, the FTIR gas-phase technique employed a filtered xenon source and the carbonyl method used fluorescent tubes as UV source which may account for some of detailed differences in the observation. TiO_2 pigmented PE films are not sensitive to variations in short UV light, different UV distributions have little effect on rank position. The rank position for unpigmented PE film changes with the UV distribution. Their CO_2 evolution rates depended on the different filter combinations because unpigmented PE film is more sensitive to shorter UV wavelengths.

In the most recent studies, the sensitivity of the method has been still further improved by reducing the background signal by moving the sample nearer to the UV light port at the front of the cell. With this improvement, the observed rate of CO_2 emission for the anatase-pigmented polyethylene was enhanced much more than for the rutile-pigmented polyethylene and unpigmented polyethylene films.

It is evident from these studies that the CO_2 method could be used to study the influence of different atmospheres. The rate of CO_2 emission was found to increase both with humidity and with the oxygen concentration. The results in Figure 4-20 show the evolution of carbon dioxide observed after 3 hours irradiation as the function of the water vapour band intensity near 1557 cm^{-1} in the IR cell measured prior to irradiation. Even though the CO_2 evolution for both anatase pigmented and rutile pigmented PE films increased with humidity, the anatase pigmented PE film had more sensitivity to humidity than rutile pigmented PE films. This can be explained in terms of mechanism of PCD *i.e.* the primary oxidant ($OH^{\bullet}$) is produced by reaction of a hole (h^{+}) with adsorbed water on the TiO_2 surface hence affects the photodegradation. The same phenomenon was observed for the influence of oxygen concentration on the CO_2 evolution from them. These results are consistent with the known mechanism of TiO_2 semiconductor photocatalytic reaction in which the highly

oxidizing $OH^{\bullet}$ species are generated either by reaction of photo-produced holes with hydroxyl anions on the pigment surface, or with adsorbed water molecules [17]. The effect of oxygen concentration on CO_2 evolution is attributed either to (i) the formation of an oxygen radical anion by electron transfer from photoexcited TiO_2 to molecular oxygen to form singlet oxygen which then attacks any unsaturation in the polymer [17]; or to (ii) dissolved oxygen suppressing electron-hole recombination [18] through the scavenging of the photogenerated electron in the conduction band by adsorbed oxygen, generating the superoxide species $O_2^{\bullet-}$. The superoxide is highly active and can attack the organic molecules. The clear and important conclusion is that determination of the relative photo-activity of anatase and rutile based polymer must be made at constant humidity and oxygen content.

The linear dependence between the rate of CO_2 evolution and the square root incident light intensity was observed only for anatase pigmented PE film. For unpigmented PE film, the rate of photodegradation was directly proportional to the incident light intensity, as was reported in Chapter 3. For the anatase pigmented PE the dominant reaction should be the photocatalysis reaction. The square root dependence is exactly what would be expected from a process in which recombination of the photo-generated electron-hole (e^{-}-h^{+}) pair is the controlling step in the mechanism. This suggests that the mechanism of TiO_2 pigmented PE photodegradation relies on strongly catalysed activity, as suggested by Egerton and King [10]. The influence of light intensity on photocatalytic TiO_2 pigmented systems should follow the square root rule as observed here for anatase-pigmented PE. From the studies of CO_2 evolution using wavelength distributions modified by AM filters combination it can be seen that the degradation of the unpigmented PE film is more sensitive than the pigmented PE films to changes in the wavelength distribution. Pigmented PE films appear to be relatively insensitive to changes in the distribution of the UV wavelength.

4.7 CONCLUSIONS

The results in this chapter demonstrate that the CO_2 gas-phase method is versatile and permits fairly rapid assessment of the relative photo-degradability of pigmented

polyethylenes. It is shown that using an *in-situ* FTIR technique in order to obtain real-time reproducible information on the photodegradation of plastic films over relatively short irradiation periods is viable. The advantages this method has over other accelerated weathering tests is the extremely rapid results it can provide, < 10 hours when compared to over a thousand hours for a conventional test based on carbonyl group measurement. The results obtained with a series of polyethylenes prepared with different TiO_2 pigments showed that anatase is a pro-degradant whereas some rutiles can be protective and some pro-degradative. The more important thing is that the results gained by the CO_2 method are consistent with the results obtained by the conventional carbonyl group development method. This is particularly valuable, giving confidence in the CO_2 method, allowing it to be adapted from paint systems to plastic systems. It is relatively easy to assess the effect of changing the spectral distribution in the UV illumination source and of changing the atmosphere in the cell (humidity, oxygen content *etc*). Changing the spectral distribution of the irradiating UV can alter the ranking of the pigments and in some cases was found to change the effect of including a pigment from protective to pro-degradative.

4.8 REFERENCES

1. Kemp, T.J. and R.A. McIntyre, *Progress in Reaction Kinetics and Mechanism,* 2002. **26**(4): p. 337-374.
2. Giesse, R. and M.A. Depaoli, *Polymer Degradation and Stability,* 1988. **21**(2): p. 181-187.
3. Gulmine, J.V., P.R. Janissek, H.M. Heise, and L. Akcelrud, *Polymer Testing,* 2002. **21**(5): p. 557-563.
4. Gulmine, J.V., P.R. Janissek, H.M. Heise, and L. Akcelrud, *Polymer Degradation and Stability,* 2003. **79**(3): p. 385-397.
5. Valadez-Gonzalez, A., J.M. Cervantes-Uc, and L. Veleva, *Polymer Degradation and Stability,* 1999. **63**(2): p. 253-260.
6. Gijsman, P. and A. Dozeman, *Polymer Degradation and Stability,* 1996. **53**: p. 45-50.
7. Christensen, P.A., T.A. Egerton, E.J. Lawson, and J. Temperley, *Journal of Materials Science,* 2002. **37**(17): p. 3667-3673.
8. Dilks, A., *Pure and Applied Studies of the Photodegradation of Titanium Dioxide Pigmented Paint Films*, in *Chemistry*. 1999, *Newcastle upon Tyne*: Newcastle upon Tyne.
9. Christensen, P.A., A. Dilks, T.A. Egerton, and J. Temperley, *Journal of Materials Science,* 2000. **35**(21): p. 5353-5358.
10. Egerton, T.A. and C.J. King, *Journal of the Oil & Colour Chemists Association,* 1979. **62**: p. 386-390.

11. Allen, N.S., H. Khatami, and F. Thompson, *European Polymer Journal,* 1992. **28**(7): p. 817-822.
12. Allen, N.S. and H. Khatami, *Abstracts of Papers of the American Chemical Society,* 1993. **206**(Pt2): p. 182-POLY.
13. Gesenhues, U., *Polymer Degradation and Stability,* 2000. **68**(2): p. 185-196.
14. Christensen, P.A., A. Dilks, T.A. Egerton, and J. Temperley, *Journal of Materials Science,* 1999. **34**(23): p. 5689-5700.
15. Christensen, P.A., A. Dilks, T.A. Egerton, and E.J. Lawson, *Journal of Materials Science,* 2002. **37**: p. 1-9.
16. Christensen, P.A., A. Dilks, T.A. Egerton, E.J. Lawson, and J. Temperley, *Journal of Materials Science,* 2002. **37**(22): p. 4879-4887.
17. Allen, N.S., M. Edge, T. Corrales, A. Childs, C.M. Liauw, F. Catalina, C. Peinado, A. Minihan, and D. Aldcroft, *Polymer Degradation and Stability,* 1998. **61**(2): p. 183-199.
18. Mills, A. and S. LeHunte, *Journal of Photochemistry and Photobiology a-Chemistry,* 1997. **108**(1): p. 1-35.

CHAPTER 5

EFFECT OF STRESS ON PHOTODEGRADATION OF PE

5.1 INTRODUCTION

It is well known that stress accelerates the photo-oxidative degradation of polymers [1, 2]. In the book by Davis and Sims [3] it is suggested that polymers are likely to fail more rapidly if weathered under load, but it does not refer to any quantitative studies of this effect. Benachour and Rogers [2] reported that the photodegradation of low density polyethylene films is greatly accelerated by uniaxial elongation, and the acceleration process is closely related to the morphological changes induced upon drawing of the polymer films. However, despite intensive investigations separately on both photooxidation and deformation of polymers, very little work has been done to determine how deformation affects TiO_2 pigmented polyethylene films photodegradation. The focus of the research described in this chapter has been the development of a special test for the assessment of the effects of strain on photodegradation and its application to study the effect of anisotropy on a series of polyethylene samples containing different TiO_2 pigments.

Polymers that have been subjected to thermo-mechanical processing almost always possess anisotropy. Most articles that have been produced by injection moulding, blow moulding or extrusion have quite different mechanical properties in the machine direction and in the transverse to flow direction. The effect of the tensile stress was to accelerate oxidation. Tensile stress was also found to alter the rate of photo-oxidation in polypropylene by Baumhardt-Neto and De Paoli [4, 5] and by O'Donnell and White [6]. The application of tensile stress generally accelerates oxidation but Baumhardt-Neto and De Paoli claimed that in some circumstances the opposite might happen. Although it was observed that there is probably an effect of anisotropy on degradation rate, the exact relationship was not determined, and explanations remain speculative [2, 7].

The studies described in this chapter used carbonyl index measurements to follow photo-oxidation and the effect on the photo-degradation rate of oriented polyethylene

of applying a tensile stress was investigated. The effect of applying the stress parallel to the longitudinal direction was compared to that observed when the stress was applied in the transverse direction. The oxidation at different depths within multi-layers has been investigated.

5.2 TENSILE TESTING

In order to investigate the difference between longitudinal and transverse tensile properties, the tensile experiments were carried out. In each test on the unexposed materials the specimen displayed extensive drawing. In all cases there was a very well defined yield point, sometimes followed by a yield drop. Although the load-deformation characteristics for a particular type of specimen did not superimpose exactly, there was a significant type-to-type variation and the stress at yield has been taken to characterize anisotropy. The values obtained are recorded in Table 5-1. It is evident that the samples all displayed a higher yield stress when tested in the machine (longitudinal) direction. The yield stress in the machine direction was typically 10 % higher than that in the transverse direction.

Table 5-1 Yield stress in tensile tests (MPa)

	Longitudinal	Transverse
PE U-1	10.6 ±0.6	9.5 ± 1.4
PE A-1	9.4 ± 1.2	8.8 ± 1.2
PE R1-1	9.3 ± 0.9	8.5 ± 1.5
PE R2-1	9.0 ± 1.2	8.4 ± 1.4
PE R3-1	10.0 ± 1.2	9.1 ± 1.4
PE R4-1	10.6 ± 0.3	9.1 ± 1.3

5.3 INFRARED SPECTRA—GENERAL APPEARANCE

The carbonyl group centred at 1712 cm^{-1} was used to monitor the photooxidation of PE film. Typical FTIR spectra are shown in Figure 5-1. The carbonyl group absorbance was absent from unexposed samples; it is quite different for the different

materials tested and it increased with exposure. Since the TiO_2 pigment does not affect the type of spectrum under this loading, it is a convenient measure of relative oxidation of the different materials.

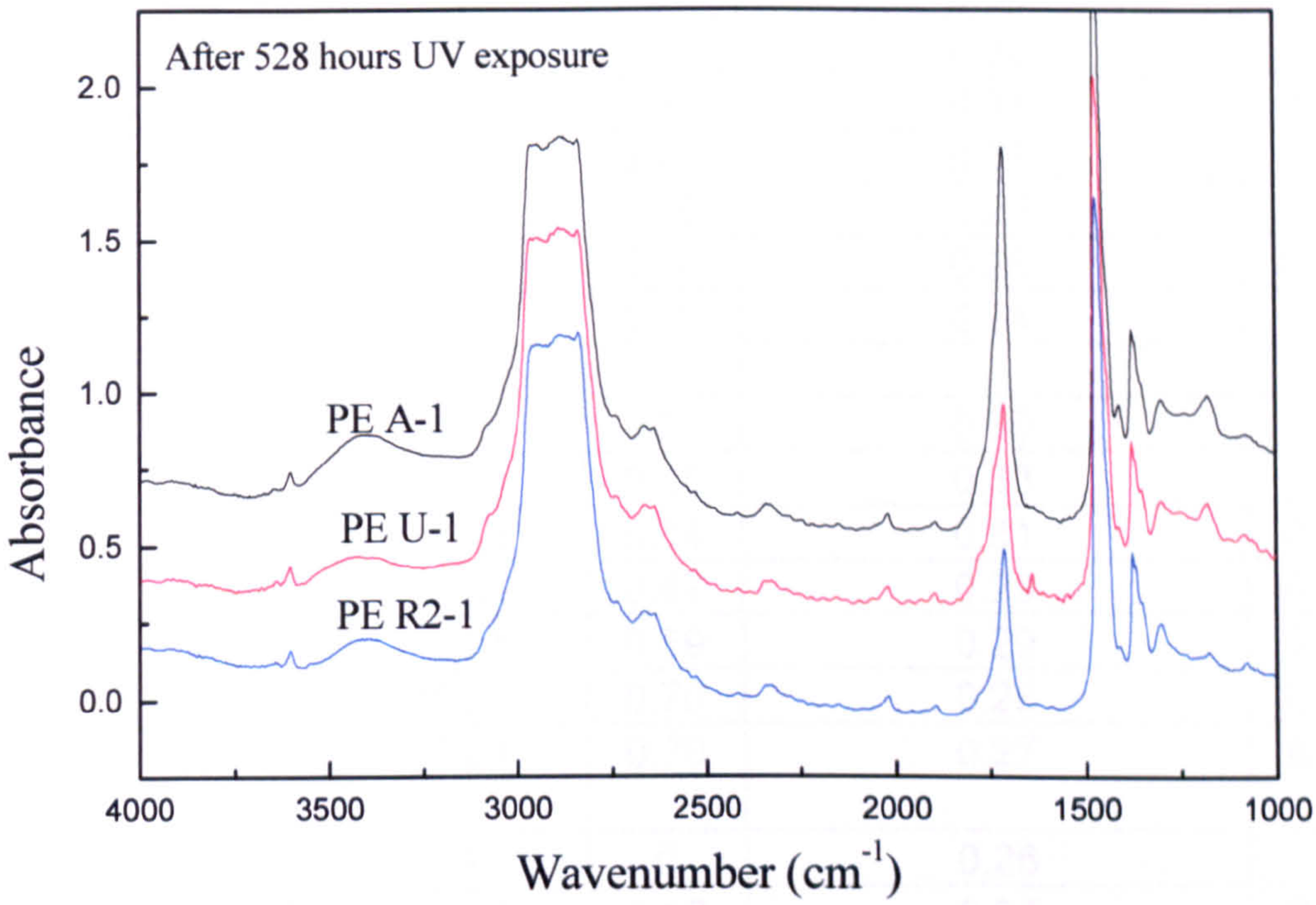

Figure 5-1 FTIR spectra for PE U-1, PE A-1 and PE R2-1 after 528 h UV exposure, showing the carbonyl band in the range 1700–1760 cm^{-1} used for the assessment of the progress of oxidation. This band was absent prior to UV exposure.

5.4 ABSORPTION IN STRAINED SAMPLES

According to the Beer-Lambert law, for the thin samples the intensity in a transmission IR absorption band will be proportional to the thickness (h) as long as the absorbing group is homogeneously distributed. For samples strained in uniaxial tension, the thickness decreases according to the equation $h = h_0(1-\nu\varepsilon)$, where h_0 is the unstrained thickness, ν is Poisson's ratio (is the ratio of transverse contraction strain to longitudinal extension strain in the direction of stretching force) and ε is the applied strain. If ε is taken to be the true strain ($= ln\ (l/l_0)$ where l is the extended length and l_0 is the unstrained length) this relationship is expected to hold for quite high strains and

a plot of (h/h_0) versus $ln(l/l_0)$ should be linear, with gradient (-ν). Table 5-2 is a summary of the effect of elongation effect on the thickness for PE U-1, PE A-1 and PE R2-1 samples.

Table 5-2 The calculation results of ε and h/h_0 for PE U-1, PE A-1 and PE R2-1

Sample	Elongation/mm	l/l_0=24.7mm	$\varepsilon=lnl/l_0$	Absorbance@1377 cm^{-1}	h/h_0
PE U-1	0	1	0	0.34	1
	5	1.20	0.18	0.33	0.98
	10	1.40	0.34	0.31	0.91
	15	1.61	0.47	0.31	0.89
	20	1.81	0.59	0.29	0.85
	25	2.01	0.70	0.26	0.76
	30	2.21	0.80	0.24	0.71
PE A-1	0	1	0	0.35	1
	5	1.20	0.18	0.33	0.95
	10	1.40	0.34	0.31	0.89
	15	1.61	0.47	0.29	0.84
	20	1.81	0.59	0.29	0.84
	25	2.01	0.70	0.28	0.79
	30	2.21	0.79	0.27	0.77
PE R2-1	0	1	0	0.26	1
	5	1.20	0.18	0.24	0.94
	10	1.40	0.34	0.24	0.93
	15	1.61	0.47	0.23	0.88
	20	1.81	0.59	0.21	0.83
	25	2.01	0.70	0.20	0.79
	30	2.21	0.80	0.20	0.77

Figure 5-2 shows this linear relationship for the IR band at 1377 cm^{-1} for samples PE U-1, PE A-1 and PE R2-1. The plots are acceptably linear and the corresponding values for Poisson's ratios (gradient in fit line equation) are 0.36 (PE U-1), 0.29 (PE A-1), and 0.29 (PE R2-1). Unpigmented PE films have Poisson's ratios around 0.4 and pigmented PE films have smaller values that depend on the volume fraction of pigment [8]. In the materials under investigation, the volume fraction of the filler was ~1 %. The values obtained were, therefore, of the correct order and ranking but were slightly smaller than expected. This is probably because, for the strip samples used, the strain was not exactly uniaxial because of constraints in the grips. Somewhat

higher values for Poisson's ratio were indicated when the same analysis was applied to the IR peak centred at 1304 cm^{-1} though this peak is less intense than the band at 1377 cm^{-1} and the results were more scattered.

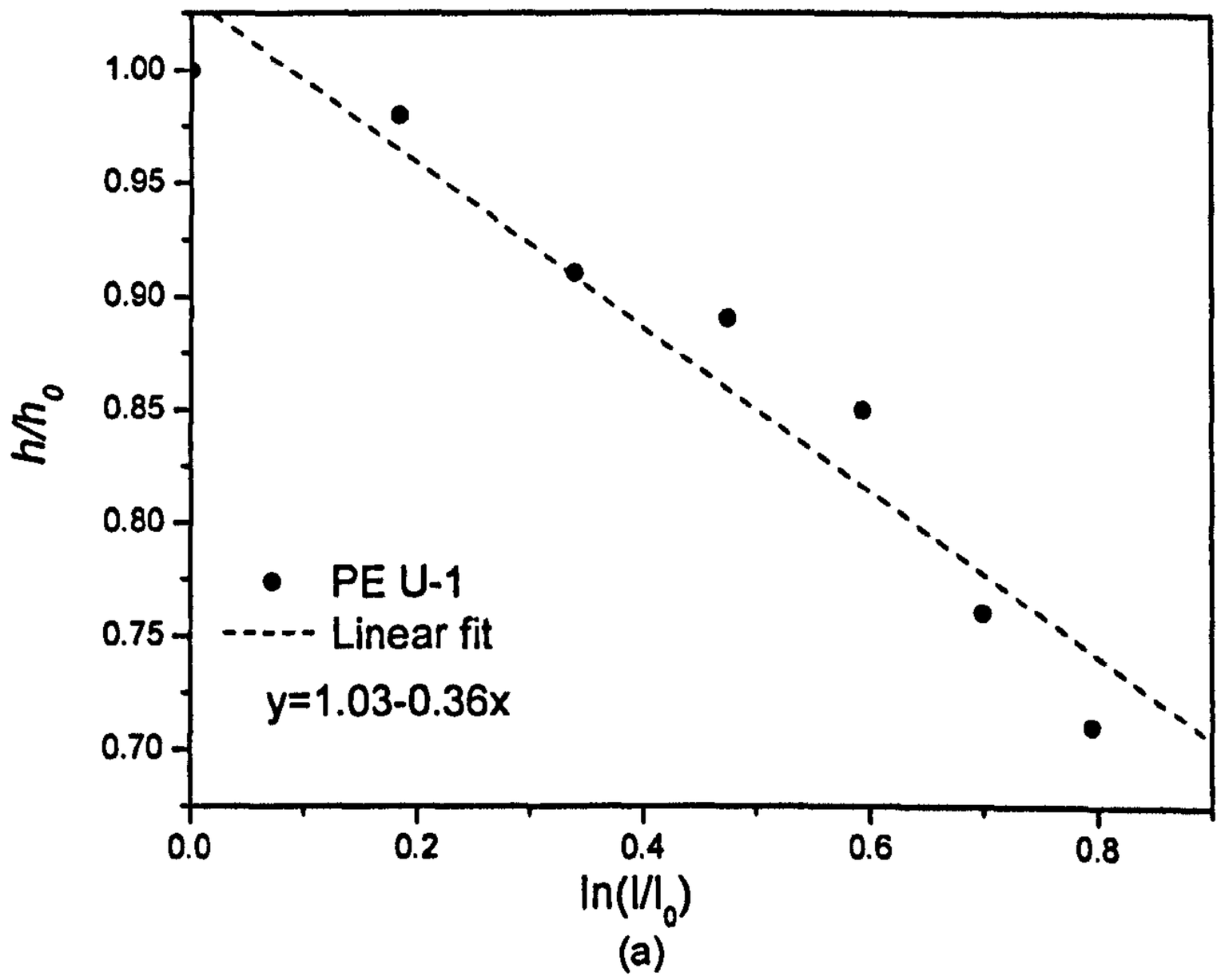

(a)

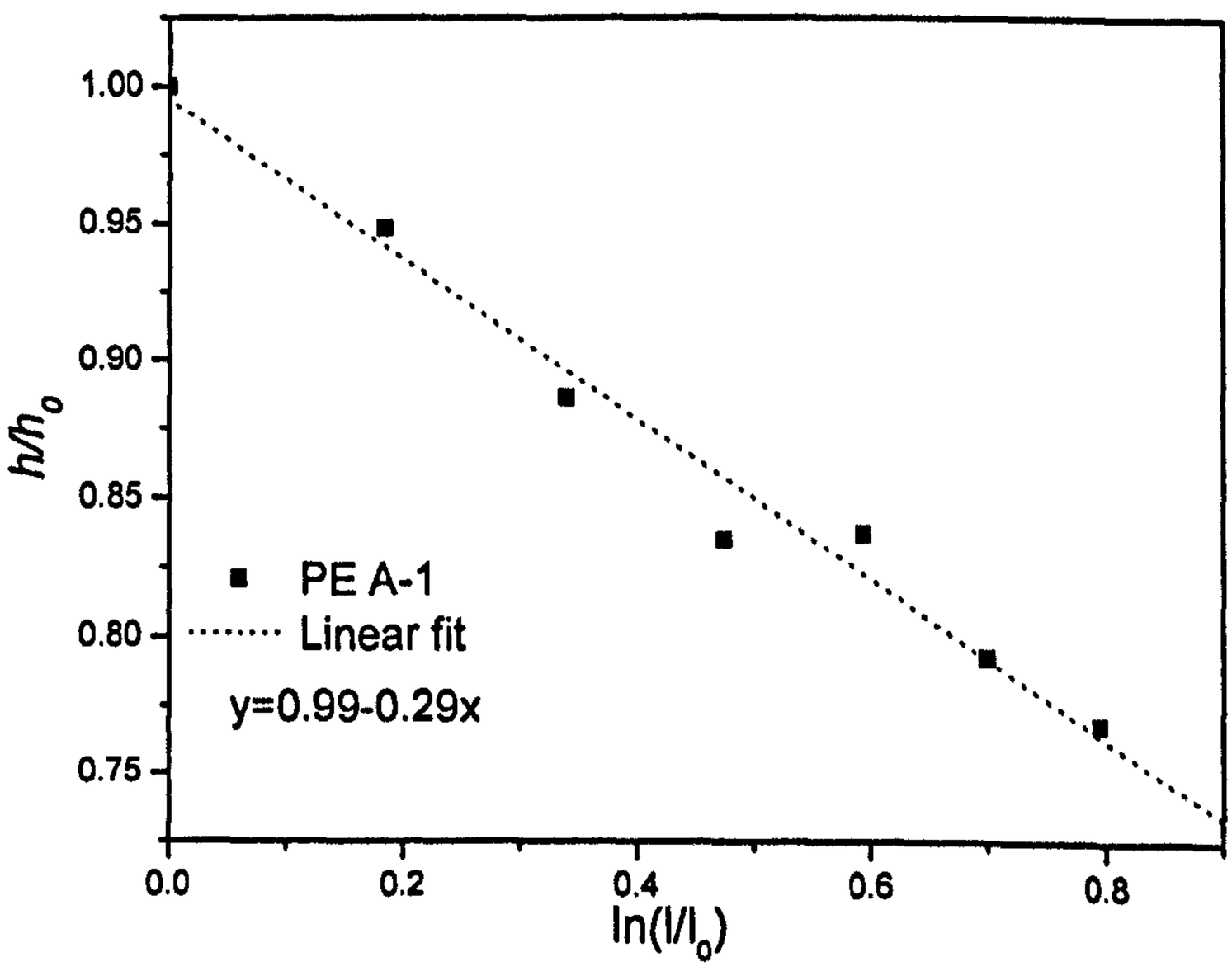

(b)

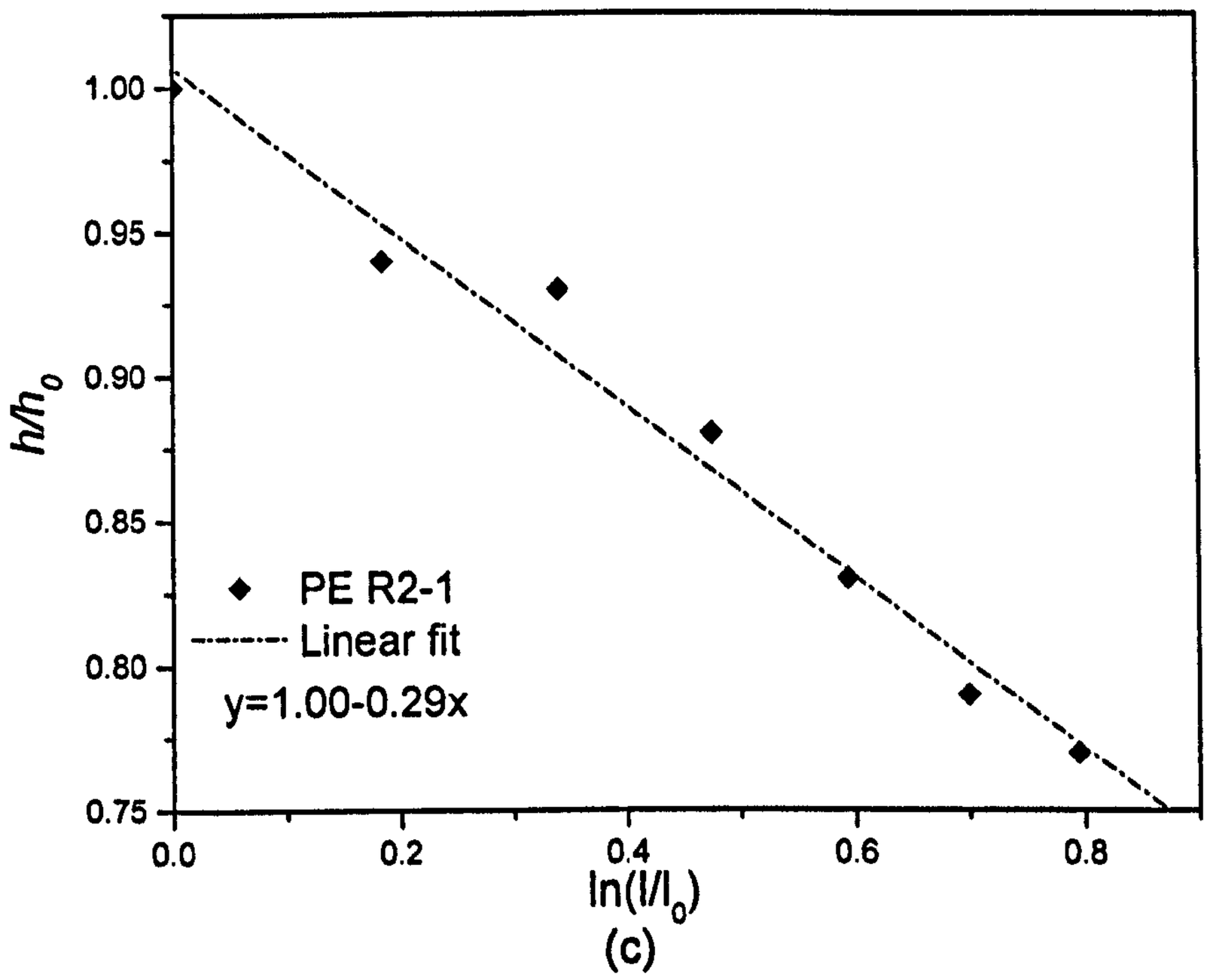

Figure 5-2 Plots of $I/I_0(= h/h_0)$ versus ε for U-1(a), A-1(b) and R2-1(c). respectively.

In accordance with the above analysis, corrections based on the intensity of the band at 1377 cm^{-1} were made to account for the contribution to changes in IR absorbance due to the thickness variations caused by straining the samples mounted in the ring clamps, and corrected data obtained using this analysis are given in section 5.5. The ratio of the intensity of the chosen band for the specimen in the stretched state and unstrained, respectively, was taken to be equal to the thickness ratio in these two conditions. It is assumed that the absorbing species is uniformly distributed and that stretching does not cause reorientation of the absorbing bonds in a way that would influence the absorption.

The dichroic ratio was found to be very close to unity for films in the unstrained state. This is what would be expected if the fabrication process achieved 'balanced orientation' between the longitudinal molecular orientation caused by passage through the die and by the 'haul-off' action, and the hoop orientation produced by the inflation of the film. Characteristic changes in the IR spectra occurred when the films were strained (Figure 5-3) and the dichroic ratio for 80 % strain was measured to be

between 1.2 and 1.3 for all specimens tested and for both transverse and longitudinal applied strain.

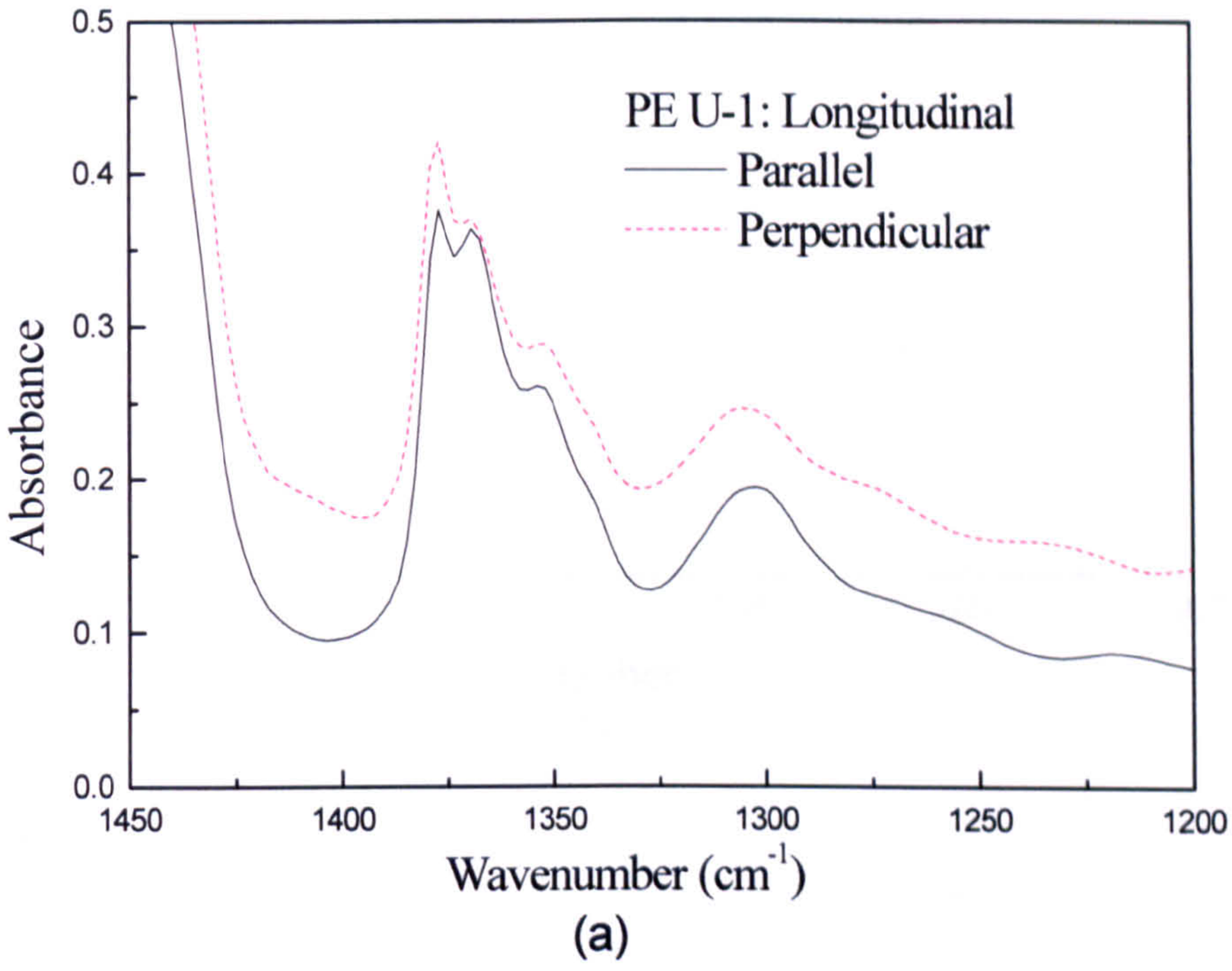

Figure 5-3 (continued next page)

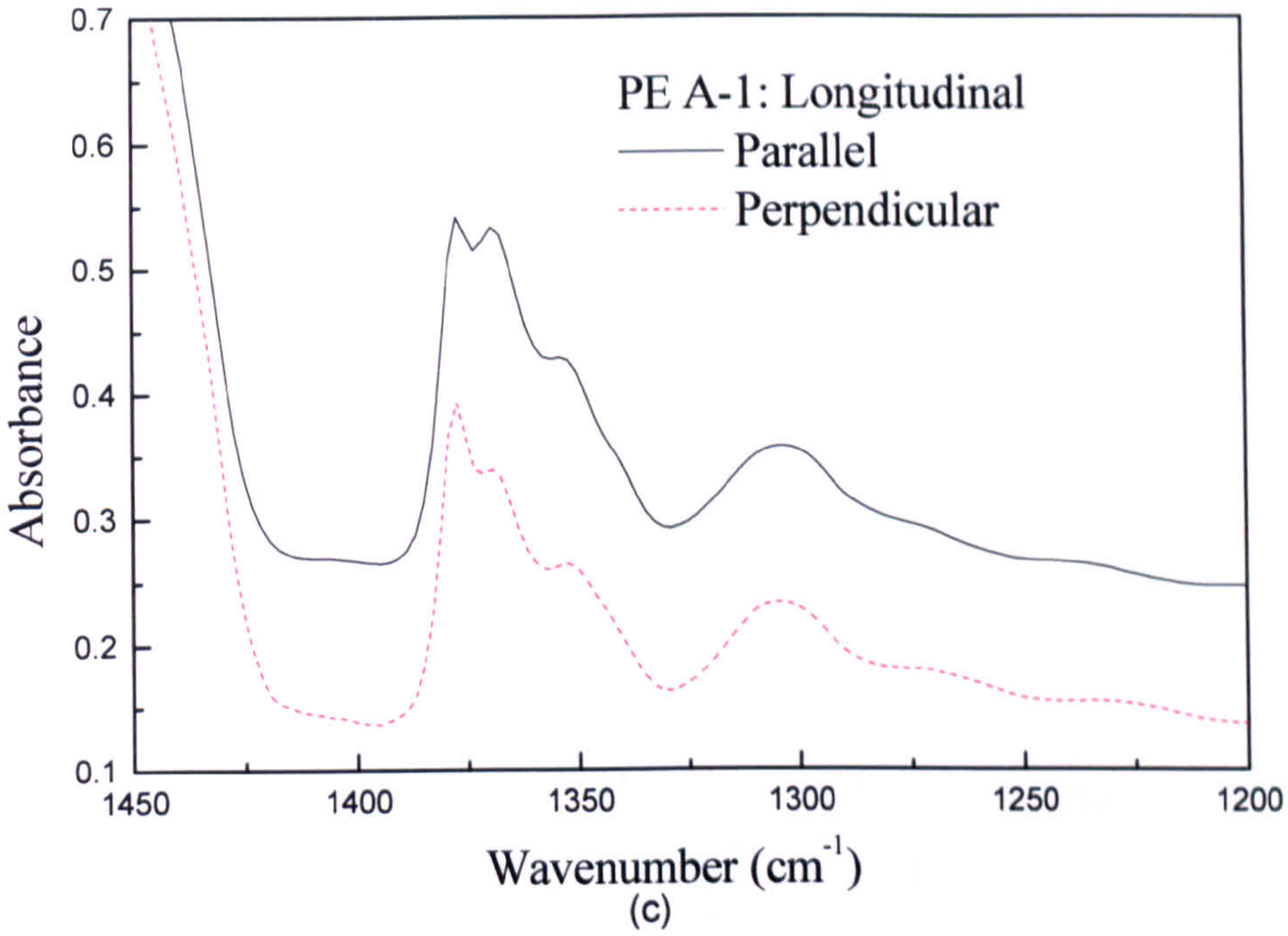

(c)

(d)

Figure 5-3 (continued next page)

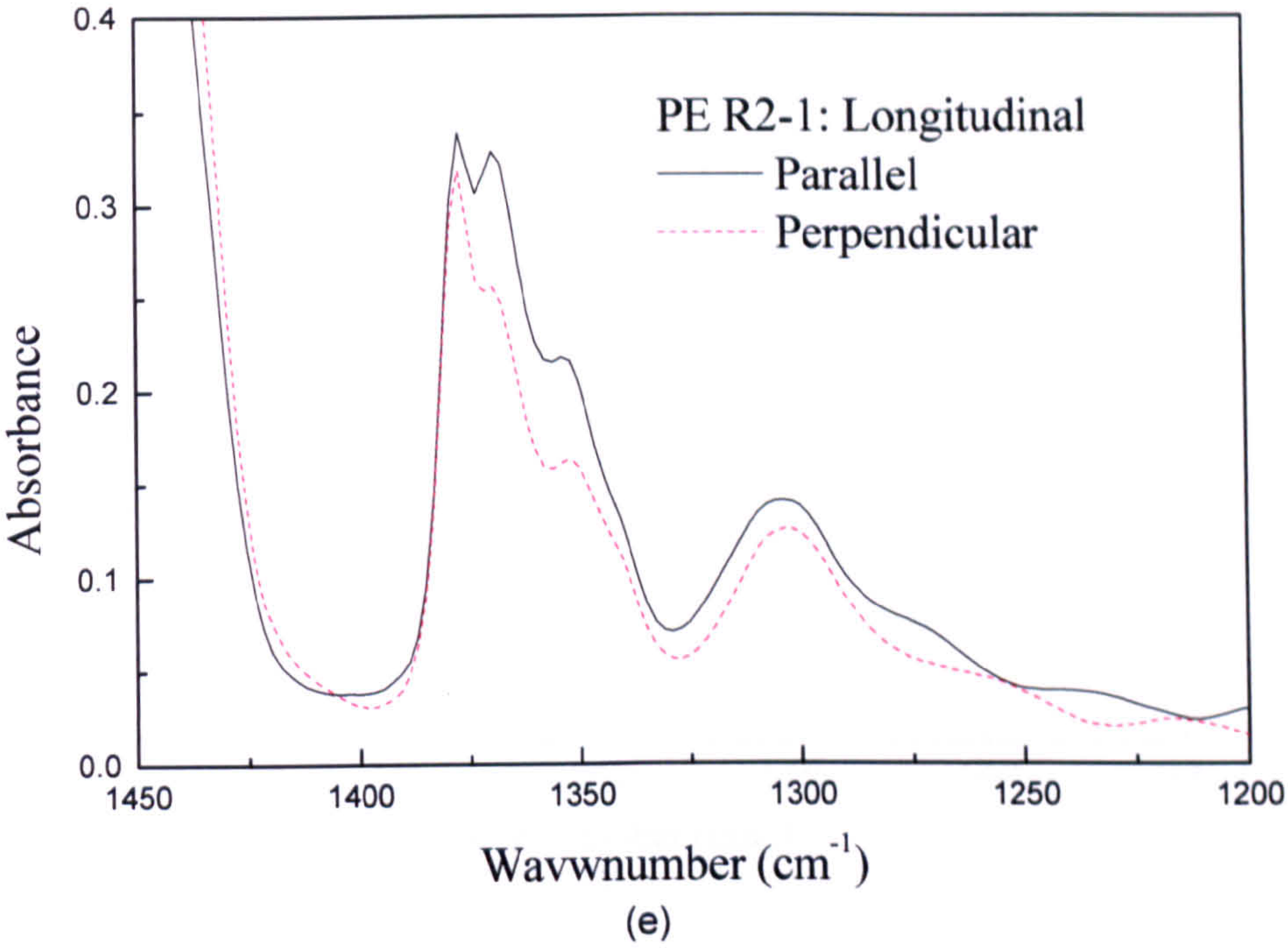

(e)

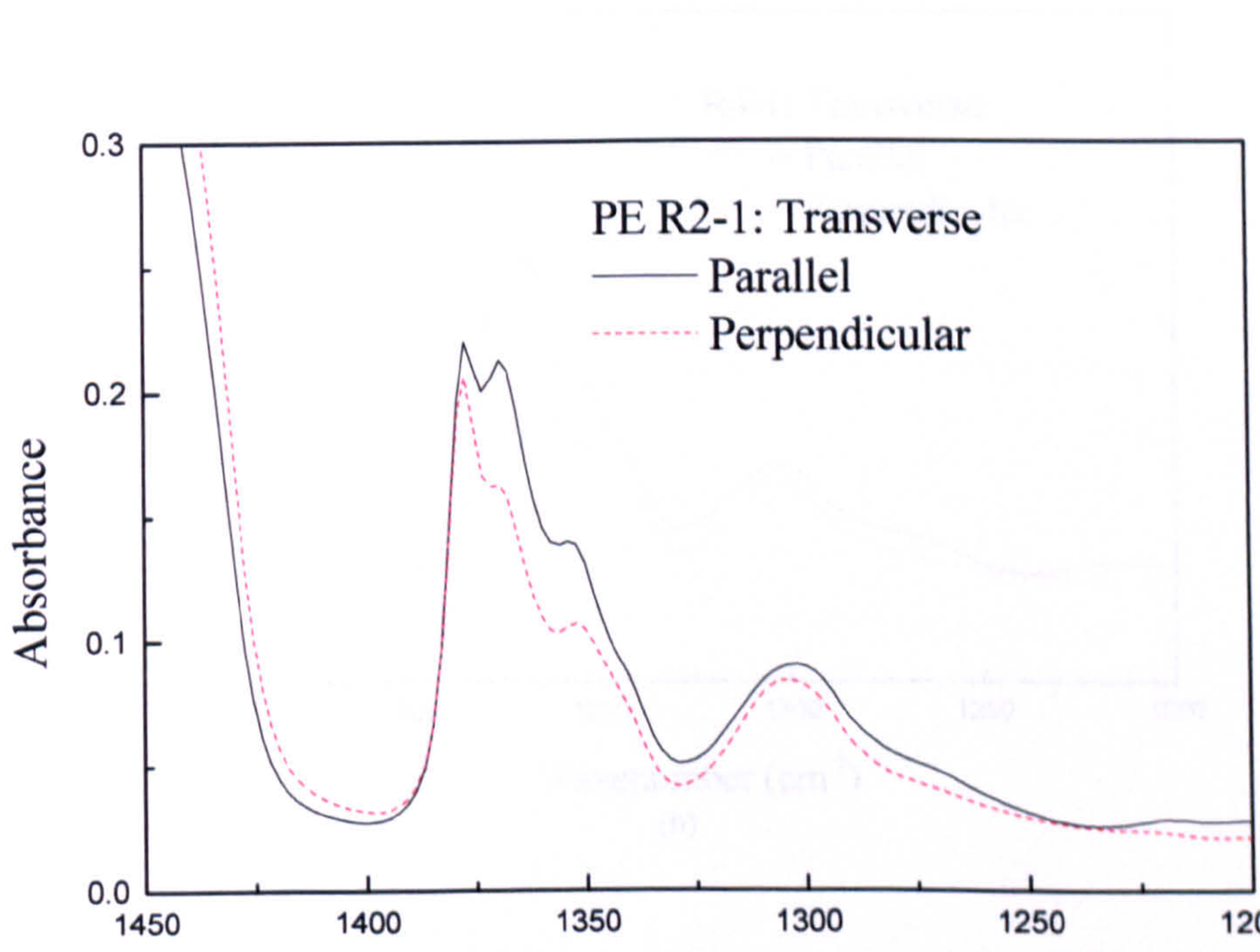

(f)

Figure 5-3 (continued next page)

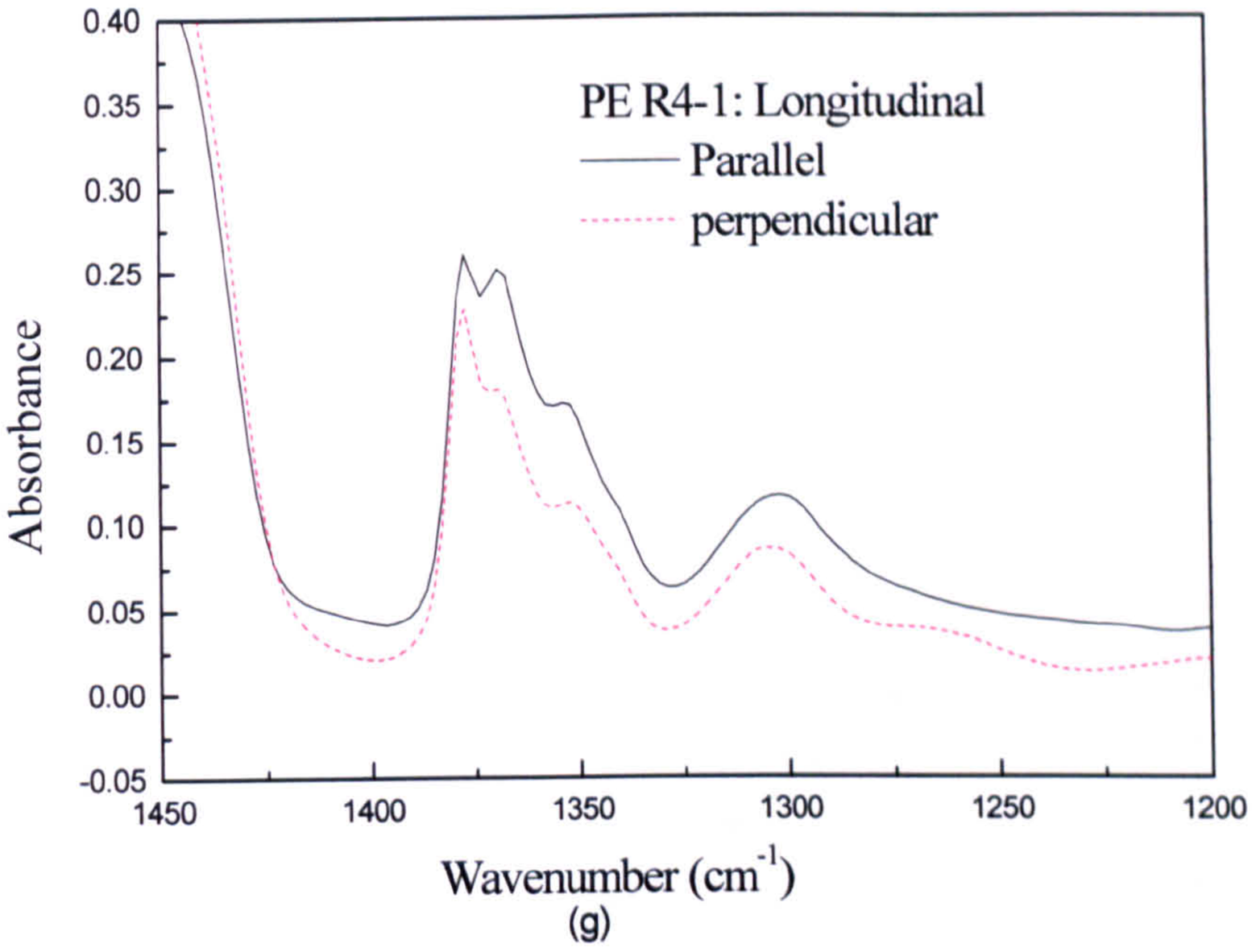

Figure 5-3 FTIR spectra of strained samples taken using polarized IR, showing the range containing the polyethylene absorbances with peaks between 1300 and 1400 cm^{-1}. (a) PE U-1 strained longitudinally; (b) PE U-1 strained transversely; (c) PE A-1 strained longitudinally; (d) PE A-1 strained transversely; (e) PE R2-1 strained longitudinally; (f) PE R2-1 strained transversely; (g) PE R4-1 strained longitudinally; (h) PE R4-1 strained transversely. 'Parallel' and 'perpendicular' refer to the orientation of the polarization axis with reference to the applied strain axis. The applied strain was 80 %.

5.5 MULTI-LAYERED EXPERIMENTS

The carbonyl group development results for the experiments with multi-layered samples are shown in Figure 5-4 for unpigmented PE film and for anatase pigmented PE film and rutile (R2-1) pigmented PE film.

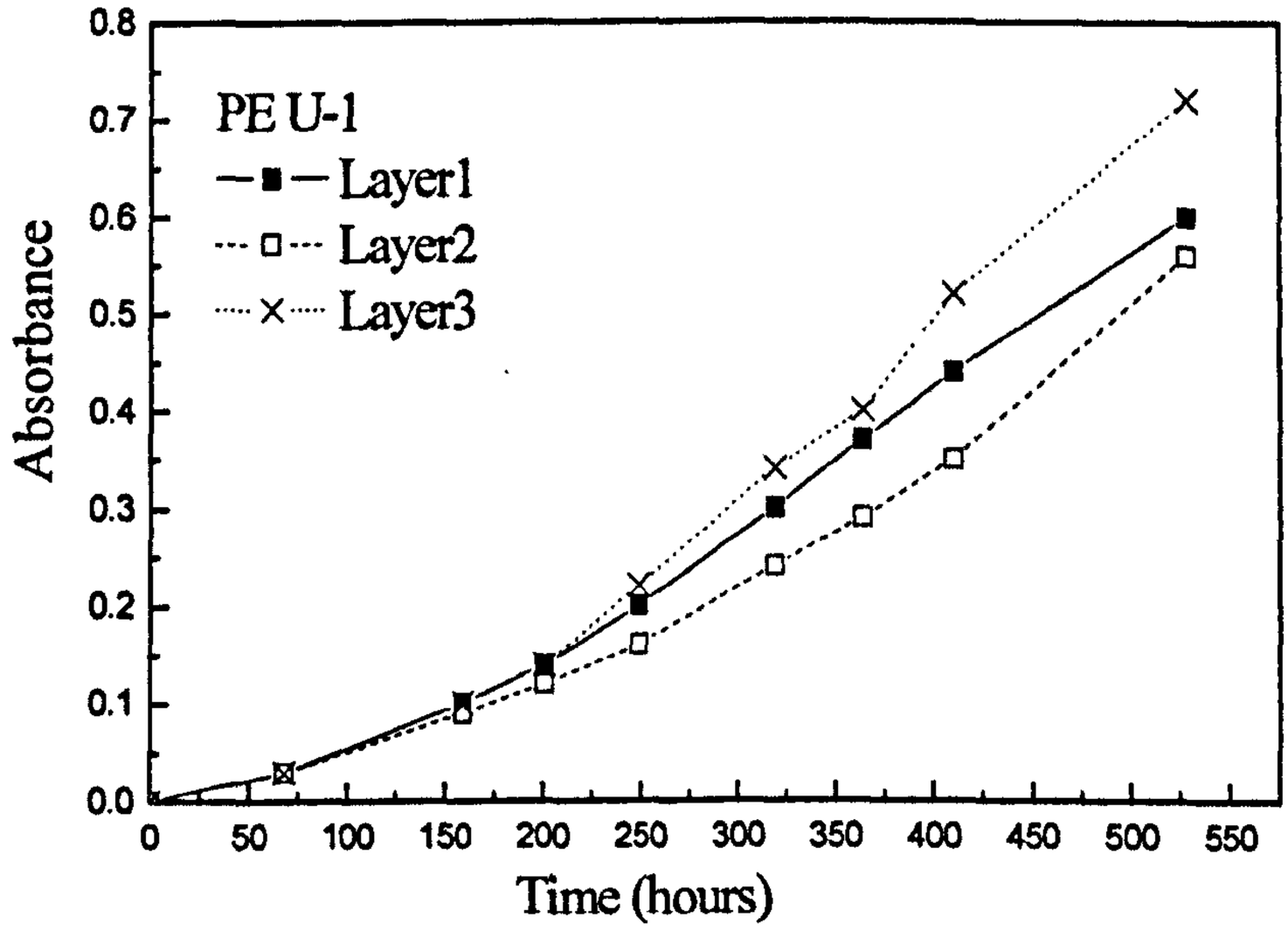

(a)

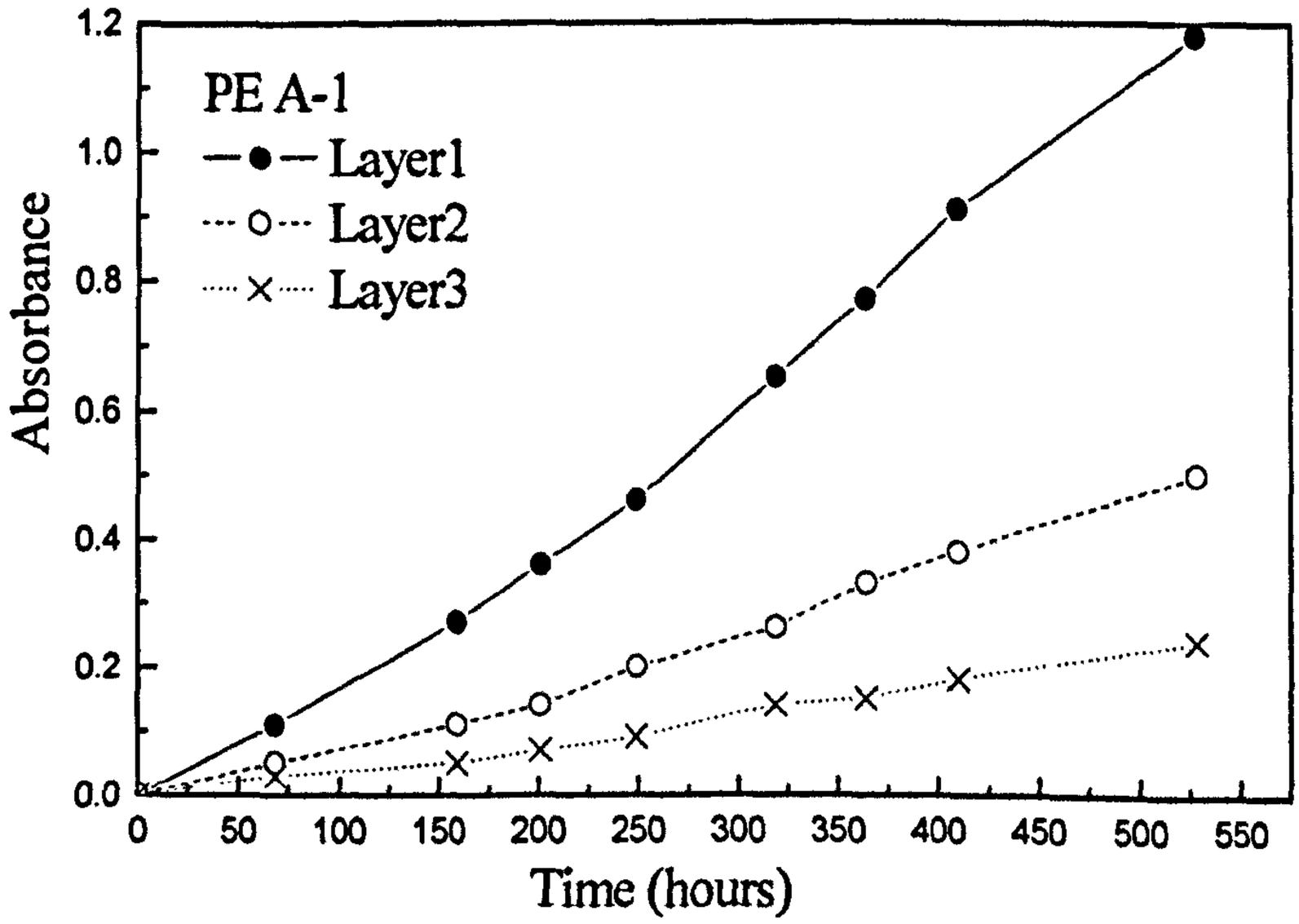

(b)

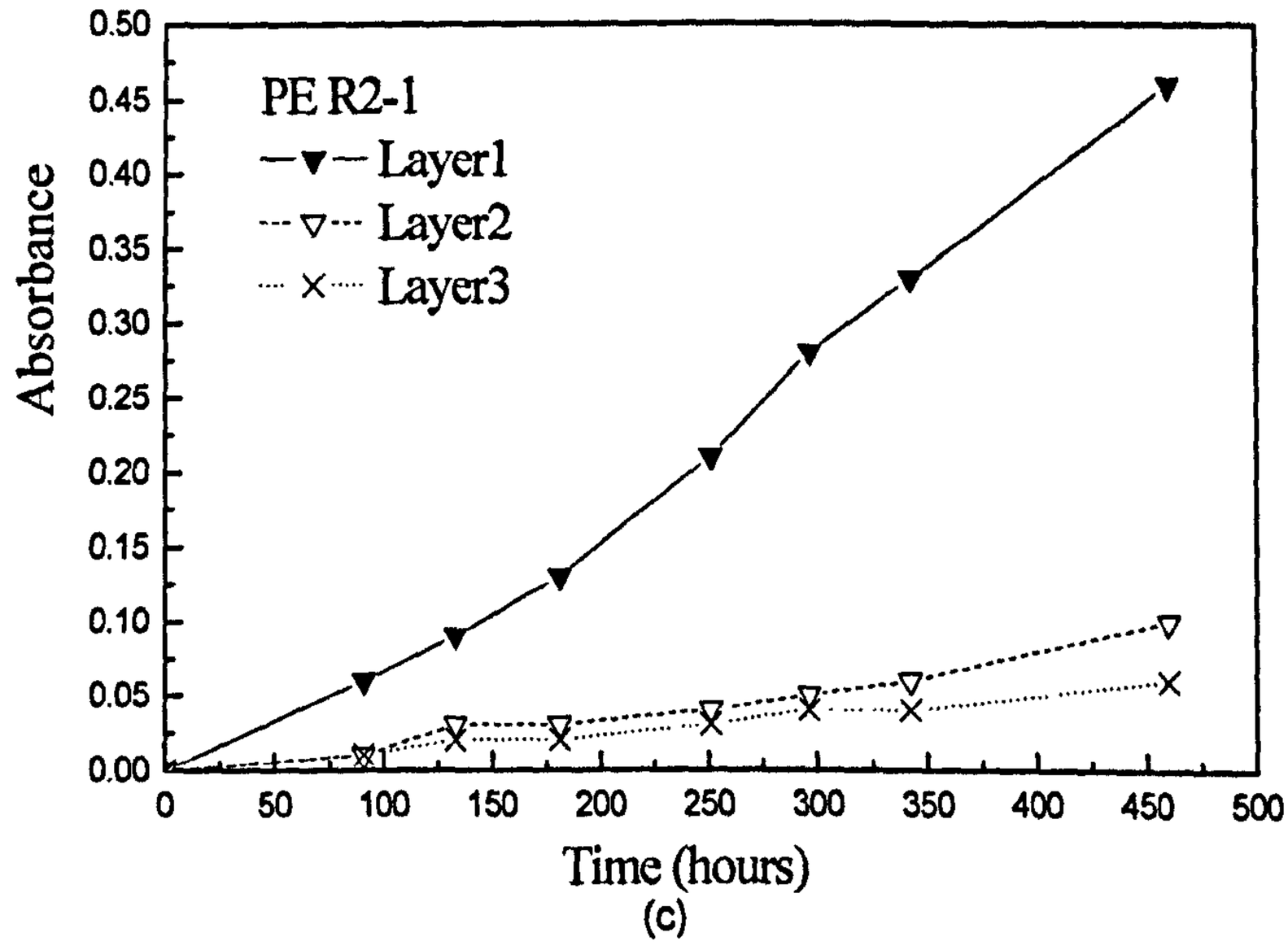

Figure 5-4 Carbonyl group absorbance versus time of UV exposure for triple layered films (a) PE U-1; (b) PE A-1; and (c) PE R2-1.

The main purpose of the experiments reported here was to investigate the effect of parameters such as UV light and oxygen diffusion on the oxidation at different depths. In unpigmented polyethylene, the slowest rate of carbonyl group formation was observed with the central layer, as would be expected if reaction was limited by oxygen starvation (Figure 5-4(a)). Whereas the UV light passes through transparent three layers with small intensity decrease (see Figure 5-5).

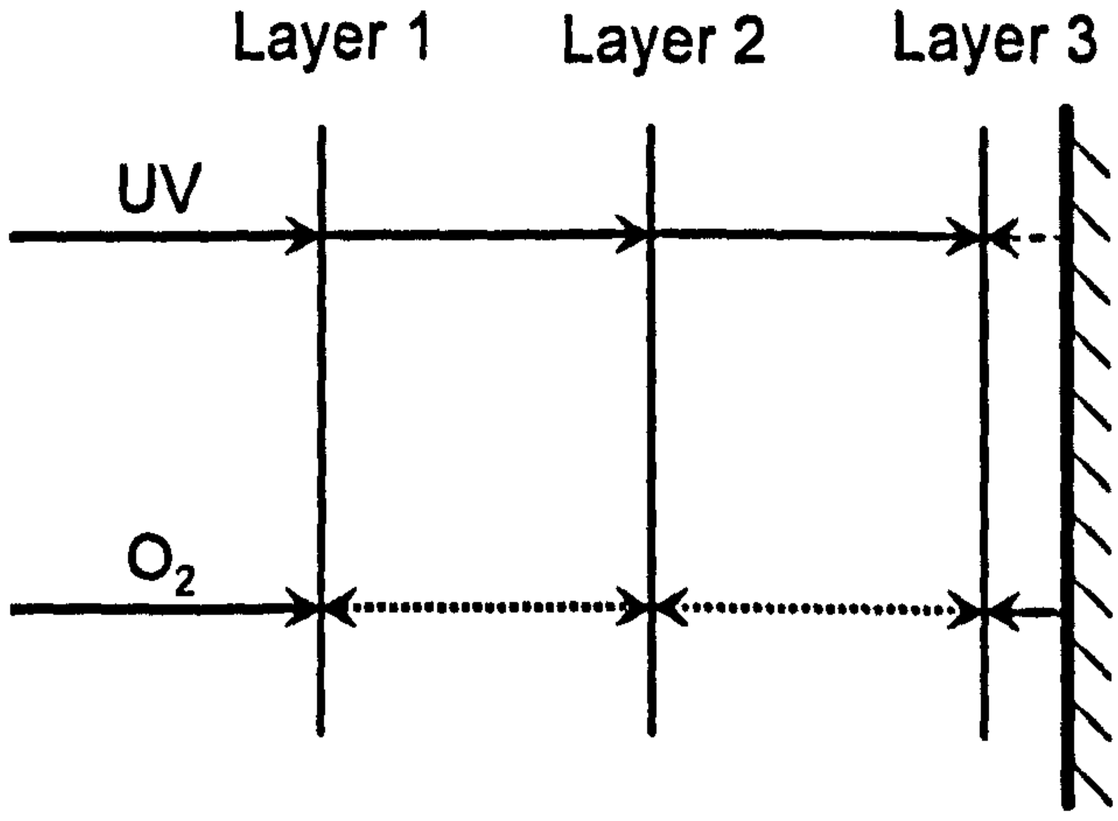

Figure 5-5 Schematics show UV light and oxygen diffusion effect on different layers for PE U-1.

The films were held tightly within the ring grips so the source of oxygen was restricted. Although there appears to be a slight oxygen-starvation effect with the unpigmented polyethylene, it is likely to be very small in a single layer sample. Both UV light and oxygen concentration are responsible for carbonyl group development.

For anatase pigmented PE film, the third layer 3 showed the slowest carbonyl group development, with the results for the central layer located between those for the directly exposed layer and those for the back-facing layer (Figure 5-4(b)). This is what would be expected if the UV intensity were the controlling factor (see Figure 5-6).

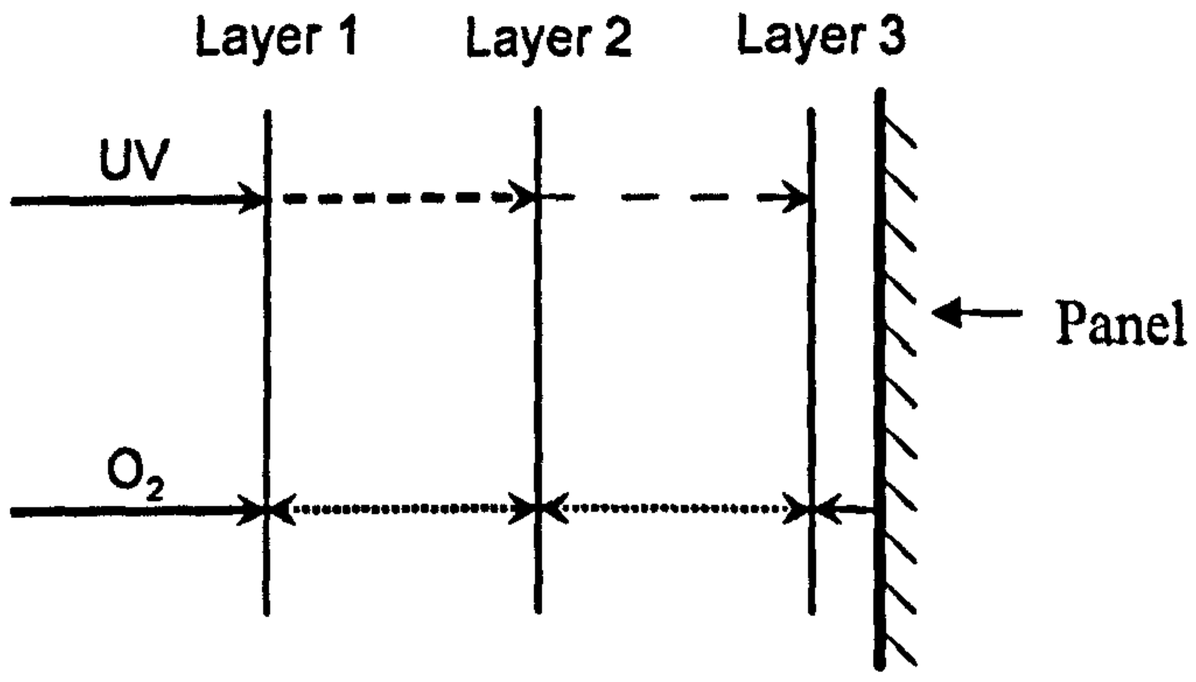

Figure 5-6 Schematics show UV light and oxygen diffusion effect on different layers for PE A-1.

For rutile (R2-1) pigmented PE film (Figure 5-4(c)) the carbonyl group development was very much slower in the central layer and in the layer that faced away from the UV source than in the directly exposed layer. The oxidation of the central layer was only slightly greater than that in the back-facing layer and it seems that UV intensity is again the controlling factor here.

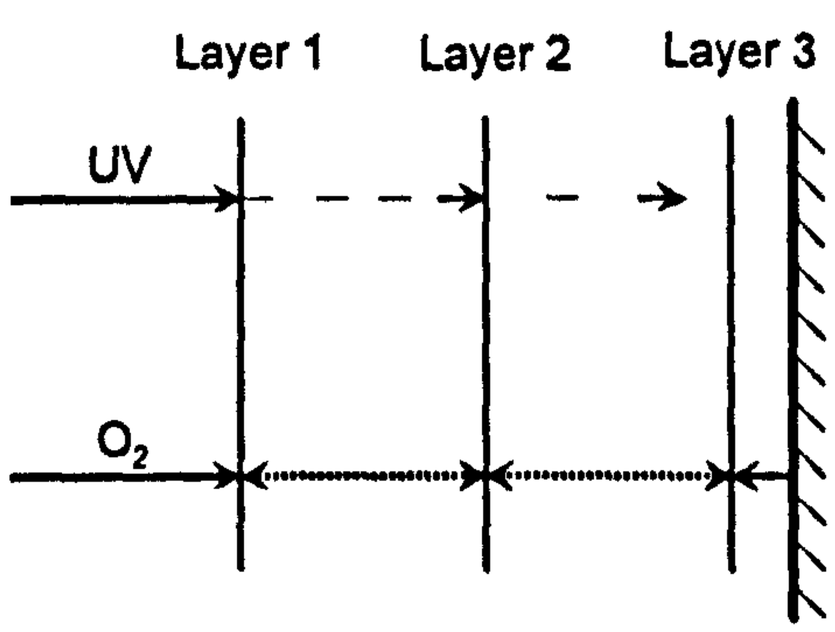

Figure 5-7 Schematics show UV light and oxygen diffusion effect on different layers for PE R2-1.

The difference between the PE A-1 and the PE R2-1 results is caused by the higher UV transmission and photocatalytic ability of anatase pigmented films than rutile pigmented films [9, 10]. Less than half the UV light probably penetrated as far as the central layer in the PE A-1 trial, giving photo-oxidation clearly greater than in the back-facing layer. Very little UV penetrated as far as the central layer in the R2-1 trial, giving a level of photo-oxidation only slightly greater than that in the back-facing layer. UV exposure of the third layer of the R2-1 stack was probably restricted to radiation scattered by the surfaces of the exposure enclosure, falling on the back face, with practically none at all transmitted through the upper two layers. This may suggest that for rutile pigmented PE film, the UV induced photooxidation just exists on the surface of PE film.

5.6 CARBONYL GROUP DEVELOPMENT UNDER STRAIN

Experiments were conducted on single-layered samples to investigate the effect of strain on carbonyl group development. The experiments were carried out for unstrained, longitudinal strain and transverse strain simultaneously *i.e.* the samples for these three sets were simultaneously exposed in the QUV machine. The unstrained set carbonyl group development is given in Figure 5-8 for exposures up to 528 hours.

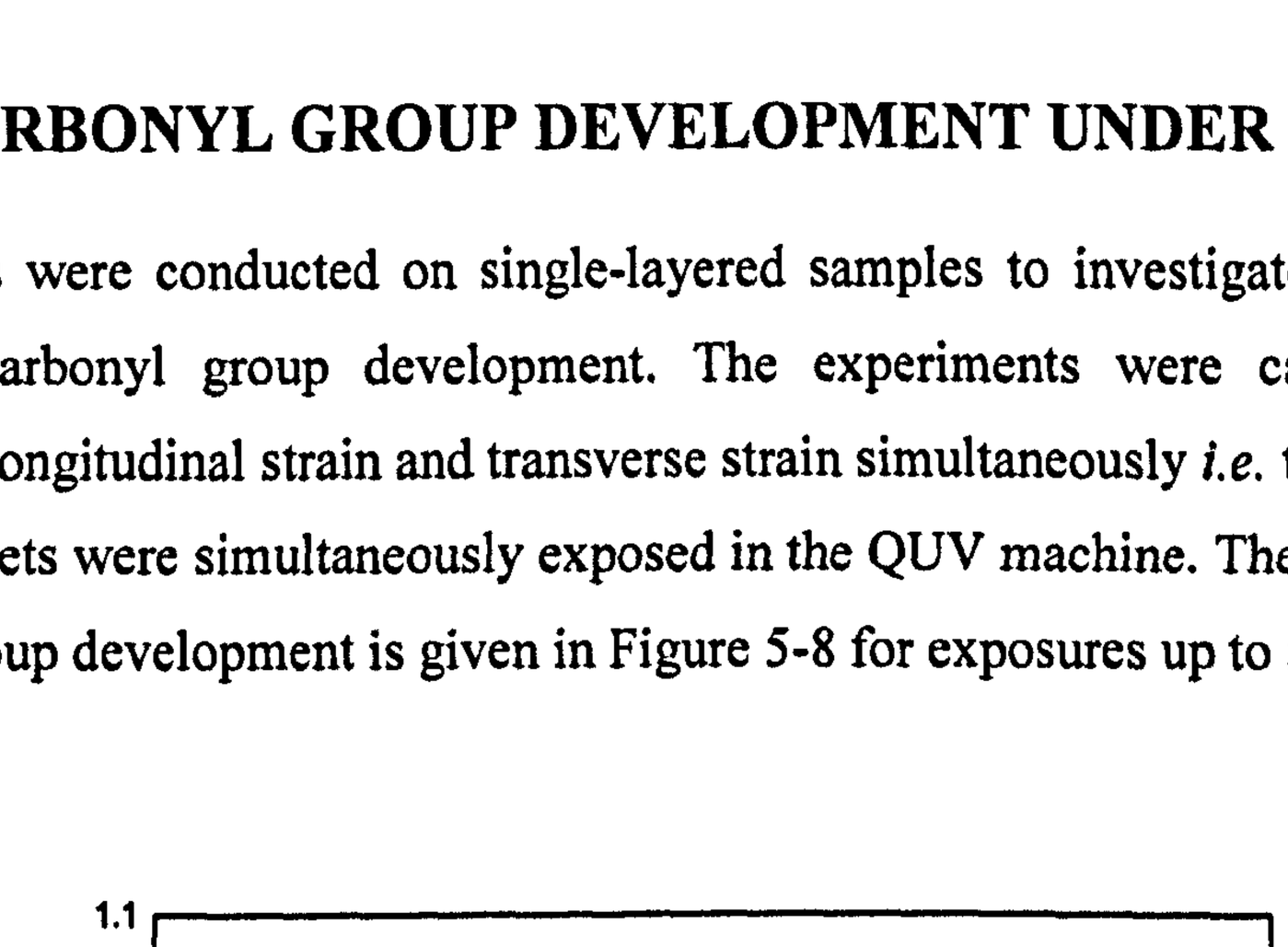

Figure 5-8 Carbonyl group absorbance versus time of UV exposure for unstrained films.

In each material the carbonyl group absorption increased progressively. Up to 400 h exposure, the curves are slightly concave upwards, possibly a consequence of auto-acceleration (see section 4.2.2). As expected the anatase-pigmented material showed the highest rate of oxidation. The rutile-pigmented materials show a range of oxidation rates. The PE R1-1 and PE R2-1 show rates that are greater than that of the unpigmented polyethylene PE U-1. The PE R3-1 and PE R4-1 produced oxidation rates below PE U-1. The ranking of the carbonyl group development is the same as the ranking when samples are exposed to QUV A lamps in the constant temperature room, but the carbonyl group development in the QUV machine was faster.

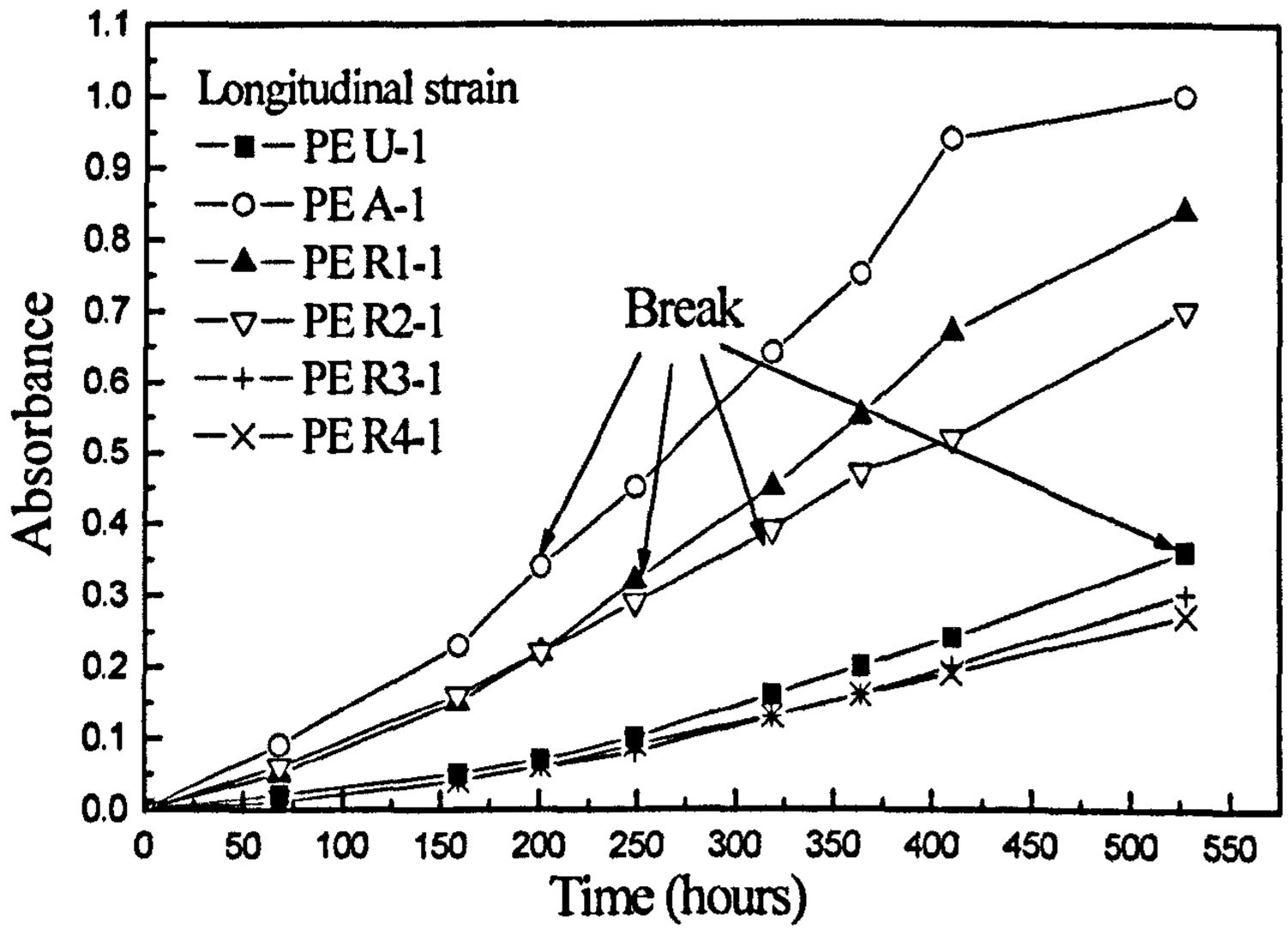

Figure 5-9 Carbonyl group absorbance versus time of UV exposure for films strained longitudinally during exposure. The times when the samples broke are shown. The data are uncorrected for thickness changes.

The carbonyl group development for samples tensile strained in the longitudinal direction are given in Figure 5-9. These results are uncorrected for thickness (see section 5.6). It is noted that the ranking of the carbonyl group development is almost identical to that in Figure 5-8. But PE R3-1 and PE R4-1 carbonyl group developments were slower than for the unpigmented PE film are again placed below it, but in this series of measurements they are almost indistinguishable, whereas, in Figure 5-8, PE R4-1 shows a detectably higher rate than PE R3-1. In the stressed

series, it seems that strain separated these 6 samples in to two groups. The strain enhanced pro-degraded pigment A-1, R1-1 and R2-1 to same degree. For the unpigmented material are much closer to those for PE R3-1 and PE R4-1 than is the case in the unstrained state (compares Figure 5-8 and Figure 5-9). Samples PE U-1, PE A-1, PE R1-1 and PE R2-1 all broke during the strained exposure, as marked on Figure 5-9. It is of interest to note that the carbonyl group absorbance at break was approximately the same for all four samples (PE U-1, PE A-1, PE R1-1 and PE R2-1) when carbonyl absorbance reached about 0.3 – 0.4 and that this level of absorbance was not reached by the PE R3-1 and PE R4-1 samples that did not break during the exposure.

The carbonyl group developments for samples strained in tension in the transverse direction are given in Figure 5-10.

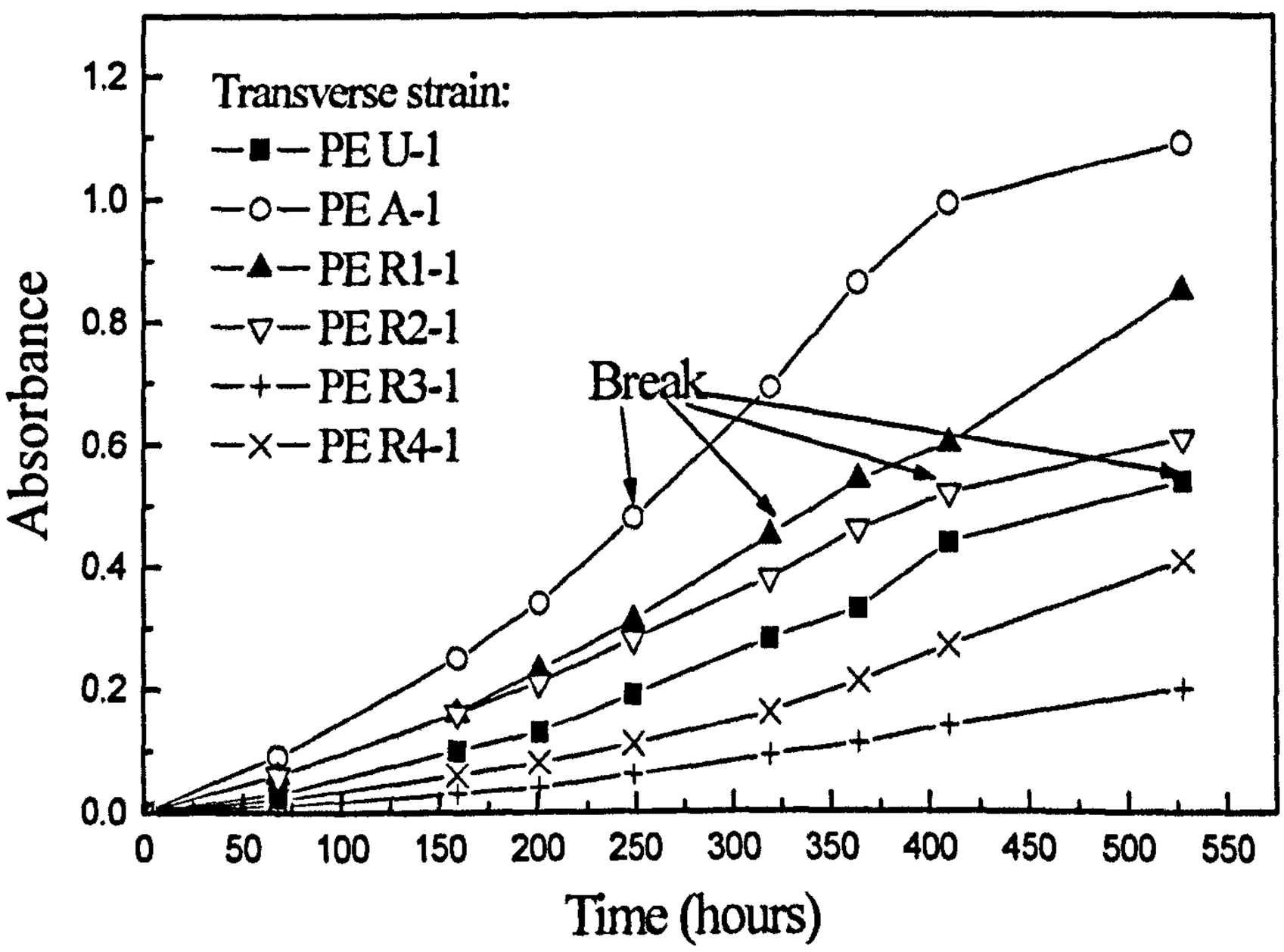

Figure 5-10 Carbonyl group absorbance versus time of UV exposure for films strained transversely during exposure. The times when the samples broke are shown. The data are uncorrected for thickness changes.

These results are not corrected for thickness. This time the manner of carbonyl group development is identical to that in Figure 5-8. Samples PE U-1, PE A-1, PE R1-1 and

PE R2-1 again all broke during the exposure, as with the longitudinal samples, and the carbonyl absorption at this point was almost identical in all cases but the carbonyl absorbance(> 0.4) was bigger than carbonyl absorbance (0.3 – 0.4) in longitudinal strain. Samples PE R3-1 and PE R4-1 did not reach this level of carbonyl group development by the time the tests were terminated, and did not break. The PE A-1, PE R1-1 and PE R2-1 transverse samples all broke after a significantly longer time than it took for the corresponding longitudinal samples to break; the PE U-1 samples broke after approximately the same exposure time.

5.7 CORRECTION FOR SAMPLE THICKNESS

From an inspection of the results presented in the previous section, it seems that there is very little effect on the rate of carbonyl group development when stress is applied in the transverse direction, and that the larger effect of stress in the longitudinal direction is to reduce the rate of oxidation in the unpigmented material, while having little effect on the pigmented PE films. However, the results as presented above do not take any account of sample thickness and the effect of this must be considered.

In Figure 5-11, the results presented in Figure 5-8, Figure 5-9 and Figure 5-10 are replotted, together with thickness-corrected plots for the two sets of data for strained samples (for longitudinal and transverse deformation).

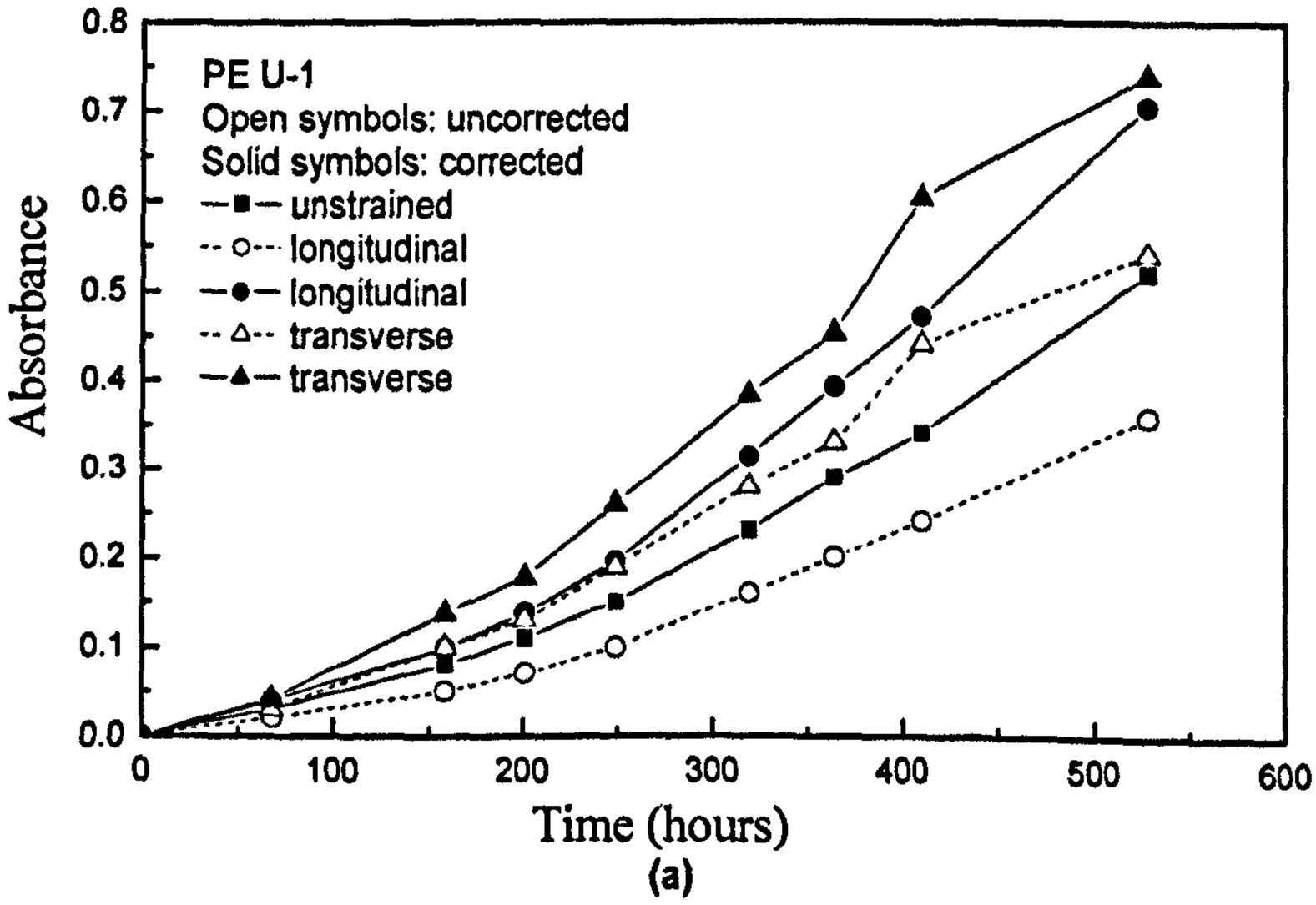

(a)

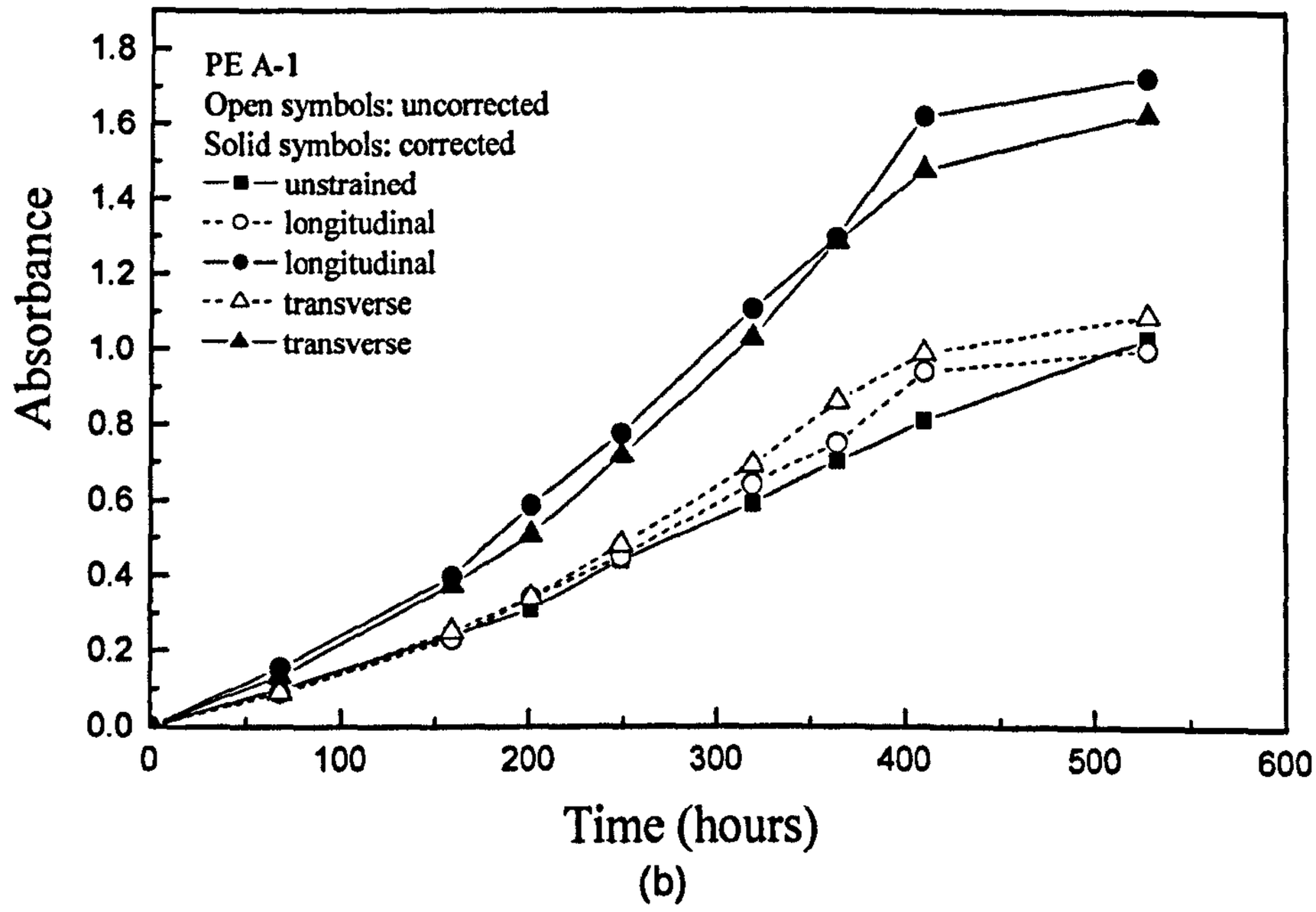
PE A-1
Open symbols: uncorrected
Solid symbols: corrected
unstrained
longitudinal
longitudinal
transverse
transverse
Absorbance
Time (hours)

(b)

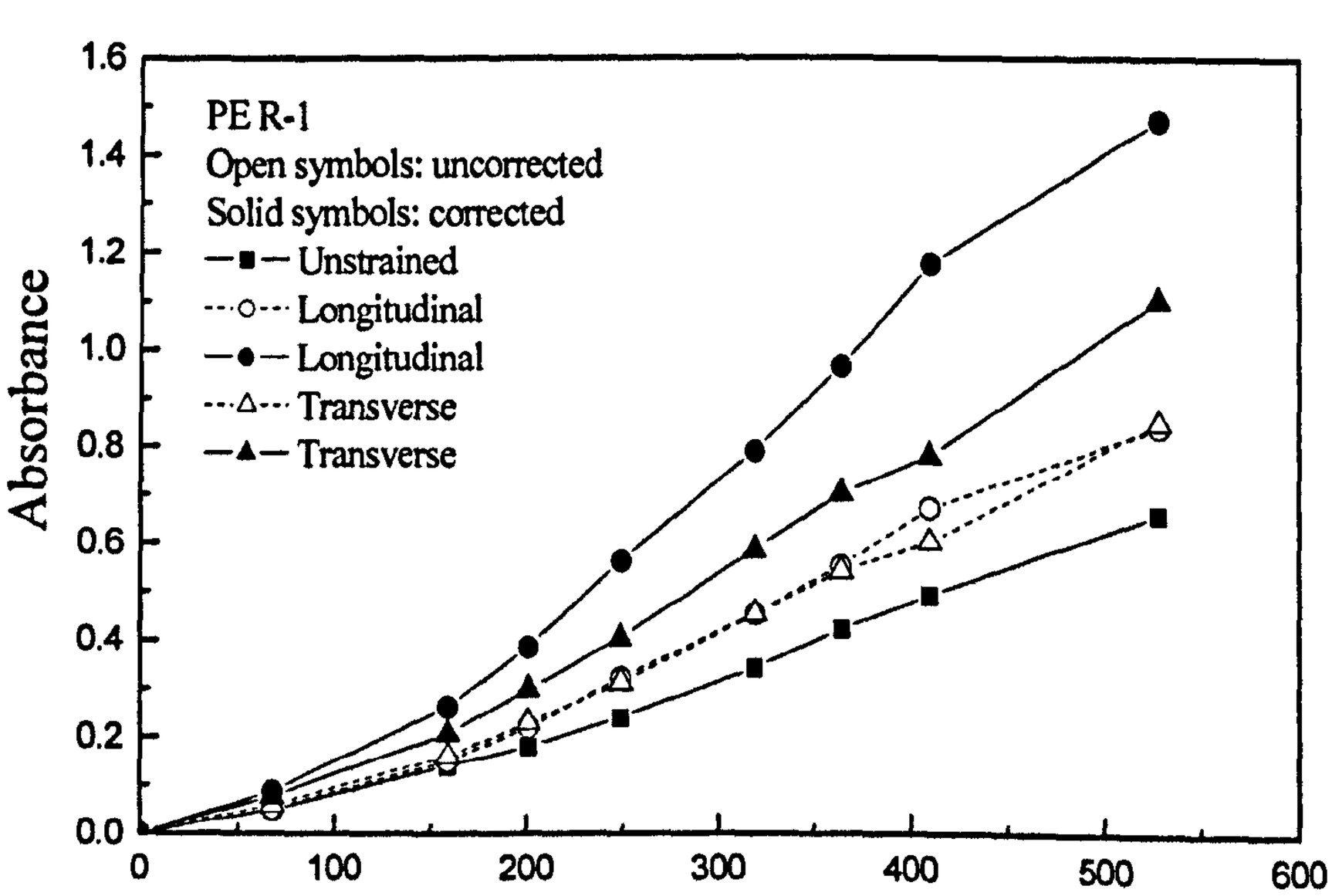
PE R-1
Open symbols: uncorrected
Solid symbols: corrected
Unstrained
Longitudinal
Longitudinal
Transverse
Transverse
Absorbance
Time (hours)

(c)

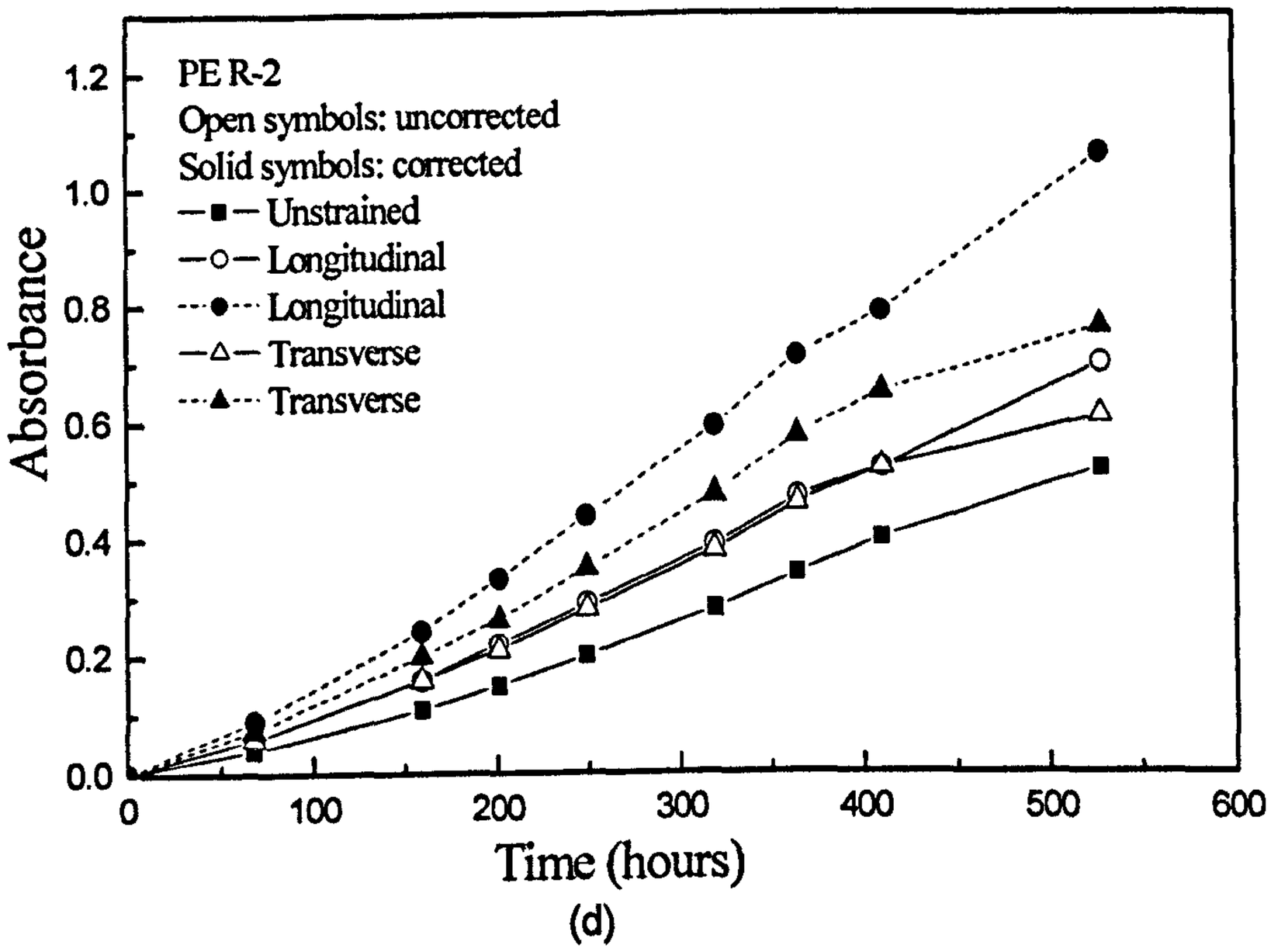
PE R-2
Open symbols: uncorrected
Solid symbols: corrected
Unstrained
Longitudinal
Longitudinal
Transverse
Transverse
Absorbance
Time (hours)
0.0
0.2
0.4
0.6
0.8
1.0
1.2
0
100
200
300
400
500
600

(d)

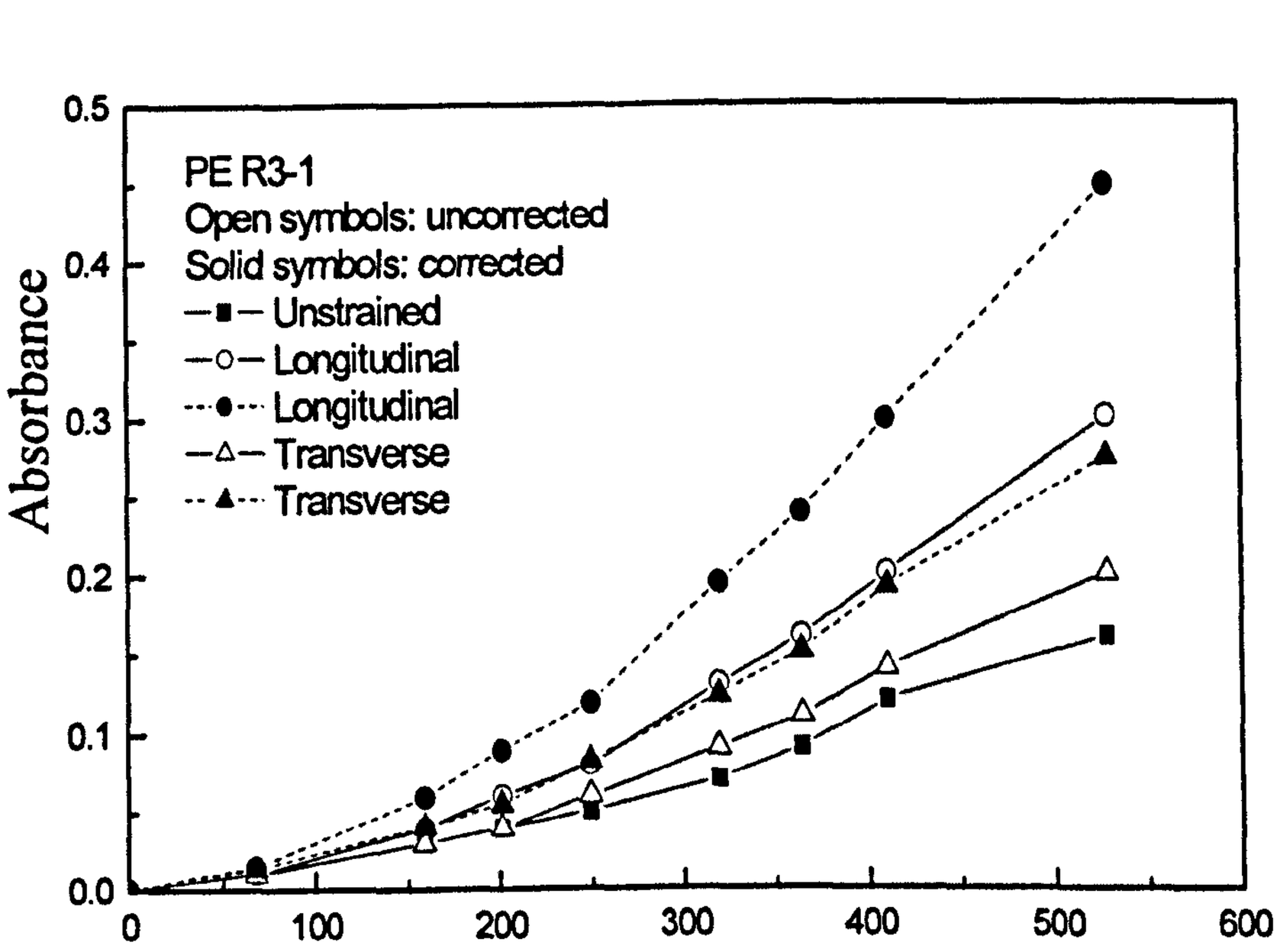
PE R3-1
Open symbols: uncorrected
Solid symbols: corrected
Unstrained
Longitudinal
Longitudinal
Transverse
Transverse
Absorbance
Time (hours)
0.0
0.1
0.2
0.3
0.4
0.5
0
100
200
300
400
500
600

(e)

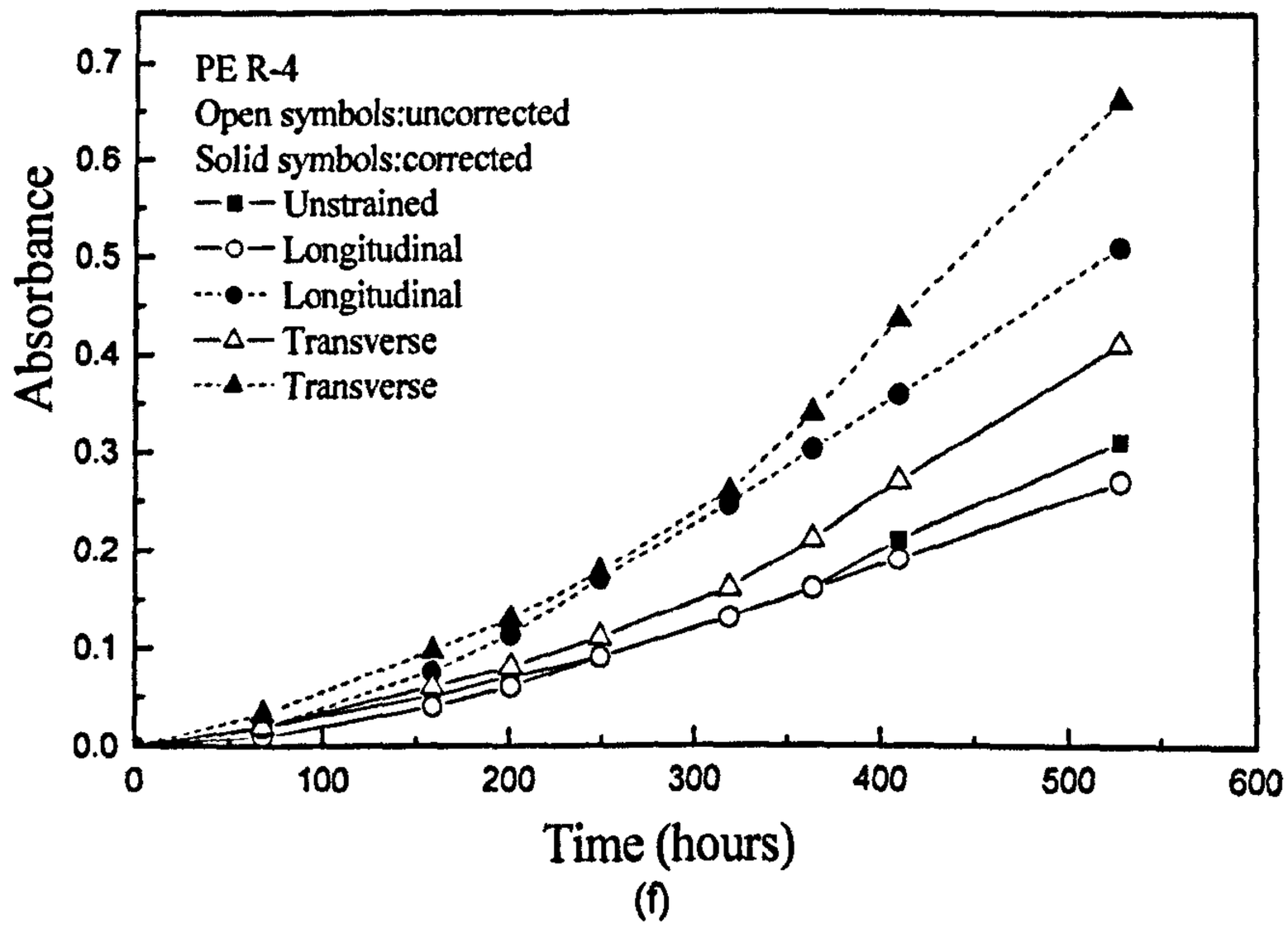

Figure 5-11 Carbonyl group absorbance versus time of UV exposure, comparing data from samples exposed unstrained, longitudinally strained and transversely strained, and showing uncorrected and thickness-corrected measurements for the strained experiments: (a) PE U-1; (b) PE A-1; (c) PE R1-1; (d) PE R2-1; (e) PE R3-1; and (f) PE R4-1. Note that the correction is almost certainly invalid for PE R2-1 and probably invalid for the other three rutile-pigmented materials (PE R1-1, PE R3-1, PE R4-1). Thus the solid lines are the ones to be used to assess the effect of stress in all graphs, and the broken lines are shown for completeness.

The correction takes account of the thickness reduction in the strained samples, based on the intensity of the IR band at 1377 cm^{-1} and implicitly assumes that the carbonyl groups are homogeneously distributed throughout the thickness of the film. When the thickness change caused by applying a tensile deformation is taken into account, the PE U-1 samples strained in the longitudinal and the transverse directions during UV exposure both show an increase in carbonyl group generation rate compared to the unstrained film.

For the anatase-pigmented polyethylene, PE A-1 is the same as unpigmented PE film. In the case of the rutile-pigmented polyethylene, PE R2-1, the thickness correction should not be applied because photodegradation just happen in very short thin surface. Even if the thickness correction is not applied in this case (Figure 5-11 (d)), the strained samples still show significantly higher carbonyl group development than the

unstrained sample exposed under the same conditions. The thickness correction is shown for completeness, despite the belief that it is not appropriate to use it. (If the thickness correction were valid, it would indicate even greater sensitivity of oxidation to stress than is represented by the original data).

No IR measurements were made for triple layered samples of PE R1-1, PE R3-1 and PE R4-1 and it is assumed, without verification, that a thickness correction would be inappropriate, as with PE R2-1. The carbonyl absorption data for PE R1-1 and PE R3-1 are similar to those for PE R2-1, showing that strain enhanced the oxidation rate significantly, whether or not the thickness correction is needed. The interpretation for PE R4-1 is a little less straightforward, since the uncorrected carbonyl absorbance for longitudinal strain falls close to or just below that for the unstrained sample. When the thickness correction is applied, the strained sample appears to have oxidised more rapidly, though the validity of the thickness correction for this compound is not known. The uncorrected carbonyl absorbance for transverse strain is greater than that for the unstrained sample, showing unambiguously that strain applied in this direction enhanced oxidation.

It is evident from Figure 5-11 that the thickness correction is greater for longitudinal testing than for the transverse samples. This indicates that the Poisson ratio is anisotropic; this is common in oriented polymers and is not entirely unexpected.

5.8 COMPARISON OF DIFFERENT STRESS ON CARBONYL GROUP DEVELOPMENT

In order to assess the enhancement of carbonyl group development caused by the application of stress, the carbonyl group absorbance at 200 h exposure for each of the strained samples was compared with that for the corresponding unstrained sample at the same time. The data taken for the strained PE U-1 and PE A-1 samples were corrected for thickness whereas the rutile-pigmented polyethylenes did not have the thickness correction applied. The ratios of the two absorbances are listed in Table 5-3.

Table 5-3 Carbonyl group enhancement in 80 % strained film after 200 h UV exposure (ratio of strained sample absorbance to unstrained sample absorbance)

	Longitudinal	Transverse
PE U-1	1.4	1.6
PE A-1	2.0	1.7
PE R1-1	1.3	1.3
PE R2-1	1.5	1.4
PE R3-1	1.6	1.0
PE R4-1	0.9	1.2

The time of 200 h was chosen because some of the samples broke at times longer than this. For pigmented polyethylenes PE A-1 and PE R3-1 the ratio for samples exposed while strained in the longitudinal direction exceeded that for the corresponding material strained in the transverse direction. There was hardly any effect of test direction for PE R1-1 and PE R2-1. For PE R4-1 the ranking was reversed, with the transverse sample showing the greater rate. In unpigmented PE U-1 the transverse sample also appeared to degrade more rapidly than the longitudinal one.

5.9 DISCUSSION

There are several ways in which stress may be expected to influence oxidation in polymers. Firstly, it may directly assist any thermally activated process in the manner proposed by Zhurkov and White et al [11-14]. It may influence the rate of recombination of radicals formed by photo-chemical scission reactions, effectively separating them before the molecules have a chance to repair themselves. This would explain why tensile stress was found to increase the rate of chain scission near to the surface of polypropylene bars but had very little influence on crosslinking rate, even though oxidation processes are involved in both scission and crosslinking [15]. Finally, stress may influence the diffusion rate of oxygen (or other reactants).

In the studies reported in this chapter, it is again evident that the application of tensile stress has increased the degradation rate, here represented by carbonyl group

development. The unique feature of the work presented here is that data are obtained for tensile stresses applied both parallel to and transverse to the machine direction during fabrication of the polyethylene, in this case a blown lay-flat film, in which the tube axis is taken to be the machine (longitudinal) direction. The rate of carbonyl group development is increased by stress applied both parallel and transverse to this direction. With unpigmented polyethylene the effect of transverse strain was greater than that of longitudinal strain. The same was observed with rutile-pigmented polyethylene PE R4-1. With the polyethylene samples pigmented with the other rutiles and with the anatase-pigmented polyethylene, the rate of carbonyl production was greater for tensile stress applied in the longitudinal direction than for the transverse direction. Tensile tests showed that the films were clearly anisotropic though it is noted that measurements of dichroic ratio did not indicate any significant molecular orientation was present.

The majority of the pigmented materials gave a greater rate of carbonyl group development for longitudinal strains, as would be the case if the effect depended on stress (which is expected to be higher for a fixed strain applied parallel to the machine direction). An exception was PE R4-1, however, for which the greater rate was observed for the transverse applied strain.

Another new observation was that strained samples that broke while under UV exposure did so at approximately the same level of carbonyl group development and that this level was different for longitudinal and transverse straining. Longitudinal samples broke at a much lower level of carbonyl group concentration than transverse samples. Bonds that are oriented during fabrication will be affected the most by stress applied in the longitudinal direction, and it is expected that they will be oxidised preferentially. This will lead to chain scission as well as to the production of carbonyl groups.

5.10 CONCLUSIONS

The effect of stress on the rate of photo-oxidation in a series of blown film polyethylene samples in unpigmented form and containing different forms of TiO_2 pigment has been investigated, using carbonyl group development as the method of assessment. Tensile tests on unexposed samples revealed that they were anisotropic;

all films gave a higher yield stress when tested parallel to the machine direction than when tested transverse to it. Tensile stress has been shown to increase the rate of photodegradation. The carbonyl group measurements were made with the samples in the stretched state, which produced a reduction in thickness compared to the unstrained state. Therefore, to analyse the infrared absorption data it was necessary to perform a correction for thickness differences between samples.

5.11 REFERENCES

1. O'Donnell, B. and J.R. White, *Polymer Degradation and Stability,* 1994. **44**(2): p. 211-222.
2. Benachour, D. and C. Rogers, E., *Photodegradation and Photostabilization of Coating,* 1981. **17**: p. 263-274.
3. Davis, A. and D. Sims, Weathering of Polymers. 1983: *Applied Science, Barking,*.
4. Baumhardt-Neto, R. and M.-A. De Paoli, *Polymer Degradation and Stability,* 1993. **40**(1): p. 53-58.
5. Baumhardt-Neto, R. and M.-A. De Paoli, *Polymer Degradation and Stability,* 1993. **40**(1): p. 59-64.
6. O'Donnell, B. and J.R. White, *Journal of Materials Science,* 1994. **29**(15): p. 3955-3963.
7. Vink, P., Degradation and stabilization of polyolefins. In: N.S. Allen, Editor. London: Applied Science; 1983. p. 213–246.
8. McCrum, N.G., C.P. Buckley, and C.B. Bucknall, Principles of polymer engineering (2nd ed ed.),, Oxford University Press, New York (1997).
9. Hird, M.J., J *Coat Technol,* 1976. 48(620): p. 75-82.
10. Egerton, T.A., Titanium products, 4th ed. Kirk-Othmer encyclopaedia of chemical technology, 24.; 1997. 225-274.
11. Zhurkov, S.N., V.A. Zakrevskyi, V.E. Korsukov, and V.S. Kuksenko, Jo*urnal of Polymer Science, Part A-2 (Polymer Physics), 1*972. 10(**8**): p. 1509-1520.
12. Zhurkov, S.N., In*t J Fract Mechs, 1*965. 1: p. 11-23.
13. White, J.R., In: L.G. Mallinson, Editor, Ageing studies and lifetime extension of materials, Kluwer Academic/Plenum, New York (2000), pp. 475-482.
14. White, J.R. and A. Turnbull, Jou*rnal of Materials Science, 1*994. 29(**3**): p. 584-613.
15. Shyichuk, A.V., Stavychna, D. Y., and J.R. White, Pol*ymer Degradation and Stability, 20*01. **72**(**2**): p. 279-285.

CHAPTER 6

PHOTO-OXIDATION OF RIGID PVC MEASURED BY CO_2 METHOD

6.1 INTRODUCTION

A large proportion of the 23 million tonnes of poly (vinyl chloride) (PVC) produced per year in the world is consumed for outdoor applications, *e.g.* house siding panels, wastewater tubes and window profiles [1]. However, these PVC products are degraded by environmental exposure, especially under sunlight [2]. According to the structure of the repeating units of PVC, $[-CH_2-CHCl-]_n$, the final gaseous production of photoreaction would mainly be CO_2 and HCl. IR spectroscopic measurements are usually carried out to monitor the development of carbonyl groups in the ageing polymer film as a measure of the polymer degradation, but this is not convenient with rigid PVC panels because IR cannot pass through the sample. The studies [3] detailed in Chapter 3 and Chapter 4 have demonstrated both that the CO_2 method is sufficiently sensitive to be applied to either unpigmented or TiO_2 pigmented polyethylene films and that it differentiates between the activities of different pigments. The preliminary investigation reported next seeks to determine if the method could be extended to PVC. The experiments were needed to test whether the sensitivity of the CO_2 method is sufficient to give a significant signal *i.e.* any difference in CO_2 evolution between different PVC samples can be detected. Studies are therefore reported below for 5 PVC samples, which were unpigmented; filled with the rutile form of TiO_2 (R1 and R3 which are the same pigments as used in the PE films); and in some, but not all samples, are filled with $CaCO_3$, as shown in table 2-2. The purposes of the studies were two-fold: firstly to evaluate whether the FTIR gas-phase technique could be extended to distinguish between the differences in the photoactivity of the rigid PVC panels of different compositions, and secondly, to elucidate whether the FTIR CO_2 method was able to test the gas phase HCl signal from the volatile production of photodegradation of PVC samples. The same glass cell used for polyethylene films described in Chapter 2 was employed, and a moist oxygen atmosphere was developed in the cell as described in section 2.5.6. The PVC samples were cut as 11.5 mm diameter discs.

Carlsson *et al* [4, 5] reported that a wide array of chloroorganic and organic compounds is released from both naturally weathered and artificially exposed PVC construction materials (siding panels for exterior cladding). Species directly evolved during ultraviolet (UV) exposure were trapped and concentrated in sorbents, then desorbed for analysis by gas chromatography with electron capture (GC-EC) or mass spectrometry (GC-MS) detection. The accumulated HCl emission was measured by conductometry. Compared to this technique, the CO_2 method utilizes the high extinction coefficient of CO_2 in the infrared region to evaluate the photoactivity of different formulations of PVC. Other volatile organic species are negligible. The same idea using CO_2 evolution to assess TiO_2 pigmented PVC coating photodegradation was used by Searle and Worsley [6]. They used a specially developed irradiation cell and a circulatory system connected to an FTIR spectrometer, and showed that it is possible to evaluate both the kinetics and chemical mechanism of the PVC photodegradation.

6.2 EXPLORATION AND REPRODUCIBILITY CHECK FOR PVC-U SAMPLE PVC 1

The sample PVC 1 was rutile R1 pigmented (3 phr) PVC sample. It also contains 6 phr $CaCO_3$ filler. The TiO_2 pigment of R1 acts as a pro-degradant in polyethylene film (see section 4.2.2) as seen when its CO_2 emission was compared to that for unpigmented PE film. The experiments were carried out in order to explore the sensitivity of the CO_2 method to the degradation of the PVC samples, and to check experimental reproducibility. The sample was placed in the back position in the cell. Degradation of a PVC 1 under moist atmosphere with AM0+AM1.5 filtered UV irradiation was investigated. Duplicate sample results are shown in Table 6-1. The numbers in brackets give the relative humidity of the cell when the experiment took place.

Table 6-1 The CO_2 band intensity after 180 minutes irradiation and values for the intensity of the water vapour band near 1557 cm^{-1} for PVC-u PVC 1 sample

Run	CO_2 band intensity / 10^{-4} a.u.	Water vapour band intensity / 10^{-4}a.u.	Atmosphere
1	57	1208 (84 %)	Moist O_2
2	53	1100 (75 %)	Moist O_2
Average	55	1154	

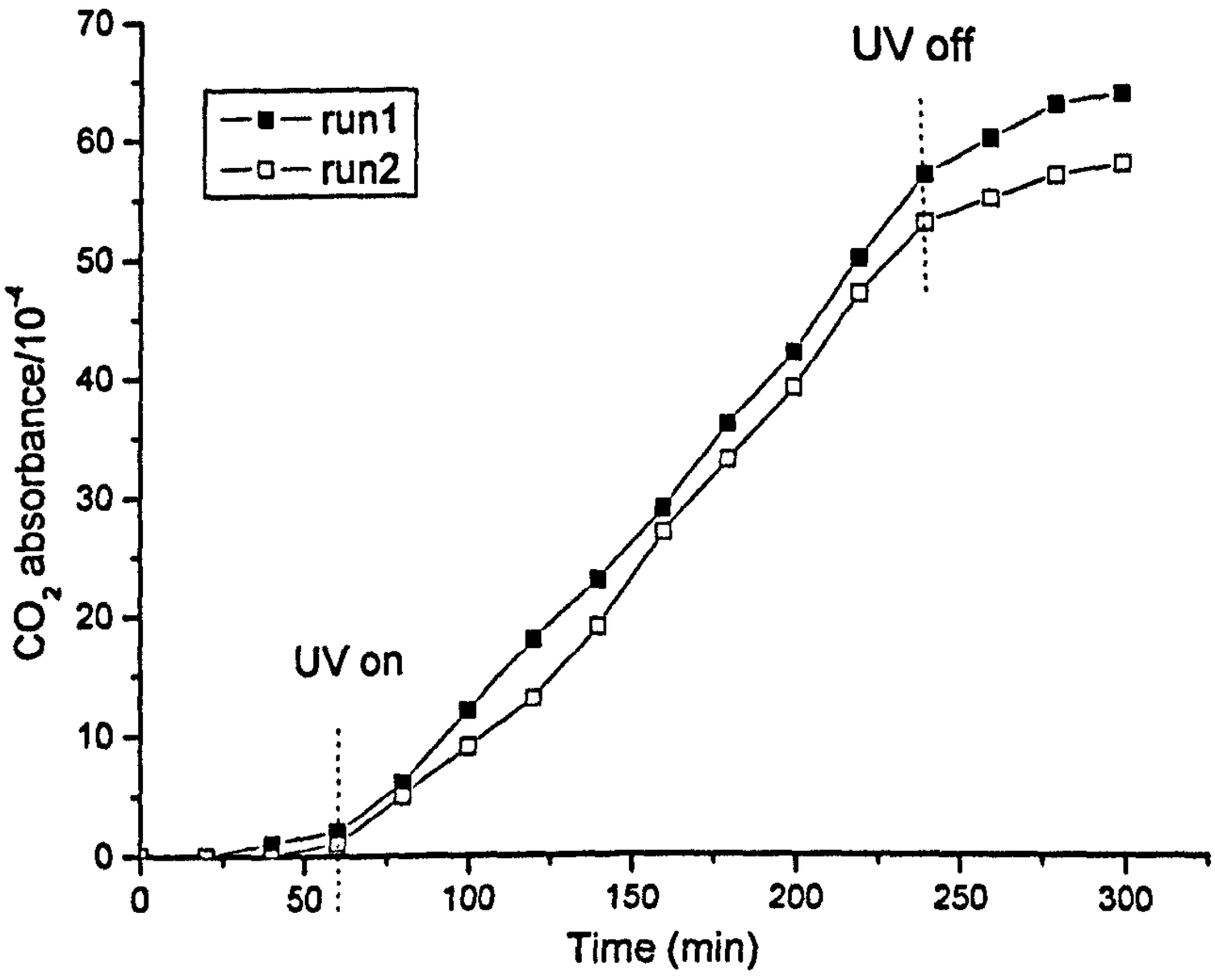

Figure 6-1 The infrared absorbance of gaseous CO_2 before, during and after UV irradiation of duplicate PVC 1 samples (different samples were taken from the same PVC sheet).

Figure 6-1 shows the typical results for the evolution of CO_2 from rigid PVC sample PVC 1. There is little apparent evolution of carbon dioxide in the dark (The small CO_2 growth in the dark is attributed to the temperature increase in the FTIR instrument chamber). As soon as the samples were exposed to UV light, CO_2 was evolved and the carbon dioxide bands increased during UV irradiation. The rate of CO_2 evolution was almost constant during the course of the UV irradiation. The experiments show a good reproducibility for two duplicate runs. The two duplicated experiments gave a rate of CO_2 evolution of 57 a.u. and 53 a.u. in the 3 hours irradiation. It is evident that the CO_2 method can probably be extended to use to test the photoactivity of rigid

PVC samples pigmented with rutile pigment R1. One aspect of the behaviour of PVC-U was unlike that of PE film. When the UV light was switched off after 3 hours irradiation, the PE sample carbon dioxide bands stopped increasing immediately; for the PVC-U sample PVC 1 it can be seen that the carbon dioxide bands continued increasing during the dark, but the evolution rate was lower than when the sample was illuminated with UV light.

However no HCl absorbance peaks were observed in the FTIR spectra during 3 hours UV irradiation. It seems that gaseous CO peaks were observed in FTIR spectra recorded during 3 hours UV exposure (see figure 6-2), but the CO peak around 2143 cm^{-1} did not keep stable during the photoreaction stage. The CO peaks are suitable to monitor the ability of photodegradation of PVC. These results are consistent with previous studies by Cho and Choi [7]. They monitored the volatile products that evolved from the degrading PVC film during UV irradiation by using a FT-IR gas cell. A small amount of CO and trace hydrocarbons that were evidenced by the C–H stretching peaks around 3000 cm^{-1} were also observed. No sign of HCl production could be seen even though it is a well-known main product of thermal and direct photolytic degradation of PVC [4].

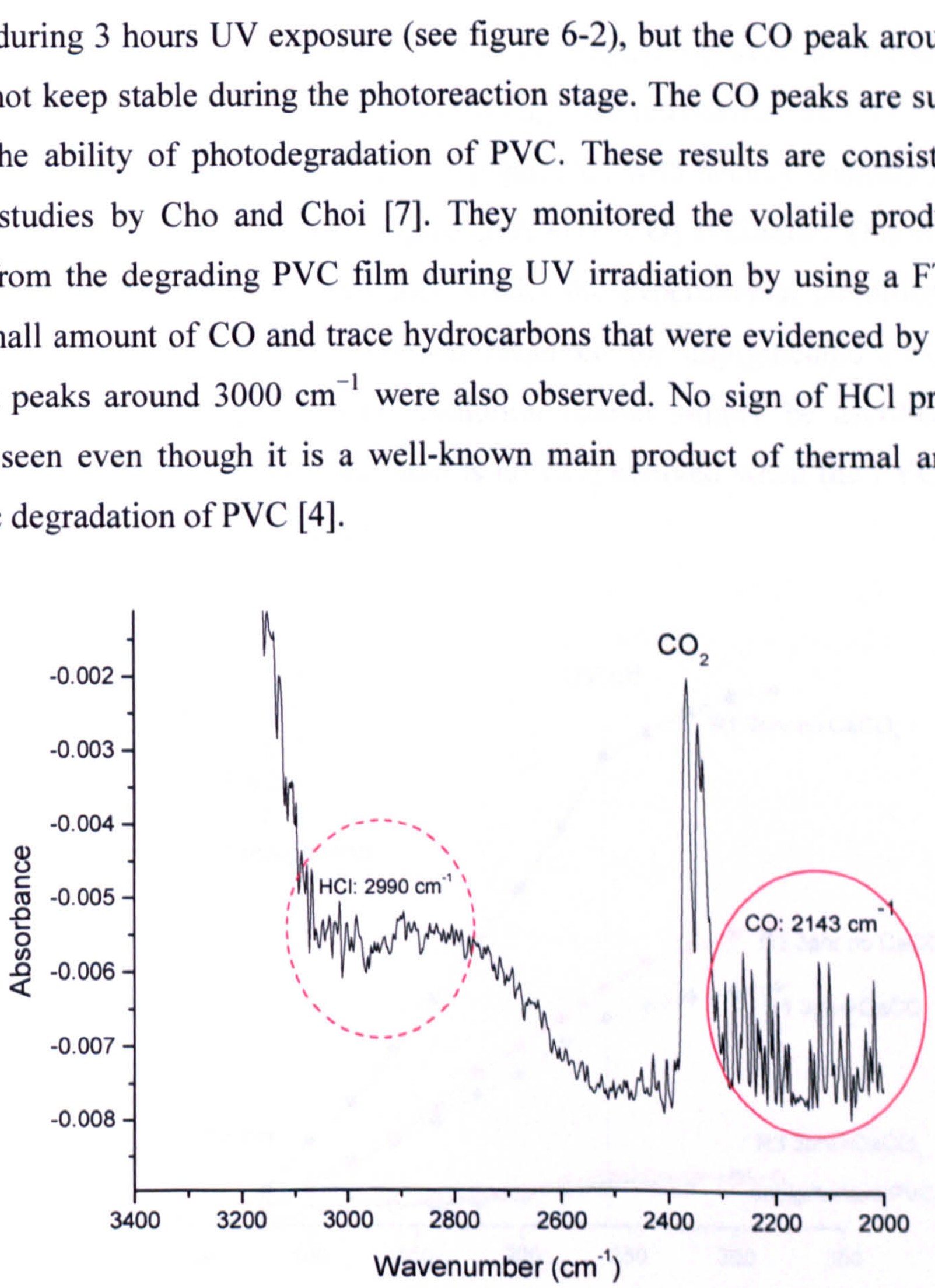

Figure 6-2 FTIR gas-phase spectra observed after 3 hours UV irradiation with PVC sample PVC 1.

6.3 CO_2 EVOLUTION WITH FIVE PVC SAMPLES

Figure 6-3 shows the CO_2 production profiles due to the UV-induced oxidation obtained for the five PVC samples (see in Chapter 2, table 2-3). As can be seen from figure 6-3, the CO_2 method was able to differentiate between them but two of the PVC samples, PVC 3 and PVC 5, were found to have no significant CO_2 evolution under the experimental condition. The intensity of CO_2 bands measured with these two samples is the same as the CO_2 background level.

The FTIR gas-phase technique was unable to distinguish between the photo-activity of these two PVC samples. It was unsurprising and reassuring, as PVC 3 was an unpigmented PVC sample and PVC 5 was pigmented with heavily coated rutile TiO_2 (R3). The R3 pigmented PE film also gave quite slow CO_2 evolution. This shows that R3 pigment always protects the polymer. Under the experimental condition used in these experiments, no CO_2 evolution was observed for unpigmented PVC sample either. Therefore the negligible CO_2 evolution cannot simply be ascribed to UV absorption. It can be concluded that there is no CO_2 evolved when the PVC samples contains protected rutile pigment R3.

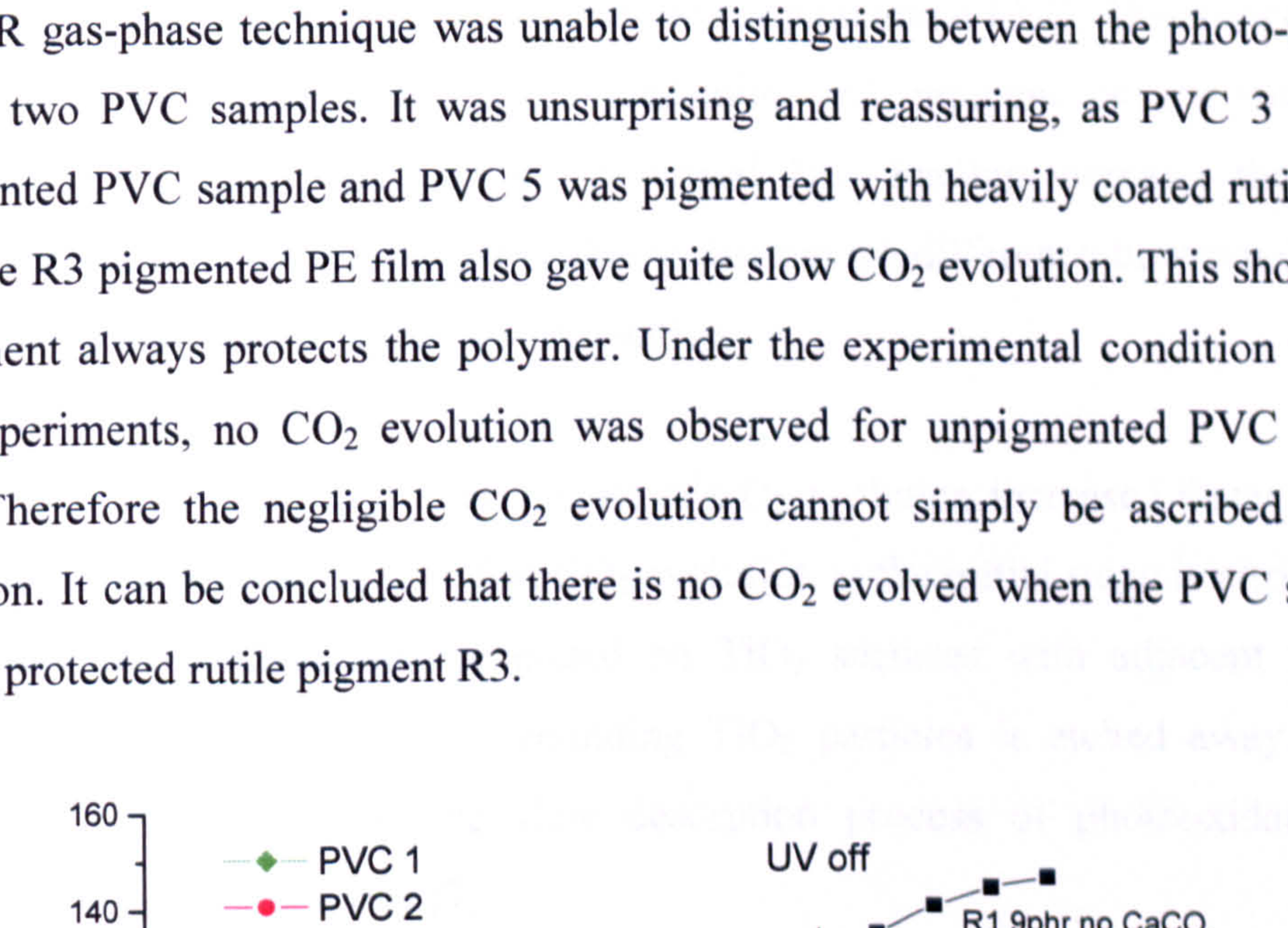

Figure 6-3 CO_2 evolution from the photo-oxidation of five PVC-u samples.

PVC sample, PVC 4, was observed to be the most photoactive of the PVC disc with an average CO_2 band intensity of 124×10^{-4} a.u. after 180 minutes UV irradiation. The PVC 4 PVC sample was pigmented with 9 phr R1 pigment which is lightly coated with Al_2O_3 (see section 2.2) and normally shows pro-degradation activity. The second most active was the PVC 2 disc with 3 phr R1, giving a CO_2 evolution ca. 65×10^{-4} a.u. after 180 minutes UV irradiation. Neither of these samples contains $CaCO_3$ filler. The PVC 1 sample is pigmented the same as PVC 2 with 3 phr R1 but contained 6 phr $CaCO_3$ filler, giving a little smaller carbon dioxide evolution than the PVC 2 sample.

There is small and neglected CO_2 evolution for unpigmented PVC. This suggests that all of the CO_2 evolution for PVC containing R1 pigment is attributable to photocatalytic reaction caused by R1. Increased TiO_2 loading increases the carbon dioxide evolution. The CO_2 method is able to distinguish difference between different loading and different filler under UV irradiation.

It can be seen from Figure 6-3 that the rate of CO_2 evolution increased faster near the beginning of UV irradiation. The fast CO_2 evolution at the initial stage is attributed to the reaction of photooxidants generated on TiO_2 surfaces with adjacent polymer chains. As the polymer matrix surrounding TiO_2 particles is etched away, further oxidation should depend on the slow desorption process of photooxidants with decelerated CO_2 evolution rate [7].

6.4 HUMIDITY EFFECT ON UV DEGRADATION OF PVC 4

In contrast to some other polymeric materials, moisture is reported not to be an important factor for unpigmented PVC [1]. The underlying chemical reactions are the formation of carotinoid polyenes from intrinsic defects by elimination of HCl, and their oxidation *via* allyl peroxy radicals, breaking residual C–C bonds [8-10]. When PVC was pigmented with TiO_2, the degradation of the PVC occurred by photo-catalysed oxidation. The moisture becomes an important factor because it affects the rate of photocatalytic degradation of PVC. In order to assess the effect of humidity on CO_2 evolution under UV irradiation, the method used was the same as for PE films to

get different humidity atmospheres. Results are shown in Figure 6-4. The experiments used the same UV intensity and with AMO + AM1.5 filtered UV light.

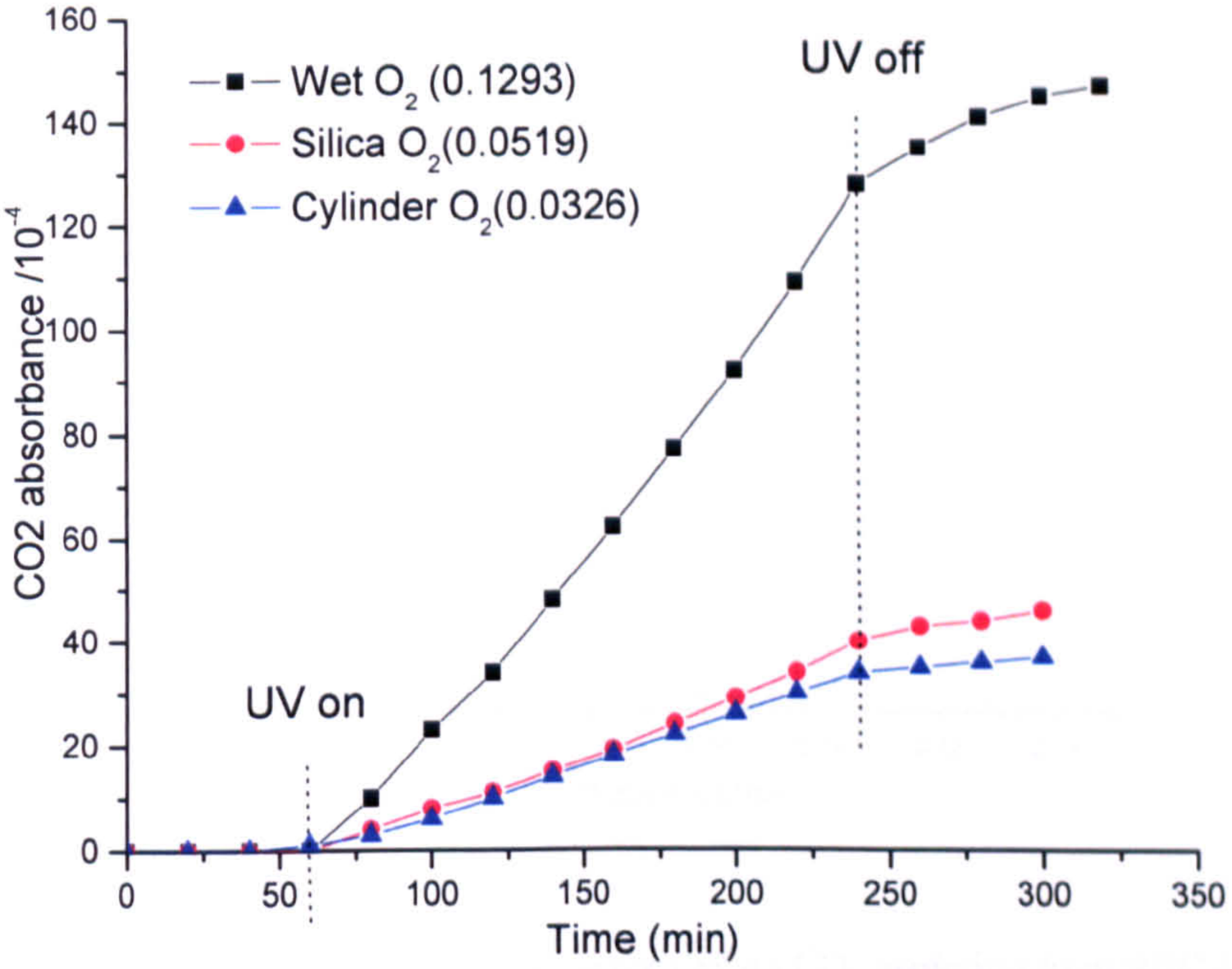

Figure 6-4 Carbon dioxide evolution in different humidity atmospheres from PVC 4 (9 phr R1) samples.

It can be clearly seen from Figure 6-4 that the rate of carbon dioxide generation is sensitive to humidity in the presence of oxygen atmosphere for PVC 4 sample. The minimum water peak height, corresponding to residual water in the spectrometer chamber, was consistently ~ 100×10^{-4} a.u., but the value of 300×10^{-4} a.u. was obtained after the cell had been purged with essentially water free cylinder oxygen and was then equilibrated overnight. It seems that the humidity bands are lower with PVC samples than with polyethylene samples (see section 4.4.1) which are normally higher than 600×10^{-4} a.u.. This difference is probably attributed to different water absorption in the PVC samples.

Carbon dioxide generation is greatest in the presence of wet oxygen. Figure 6-4 gives the data for PVC 4 showing a clear reduction in the rate of CO_2 evolution under UV with decreasing humidity. The absorbance rates for PVC 4 are replotted against H_2O peak height in Figure 6-5 and demonstrate that it is essential to control humidity if

reproducible comparative experiments are to be made by monitoring the carbon dioxide produced during UV degradation.

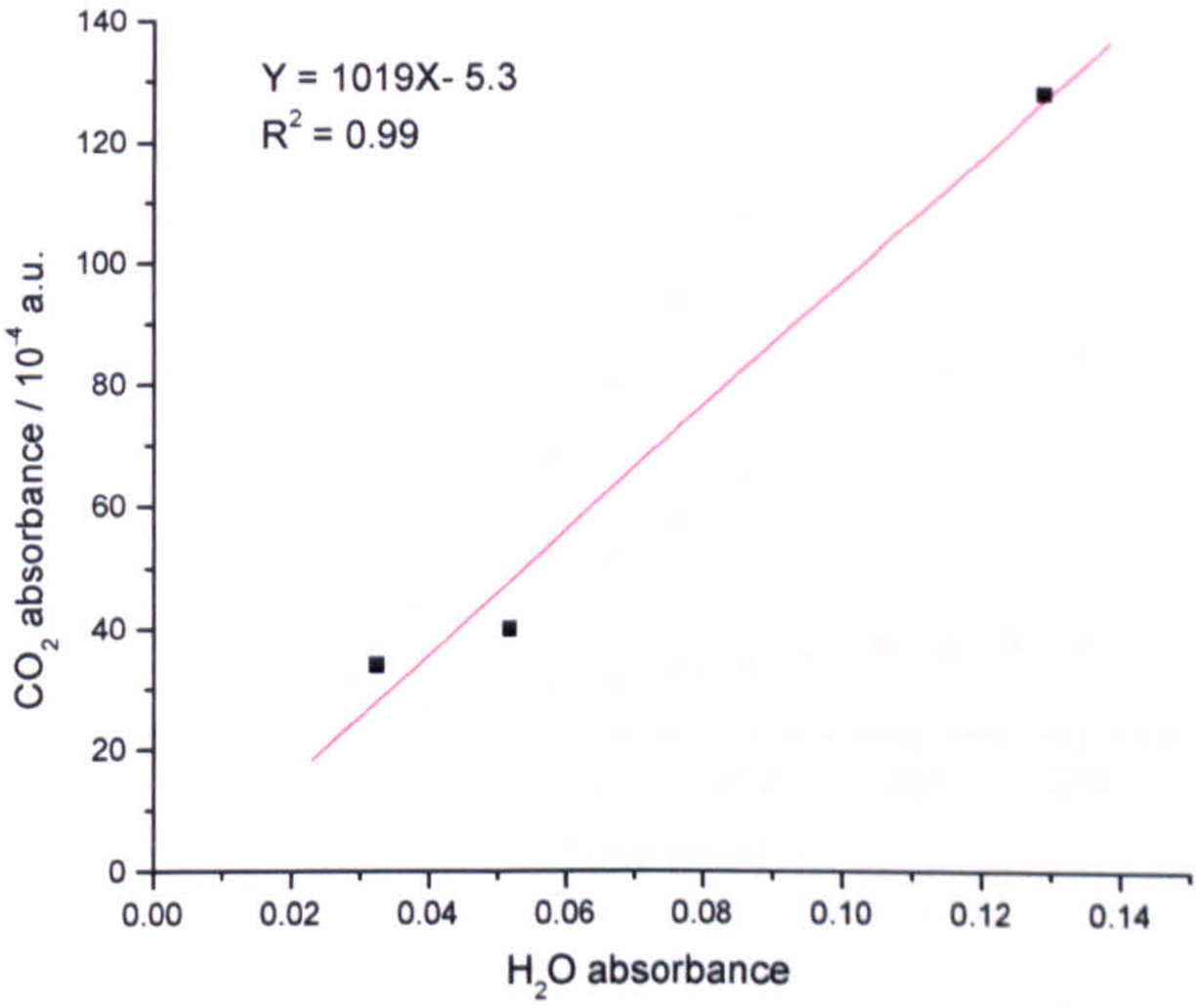

Figure 6-5 The effect of varying humidity in the cell on CO_2 evolution from PVC 4.

6.5 EFFECT OF OXYGEN CONCENTRATION

PVC may degrade thermally as well as photochemically or photocatalytically, and solar irradiation (UV light and heating effect) and oxygen from the atmosphere may trigger both mechanisms [1]. The oxygen and UV light are essential factors in both direct photochemical and indirect photo-catalysed oxidation on polymer systems. The oxygen concentration was expected to play an important role in the reaction. The effect of reducing the oxygen concentration was therefore investigated first by purging with a 20/80 v/v O_2/N_2 mixture and or by purging with N_2 alone to get different oxygen concentration atmospheres. All gases were bubbled through de-ionised water. Table 6-2 shows the results of CO_2 evolution from these three different atmospheres and was plotted as the function of time in Figure 6-6.

Table 6-2 Effect of oxygen concentration on CO_2 evolution

Experiment	Atmosphere	CO_2 absorbance /10^{-4}
1	O_2	124
2	20/80 O_2/N_2	63
3	N_2	15

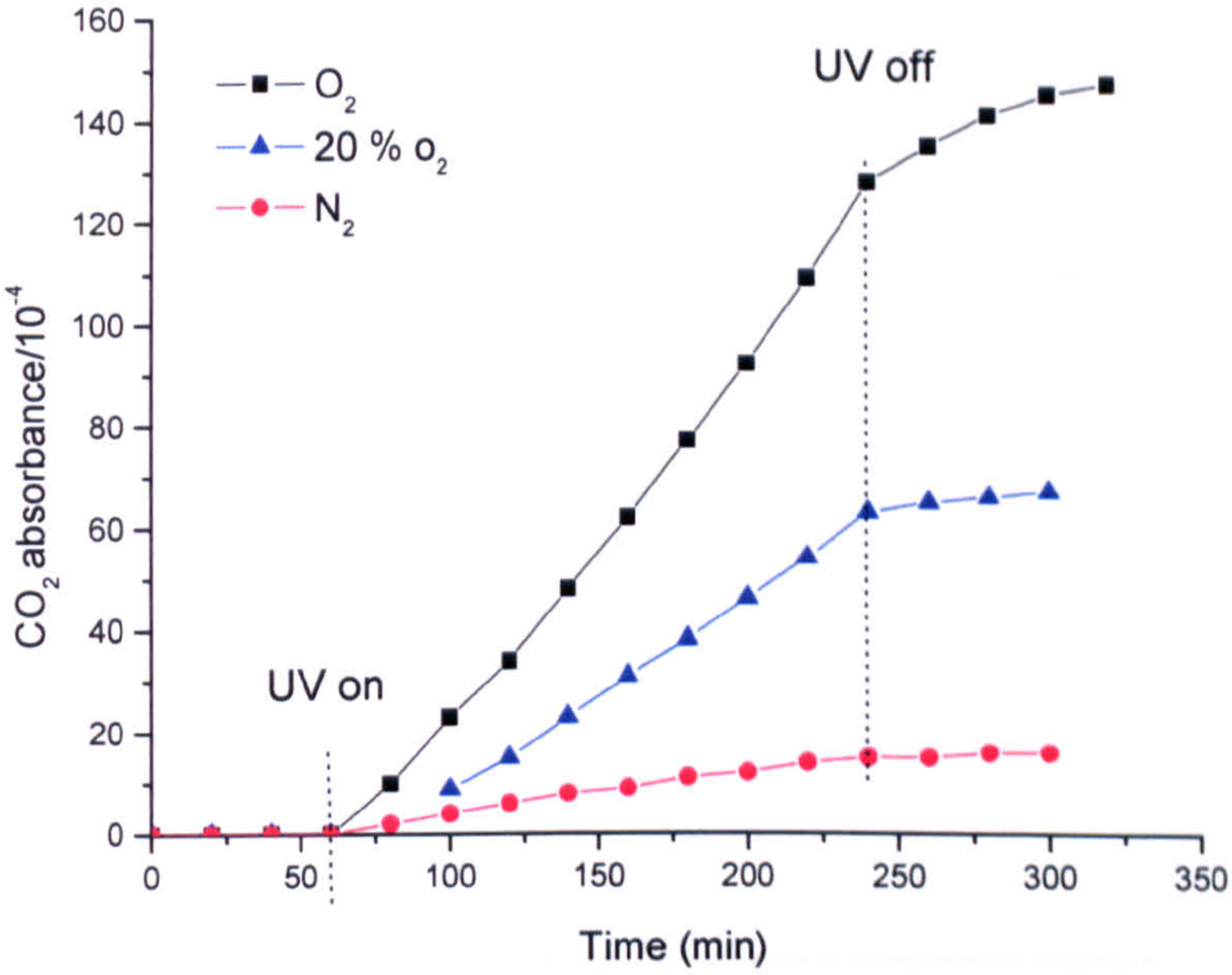

Figure 6-6 Carbon dioxide evolution in different oxygen concentration atmospheres from PVC 4 sample.

It can be seen from Figure 6-6 there was a strong effect on the rate of CO_2 evolution of different oxygen concentrations. With pure oxygen, the CO_2 concentration was raised to 124×10^{-4} a.u. after 3 hours UV irradiation. Wet nitrogen gave the lowest rate of CO_2 emission which was almost equal to the background CO_2. The rate of CO_2 evolution was intermediate, 63×10^{-4} a.u., for the 20:80 volume % O_2:N_2 mixture. It is evident that for the PVC sample containing R1 pigment, a clear reduction in the rate of CO_2 evolution under UV was observed with decreasing oxygen concentration.

The CO_2 evolution of 15×10^{-4} a.u. after 3 hours UV irradiation with AM0+AM1.5 filters for PVC 4 (9 phr loading) was measured with nitrogen. It is very much less than that CO_2 evolution from polyethylene film (5 phr pigment) which has lower pigment loading. This may be the result of the low absorption of oxygen in the PVC matrix. A special observation in UV degradation of the PVC 4 with N_2 was that the exposed sample area became grey. This phenomenon was not observed in UV degradation experiments with any pigmented polyethylene. The phenomenon may be probably caused by UV light inducing the redox reaction of $Ti^{4+}+ e^{-}\rightarrow Ti^{3+}$. If little

oxygen absorbs in the PVC matrix there would be little driving force for $Ti^{3}+ + O_2 \rightarrow Ti^{4+} + O_2^{-}$.

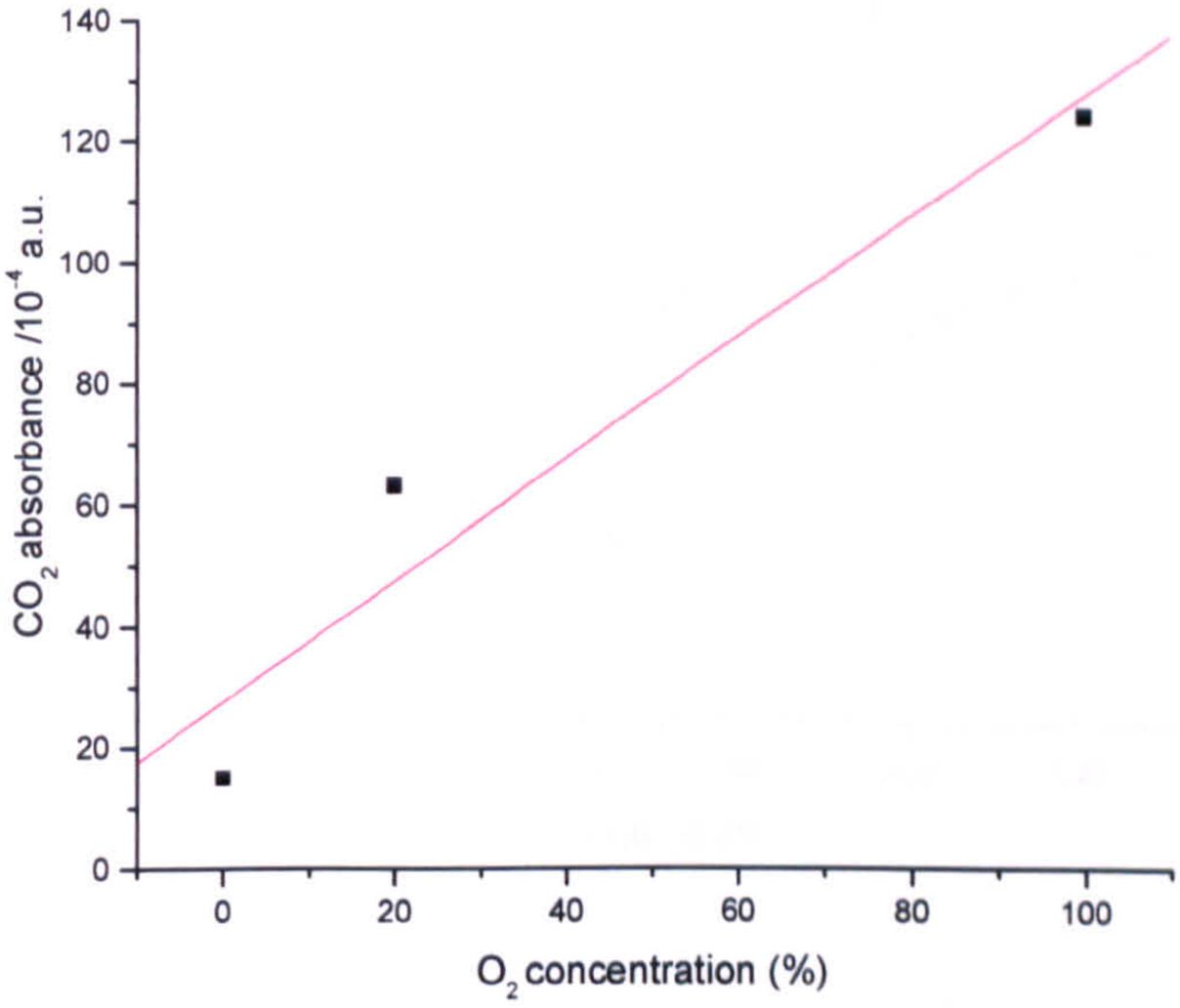

Figure 6-7 CO_2 absorbance rate against O_2 concentration in the cell for PVC 4.

6.6 EFFECT OF PIGMENT CONCENTRATION ON CO_2 EVOLUTION

The PVC 2 was the sample containing R1 pigment with 3 phr loading and PVC 4 was the sample containing R1 pigment with 9 phr loading. Figure 6-8 shows the effects of the different pigment concentrations on CO_2 evolution under UV irradiation.

The results clearly show a dramatic increase in CO_2 evolution with increasing TiO_2 pigment loading. With 3 phr pigmentation of sample PVC 2, the accumulated CO_2 concentration was *ca.* 65×10^{-4} a.u. after 3 hours UV irradiation. When the pigmentation increased to 9 phr in the sample, the accumulated CO_2 concentration increased to 124×10^{-4} a.u. after 3 hours UV irradiation. If the background level of CO_2 absorbance 12×10^{-4} a.u is subtracted from the different results. For the corrected data are (0, 3); for 3 phr R1 pigment loading PVC is (3, 53) and 9 phr is (9, 113), where (x, y) denotes the rate of CO_2 evolution corresponding to x phr TiO_2.

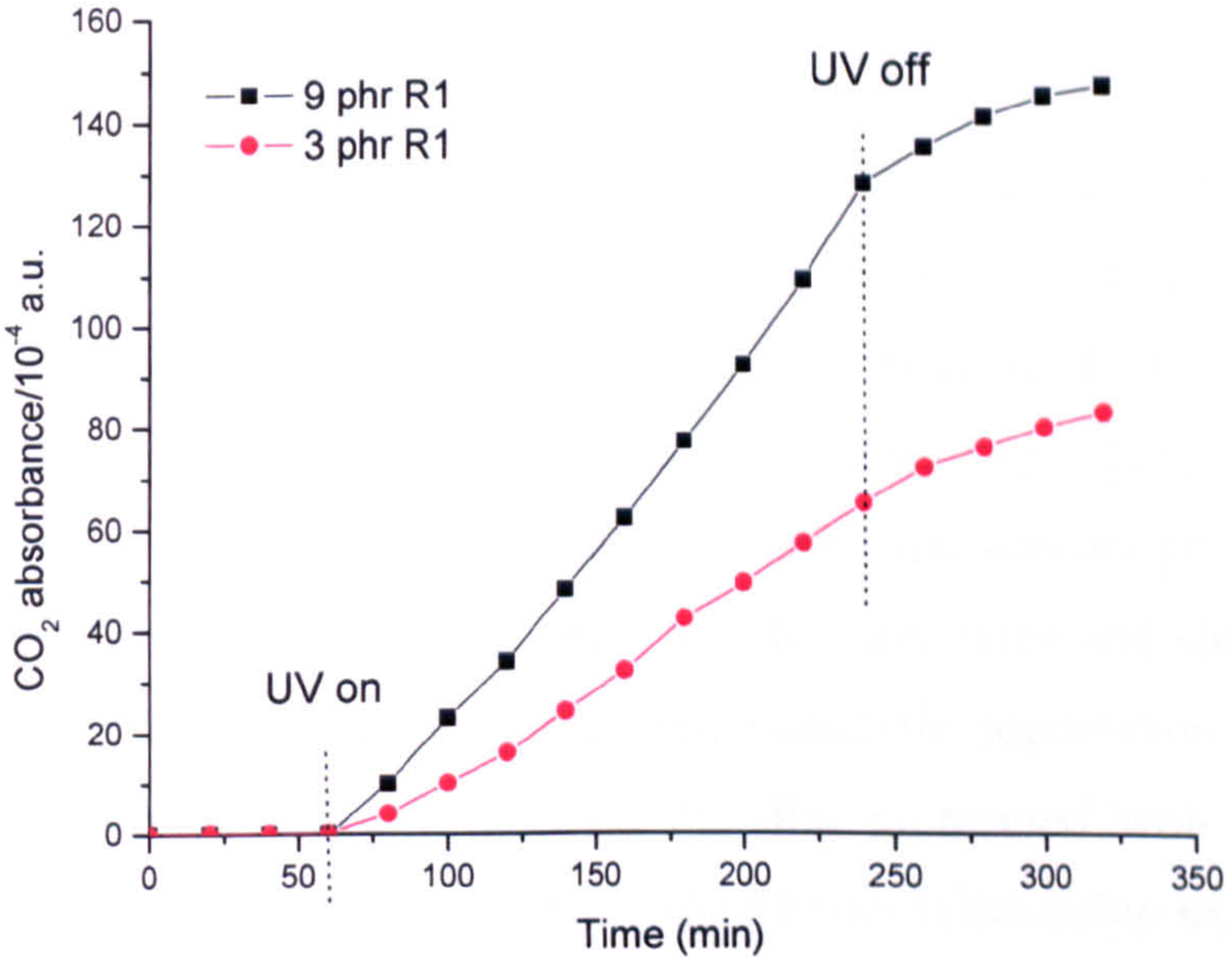

Figure 6-8 Pigment loading effect on CO_2 evolution in UV degradation.

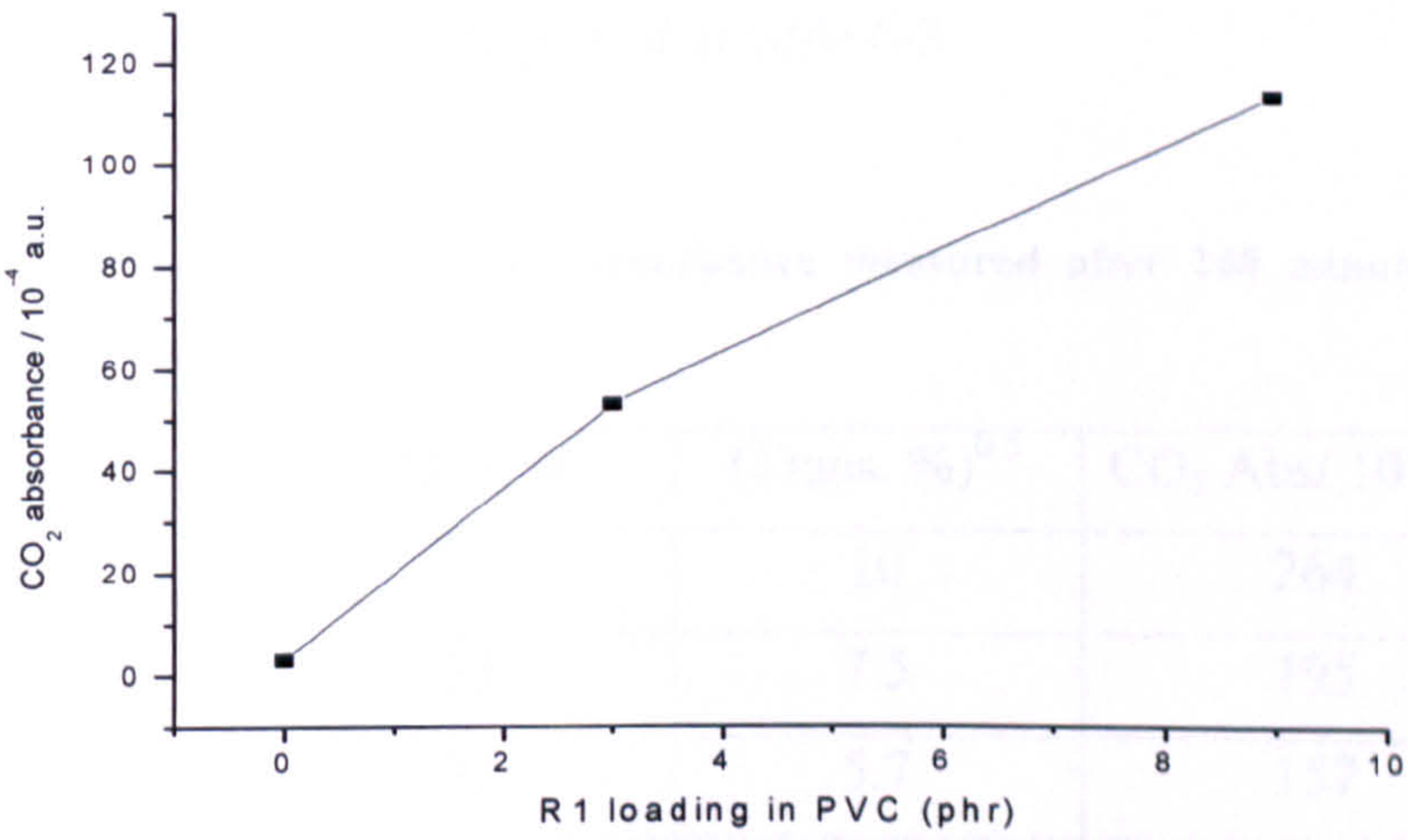

Figure 6-9 CO_2 evolution as the function of TiO_2 (R1) loading.

Surprisingly, near linear relationship was obtained as between the rate of CO_2 evolution and the TiO_2 loading. At high loadings of CO_2 evolution decreased slightly probably because of the TiO_2 screening effect.

6.7 DEPENDENCE OF CARBON DIOXIDE EVOLUTION RATE ON UV INTENSITY

As described in section 6.3, no photochemical reaction occurred for unpigmented PVC samples. For photocatalytic reaction, a CO_2 evolution proportional to the square root of UV intensity is explained by the effective concentration of holes or of radicals being controlled by recombination processes. An earlier paper [11] by this group described the study of the effect of irradiation intensity and wavelength on the photo-oxidative formation of carbon dioxide from acrylic paint films and showed that the square root relationship was obeyed for the photocatalytic degradation of a practical paint film. Also similar measurements on PE film pigmented with anatase TiO_2 described in section 4.5.2, demonstrated the square root relationship existed between CO_2 evolution and UV intensity.

Experiments therefore were carried out to test whether the rate $\propto I^{0.5}$ relationship was obeyed by PVC. The results are displayed in table 6-3.

Table 6-3 Table showing the CO_2 absorbance measured after 240 minutes irradiation under different UV intensities.

Sample	Trans. %	(Trans. %)$^{0.5}$	CO_2 Abs/ 10^{-4}a.u.
PVC 4	100	10	264
PVC 4	55	7.5	195
PVC 4	33	5.7	157
PVC 4	7	2.7	78
PVC 4	0	0	9

The UV intensity was varied using neutral density filters. The sample selected was PVC 4 because it gives the most CO_2 evolution. Figure 6-10 shows the effect of changing UV intensity on carbon dioxide evolution from R1 pigmented (9 phr) PVC samples.

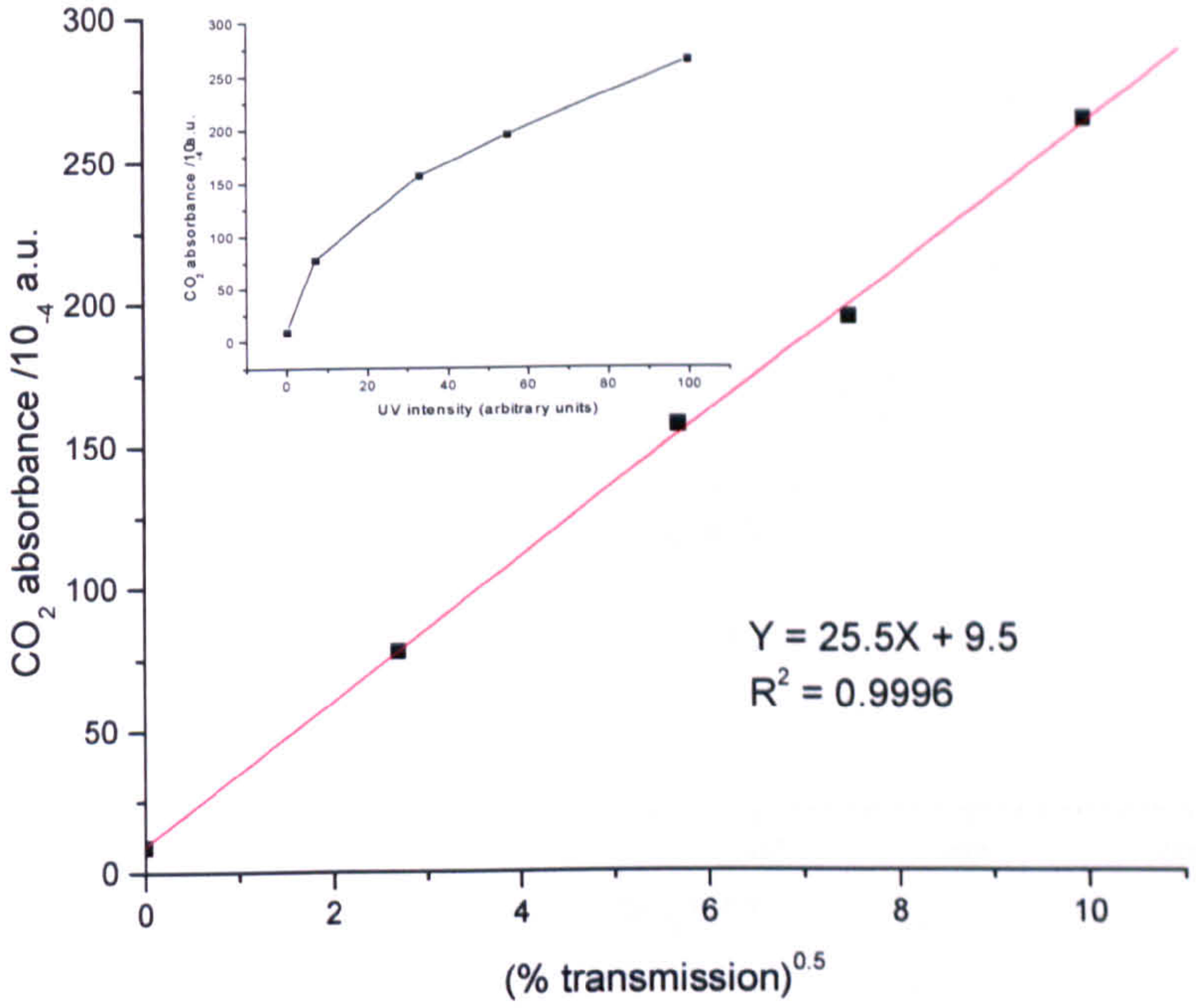

Figure 6-10 CO_2 evolution after 240 minutes irradiation from PVC 4 as a function of variation in incident UV intensity.

It can be seen from the Figure 6-10 that the linear relationship between the rate of carbon dioxide evolution (UV intensity)$^{1/2}$ is obeyed and that therefore the degradation rate varies as the square root of the intensity of the incident radiation. Also in Figure 6-10 the best fit line can be extrapolated to cut the y-axis, with the intercept equal to the background carbon dioxide.

6.8 THE EFFECT OF FILTERS

The solar filters were employed in order to modify the spectral distribution of the arc lamp to simulate specific natural solar conditions. Two filters were used. When the filter combination is charged box, both UV intensity and wavelength are changed. The details are described in Chapter 2. The intensities of UV distribution with AM0+AM1.5, AM1.5 only and with no filter were shown in figure 4-31. Figure 6-11 and Figure 6-12 show the effect of filters on CO_2 evolution from PVC 1 and PVC PVC 5, respectively.

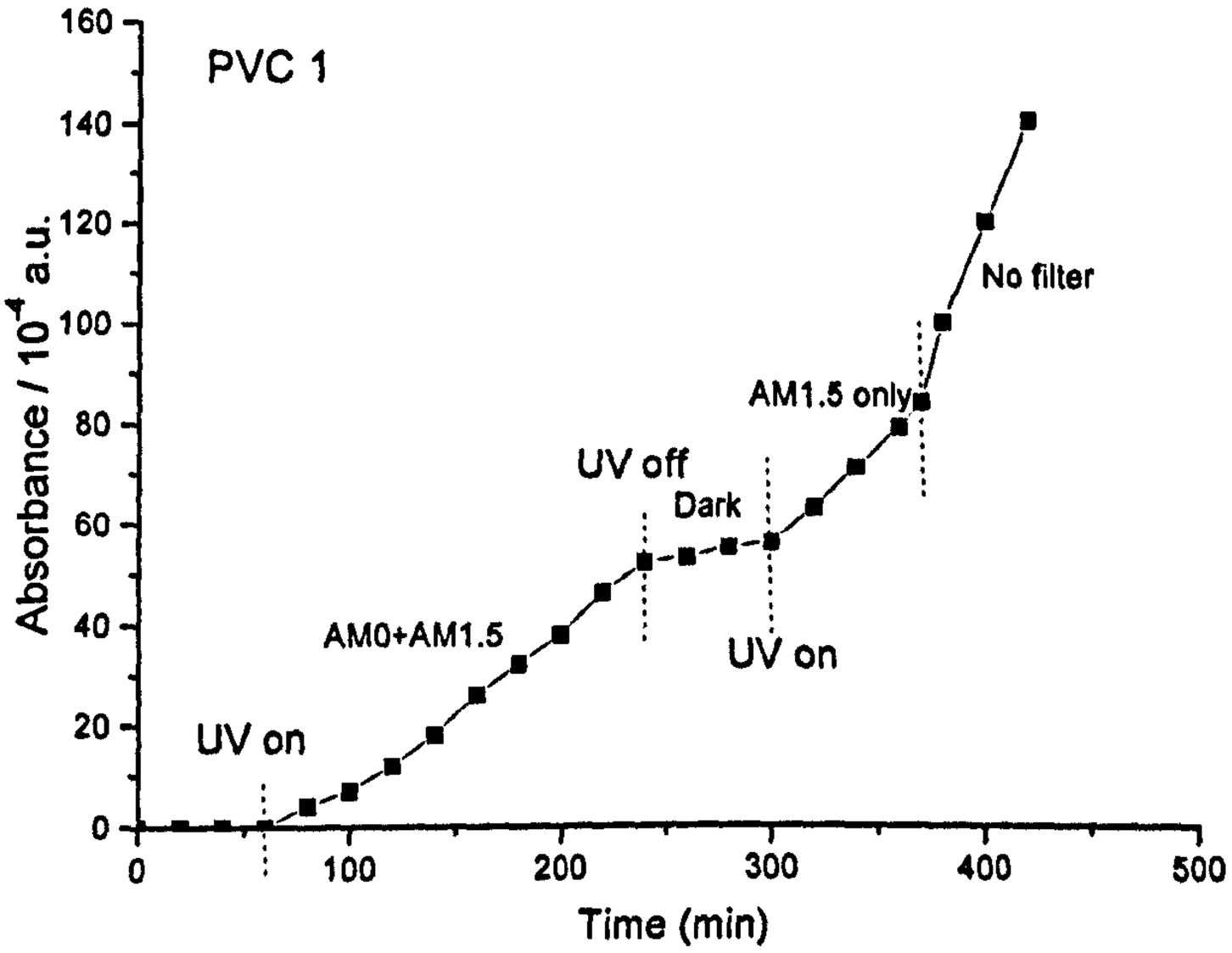

Figure 6-11 The effect of the AM filters on CO_2 evolution for PVC sample PVC 1.

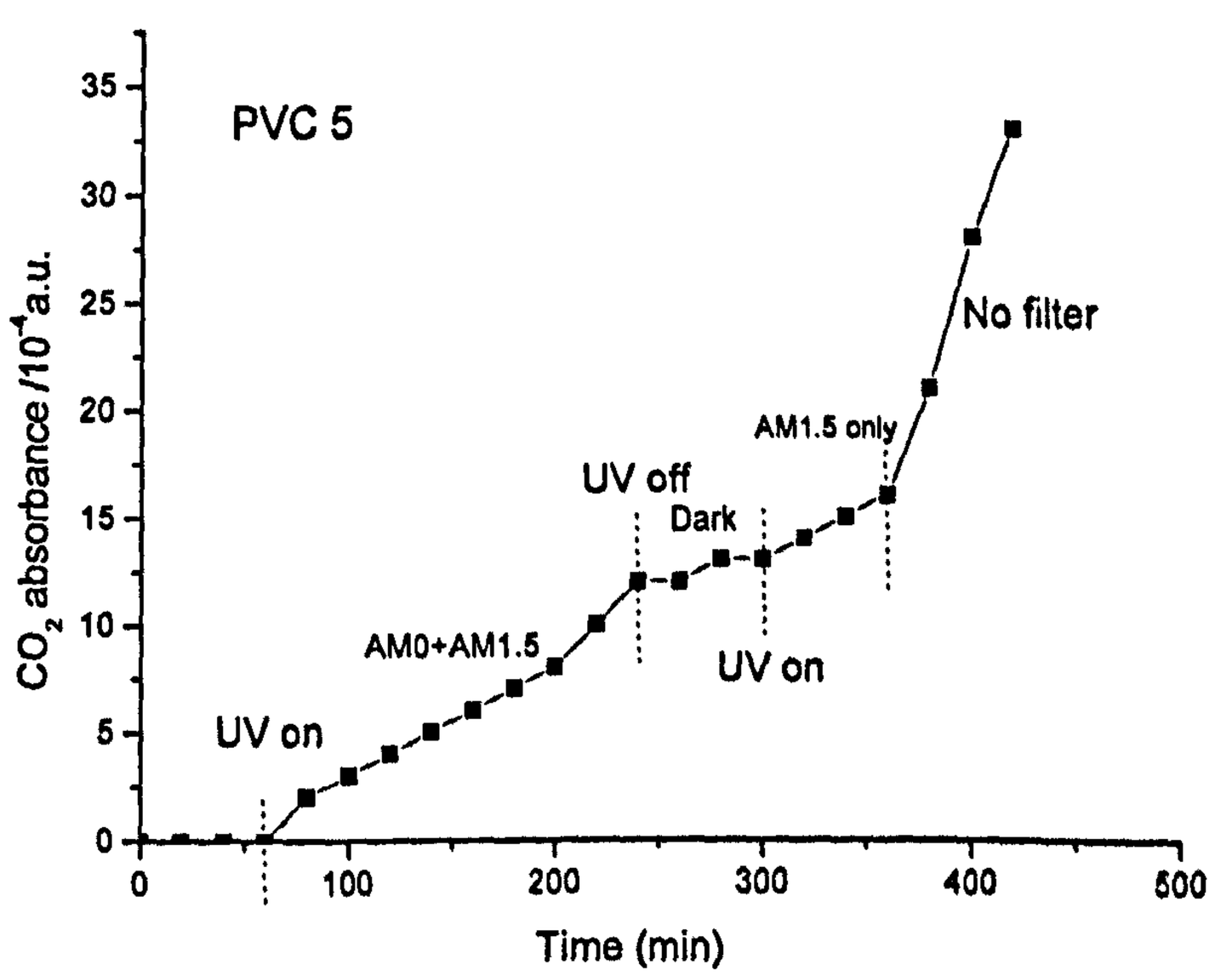

Figure 6-12 The effect of the AM filters on CO_2 evolution for PVC sample PVC 5.

Figure 6-11 shows a set of measurements of CO_2 evolution for the R1 pigmented sample — PVC 1 when using different filters. The CO_2 evolution of 14 a.u. per hour was observed when using AM0+AM1.5 filtered UV light. As described above, this

CO_2 evolved is attributed to photocatalytic reactions caused by R1 because no photochemical reaction occurred with two filters used in combination. On switching off the UV source after 3 hours irradiation, the rate of increase in CO_2 concentration fell. The small CO_2 emission in the dark may be the result of residual radical reactions continuing after UV was switched off.) There is a clear increase in rate of CO_2 evolution to 23 a.u per hour from PVC 1 when using the AM1.5 filter only to modify the Xenon lamp output. When using unfiltered UV light the rate of CO_2 emission was enhanced again to 56 a.u. per hour giving the greatest value CO_2 evolution.

Figure 6-12 shows a similar set of measurements for the R3 pigmented PVC panel. When using UV filtered by both AM0+AM1.5 filters, there is no significant CO_2 evolution from the PVC *i.e.* the level ~15 a.u. after 3 hours. When using AM1.5 filter only in the filter box, the same rate of CO_2 evolution as for the AM0+AM1.5 combination was observed. This suggests that with the AM0 filter out, shorter wavelength irradiation was provided and the UV intensity increase was not enough to induce photochemical reaction or photocatalytic reaction for the R3 pigment which has very low photocatalytic activity. However, it is clear that CO_2 evolution was observed from PVC 5 when using unfiltered UV light irradiated onto the sample, which gave a larger proportion of short wavelength and stronger UV intensity compared to filtered UV light. This may suggest that unfiltered UV light is strong enough to induce in the PVC sample direct photochemical reactions even with strongly protecting TiO_2 pigment (R3).

It can be concluded that even when the AM0 filter was taken out from the filter box, giving more short wavelength UV light, this was not enough to induce CO_2 evolution for R3 pigmented PVC. This is consistent with work reported by Gesenhues [1] 'in dry irradiation, the photooxidation of PVC comes to a standstill when the irradiation intensity is reduced by only 50 %'. With unfiltered UV light, the UV intensity was strong enough to induce photodegradation in R3 pigmented PVC giving CO_2 evolution under UV irradiation. It also suggests a complex relationship exists between CO_2 evolution and UV wavelength or intensity for PVC.

6.9 DISCUSSION

The CO_2 method for the study of photo-degradation of poly (vinyl chloride) was shown to have some limitation when two filters were used in combination. There was no significant CO_2 emission for the unpigmented PVC and the sample with durable TiO_2 pigment (R3). However, it allows elimination of the photochemical reaction from the whole results, and puts the focus only on photocatalytic reaction. It is clear from these preliminary studies that the method could be convenient to study the influence of pigments, pigment loading and other factors on photodegradation. The rate of CO_2 evolution was found to increase both with humidity and with the oxygen content. Because it is relatively easy to assess the effect of changing the spectral distribution in the UV illumination source, the method can be developed to study durable PVC samples. The results of Figure 6-11 illustrate that the FTIR method can monitor the CO_2 evolution in R3 pigmented PVC sample when they are irradiated with an unfiltered Xe UV light.

The results in Figure 6-3 also show that evolutions of carbon dioxide from UV irradiated PVC— PVC 1 and PVC 2 were slightly affected by $CaCO_3$ filler. As expected the $CaCO_3$ filler reduced CO_2 evolution compared to unfilled PVC with $CaCO_3$ filler. One reason is probably that the $CaCO_3$ filler scattered some UV light to reduce the efficiency of TiO_2 pigment absorption.

In section 2.5.7, 10^{-4} a.u of CO_2 is calculated to equal 0.41 μm CO_2 gas fill in the cell used in these experiments. For the most CO_2 evolution sample, PVC 4 gave 124×10^{-4} a.u CO_2 evolution in 3 hours UV irradiation. After correcting for a CO_2 background of 12×10^{-4} a.u , the CO_2 evolution from PVC is 112×10^{-4} a.u equivalent to 46 μg = 4.6×10^{-5} g CO_2 evolution from the PVC sample in 3 hours UV irradiation. The 4.6×10^{-5} g CO_2 includes 1.255×10^{-5} g carbon atoms. It is equal to 3.27×10^{-5} g pure PVC degraded in 3 hours UV irradiation assuming that two CO_2's comes from one CH_2 unit, and one CHCl. This is equivalent to the removal of 1.45 μm thickness from the PVC surface. The PVC sample weight was *ca.* 0.212 g. The pure PVC is 0.212× 100/123= 0.172 g in this sample. Assuming this rate of photodegradation can be maintained until the whole of the PVC consumed, the time needed is $0.172/1.255\times10^{-5}\times3 = 41201$ hours *i.e.* 4.7 years full 24 hours per day irradiation. Alternatively, using

the hypothesis that there is 6 hours effective irradiation on the sample per day, the PVC needs 18.8 years to be degraded completely.

Worsley and Searle (W&S) [12] described a new testing procedure that enables a rapid assessment of TiO_2 photoactivity to be made. The ability to study reaction via the FTIR monitoring of the headspace CO_2 concentration provide quick and simple feedback on the rate of reaction. However, their work has not considered other environmental conditions such as relative humidity and light intensity and as such further research is necessary to quantify their effects. A direct comparison of our results with those of Worsley and searle is not possible because UV light intensity at the film has not been directly measured in either study. If it is assumed that 50 % of W&S's 6 × 8 W is incident on 300 cm^2 of sample area, the intensity per cm^2 is 24/300 = 0.08 W cm^{-2}. If we assume 5 % of Xe lamp output is in the form of UV incident on the disc, the intensity is 6 Wcm^{-2}. It is shown in that the oxidation rate of PVC sample is proportional to $I^{0.5}$. Therefore relative CO_2 emission rates would be $(6/0.08)^{0.5}$ = 8.7. The CO_2 concentration from the W&S would be proportional to (sample area) / whole volume *i.e.* 300/771 = 0.4 cm^{-1}; the CO_2 concentration in this *in-situ* method would be proportional to 0.55/13.7 = 0.04 cm^{-1}. The relative rate between these two method is 8.7 × (0.4/0.04) ≈ 1. Obviously this comparison is only as good as the crude estimates of light intensity but it appears that sensitivity of the two methods is of the same order of magnitude. However, *in-situ* method here is simpler, less subject to leaks and more convenient.

6.10 CONCLUSIONS

The experiments have given a clear picture of the role that pro-degradant TiO_2 pigments play in the photodegradation of PVC. This method can provide a reproducible measurement of the photoactivity of the PVC by amount of carbon dioxide evolution. Even though unpigmented PVC is stated to be not sensitive to water, the CO_2 method showed that the photodegradation of PVC pigmented with active TiO_2 was sensitive to water. The presence of oxygen was essential for the efficient photolytic degradation of PVC and had strong effect on the CO_2 evolution. The photocatalytic reaction rate follows the square root of UV intensity.

6.11 REFERENCES

1. Gesenhues, U., *Polymer Degradation and Stability,* 2000. **68**(2): p. 185-196.
2. Allen, N.S., M. Edge, T. Corrales, A. Childs, C.M. Liauw, F. Catalina, C. Peinado, A. Minihan, and D. Aldcroft, *Polymer Degradation and Stability,* 1998. **61**(2): p. 183-199.
3. Jin, C., T.A. Egerton, J.R. White, P.A. Christensen, and N. MacDonald, *SPE ANTEC2003,* 2003. **49**: p. 1976-1980.
4. Carlsson, D.J., M. Krzymien, D.J. Worsfold, and M. Day, *Journal of Vinyl & Additive Technology,* 1997. **3**(2): p. 100-106.
5. Carlsson, D.J., M. Krzymien, G. Pleizier, D.J. Worsfold, and M. Day, *Polymer Degradation and Stability,* 1998. **62**(3): p. 413-419.
6. Searle, J. and D. Worsley, *Plastics Rubber and Composites,* 2002. **31**(8): p. 329-335.
7. Cho, S. and W. Choi, *Journal of Photochemistry and Photobiology A: Chemistry,* 2001. **143**(2-3): p. 221-228.
8. Skowronski, T.A., J.F. Rabek, and B. Ranby, *Polymer Degradation and Stability,* 1984. **8**(1): p. 37-53.
9. Gaumet, S. and J.-L. Gardette, *Polymer Degradation and Stability,* 1991. **33**(1): p. 17-34.
10. Gardette, J.-L. and J. Lemaire, *Polymer Degradation and Stability,* 1991. **34**(1-3): p. 135-167.
11. Christensen, P.A., A. Dilks, T.A. Egerton, and J. Temperley, *Journal of Materials Science,* 2000. **35**(21): p. 5353-5358.
12. Worsley, D.A. and J.R. Searle, *Materials Science and Technology,* 2002. **18**(6): p. 681-684.

CHAPTER 7

CONCLUSIONS AND POSSIBLE AREAS FOR FUTURE WORK

7.1 MEASUREMENT OF PHOTODEGRADATION

The CO_2 gas-phase method is versatile and permits rapid assessment of the relative photo-degradability of pigmented polyethylenes. It is shown that using an *in-situ* FTIR technique to obtain reproducible information on the photodegradation of plastic films over relatively short irradiation periods is viable. The advantages this method has over other accelerated weathering tests is the extremely rapid results it can provide, < 10 hours when compared to over thousands of hours for a conventional test based on carbonyl group measurement. Not only do the results obtained with a series of polyethylenes prepared with different TiO_2 pigments show that anatase is a pro-degradant whereas some rutiles can be protective and some pro-degradative, but most importantly for a suite of samples (nine) the results gained by the CO_2 method are consistent with the results obtained by the conventional carbonyl group development method. This is particularly valuable, giving confidence in the CO_2 method, allowing it to be adopted from paint systems to plastic systems.

Using the CO_2 method, it is relatively easy to assess the effect of changing the UV spectral distribution and of changing the atmosphere in the cell (humidity, oxygen content *etc*). Changing the spectral distribution of the irradiating UV can alter the ranking of the pigments and in some cases was found to change the effect of a pigment from protective to pro-degradative.

The results of *in-situ* gas phase studies have indicated that atmosphere, pigments, radiation intensity and radiation distribution all affect the rate of photodegradation of practical polymer films. It was found that both the oxygen concentration and humidity in the cell strongly affect the evolution of CO_2 from the irradiated polymer sample. Changing the dominant gas in the cell atmosphere from pure oxygen to 20% oxygen/

80% nitrogen caused a decrease in the rate of photodegradation of PE and PVC samples, but the extent of the decrease was found to be different for the different polymers. For example, the PE sample still gave a measurable amount of carbon dioxide evolution with the nitrogen atmosphere, whereas for PVC samples, no carbon dioxide was observed in the course of irradiation under nitrogen atmosphere. Further studies demonstrated that both direct photochemical and photocatalytic degradation of the polymer films depend on the humidity of the cell. The faster rates of degradation of polymer are obtained for higher humidity levels. It is therefore essential that a stable atmosphere (*i.e.* humidity and oxygen concentration) is mantained in the cell to get comparable results. These results are fully consistent with the known semiconductor photocatalysis mechanism and the inherent importance of water and oxygen for pigmented plastic films.

The mechanisms of degradation of pigmented and unpigmented polymer film are different. *Ex-situ* multiple layers experiments, monitoring carbonyl group development in the films, showed that although both direct photochemistry and photocatalytic action are surface phenomena. For direct photochemical reaction the oxygen starvation is a main reason why reaction is limited in the inner portion material; for pigmented polymer films, the pigment absorbing UV light is a main reason why inner material degradation is limited.

The study of the effect of irradiation intensity and wavelength on the photo-oxidation formation of carbon dioxide from polyethylene films shows that the mechanism is different for unpigmented and TiO_2 pigmented films. Preliminary measurements demonstrate that, for anatase pigmented polyethylene and rutile R1 pigmented poly (vinyl chloride) samples, the rate of carbon dioxide is proportional to $I^{0.5}$, the square root of the UV intensity. For unpigmented polyethylene films, the rate of carbon dioxide is proportional to the UV intensity, I, under the experimental conditions used with these experiments. In turn, the *in-situ* gas-phase FTIR technique has allowed the effect of radiation wavelength to be conveniently and directly measured for both unpigmented and pigmented plastic samples. The results showed that unpigmented polymer is more sensitive to UV light distribution than the TiO_2 pigmented polymer.

7.2 TENSILE STRESS STUDIES

The effect of stress on the rate of photo-oxidation in a series of blown film polyethylene films in unpigmented and pigmented form has been investigated, using carbonyl group development as the method of assessment. Tensile tests on unexposed samples revealed that they were anisotropic; all materials gave a higher yield stress when tested parallel to the machine direction than when tested transverse to it. Tensile stress has been shown to increase the rate of photodegradation. The carbonyl group measurements were made with the samples in the stretched state, which produced a reduction in thickness compared to the unstrained state. Therefore, to analyse the infrared absorption data it was necessary to perform a correction for thickness differences between samples.

In some cases, different rates of carbonyl group development were found for samples strained parallel and transverse to the machine direction. With unpigmented polyethylene, carbonyl group development was slightly faster when UV exposure was conducted with tensile stress applied in the transverse direction. Pigmented samples PE A-1 and PE R3-1 gave the greatest carbonyl production rates when strained parallel to the machine direction whereas the rutile-pigmented polyethylene PE R4-1 displayed a greater rate for transverse stress. The oxidation of PE R1-1 and PE R2-1 under UV-stress conditions showed little effect of strain application direction. It is evident that the underlying anisotropy in some samples is sufficient to provoke a strong response in the oxidation behaviour under applied loading, even though it was not revealed by measurements of dichroic ratio. Samples loaded in the machine direction during UV exposure broke after a shorter time than samples of the same material loaded transversely. The carbonyl index was higher at the time of break in those samples strained transversely than those stressed longitudinally during exposure.

7.3 FUTURE WORK

The studies reported above have shown that the *in-situ* FTIR method of monitoring CO_2 can be used in conjunction with a suitable artificial light source to provide a reproducible measure of the carbon dioxide evolution to evaluate the photooxidation of polyethylene and poly(vinyl chloride). It was also shown that the technique could

not only distinguish the photoactivity of unpigmented and different pigmented materials, but also could be used to demonstrate the effects of UV intensity, wavelength, humidity, concentration of oxygen and others factors for the same material.

The CO_2 method is not restricted to the studies described above. The versatility of the *in-situ* FTIR method of monitoring CO_2 to evaluate the material photoactivity have been explored by considering a variety of samples drawn from others polymers and materials. Preliminary results are now presented on the use of the CO_2 method to evaluate photodegradation of polyester or rubbers or the photoactivity of different layers coating on TiO_2.

7.3.1 Polyesters

Polyesters have hydrocarbon backbones which contain ester linkages, hence the name.

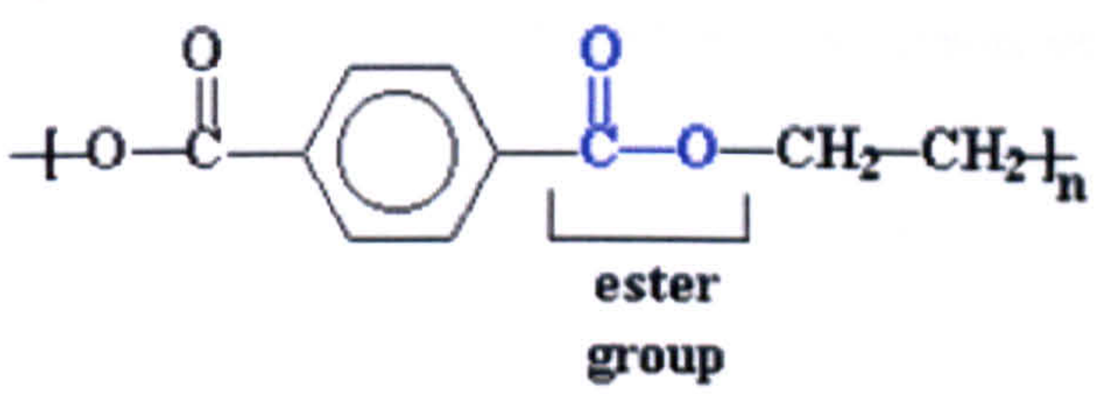

The structure in the picture is called poly(ethylene terephthalate), or PET for short, because it is made up of ethylene groups and terephthalate groups.

FTIR has been used to monitor the presence of new carbonyl groups on the polymer weathering, although this is not possible for polyesters because there are carbonyl groups existing in their structure. However many polyesters can be weathered by UV radiation, and the consequent release of CO_2 at the beginning of the oxidation can be followed by the CO_2 method. Figure 8-1 shows the CO_2 evolution from different PET samples, with different crystallinities. It can be seen that the CO_2 method gave a clear indication which sample emitted more CO_2. The most photostable film (PET4) is the only one that contains an organic stabilizer. Hence these results demonstrate (a) the

possibility of using the method to study PET oxidation and (b) the possible use of the method to determine the efficacy of UV stablizers.

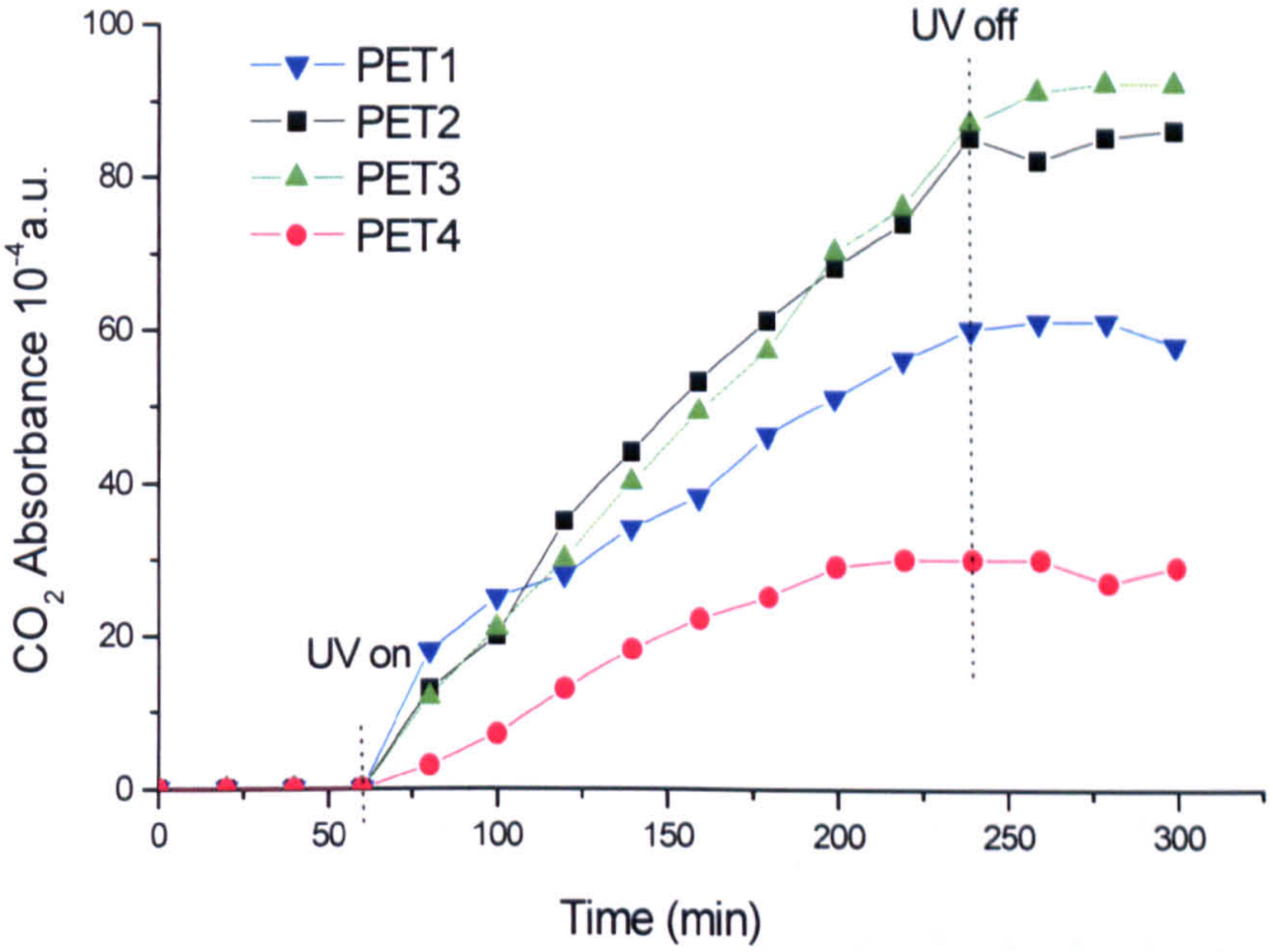

Figure 7-1 Carbon dioxide evolution from PETs UV irradiated, under wet O_2 atmosphere.

7.3.2 Rubbers testing

Rubbers are highly susceptible to degradation, due to the presence of double bonds in the main chain. Degradation of rubbers is accelerated mainly by heat, humidity, light, ozone, radiation *etc*. Various methods exist for characterization of weathered rubbers such as chemical, physical or mechanical. Several authors studied degradation of elastomers due to UV irradiation[1-6]. However, the CO_2 method has a potential to extend for rapid testing. Figure 7-2 shows four different type rubbers gave the different CO_2 evolutions. It is clear that the CO_2 evolution from UV irradiated rubbers were big difference between different types of rubber. The silicone gave about thirty times more CO_2 evolution than Nitrile. The results were obtained from these four samples are as expected. It is possible to evaluate a good correlation between the light resistance and outdoor weathering behaviour. Also the versatility of the *in-situ* FTIR

method of monitoring CO_2 will provide a convenient method to explore the effect of other parameters such as water, the concentration of oxygen *etc*, on photodegradation.

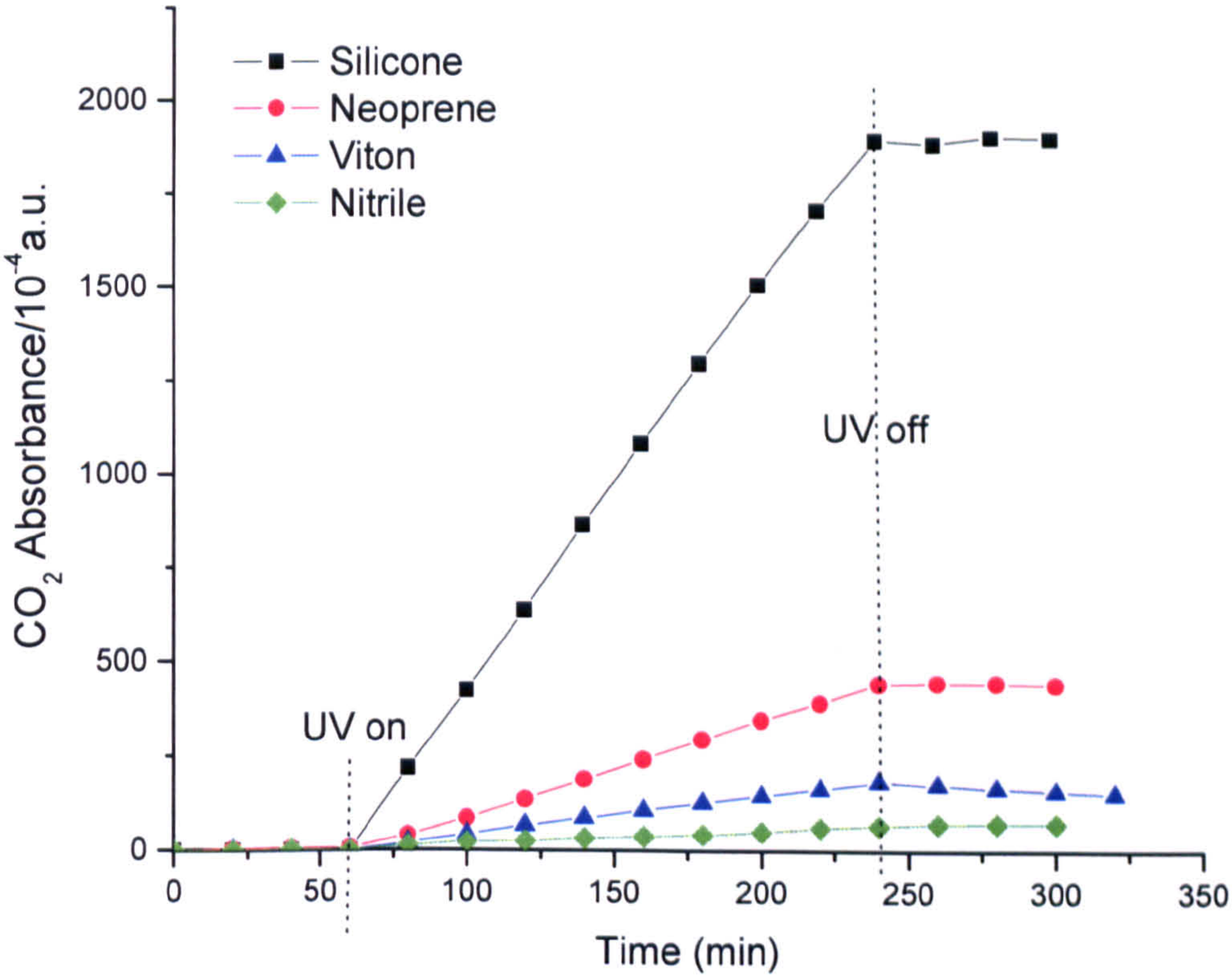

Figure 7-2 CO_2 evolution under UV irradiation in wet O_2 atmosphere from different rubbers.

7.3.3 TiO_2 powder testing

TiO_2 nanoparticles may be coated with sodium stearate to reduce their photoactivity when used as sunblocks. However this stearate layer may itself be photo-oxidized.

The results in Figure 7-3 were measured on the different grades of TiO_2 powder were coated with sodium stearate. The same types of TiO_2 were pressed into disks like a KBr disc used in FTIR transmission method and were then placed in the *in-situ* cell under UV irradiation. The CO_2 evolutions were monitored by *in-situ* FTIR for the different TiO_2 disks. Figure 7-3 shows a typical plot of the CO_2 evolution against exposure time for these three kinds of TiO_2.

Sample A and B are both predominantly anatase. However the high area 50 m^2g^{-1} sample A is clearly more photoactive than the low area, 10 m^2g^{-1}, sample B. Sample C is a high area (140 m^2g^{-1}) rutile. These rutile particles are less photoactive than A and B despite their high area. These results demonstrate a potential application of the technique to the study of catalytically active nanoparticles.

All three of these examples could form the basis of future research.

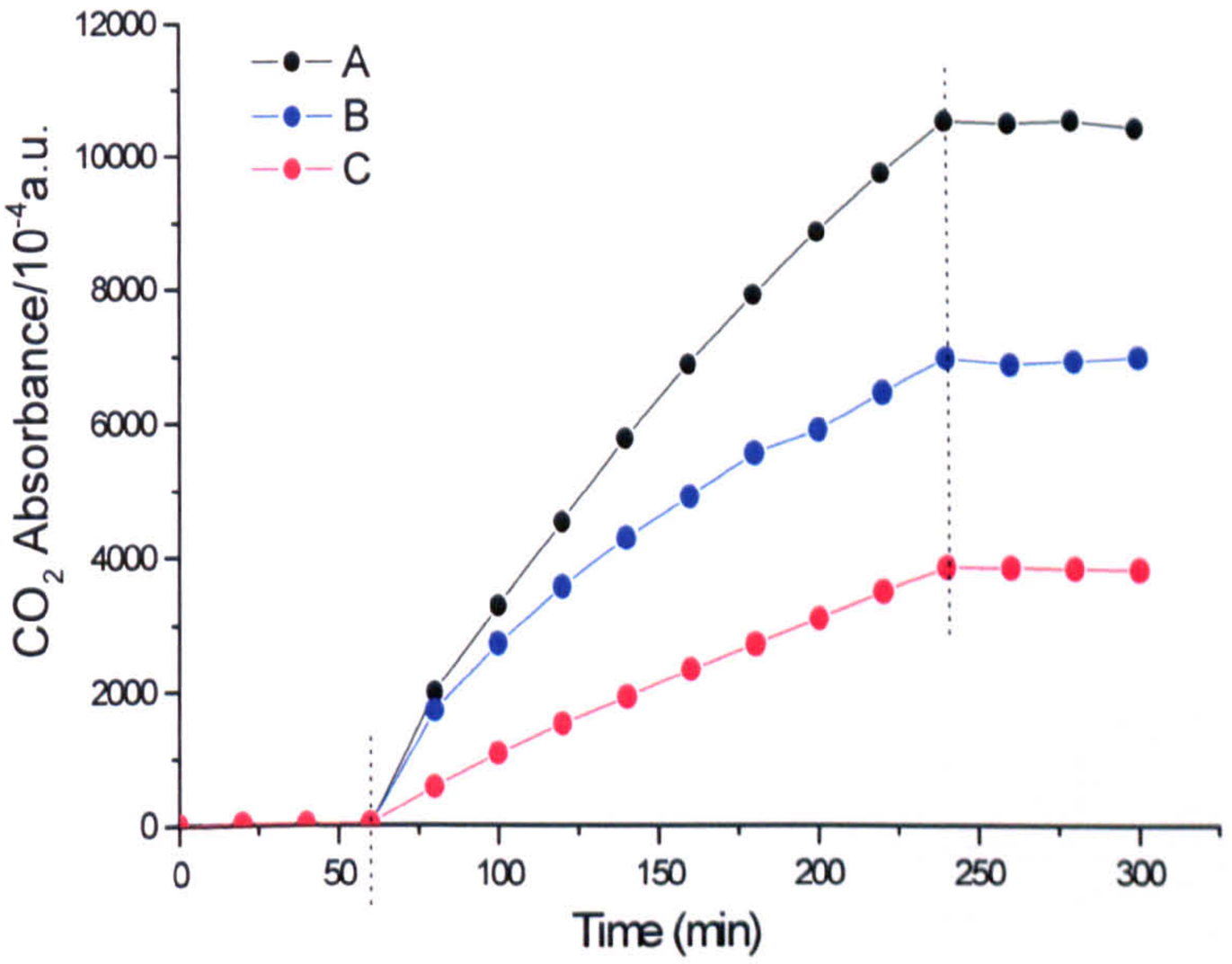

Figure 7-3 CO_2 evolution under UV irradiation in wet O_2 atmosphere for the three different kinds of TiO_2.

7.4 REFERENCES

1. Sommer, A., E. Zirngiebl, L. Kahl, and M. Schonfelder, *Progress in Organic Coatings,* 1991. **19**(1): p. 79-87.
2. Govorcin Bajsic, E., V. Rek, A. Sendijarevic, V. Sendijarevic, and K.C. Frish, *Polymer Degradation and Stability,* 1996. **52**(3): p. 223-233.
3. Guzzo, M. and M.-A. De Paoli, *Polymer Degradation and Stability,* 1992. **36**(2): p. 169-172.
4. Decker, C., K. Moussa, and T. Bendaikha, *Journal of Polymer Science, Part A: Polymer Chemistry,* 1991. **29**(5): p. 739-747.
5. Decker, C. and K. Zahouily, *Journal of Polymer Science, Part A: Polymer Chemistry,* 1998. **36**(14): p. 2571-2580.
6. Bhowmick, A.K., J. Heslop, and J.R. White, *Polymer Degradation and Stability,* 2001. **74**(3): p. 513-521.